THERMAL DECOMPOSITIONS OF INORGANIC AND ORGANOMETALLIC TIN COMPOUNDS.

by Michelle Hornby Jones.

Thesis submitted for Doctor of Philosophy

Chemistry Department

The City University.

November, 1985.

ORIGINAL COPY TIGHTLY BOUND

Acknowledgements.

I would like to thank Prof. J.D. Donaldson for providing the financial support for this work, for his supervision and advice throughout, and with [redacted] for the concept of the research programme.

Particular thanks go to [redacted] for his kindness and assistance, especilly with regard to the construction of the thermal decomposition apparatus.

Large portions of the research would not have been possible without the support of the technical staff within the Chemistry department. I hope that I will be forgiven for merely listing a number of them:

[redacted], (GC/MS); [redacted] (I.R., UV); [redacted], (elemental analyses); and [redacted], (nmr).

My grateful thanks also go to my colleagues for their encouragement and innumerable games of Badminton.

Abstract.

An apparatus is constructed to study the products of decomposition of a range of inorganic and organometallic tin compounds. The apparatus incorporates gas,liquid and solid sample collection and separates the decomposition products into gaseous, volatile and non-volatile fractions. The products of pyrolysis can be collected in sufficient quantities to permit full analyses using techniques such as: Gas Chromatography-Mass Spectroscopy, i.r. spectroscopy, uv spectroscopy, elemental analysis, X-ray diffraction,TLC, titrimetric analysis, and nmr spectroscopy.

A pyrolysis head attachment for a mass spectrometer was also constructed to permit gas chromatographic -mass spectroscopic identification of the gaseous products of pyrolysis.

The inorganic compounds studied were tin(ii) carboxylate derivatives including complex tin(ii) formates, acetates, oxalates and malonates. For the complex tin(ii) formates , the transition metal was seen to affect the order of cleavage of the metal-formate bonds, (ie. Sn or M-formate bond broken in first pyrolysis reaction), and to have different catalytic effects on the volatile products formed. The Na, K, and Ca tin(ii) acetates followed similar decomposition pathways with formation of SnO and metal acetate in the first pyrolysis step, with subsequent breakdown of the metal acetate to give the carbonate in the final decomposition stage. For the NH_4^+ derivative, the ammonium acetate portion of the complex decomposed initially, rapidly followed by decomposition of the stannous acetate. The metal carbonates were also the final decomposition product of pyrolysis of the oxalates and malonates although as with the formates, the different metals are seen to have different catalytic effects on the volatile gaseous products.

The organotin compounds studied included triphenyltin hydroxide, dialkyltin oxide polymers, dialkyl and diaryltin nitrates, dialkyl and diaryltin sulphates, and organotin(iv) carboxylates. For the majority of compounds full decomposition

pathways are presented. The oxides and hydroxide show quite complex pyrolysis pathways involving partial reduction of Sn(iv) to Sn(ii) in the final decomposition stage to give solid residues comprising both Sn(ii) and Sn(iv) oxides. Both the nitrates absorb moisture initially to form hydroxides which breakdown to give SnO_2 as the final solid residue. Complicated partial decomposition pathways were followed for the carboxylates, which incorporated several pyrolysis steps.

Index.

Index - Chapter 1.

1.1. Introduction.

Although thermal decomposition studies dating back to the end of the last century are recorded in the literature, relatively little work has been published on the decomposition of either organotin compounds or tin carboxylates and their complexes. In this chapter, published work on the thermal decomposition of organotin compounds from papers from about 1860 to date and more recent information on the thermal behaviour of metal carboxylates is presented as background information to the topic of this thesis.

Three main conclusions can be drawn from the literature surveys contained in this chapter, viz. (i) there is a considerable amount of disagreement between authors on the exact nature of the thermal decompositions of many of the compounds considered, (ii) that the conditions of pyrolysis can effect the nature of the products, and (iii) that great care has to be taken in controlling experimental conditions and in analysing for all pyrolysis products to permit proper interpretation of decomposition routes.

1.2. Metal Carboxylates.

1.2.1. Formates.

Over the past 25 years, a wide range of metal formates have been prepared and their thermal behaviour studied but it is only during the last few years that complex metal formates of any type have been investigated.

In 1973, Shishida and Masuda[1] identified the gaseous thermal decomposition products of sodium and potassium formates which were decomposed using a thermogravimetric technique incorporating gas chromatographic analysis. For both compounds, the final residue was found to be the metal oxide, M_2O, while the main gaseous products were CO_2, CO, and H_2. The following mechanism was used to explain these results.

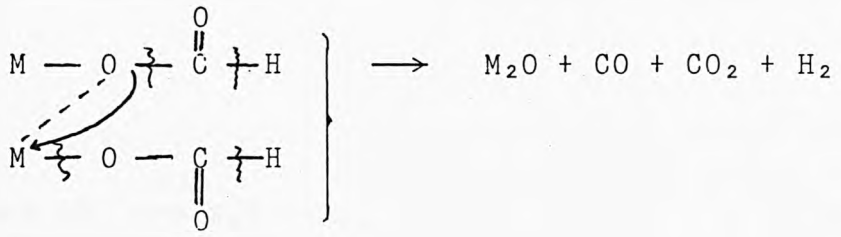

Secondary reactions resulting in the formation of small amounts of CH_4, HCOH, $HCOOCH_3$, and CH_3OH also occurred. These gaseous products were said to be formed by the catalytic action of the solid metal oxide residue on the primary products:

$$2H_2 + CO \longrightarrow CH_3OH \; ; \qquad H_2 + CO \longrightarrow HCHO \; ;$$

$$2HCHO \longrightarrow HCOOCH_3 \; ; \qquad CO + 3H_2 \longrightarrow CH_4 + H_2O \; .$$

Other authors [4] have observed side reactions in which gaseous organic compounds are formed, and have proposed a direct route to the metal oxide.

The single step formation of the alkali metal oxide suggested by Shishida and Masuda was later refuted by Meisel et al.[2], who proposed a two or three stage process with M_2CO_3 and $M_2C_2O_4$ as intermediates. The mechanism suggested involved the formation of the intermediates:

$$2HCOOM \begin{cases} \longrightarrow M_2CO_3 + CO + H_2 & \text{I} \\ \longrightarrow M_2C_2O_4 + H_2 & \text{II} \end{cases}$$

and their subsequent decomposition to give the final M_2O product.

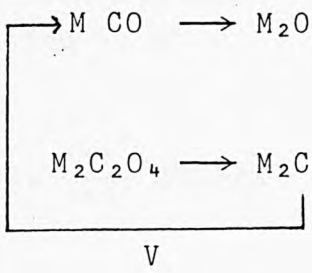

These reactions leading to the matal oxide were said to proceed separately and independantly, both from each other and from reactions I and II. The only gas phase reactions considered in the mechanism were:

$$2CO \rightleftharpoons CO_2 + C \; ; \qquad 2H_2 + O_2 \longrightarrow 2H_2O \; ;$$

$$2CO + O_2 \longrightarrow 2CO_2 .$$

and no reactions giving organic molecules were included.

The Meisel at al. mechanism was further substantiated in 1979 by Baraldi [3], who found that although in air alkali metal formates form the carbonate directly on decomposition, in vacuo both the Na and K salts undergo a phase change above the dehydration temperature but below the decomposition temperature. The phase changes were attributed to formation of the oxalates which subsequently decomposed below 500°C to give the carbonate, ie.

in air: $$2HCOO^- \longrightarrow CO_3^{2-} + CO + H_2$$

in vacuum: $2HCOO^- \longrightarrow C_2O_4^{2-} + H_2 \longrightarrow CO_3^{2-} + CO$

The thermal decomposition of sodium hydroformate, $NaH(HCOO)_2$ has also been studied[5] and the following pathway proposed for the reaction in air:

$$NaH(HCOO)_2 \xrightarrow[\text{exo}]{150^0} HCOONa + HCOOH \xrightarrow[\text{endo}]{210^0} \alpha\text{-}HCOONa \xrightarrow{500^0} \text{mixture of } Na_2C_2O_4 \text{ and } Na_2CO_3$$

The endothermic phase change at 210°C was reported to be irreversible and no metal oxide was found among the products.

Thermal studies on group II metal formates have received much greater attention. In 1965, Hartman and Hisatsune[6] studied the pyrolysis of $Ca(HCOO)_2$ in a KBr matrix, following the decomposition process by infra-red spectroscopy. They found that $Ca(HCOO)_2$ decomposed to give $CaCO_3 + CO + H_2$, and the CO disproportionated to give $CO_2 + C$. The proposed decomposition mechanism was:

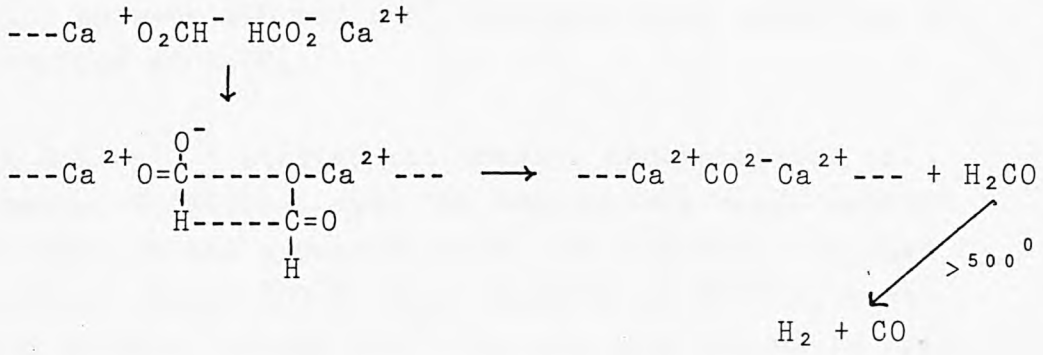

The $BaCO_3$ formed then decomposed in two steps to give BaO. Secondary reactions commencing at 600°C for both the Ba and Sr salts were believed to be:

$$MCO_3 + C \longrightarrow M + 2CO$$

This was implied by analysis of the gaseous products, which showed the presence of CO, CH_4, CO_2, and H_2, and at maximum heating rate, formaldehyde. All these products are accounted for by formation of CO_3^{2-} and CH_2O, which break down to give the side products. Canning and Hughes[9] obtained the same results in their study of the alkali metal formates, although they also identified formic acid in the reaction products.

A two stage decomposition mechanism has , however, been suggested for the Ca and Sr compounds[7], with the residue from the first decomposition stage having a slightly lower weight than would bave been expected from the direct formation of MCO_3. Above 550°C, the MCO_3 decomposes to give CaO, with a slightly higher experimental weight loss than the calculated value. These slight anomalies were explained by formation of elemental carbon in the first stage, which is only partially removed at higher temperatures.

The thermal decomposition of barium hydroformate[5] commenced at 130°C, giving barium formate and formic acid. The intermediate formate melted at 340°C, then decomposed exothermically between 400 and 425°C probably with oxidation of H_2CO and formation of $BaCO_3$.

Head and Holley[10] studied the thermal decomposition of scandium formate, $Sc(HCOO)_3$, over the temperature range ambient to 500°C. As well as the expected gases, (CO and H_2O), CO_2 and H_2 were also evolved. Below 500°C, trace amounts of $HCOOCH_3$ were detected, and between 340 and 500°C CH_4 was also formed in trace amounts. No free carbon was found and by 500°C the only residue was Sc_2O_3. Masuda and Shishido[11] in their study of the thermal decomposition of $Sc(HCOO)_3$ in nitrogen found that $Sc_2O_2CO_3$ and Sc_2O_3 were formed in the first stage between 210 and 380°C. This they explained by the following reaction:

$$4Sc(HCOO)_3 \longrightarrow Sc_2O_3 + Sc_2O_2CO_3 + 6H_2 + 6CO + 5CO_2$$

At temperatures between 380 and 1000°C the only solid residue detected was Sc_2O_3 so that the basic salt must have decomposed:

$$Sc_2O_2CO_3 \longrightarrow Sc_2O_3 + CO_2$$

Thermal studies on $Y(CHOO)_3.2H_2O$ [12] in nitrogen and CO_2 provided evidence for a three stage decomposition. The first stage was complete dehydration to give the anhydrous compound, which decomposed to YO(HCOO), which in turn decomposed to give the final residue $Y_2O_2CO_3$.

Thermal decomposition studies on $Sn(HCOO)_2$, carried out in both inert and oxidising atmospheres have shown that only SnO is formed in the final decomposition stage [13]. In oxidising atmospheres, SnO disproportionated at 827K to give SnO_2 and metallic Sn. At 873K, metallic Sn was oxidised to Sn(IV) oxide. The following decomposition schemes have been proposed:

$$Sn(HCOO)_2 \longrightarrow SnO + CO_2 + H_2CO \; ; \qquad SnO + \tfrac{1}{2}O_2 \longrightarrow SnO_2 \quad *$$

$$2SnO \longrightarrow Sn + SnO_2 \; ; \qquad Sn + O_2 \longrightarrow SnO_2 \quad *$$

(* these two reactions take place in oxidising atmospheres only). Evolved gas analysis confirmed that CO_2 and formaldehyde were formed.

Although the final products in the decomposition of lead formate were found to be a mixture of Pb and PbO, three different pathways have been proposed. One group have suggested that lead formate decomposes at 325°C in air to give Pb and C [14]. The finely divided lead formed in the decomposition reacts vigerously with oxygen to give the following reaction sequence:

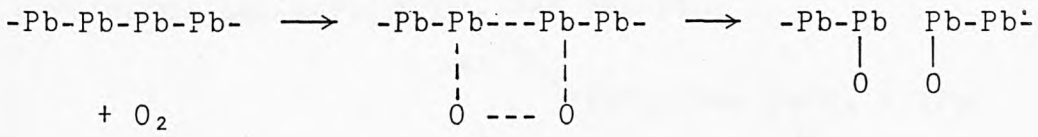

Although the finely divided lead is adsorbed onto the C matrix, C is said to play no part in the oxidation process. The second group, Shishido and Masuda[11], reported that lead formate belongs to the class of formates which include the Ni, Cu, and Sr salts, and in which the main decomposition pathway is:

$$M(HCOO)_2 \longrightarrow M + 2CO_2 + H_2$$

and suggested the mechanism:

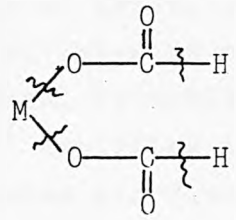

with the side reactions arising from

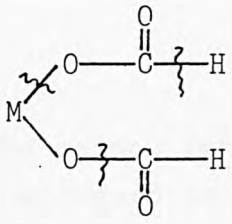

and giving $MO + CO + CO_2 + H_2$

The third group proposed a decomposition mechanism involving two simultaneous reactions occurring in both air and vacuum:

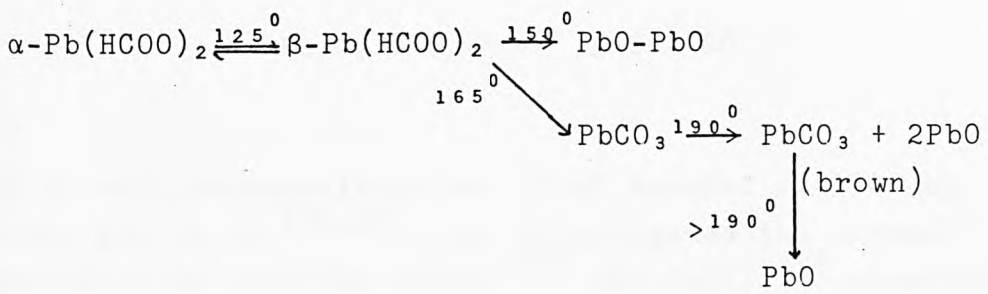

Nirsha et al., in 1979[16] investigated the thermal decomposition of the complex $Ti_2OCl(HCOO)_3(OH)_2$ over the temperature range 200 to 350°C. This complex was found to decompose to give TiO_2, H_2O, CO, and HCl, ie:

$$Ti_2OCl(HCOO)_3(OH)_2 \longrightarrow 2TiO + 2H_2O + 3CO + HCl$$

The pyrolysis reactions of transition metal formates have aroused a considerable amount of interest over recent years[17,18]. Hydrous iron (II) formate, $Fe(HCOO)_2 2H_2O$ when decomposed in an atmosphere of argon[19] exhibited a five stage decomposition process with two exotherms and five endotherms. The exotherms were attributed to recrystallisation processes, while the five endotherms were represented by the following decomposition scheme:

$$Fe(HCOO)_2 2H_2O \xrightarrow[1]{} Fe(HCOO)_2 H_2O \xrightarrow[2]{} ? \xrightarrow[3]{} Fe(HCOO)_2 \xrightarrow[4]{} Fe_3O_4 \xrightarrow[5]{} FeO$$
magnetite

The nature of the second intermediate was unknown, although it was tentatively assigned as one of three materials, viz., Fe_3O_4, Fe carbonyl carbonate or Fe carbonate. The magnetite produced in the fourth decomposition step may have contained some C from the decomposition of the formate group, and this would explain the presence of 0.3 mole of CO in the gaseous products of the fifth decomposition step, ie.:

$$Fe_3O_4 + C \longrightarrow 3FeO + CO$$

Copper formate decomposition was first studied on 1962 by Schuffenecker et al.[20,21], who investigated the thermal decomposition of both the Cu(II)[20] and Cu(I)[21] compounds in vacuo. CuCOOH decomposed to give metallic Cu, CO_2 and formic acid, ie.:

$$Cu(HCOO) \longrightarrow Cu + \tfrac{1}{2}CO_2 + \tfrac{1}{2}HCOOH$$

There is a great deal of discrepancy in the published data on the thermal decomposition of copper (II) formate, ($Cu(COOH)_2$). Schuffenecker stated that the Cu(II) compound was first reduced to $Cu^{I}COOH$ with evolution of CO_2 and H_2, but the CuCOOH formed in this decomposition did not decompose in the same manner as CuCOOH not produced in situ. The intermediate, CuCOOH, decomposed to give Cu + CO_2 + H_2, with no formic acid. Which has also been reported by another group of workers[23]. Shishida and Masuda[1], however, stated that CuO was also present as a minor constituent of the decomposition residue, with the major product being Cu metal.

Rao et al.[22] suggested that hydrated $Cu(COOH)_2$ underwent a two-stage decomposition, in which the first intermediate was the anhydrous material which was found to decompose subsequently to give CuO, CO, CO_2, H_2O and H_2, according to the reaction:

$$2Cu(HCOO)_2 \longrightarrow 2CuO + 3CO + H_2O + H_2$$

Dollimore and Tong[24] found that anhydrous zinc formate decomposed via two main routes, each giving ZnO as the solid residue:

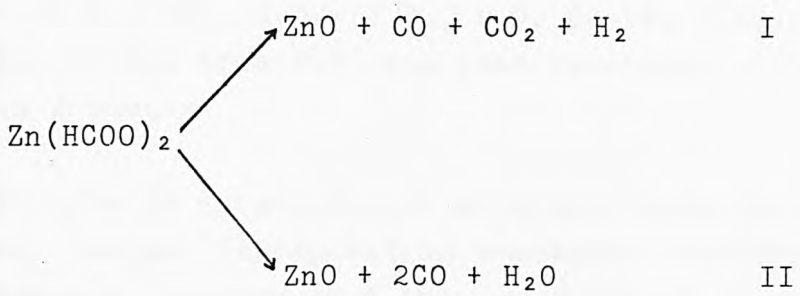

The two routes were said to arise from the presence of two types of formate group in the zinc formate lattice; (i) those with both oxygen atoms as nearest neighbours to the Zn^{2+} ions in an octahedral arrangement, and (ii) those with one oxygen atom as the nearest neighbour to the Zn^{2+} ion in a dihedral arrangement. Although the primary gaseous decomposition products of the second route were CO and H_2O, they were said to be catalysed in the gas phase by ZnO to give formaldehyde and CO_2:

$$2CO + H_2O \rightleftharpoons CO + CO_2 + H_2 \rightleftharpoons HCHO + CO_2$$

Similar results were obtained for $Zn(HCOO)_2.2H_2O$[25] where numerous gas phase reactions resulted in a diversity of gaseous products. The initial decomposition process involved loss of both water molecules, and was accompanied by an endothermic and an exothermic effect. The exothermic energy change has been attributed to recrystallisation of the amorphous portion of the anhydrous intermediate. Gas chromatographic analysis of the gaseous products indicated the presence of CO, CO_2, HCHO, and HCOOH, said to be formed in three simultaneous decomposition reactions:

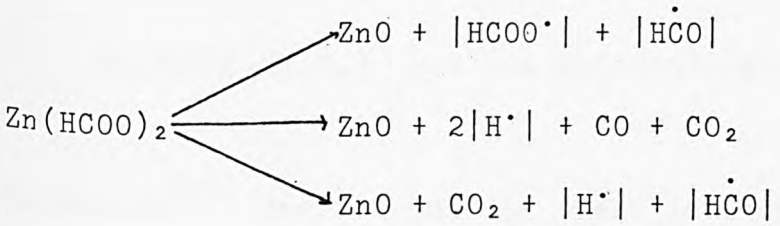

Smaller amounts of H_2, CH_4, C_2H_4, C_2H_6, H_2O, CH_3OH, $(CH_3)_2O$, and $HCOOCH_3$ were also formed from ZnO catalysed reactions of the original gaseous products.

Manganese formate is isostructural with zinc formate, and it undergoes similar thermal decomposition reactions. Dollimore and Tong[24], for example, claimed that the pyrolysis of the Mn compound was the same as that for zinc formate except that reaction (II) above is relatively fast compared with reaction (I), and that the MnO formed had no catalytic effects on the gaseous products

In the thermal decomposition of $Cr(HCOO)_3.H_2O$ in air, Berezin et al.[26] noted an exothermic reaction at ca. 500°C which corresponded to oxidation of Cr(III) to Cr(IV) with formation of CrO_3. This decomposition was preceded by an endothermic effect between 250 and 270°C due to dehydration of the hydrous compound.

Nadzharyan et al.[17] reported that the Cd-NH_4 complex, $NH_4|Cd(CHOO)_3|$ underwent a monotropic transformation when heated in an Ar atmosphere. The thermal bahaviour of a number of transition metal hydrazine complexes of the type $|M(HCOO)_2.(N_2H_4)|$ have also been studied[18]. The Co, Zn, and Cd complexes were found to lose both hydrazine molecules above 100°C in a single step to give the metal formate. Whereas the Ni complex decomposed directly to a mixture of metallic Ni and NiO, and the Mn complex lost only one molecule of hydrazine initially in two endothermic reactions. Further heating of the Mn residue did not give the same product as in the decomposition of manganese formate, but, instead a mixture of MnO and Mn_2O_3 was formed from the intermediate $Mn(HCOO)_2.N_2H_4$ in the temperature range 197 to 320°C, ie:

$$Mn(HCOO)_2(N_2H_4) \longrightarrow\longrightarrow Mn(HCOO)_2.N_2H_4 \longrightarrow MnO + Mn_2O_3$$

Dabkowska[27] carried out the first investigations into the thermal decomposition of lanthanide formate compounds, $M(HCOO)_3$, (M=Eu, Tb, Lu). Eu and Tb formates decomposed in three stages to give oxide (M_2O_3)final residue. For $Eu(HCOO)_3$, the intermediates were found to be carbonate and the oxycarbonate:

$$Eu(HCOO)_3 \xrightarrow{>200^0} EuCO_3 \longrightarrow Eu_2O_2CO_3 \longrightarrow Eu_2O_3$$

While $Tb(HCOO)_3$ decomposed directly to the oxycarbonate, and then via Tb_4O_7 to Tb_2O_3. $Lu(HCOO)_3.2H_2O$ decomposed in four stages, the first, below 220°C was dehydration, and subsequent stages were interpreted as follows:

$$Lu(HCOO)_3 \xrightarrow{>200^0} Lu_2O(CO_3)_2 \longrightarrow Lu_2O_2CO_3 \longrightarrow Lu_2O_3$$

Lanthanide metal carboxylates have been studied quite extensively by a number of workers. However, their decomposition mechanisms are complex and there are many discrepancies in the pathways which have been recorded. One particular example is provided by lanthanum formate, ($La(HCOO)_3$), for which two groups of workers have reported two different pyrolysis mechanisms. Dharwadker et al.[28] in their study on the thermal decomposition of $La(HCOO)_3$ proposed the following decomposition pathway, and identified the gaseous products:

$$2La(HCOO)_3 \longrightarrow La_2(C_2O_4)_3 + 3H_2 \longrightarrow La_2O(CO_3)_2 + 3CO + CO_2$$

$$\longrightarrow La_2O_2CO_3 + CO_2 \longrightarrow La_2O_3 + CO_2$$

Traces of HCHO and CH_4 from gas-phase reactions were also found. In contrast, Masuda[29] did not obtain $La_2(C_2O_4)_3$ as the first intermediate for $La(HCOO)_3$, but instead obtained a 70:30% mixture of $La_2O_2.CO_3$ and LaO(HCOO) which he used to explain the presence of two endotherms in the Differential Thermal Analysis (DTA) trace of $La(HCOO)_3$ at 435-572°C and 665°C. Masuda claimed that the intermediates decomposed to give La_2O_3 and CO_2, and La_2O_3, CO_2, H_2, and CO, respectively. The Tb compound, $Tb(HCOO)_3$ was found to decompose to give initially TbO(HCOO) + H_2 + CO_2 + CO, followed by the oxycarbonate, and finally Tb_2O_3. Decomposition of

the other rare earth formates were said to be similar to that of terbium formate, except that they melt during pyrolysis. Different thermal behaviour was noted for dysprosium formate, which decomposed directly to the oxycarbonate, and then to Dy_2O_3. The dehydration temperature of the hydrated formates has been found to increase with increasing reciprocal ionic radius of the Ln^{3+} ion [30]

In 1968 the Th formate decompositions were studied by Mentzen [31] who carried out a detailed thermal analysis/X-ray diffraction study of the thermal decomposition of $Th(HCOO)_4.3H_2O$, using a Gas Chromatography-Mass Spectrometry method for analysis of volatile phases. The only solid product obtained in the temperature range 225-411°C was ThO_2. Gas-phase reactions occurred to give secondary products: H_2, CO, H_2O, CH_3OH, $HCOOCH_3$, HCOOH, and $(CH_3)_2O$.

For uranium formate, $|U(CHOO)_4|$, two conflicting decomposition reactions have been reported in air:

|Ref. 32| $U(HCOO)_4 \xrightarrow{220^0} UO_2(HCOO)_2 \longrightarrow \alpha\text{-}UO_3 + 8.5\%\ UO(OH)(HCOO)$

UO_3

|Ref. 36| $\beta\text{-}U(CHOO)_4 \xrightarrow{150^0} \gamma\text{-}U(CHOO)_4 \longrightarrow UO_2(CHOO)_2 \xrightarrow{200^0} UO_3 \xrightarrow{315^0} U_3O_8$

In nitrogen and argon, a two stage reaction has been recorded, to give a final residue of UO_2 [32,36] :

$$\alpha\text{-}U(CHOO)_4 \longrightarrow \gamma\text{-}U(CHOO)_4 \longrightarrow UO_2$$

For uranyl formate $|UO_2(CHOO)_2|$, three conflicting reports have been recorded for the decomposition in air:

|Ref. 32| $UO_2(CHOO)_2 \xrightarrow{340^0} \alpha\text{-}UO_3 + 8.5\%\ UO(OH)(HCOO) \xrightarrow{370^0} U_3O_8$

|Ref. 33| $UO_2(CHOO)_2 \xrightarrow{200^0} UO(OH)(HCOO) \xrightarrow{285^0} UO_3O.H_2O \xrightarrow{300^0} U_3O_8$

|Ref. 34| $UO_2(CHOO)_2 \longrightarrow UO(OH)(HCOO) \longrightarrow UO_{2+x}$

The mechanism of breakdown of the formate group has been suggested to be|32|:

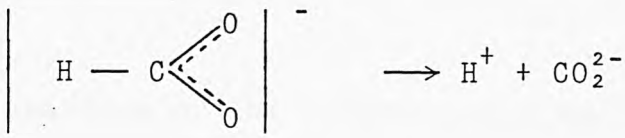

This mechanism was used to explain the formation of formic acid in the evolved gases, by H-abstraction on the formate group:

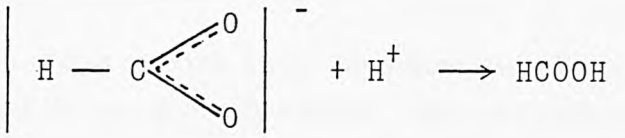

and formation of the uranium formates by reaction of the CO_2^{2-} ions:

$$UO_2^{2+} + CO^{2-} \longrightarrow UO_3 + CO; \qquad U^{4+} + 2CO_2^{2-} \longrightarrow UO_2 + 2CO.$$

The thermal bahaviour of three nitrogen-containing dioxouranium (VI) formate complexes, $UO_2(HCOO)_2.2L$, (where

L= $CO(NH_2)_2$, $HCONH_2$, and $CO|N(CH_3)_2|_2$), was studied by Spitsyn et al.[37] in nitrogen and air. In all three instances, the complexes lost one ligand molecule in the first decomposition stage, and gave a final residue of U_3O_8, which in air was preceded by formation of UO_3. When the ligand was $CO|N(CH_3)_2|_2$, a polymorphic transformation occurred at 32°C in nitrogen prior to decomposition. When L= $CO(NH_2)_2$ the gaseous decomposition products were CO_2, HNCO, and H_2O. When L= $HCONH_2$, the gaseous products were CO_2, CO, H_2O, HNC, and N_2C_2; and when L= $CO|N(CH_3)_2|_2$ the gaseous products were HCOOH, CO_2, CO, and H_2O.

1.2.2. Acetates.

The initial reaction of the acetate group during thermal decomposition is believed to be the following rate determining step[38]:

$$CH_3CO_2^- \longrightarrow CH_3^{\bullet} + CO_2^-$$

The CO_2^- formed at this point then becomes involved in a rapid H-abstraction reaction to give formate. The principal source of H is any water present, but minor sources are $CH_3^{\bullet}$ and $CH_3CO_2^-$. The $CH_3^{\bullet}$ formed in the rate determining step can either dimerise, or abstract a H to form CH_4. Together with CO, CH_3 may also be a source of C, which has also been identified in the thermal decomposition of acetates.

A second process, in which carbonate ion is formed, can occur independantly of the reaction above, ie:

$$2CH_3CO_2^- \longrightarrow (CH_3)_2CO + CO_2^{2-}$$

In the presence of a metal ion the CO_3^{2-} reacts with the metal to give the metal carbonate, which remains as a solid residue.

Pyrolysis experiments on alkali metal acetates suggest a one, or possibly two stage decomposition process to give a final residue of M_2CO_3 (M= Li, Na,K,Rb). For the Na salt, the following decomposition reaction was proposed:

$$2Na(CH_3COO).3H_2O \longrightarrow Na_2CO_3 + CH_4 + O_2$$

The same decomposition reaction has been reported for caesium acetate[39,40,41], but for the Li, K, and Rb salts no CH_4 was formed and pyrolysis produces acetone:

$$2M(CH_3COO) \longrightarrow M_2CO_3 + CH_3COCH_3$$

Baraldi[43] , however, suggested a two stage decompostion pathway for all the hydrated alkali metal acetates, with the metal oxalate, $M_2C_2O_4$, as the intermediate formed after dehydration:

$$2M(CH_3COO).xH_2O \longrightarrow 2M(CH_3COO) \longrightarrow M_2C_2O_4 \longrightarrow M_2CO_3$$

the dehydration process occurs at low temperatures, indicative of weak bonds between the coordinated water molecules and the metal ion. Metal oxalate has also been suggested as a possible intermediate in the final decomposition of acid potassium acetate, $KH_2(CH_3COO)_3$[44]. Decomposition of this complex compound at 30°C with evolution of acetic acid as follows:

$$KH_2(CH_3COO)_3 \xrightarrow{32-115^0} KH(CH_3COO)_2 + CH_3COOH \xrightarrow{115-195^0} CH_3COOK + CH_3COOH$$

Bernard and Fusnot[45] have shown that the hydrated alkaline earth acetates undergo four or five stage decompositions to give metal carbonates and acetone. Both $Mg(CH_3COO)_2.4H_2O$ and $Ca(CH_3COO)_2.H_2O$ undergo two stage dehydration processes in air and Ar. Magnesium acetate then partially decomposes to give a mixture of the anhydrous compound and the basic acetate, or as proposed by Grigor'ev et al.[47] an oxyacetate with the formula $Mg_4O(CH_3COO)_6$ together with acetic anhydride, $|(CH_3CO)_2O|$. Undecomposed $Mg(CH_3COO)_2$ fuses between 320 and 325°C and is identified by an endotherm in the DTA trace, and then decomposes to give $MgCO_3$. Grigor'ev et al. did not identify $MgCO_3$ in the final residue, but report that the oxide, Mg_2O_3 is formed instead.

Three groups of workers have carried out pyrolysis experiments on hydrated lead (II) acetate, ($Pb(CH_3COO)_2.3H_2O$), and obtained different decomposition schemes. Manabe and Kubo[48] suggested that hydrated lead acetate underwent a five stage decomposition in inert atmospheres to give Pb metal as the final residue,[48] with dehydration commencing at ca. 40°C. Although the amount of water lost, and the stoichiometry of the lower hydrate formed were unknown. Dehydration was complete by 200°C and the anhydride melted and decomposed above 200°C to give an intermediate with the formula $3Pb(CH_3COO)_2.2PbO$ which decomposed directly to metallic Pb. Other authors[49] report a single stage dehydration reaction followed by decomposition by the route:

$$6Pb(CH_3COO)_2 \longrightarrow 3|Pb(CH_3COO)_2 + PbO| \longrightarrow 2|Pb(CH_3COO)_2 2PbO|$$

$$\longrightarrow 6PbO + CO_2 + CH_3COCH_3$$

The two lead acetate-lead oxide intermediates were said to have different $Pb(CH_3COO)_2$:PbO ratios, but both decompose to give PbO not metallic Pb, although small amounts of lead, which arise from the following side reaction are formed:

$$Pb(CH_3COO)_2 \longrightarrow Pb + CH_3COOH + CO_2 + H_2 + C$$

$(CH_3CO)_2O$ and ketene were also identified, and their formation assigned to the side-reactions:

(i) $CH_2CO \longrightarrow C + H_2 + CO$; (ii) $2CH_2CO \longrightarrow C + CH_4 + 2CO$.

For Pb (IV) acetate decomposition was reported to take place in three stages[50] and to give a final residue of PbO. The first decomposition stage involved reduction of Pb(IV) to Pb(II) and the formation of two acetoxy radicals. The acetoxy radicals combined to form CH_3COOCH_3 and CO_2. $Pb(CH_3COO)_2$ was reported to decompose directly to $PbCO_3$ and acetone (in contrast to the results obtained from the decomposition of $Pb(CH_3COO)_2$ not obtained in a decomposition reaction), prior to a final decomposition to PbO and CO_2.

In the initial decomposition stage for hydrated Co and Ni acetates there are differences of oppinion between the three groups of workers who have conducted the pyrolysis experiments. One group of authors has reported a single stage dehydration to the anhydrous compounds of the same crystal structure[51], while other authors suggested a two stage dehydration[52,53], while Baraldi[43] claimed that the first stage in the decomposition of cobalt acetate was not dehydration but the formation of an intermediate hydroxyacetate, $|Co(CH_3COO)_{2(1-x)}(OH)_{2x}|$. In the two stage dehydration process, the first stage was formation of a lower hydrate with an unknown number of water molecules. Above 100^oC, anhydrous Co and Ni acetates partially decomposed to give a mixture of the anhydride and metal oxide. In the case of $Ni(CH_3COO)_2$ the ratio of anhydride to NiO was 10:3. The final stage was formation of Ni metal oxides, NiO and some chemisorbed oxygen for nickel acetate, and Co_3O_4 with traces of CoO for cobalt acetate.

In Baraldi's work, the first intermediate, $Co(CH_3COO)_{2(1-x)}(OH)_{2x}$ decomposed on further heating to give a mixture of $Co_6O(CH_3COO)_{10}$, (blue in colour), and $Co_3O(CH_3COO)_4$, (pink). The blue complex converted into the more stable pink complex after it had been formed. At higher temperatures, $Co_3O(CH_3COO)_4$ broke down to give a mixture of CoO and $Co(CH_3COO)_2$ which was green. On complete decomposition, the residue was CoO with traces of Co metal.

For the Ni salt, Baraldi suggested that a basic acetate was formed after dehydration, which decomposed to give metallic Ni. Anhydrous cobalt acetate was reported to decompose directly to Co metal.

It was reported that hydrated zinc acetate, $Zn(CH_3COO)_2.2H_2O$ lost water in a single step[55], followed by slow sublimation of the anhydrous compound with maximum rate of weight loss above 180°C to give octahedral zinc oxyacetate and acetic anhydride:

$$4Zn(CH_3COO)_2 \longrightarrow Zn_4O(CH_3COO)_6 + (CH_3CO)_2O$$

The zinc oxyacetate formed melted at 252°C, and immediately decomposed to ZnO with evolution of CH_3COCH_3 and CO_2. Baraldi, however, disagreed with this reaction scheme, proposing instead that a crystalline modification of the anhydrous zinc acetate melted then decomposed directly to ZnO[39,56].

Baraldi[43] and Patil[50] disagree in their decomposition schemes for $Cu_2(CH_3COO)_4.2H_2O$. Baraldi stated that decomposition proceded via a crystalline modification of the anhydrous phase to metallic Cu. Patil et al. observed no crystalline modification and the final product was found to be CuO with gaseous products acetone and CO_2.

Dehydration and decomposition of hydrated rare earth acetates have been extensively studied, and with good agreement on the residue composition between the researchers[50,57,58]. Although

once again the nature of the intermediates formed varies between the groups of authors. Neodymium acetate, $Nd(CH_3COO)_3.H_2O$ has received most of the attention. Three possible decomposition schemes have been obtained from the various authors:

|Ref. 50| $M(CH_3COO)_3.H_2O \longrightarrow$ anhydrous compound $\longrightarrow MCO_3(CH_3CO_2)_2$

$\longrightarrow \frac{1}{2}M_2(CO_3)_3$ + acetone $\longrightarrow \frac{1}{2}M_2O_3$ (M = Nd, La)

|Ref. 57| $M(CH_3COO)_3H_2O \xrightarrow{>120^0}$ amorphous dehydrated compound $\xrightarrow{170^0}$ crystalline dehydrated compound

$\xrightarrow{220^0}$ crystalline dehydrated compound $\xrightarrow{240-400^0}$? $\longrightarrow M_2O_3CO_2$ + CO + acetone
high temperature form

(it was suggested that the unknown intermediate could be $\frac{1}{2}M_2O(CH_3COO)_2$).

|Ref. 58| $M(CH_3COO)_3.H_2O \longrightarrow M(CH_3COO)_3 \longrightarrow \frac{1}{2}M_2O(CO_3)_2 \longrightarrow \frac{1}{2}M_2O(CO_3)_2$

$\longrightarrow \frac{1}{2}M_2O_3$.

Patil et al.|50| also investigated the thermal decomposition of Gd, Dy, Lu, La, and Sm acetates, and found that for those acetates with more than one water of crystallisation, that dehydration occurred in more than one step|50,58|. One anomalous compound was $Pr(CH_3COO)_3H_2O$, which dehydrated in two steps to give the sub-hydrate $Pr(CH_3COO)_30.1H_2O$ prior to complete loss of water.

The acetates, $M(CH_3COO)_3.3H_2O$, were reported to decompose after dehydration to give $M_2O_2CO_3$, (where M = Gd, Dy, and Lu), in the temperature range 420-460°C, decomposing above 750°C to the oxide M_2O_3. In the Gd system, Shaplygin et al.|58| identified

another intermediate formed before $Gd_2O_3CO_2$, with the formula $Gd_2O(CO_3)_2$. These two groups of workers again disagree in their results on the pyrolysis of $Sm(CH_3COO)_3$, Patil et al. suggested that decomposition proceded as follows:

$$Sm(CH_3COO)_3 \longrightarrow \tfrac{1}{2}Sm_2O(CO_3)_2 \longrightarrow \tfrac{1}{2}Sm_2O_2(CO_3) \longrightarrow \tfrac{1}{2}Sm_2O_3$$

Holmium acetate, $Ho(CH_3COO)_3.3H_2O$ was said to decompose as follows:

$$Ho(CH_3COO)_3 3H_2O \longrightarrow Ho(CH_3COO)_3 0.5H_2O \longrightarrow Ho(CH_3COO)_3 \longrightarrow \tfrac{1}{2}Ho_2O_2(CO_3)$$

$$\longrightarrow \tfrac{1}{2}Ho_2O_3$$

The decomposition of cerium acetate is more complex than any of the other lanthanide acetates. Anhydrous cerium acetate was reported to decompose in five stages in inert atmospheres to give a final residue of CeO_2 [59]:

$$Ce(CH_3COO)_3 \xrightarrow{230^0} \text{Crystallographic transformation} \xrightarrow{300-50^0} Ce_8O_3(CH_3COO)_{18}$$

$$\longrightarrow CeO(CH_3COO) \longrightarrow Ce_2O_3 \longrightarrow CeO_2$$

The crystallographic transformation which was said to occur at 230^oC resulted in the formation of a high temperature polymorph of the starting material.

A number of researchers have carried out thermal decomposition studies on $U(CH_3COO)_4$ and $UO_2(CH_3COO)_2.xH_2O$ [60-62], and have reported that after dehydration, decomposition proceeds in a single step to uranium oxide. The stoichiometry of the oxide formed in the final stage was stated to be dependent on the atmosphere under which decomposition had taken place. In air and nitrogen, uranyl acetate, $UO_2(CH_3COO)_2.2H_2O$ was said to lose both

water molecules in one stage over the temperature tange 96-145°C. In air, a very small endotherm and a large exotherm were reported at 295 and 320°C, respectively. The small endotherm was believed to be due to the reaction:

$$UO_2(CH_3COO)_2 \longrightarrow UO_2 + \text{products}$$

The exotherm was suggested to be due to oxidation of organic radicals and molecules, and lower uranium oxides to give U_3O_8. In nitrogen, no exotherm was reported, only two endotherms. The final residue was consistently reported to contain 4.9% C, non-stoichiometric UO_{2+X} , and ~8% U_3O_8, and major gaseous products CO_2 and CO with minor contributions from CH_3COOH and CH_3COCH_3. Cleavage of the carbonyl C-O band and formation of a new O-U bond was used to explain formation of an acetic anhydride type structure[61]:

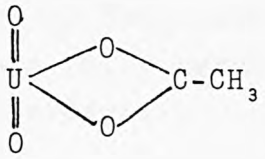

which combined in the following manner:

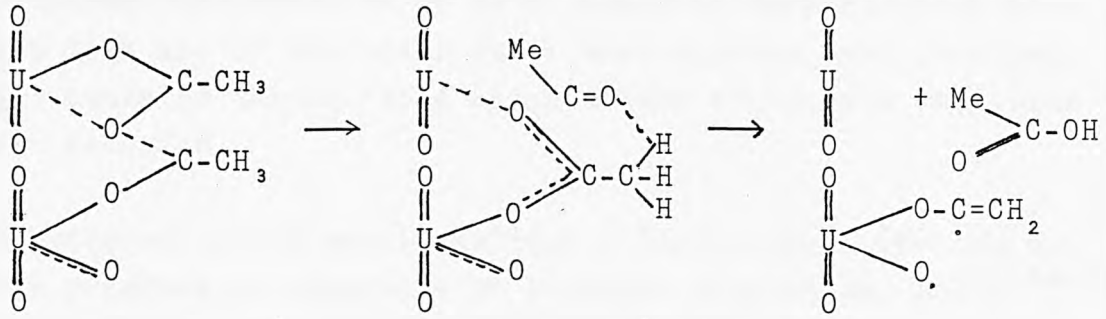

In uranyl acetate, the next decomposition stage was reported to be:

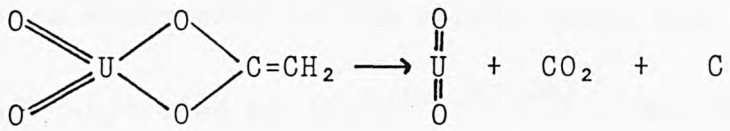

Whereas, in uranium (IV) acetate, the acetate group was said to be cleaved to give:

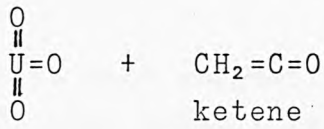

Similar decompositions to the uranium acetates were reported for the thorium and plutonium acetates, to give a final residue of the metal dioxide[62,63]. $Th(CH_3COO)_4$ was said to decompose initially to ThO_2 and $2(CH_3CO)_2O$, but with other gaseous products formed in the vapour phase by ThO_2 catalysis. The decomposition steps to ThO_2 have not been fully resolved, but were believed to pass through activation barriers.

1.2.3. Oxalates.

The thermal decompostion of metal oxalates have received more attention than any of the other metal carboxylates, and pyrolysis of simple oxalates through to a large number of oxalate complexes have been recorded.

The hydrated alkali metal oxalates , $|M_2C_2O_4.H_2O$, (M= Li, Na, K)|, were reported to dehydrate in a single step at ca. 100°C[64,65], to give anhydrous salts, which were stable up to fairly high temperatures. For example, potassium oxalate, ($K_2C_2O_4$), decomposed above 540°C in air and above 600°C in vacuum. At higher temperatures the hydrated salts were reported to decompose to give the metal carbonate and CO. Li_2CO_3 was said to melt at 710°C in air, followed

by decomposition to Li_2O_2 at ca. 1000°C, whereas the potassium and sodium oxalates decomposed to the simple oxide M_2O.

$(NH_4)_2C_2O_4H_2O$ dehydrated at 105°C[64,67,68], but the nature of the intermediate formed was not known. Fialko and Ushenko[67] obtained an intermediate with the formula $NH_4HC_2O_4$, but this compound was not identified by other workers[64,68] who suggested a single stage decomposition mechanism giving ammonia and other gaseous products, which were stated to be either CO_2, CO, and H_2O[68] or CO_2 and CO only[64].

Two decomposition pathways were suggested for hydrated calcium oxalate, $CaC_2O_4.H_2O$. Some authors reported a two stage decomposition going from the monoclinic hydrated oxalate, via the orthorhombic anhydrous compound, directly to the final residue $CaCO_3$[69-71]:

$$CaC_2O_4.H_2O \longrightarrow CaC_2O_4 \longrightarrow CaCO_3 + CO$$

Whereas, other workers[65,66,72] suggest a three stage decomposition with formation of a mixture of $CaCO_3$ and CaC_2O_4 after dehydration. In addition to this extra step, Nagase et al.[72] also reported an irreversible exothermic transformation at 290°C which was not associated with a weight loss.

Ba and Sr oxalates were said to decompose in two stages, in the same way as calcium oxalate[65,66,70,73]:

$$MC_2O_4.xH_2O \longrightarrow MC_2O_4 \longrightarrow MCO_3 + CO$$

(for Ba, $x=\frac{1}{2}$, for Sr, $x=1$)

Although Nagase et al.[72] also suggested that an exothermic energy change occurred at 259°C in strontium oxalate which was attributed to recrystallisation of poorly crystalline SrC_2O_4 formed during

dehydration. There is disagreement in the nature of the subsequent decomposition of the strontium carbonate formed in the pyrolysis of the oxalates with suggestion (a) that the carbonate decomposes above 800°C to give SrO[73] and (b) that $SrCO_3$ is stable to any further decomposition.

The presence of C and the observation of $CO:CO_2$ ratio greater than one in barium oxalate residues has also been reported[73] over the temperature range 440-650°C. The following mechanisms used to explain these results:

$$\begin{aligned} &470\text{-}550^{\circ}C && 2CO \longrightarrow C + CO_2 \\ &600\text{-}725^{\circ}C && BaCO_3 + C \longrightarrow BaO + 2CO \\ &700\text{-}1050^{\circ}C && BaCO_3 \longrightarrow BaO + CO_2 \end{aligned}$$

The nature of the decomposition of $MgC_2O_4.2H_2O$ is a confused subject in the literature with the following suggestions being made:

a) that dehydration occurs in one step[65,66,73];
b) that a subhydrate of unknown composition is formed prior to complete loss of water[74];
c) that MgC_2O_4 decomposes directly to MgO above 380°C[65];
d) that $MgCO_3$ is formed as an intermediate between MgC_2O_4 + MgO[73].

The rapid initial decomposition of lead acetate was attributed to chain reactions that induced latteral strains within the crystal lattice, which were then relieved by formation of Smekel cracks along which decomposition occurred. Decomposition of the anhydrous compound was found to be a simple, one stage reaction giving either PbO[65,66,75] or a mixture of Pb and PbO[76,77]. The amount of metallic lead present was found to be proportional to the time of contact between solid and gaseous products[77].

The decomposition of stannous oxalate, $Sn(C_2O_4)$ in air was found to give SnO_2 [65,66], although at lower pressures the final product was SnO.

The fovoured mechanism for the dehydration and decomposition of transition metal oxalates involves a single step loss of water [78] above 100°C followed by decomposition of the anhydrous compound by rupture of a C-O bond to give metal oxide residues and CO and CO_2 gases. The subsequent stages of the decomposition depend on the nature of the metal formed. In nitrogen, the Ni and Co oxides were found to undergo further decomposition due to reduction of the metal oxide to the corresponding metal by CO formed in the first step of the reaction [72,79-81]. The influence of atmosphere on the decomposition of $FeC_2O_4.2H_2O$ was quite pronounced. In inert atmospheres the final product was said to be FeO, although this was not isolated due to a rapid disproportionation reaction in which a mixture of Fe and Fe_3O_4 were formed [82]:

$$4FeO \longrightarrow Fe + Fe_3O_4$$

or in the presence of some moisture:

$$4FeO + H_2O \longrightarrow Fe_3O_4 + H_2$$

In oxidising atmospheres the anhydrous iron oxalate was reported not to decompose directly to Fe_3O_4 but was oxidised to Fe_2O_3 [84], the final product. Wang et al. [85] reported a FeC_2O_4 crystal phase change below 240°C, which was not recorded by other authors. The presence of side reactions in the decomposition of the anhydrous oxalate whilst in contact with water vapour from the dehydration step was used to explain the presence of Fe, Fe_3O_4 and C in the final residue [86]. The side reactions recorded were:

$FeO + H_2O \longrightarrow Fe_3O_4 + H_2$; $4FeO \longrightarrow Fe_3O_4 + Fe$;

$FeO + H_2 \longrightarrow Fe + H_2O$; $2CO \longrightarrow CO_2 + C$;

$Fe_3O_4 + 4H_2 \longrightarrow 3Fe + 4H_2O$; $CO_2 + H_2 \longrightarrow H_2O + CO_2$;

$FeO + CO \longrightarrow Fe + CO_2$.

Zinc oxalate was reported to decompose in the same way as the other transition metal oxalates, but giving zinc metal above 290^oC in a reversible decomposition with ZnO. In vacuo, a weight loss slightly in excess of the calculated value was recorded for the reaction:

$$ZnC_2O_4 \longrightarrow ZnO$$

This was explained by partial reduction of ZnO to give non-stoichiometric ZnO_{1-x}. From an EPR study of the last two products in this decomposition, five different paramagnetic species were reported: CO*,(an excited radical which is neutral or δ-positive, adsorbed on the ZnO surface), ZnO_{1-x}, trapped e^- or Zn^+, CO_4^-, and O_3^{3-} or $V_{11}\ O_2^-$.

A decomposition mechanism for the decomposition of nickel oxalate to metallic nickel was suggested which involved: (a) loss of electons from the $C_2O_4^{2-}$ anion at a favourable site on the surface of the bulk material[79,80], ie:

$C_2O_4^{2-} \longrightarrow C_2O_4 + 2e^-$; $Ni^{2+} + 2e^- \longrightarrow Ni$.

(b) Electrons being trapped at existing vacant anion sites. (c) The oxalate radical breaking down to give CO_2 which escapes to leave a vacant anion site which may act as a further electron trap. (d) The defective lattice surface then collapsing

with electron migration to a cation adjacent to a metallic nucleus. (e) The decomposition rate increasing with continuous exposure of oxalate anions at the free surface. The decomposition of $CoC_2O_4.4H_2O$ was recorded as being one exception to the single-stage dehydration of transition metal oxalates. The decomposition suggested was:

$$CoC_2O_4.4H_2O \xrightarrow[\text{room temperature}]{} CoC_2O_4.2H_2O \xrightarrow{170-180^0} CoC_2O_4 \xrightarrow{290^0} Co_3O_4$$

Low pressure studies on the transition metal oxalates[66] indicated a tendency towards formation of lower oxides or metals in some cases. Particular examples are Cd, Cu, Pb, and Mn oxalates which were said to decompose to give CdO, CuO, PbO, and Mn_2O_3 in air at atmospheric pressures, but low pressures gave Cd + CdO, Cu + CuO, Pb + PbO, and MnO. Wang et al.[85] also studied the thermal decomposition of hydrated Fe(III) oxalate, $Fe_2(C_2O_4)_3.5H_2O$, which was said to undergo the following decompostition reaction:

$$Fe_2(C_2O_4)_3.5H_2O \xrightarrow{240^0} \alpha\text{-}FeC_2O_4 \xrightarrow{>380^0} \alpha\text{-}Fe + Fe_3C$$

The rare earth oxalates have been found to lose water of crystallisation at temperatures between 40 and 60°C[89]. However, in many cases initial, rapid water loss was reported to leave a lower hydrate which could re-absorb water at low temperatures[90]. Another example of the problems encountered in the elucidation of decomposition pathways for lanthanide metal carboxylates is lanthanum oxalate, $|La_2(C_2O_4)_3|$, where four possible schemes are recorded:

[Ref. 91] $La_2(C_2O_4)_3 \longrightarrow La_2(C_2O_4)_x(CO_3)_y \longrightarrow La_2(CO_3)_3 \longrightarrow$

$La_2O_2CO_3 \longrightarrow La_2O_3$

|Ref. 89,92| $La_2(C_2O_4)_3 \longrightarrow La_2O_3CO_2 \longrightarrow La_2O_3 + CO_2$.

|Ref. 94| $La_2(C_2O_4)_3 \longrightarrow La_2(C_2O_4)_{1.5}(CO_3)_{1.5} \longrightarrow La_2(CO_3)_3$

$\longrightarrow La_2O(CO_3)_2$

For Y and Sc oxalates, no other workers have recorded the above general reaction[10,89,93] presented in equation referance 91. Two decomposition schemes have been suggested for anhydrous yttrium oxalate[89,93]:

|Ref. 89| $Y_2(C_2O_4)_3 \longrightarrow Y_2O_3$

|Ref. 93| $Y_2(C_2O_4)_3 \longrightarrow Y_2O_3CO_2 \longrightarrow Y_2O_3$

For scandium oxalate, Head and Holley[10] obtained no evidence to support the formation of either basic or normal oxalates during decomposition, instead, Sc_2O_3 was said to be formed directly from the anhydride. For a number of the lanthanide oxalates, stable compounds have been obtained with various water contents. Scandium oxalate has been prepared with 11.8 and 6 water molecules in the coordination sphere[10,89]. The 11.8 hydrate was reported to decompose to the hexahydrate at 70°C, which then reversibly dehydrated to the dihydrate at 160°C. The dihydrate which was stable to 260°C, was said to lose the remaining water to form the anhydrous compound. Both Eu(II) and Eu(III) oxalate hydrates have been prepared[95,96]. $Eu_2(C_2O_4)_3$ has been obtained with 5.8 and 10 waters of crystallisation[95]. The 5.8 hydrate dehydrated in two stages, the first below 235°C, the second at 300°C, which was accompanied by decomposition to give EuC_2O_4. The decahydrate also dehydrated in two stages to give EuC_2O_4. After dehydration and reduction to Eu(II), a partial reoxidation process was proposed with formation of $(EuCO_3)_2O$ to give the sesquioxide at

650°C. $EuC_2O_4.1.7H_2O$ dehydrated in a single step and was then found to decompose in the same way as the Eu(III) oxalates.

Loss of water has been reported to occur in single steps and in two or three stages for various hydrated oxalates. Subsequent decomposition of the anhydrous materials gave the appropriate stable lanthanide oxide[89,92,93,97-101].

For uranium and uranyl oxalates, $U(C_2O_4)_2$ and $UO_2C_2O_4$, respectively, the following mechanisms have been proposed for their decomposition in oxidising atmospheres:

[Ref. 99] $U(C_2O_4)_2.6H_2O \longrightarrow U(C_2O_4)_2.2H_2O \longrightarrow U(C_2O_4)_2$

$\longrightarrow UO_3$ + traces of U_3O_8

[Ref. 92] $UO_2.C_2O_4.3H_2O \longrightarrow UO_2C_2O_4.H_2O \longrightarrow UO_2C_2O_4 \longrightarrow$ uranium oxides

[Ref. 103] $UO_2.C_2O_4.3H_2O \longrightarrow UO_2C_2O_4.H_2O \longrightarrow UO_2C_2O_4 \longrightarrow UO_3 \longrightarrow U_3O_8$

The equivalent thorium compound, $Th(C_2O_4)_2$, decomposes in oxidising atmospheres either via the intermediate, $Th(CO_3)_2$[102], or directly to ThO_2[92,99]. In inert atmospheres, all the actinide oxalates decompose directly to the dioxide[61,92,99,102,103].

The pyrolysis reactions of a number of main group element oxalato complexes have been studied and the following reaction pathways suggested:

1) $\underline{K_3[Co(C_2O_4)_3].3H_2O}$

[Ref. 105] $\longrightarrow K_3[Co(C_2O_4)_3] \longrightarrow ? \longrightarrow K_2CO_3 + Co_3O_4 + C$

|Ref. 106,107| $\longrightarrow K_3|Co(C_2O_4)_3.5H_2O \rightarrow K_2|Co(C_2O_4)_2|$*

$\longrightarrow K_2CO_3 + Co_3O_4 + C$

(* Co(III) reduced to Co(II) accompanied by a colour change from green to violet).

2) $\underline{K_3|Mn(C_2O_4)_3|.3H_2O}$ |107,110|

The manganese complex decomposes in the same way as the cobalt complex above, except that dehydration takes place in one step. A colour change from red-violet to white associated with reduction of Mn(III) to Mn(II) is also observed.

3) $\underline{K_3|Cr(C_2O_4)_3|3H_2O}$

|Ref. 107-109,111,112| $\longrightarrow K_3|Cr(C_2O_4)_3|.2H_2O \longrightarrow K_3|Cr(C_2O_4)_3|$

$\longrightarrow K_3|Cr(C_2O_4)_{3/2}(CO_3)_{3/2} + 1\tfrac{1}{2}CO \longrightarrow K_3|Cr(C_2O_4)_{\frac{1}{2}}(CO_3)_{5/2} + CO$

$\longrightarrow K_3|Cr(CO_3)O_2| \longrightarrow K_3CrO_3$

4) $\underline{K_3|Fe(C_2O_4)_3|.3H_2O}$

After dehydration, the following decomposition schemes were proposed in air:

|Ref. 113| $2K_3Fe(C_2O_4)_3 \xrightarrow{\frac{1}{2}O_2} 3K_2C_2O_4 + Fe_2O_3 \longrightarrow K_2CO_3 + CO + Fe_2O_3 + 4CO_2 + 2CO$

$\longrightarrow K_2Fe_2O_4 + CO_2$

|Ref. 108| $K_3Fe(C_2O_4)_3 \longrightarrow K_3|Fe(C_2O_4)(CO_3)(O)| \longrightarrow K_3|Fe(C_2O_4)(O)_2|$
$+ 2CO + CO_2$

$\longrightarrow K_3|Fe(CO_3)(O)_2| + CO$

In vacuum the following decomposition pathway was recorded:

|Ref. 113| $2K_3Fe(C_2O_4)_3 \longrightarrow 2K_3Fe(C_2O_4)_3 + K_2C_2O_4 \longrightarrow K_2C_2O_4 + FeO$

$K_2CO_3 + CO$ $\qquad$ $Fe + \frac{1}{2}O_2$

5) $\underline{A_2|MoO_3(C_2O_4)|xH\ O}$ and $\underline{A_2|Mo_2O_6(C_2O_4)|}$, (where A= Na, K, NH_4^+; for Na, x=4, for K and NH_4^+, x=1)

On decomposing in static air, the sodium complex was found to dehydrate in two stages, whereas the potassium and ammonium complexes lost water in a single step. For potassium and sodium the final products were the metal oxides, A_2O and MoO_3, for the ammonium complex the final product was MoO_3 |114-116|

6) $\underline{CuC_2O_4.(NH_3)_2}$

The three isomeric forms of this complex decomposed in three stages to give CuO as the final residue |117|.

7) $\underline{|Co_2(NH_3)_6|_2(C_2O_4)_3.4H_2O}$

After dehydration the proposed decomposition pathway was:

|Ref. 118| $|Co_2(NH_3)_6|_2(C_2O_4)_3 \longrightarrow |Co_2(NH_3)_2(NH_2)_4|C_2O_4$

$\longrightarrow 2CoO + 2CO + 2NH_3 + 2N_2H_4$

8) $\underline{(NH_4)_3|VO_2(C_2O_4)_2|}$

$$|\text{Ref. 121}| \longrightarrow (NH_4)_2|(VO)_2(C_2O_4)_3| \overset{*}{\longrightarrow} VO_2$$

(*Reduction of V(V) is reported to take place in the first decomposition to give V(IV).)

9) $\underline{A_3|Fe(C_2O_4)_3|_2.xH_2O}$

Where A= Ba or Sr, (for A= Ba, x=8, for Sr, x=2).

$$|\text{Ref. 122,123}| \longrightarrow A_3|Fe(C_2O_4)_3|_2 \xrightarrow{<300^0} A_3Fe(C_2O_4)_5 \xrightarrow{300-400^0} 3ACO_3.Fe_2O_3$$

10) $\underline{M|Co(C_2O_4)_3|xH_2O}$

Where M= La, Pr, or Nd, (for M= La, x=9, for Pr, Nd, x=8)

After loss of water, pyrolysis proceded as follows:

$$|\text{Ref. 124}| \longrightarrow M|Co(C_2O_4)_2(CO_2)| \longrightarrow MCoO_{3-x}(CO_3)_x \xrightarrow{\text{air}} MCoO_3 \xrightarrow[\text{vacuum}]{} MCoO_3 + M_2O_3 + CoO$$

The first decomposition stage after dehydration involved reduction of Co(III) to Co(II) accompanied by a colour change from green to pink.

11) $\underline{K_3Al(C_2O_4)_3mH_2O}$ $(2<m<3)$

After loss of water, the following pyrolysis mechanism was observed:

|Ref. 119| $K_3Al(C_2O_4) \xrightarrow{320-435^0} K_2C_2O_4 + 0.5Al_2O_3 + 2CO + Q.5K_2CO_3$

$K_2C_2O_4 \xrightarrow{435-475^0} K_2CO_3$

$K_2CO_3 \xrightarrow{1} KAlO_2 + CO_2$

$K_2CO_3 \xrightarrow{2} K_2O + CO_2$

Reaction (1) involved a solid phase reaction between $0.5Al_2O_3$ and K_2CO_3, (2) is a reaction between CO and K_2CO_3.

12) $\underline{(NH_4)|Tl(C_2O_4)_2|.3H_2O}$

|Ref. 120| $\xrightarrow{150^0} (NH_4)_2C_2O_4 + TlC_2O_4 \xrightarrow{400^0} TlO_2$

1.2.4. Malonates.

Very few pyrolysis experiments have been carried out on malonate compounds, of those reported in the literature, the majority are by a single author and have not been verified by other workers. The only research published, so far, is on the transition metal, alkali metal, and calcium malonate compounds, and a single article on a mixed uranium-alkali metal complex.

The products identified in pyrolysis reactions of the malonates are recorded in table 1.1.

For Na, K and Ba malonates mechanism suggested:

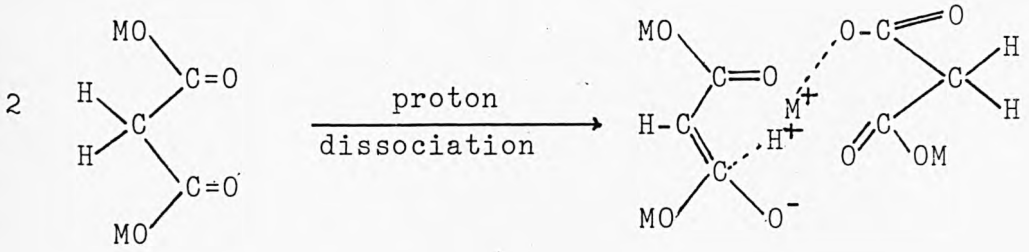

Malonate	Solid Products	Gaseous Products	Atmospheric Conditions of Pyrolysis	References
Zn	ZnO + C	CO_2 + CO	N_2	125,126
Mn	MnO	"	"	"
Ni	Ni + δC	"	"	"
Cu	Cu + 0.5C	"	"	"
Co,Fe	M + δC	CO + δCO_2	"	"
Zn,Ni, Cu, Co,Fe	MO	-	O_2	"
Mn	Mn_2O_3	-	"	"
Na,K	M_2CO_3 + δC	CO_2 + CH_3COCH_3	N_2	127
Ba	MCO_3 + δC	CO_2 + CH_3COCH_3	N_2	"
Ca	$CaCO_3$	CH_3COOH	O_2	50

Table 1.1.

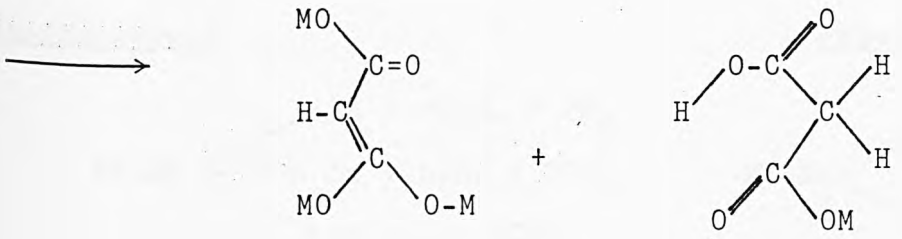

decarboxylation decomposition

$CH_3COOM + CO_2$ $(MO---H) + 2C + M_2CO_3$

Uranium-alkali metal complexes of the type, $|UO_2(CH_2C_2O_4)_2|M_2.xH_2O$ where M= Li, Na, and K, (for Li, x=3, for Na, x=2, and for K, x=1), have been prepared and their thermal behaviour studied[128]. In each case uranium (VI) is reduced to uranium (IV) after loss of water in the temperature range 260 to 340°C with the formation of $U_2O_7M_2$ and M_2CO_3. A final residue of UO_4M_2 and gaseous product CO_2 were reported.

1.3. Organotin Compounds

Very little information on the thermal decomposition of organotin compounds has been recorded. In this section, a brief summary of the pyrolysis of stannanes and organotin halides, together with a more detailed account of the thermal decomposition of other organotin and tin-sulphur compounds is presented.

The simplest organotin compounds are the stannanes, (R_4Sn) and the distannanes, $|(R_3Sn)_2|$, but even with Me_4Sn, three decomposition mechanisms have been proposed[129-132]. The earliest workers[129], suggested a combination of rearrangement and free-radical reactions as the primary pyrolysis process:

Rearrangement

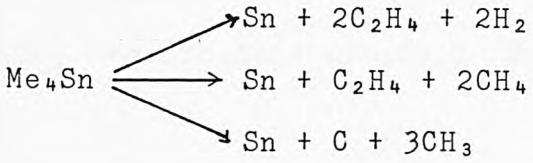

Free-radical

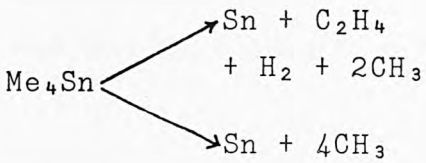

with the major product methane, and smaller amounts of H_2 and ethylene, to leave a residue of Sn and C. Other workers have suggested that at temperatures below 340°C, CH_4 is formed solely from $CH_3^{\bullet}$ radicals[130] via a multi-collision mechanism:

$$CH_3^{\bullet} + CH_3^{\bullet} \longrightarrow C_2H_6 \xrightarrow{{}^{\bullet}CH_3} CH_4 + C_2H_5 \xrightarrow{{}^{\bullet}CH_3} C_3H_8$$

$$\xrightarrow{{}^{\bullet}CH_3} CH_4 + C_3H_7 \longrightarrow CH_3 + C_2H_4$$

(C_2H_4 polymerises)

At higher temperatures, (340-600°C), a radical chain mechanism was said to predominate to be superceded by a more complicated mechanism at temperatures above 600°C. Another mechanism, including consecutive release of $CH_3^{\bullet}$ radicals[131], and rate-determining splitting off of $CH^{\bullet}{}_3$ radicals followed by radical-radical and radical-molecule reactions has also been proposed[132]

$$CH_3^{\bullet} + (CH_3)_3SnCH_3 \longrightarrow CH_4 + (CH_3)_3SnCH_2^{\bullet}$$

In higher alkane stannanes, some authors recorded polymer formation during decomposition[133,134], for example, in Bu_4Sn, a colour change from white to cherry red was explained by formation of the polymer nBu_6Sn_2[133], which was believed to be a complex molecule with branched Sn-Sn bonds. The following mechanism was proposed:

$$nBu_4Sn \longrightarrow nBu_3Sn + nBu^{\cdot} \quad ; \quad 2nBu_3Sn^{\cdot} \longrightarrow nBu_6Sn_2 \ ;$$

$$nBu_6Sn_2 \longrightarrow nBu_4Sn + nBu_2Sn \ ; \quad 2nBu_2Sn \longrightarrow nBu_4Sn + nSn.$$

Final decomposition products for Bu_4Sn and Et_4Sn of Sn metal and a range of hydrocarbons up to C_8H_{18} for Bu_4Sn and C_4H_{10} for Et_4Sn were recorded. A mechanism involving consecutive release of $Et^{\cdot}$ radicals was suggested. Stannanes were also reported to have been formed in the decomposition of distannanes and in aryl compounds of the type Ph_3SnH[137,138,140]. The compound Et_6Sn_2 was found to decompose at 260°C to give final products of Sn, Et_4Sn and $2C_2H_5$, which were explained by combination of two mechanisms:

$$(Et_3Sn)_2 \longrightarrow Et_4Sn + Et_2Sn \downarrow Sn + 2C_2H_5$$

Similarly for Ph_3SnH:

$$Ph_3SnH \longrightarrow Ph_3Sn^{\cdot} + H^{\cdot} \ ; \qquad Ph_3Sn^{\cdot} \longrightarrow Ph_2Sn + Ph_4Sn$$

$$2Ph_2Sn \longrightarrow Ph_4Sn + Sn$$

Organotin halides of the system R_nSnX_{4-n} (where n= 0-4), can be divided into two groups- (i) those which volatilise on heating (eg. R_2SnCl_2), and (ii) those which decompose to give tin(II) dihalide residues[139].

The earliest work recorded on the decomposition of alkyltin compounds was on trimethyltin hydroxide[140]. The reaction :

$$2Me_3SnOH \longrightarrow |Me_3Sn|_2O + H_2O$$

was recorded above 80°C. The distannoxide believed to be formed above 80°C was itself decomposed at 200°C to give predominantly Me_2SnO with some Me_4Sn [141]. The following series of reactions were recorded:

$$|Me_3Sn|_2O \longrightarrow Me_2SnO + Me_4Sn$$

$$2Me_2SnO \begin{cases} \nearrow Me_4Sn + SnO_2 \\ \searrow 2C_2H_6 + 2SnO \end{cases}$$

The presence of small quantities of unsaturated hydrocarbons and CH_4 in the gaseous products were also observed. In the decomposition of the analagous phenyl compound, Ph_3SnOH, a similar series of reactions were observed [142,143]. The first of these two authors suggested a direct decomposition of the hydroxide to the oxide:

$$2Ph_3SnOH.1.5H_2O \longrightarrow Ph_4Sn + Ph_2SnO + 4H_2O$$

while in the second more detailed investigation the same type of stannoxide intermediate as had been found with Me_3SnOH was suggested:

$$2Ph_3SnOH \xrightarrow{123^0} (Ph_3Sn)_2O + H_2O \xrightarrow{135-140^0} Ph_2SnO + Ph_4Sn$$

The diphenyl tin oxide formed at 140°C was believed to be polymeric and to have the structure [144]:

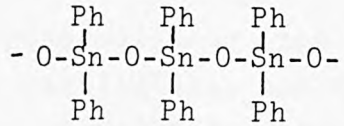

which was said to decompose further at 400°C to give Ph_4Sn + SnO_2:

$$|Ph_2SnO|_n \longrightarrow .5nPh_4Sn + .5nSnO_2$$

A mechanism was proposed in which Ph groups on adjacent sites migrated to form Ph_4Sn, leaving some Ph groups behind which had no nearest neighbours and could not undergo rearrangement.

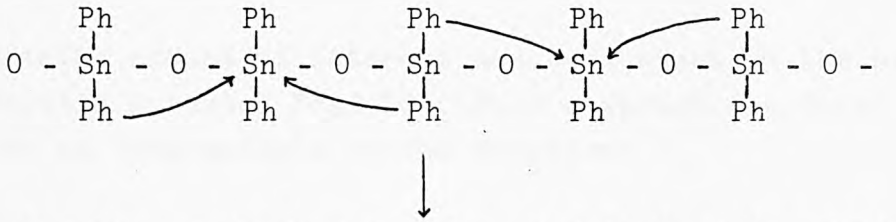

$$-O + PhSn + Ph_4Sn + O - Sn - O + Ph_4Sn + O - SnPh$$

This type of mechanism has not been suggested for the aliphatic alkyltin oxide polymers[144], where the major products were alkenes with only a small percentage of tetraalkyltin compounds. For example, the di-n-octyltin oxide polymer was reported to give a 75% yield of alkenes, 82% of which was oct-1-ene, 10.5% hex-1-ene, with smaller contributions from hept-1-ene, and possibly pent-1-ene.

Dialkyltin oxide polymers were also proposed as intermediates in the decomposition of compounds of the type R_3SnOOH, (trialkyltin hydroperoxides)[145], according to the following two simultaneous but independant routes, eg. the methyl analogue:

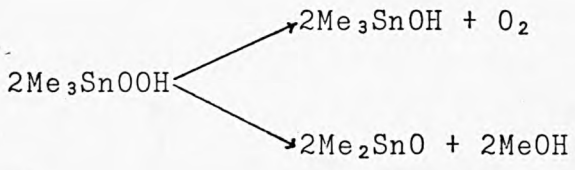

Some work has been carried out into the thermal decomposition of alkyltin carboxylates, particularly the di- and tri-phenyltin compounds[146,147]. For $Ph_2Sn(OMe)_2$ a two stage decomposition was

suggested, giving final products of PhOH, O_2, PhSn(O)OH, and $C_9H_{19}COOH$. The first stage in the decomposition was explained by an intramolecular rearrangement of the Ph groups from Sn to oxygen atoms[146]. The series of compounds $Ph_3SnOCOR$ were reported to give Sn as the final decomposition product in air and nitrogen [147], although large numbers of decomposition steps reported were found to make determination of all the intermediates very difficult. The first stage was interpreted as cleavage of Ph· probably resulting in the formation of a diphenyl complex with Sn-O bridging.

Considerable amount of interest has been shown in the preparation of triphenyltin nitrate, Ph_3SnNO_3. This compound was first reported as an intermediate in the reaction:

$$Ph_3SnH + HNO_3 \longrightarrow PhNO_2 + Ph_2SnO \text{ [148]}$$

The compound formed was said to give nitrobenzene and Ph_2SnO on decomposition[148,150,151]. Two mechanisms were proposed for the pyrolysis, one was simple rearrangement of Ph_3SnNO_3, the second reaction, favoured at higher temperatures involved H-abstraction and possible formation of more highly oxidised compounds. On carrying out the decomposition in o-dichlorobenzene, other workers[149] reported first intermediates of diphenyltin dinitrate and tetraphenyltin, followed by an intermolecular condensation reaction:

$$2Ph_3SnNO_3 \longrightarrow Ph_2Sn(NO_3)_2 + Ph_4Sn$$

$$O_3N\text{-}\overset{\overset{Ph}{|}}{\underset{\underset{Ph}{|}}{Sn}}\text{-}ONO_2 + O_3N\text{-}\overset{\overset{Ph}{|}}{\underset{\underset{Ph}{|}}{Sn}}\text{-}O\text{-}NO_2 \longrightarrow O_3N\text{-}\overset{\overset{Ph}{|}}{\underset{\underset{Ph}{|}}{Sn}}\text{-}O\text{-}\overset{\overset{Ph}{|}}{\underset{\underset{Ph}{|}}{Sn}}\text{-}NO_3 + |N_2O_5|$$

However, in conducting the reaction in the absence of solvent, this intermediate was not recorded, and none of the products which are associated with a homolytic dissociation mechanism, eg. hexaphenylditin, biphenyl, or triphenyltin phenoxide, were reported. Decomposition in the absence of solvent was therefore believed to proceed via heterolytic dissociation of the β-oxygen-nitrogen bond, and that the following reactions took place:

$$Ph_3SnO\text{-}NO_2 \longrightarrow Ph_3SnO^- + NO_2^+$$

$$Ph_3SnO^- + Ph_3CH \longrightarrow Ph_3SnOH + \text{other products}$$

$$nPh_3SnO^- \longrightarrow (Ph_2SnO)_n + nPh^-$$

$$Ph^- + NO_2^+ \longrightarrow PhNO_2$$

$$Ph^- + Ph_2NH \longrightarrow PhH + \text{other products}$$

Tris trialkyltin amines, $(R_3Sn)_3N$, have also been prepared but were found to be highly unstable and to decompose on exposure to air to give ammonia and either trialkyltin hydroxide, (methyl), or trialkyltin carbonate, (ethyl, n-propyl, or n-butyl).[152]

Virtually all the thermal decomposition studies carried out on S-containing compounds have been on dithiocarbamates. For the complexes, $Sn(Me_2NCS_2)_2$ and $Sn(Et_2NCS_2)_2$, thermal gravimetry traces have been presented which show two decomposition steps, each being loss of a dithiocarbamate group[153]:

$$Sn(S_2CNR_2)_2 \longrightarrow Sn(S_2CNR_2) + S_2CNR_2 \longrightarrow Sn + S_2CNR_2$$

From a mass spectroscopic study, this mechanism was further substantiated by the presence of tin thiocarbamate and thiocarbamate fragments. A combined pyrolysis-gas chromatography/mass spectroscopy study indicated, however, that the decomposition

mechanism was not as simple as was first thought[154-158]. In these papers, Bratspies et al. investigated the thermal decomposition of a number of Sn(II) and Sn(IV) dihalo and dialkyltin dithiocarbamate complexes.

Dihalobis(diethyldithio carbamate)tin(IV)[155] complexes were said to decompose in three steps immediately after melting. The first two steps being loss of most of the Et_2DTC ligands followed by loss of halogen ligands, In air, residual SnS was said to slowly oxidise to SnO_2, possibly via a number of mixed sulphur-oxygen intermediates. However, in nitrogen, Sn and S were found at temperatures above 750°C. As well as these primary decomposition reactions side reactions were also proposed, which were characterised by formation of Et_3N, which was not formed in the primary reaction.

Primary route

First stage:

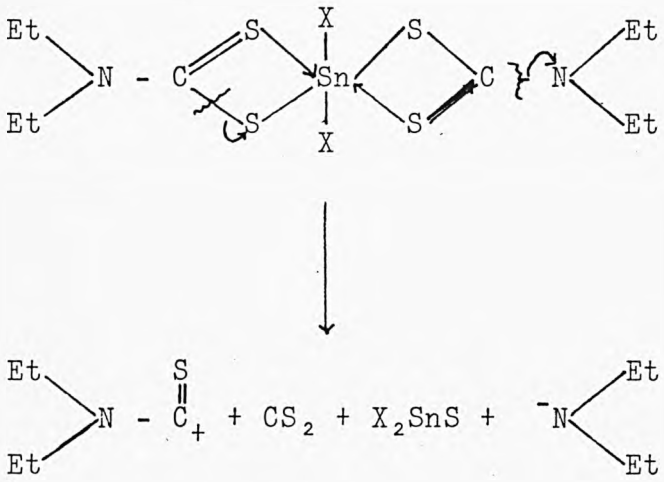

$$Et_2NCS^+ + {}^-NEt_2 \longrightarrow Et_2NC(=S)NEt_2$$

Second stage:

$$X_2SnS \longrightarrow SnS + X_2$$

Secondary reactions

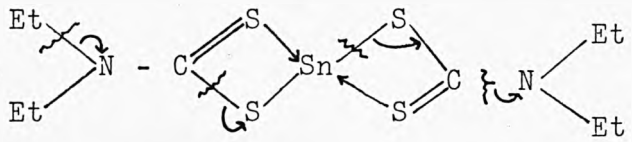

$$EtNCS + CS_2 + Et^+ + {}^-NEt_2 + X_2SnS$$

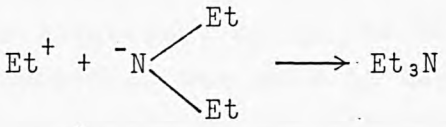

In these reactions the halide ligand was stated to have no effect on the decomposition mechanism, but in the dialkyltin dithiocarbamates, $|R_2Sn(DTC)_2|$, the mechanism was said to be dramatically influenced by the organic functional group R , with decomposition also taking place at higher temperatures in three overlapping stages over the ranges, 210-330°C in air, and 215-380°C in N_2, (cf. dihalo complexes for which decomposition accurs immediately after melting at ca. 150°C.). A wide variety of secondary reactions were also reported which abscure the primary reaction mechamism. However, the primary mechanism was believed to involve high molecular mass intermediates, and to be a combination of ionic and radical reactions. The proposed initial step in the primary mechanism was homolytic dissociation of a Sn-Ph bond and subsequent reaction of the radicals formed, which was followed by heterolytic dissociation of the remaining Sn-Ph bond:

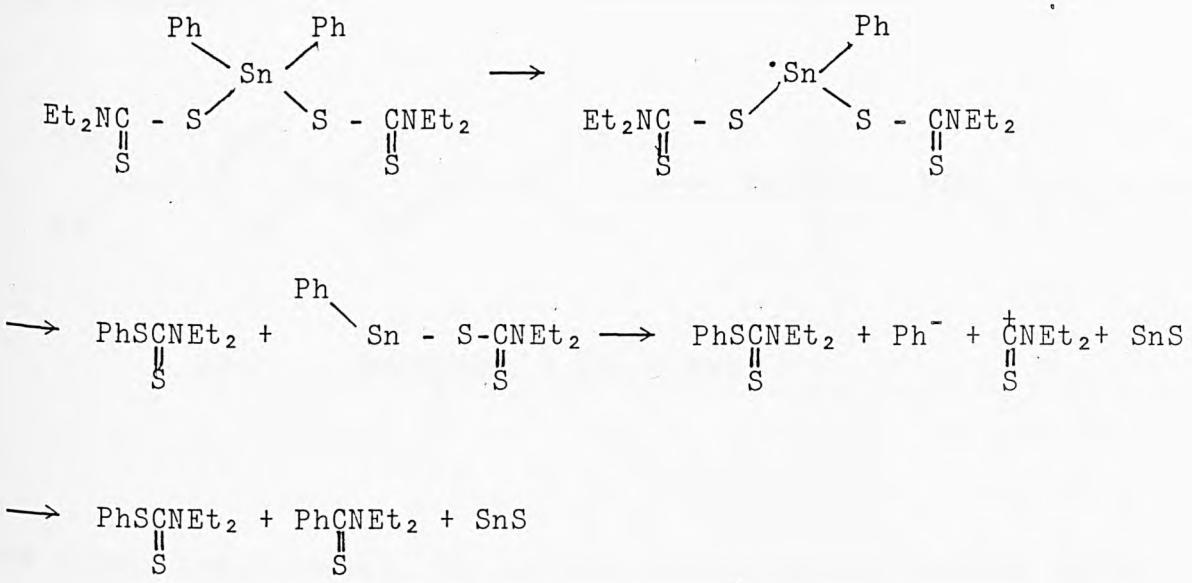

For tetrakis(diethyldithiocarbamato)tin(IV)[156] decomposition at lower temperatures was suggested, as in the dihalo complexes. Although in air, decomposition was said to take place in two steps, each of the steps involving two simultaneous processes. In the first stage, the low temperature of decomposition was implied for making the volatility of the products the rate determining step, instead of the rate of formation of the products, suggesting that highly volatile products such as CS_2 were lost immediately, whereas, less volatile products such as tetraethylthiourea were lost later. Exothermic oxidation of the Sn residue, and endothermic vaporisation of the products were proposed for the second decomposition stage, In N_2, a single stage decomposition was reported, which comprised of three consecutive endothermic processes, involving loss of dithiocarbamate ligands to leave SnS.

For the Sn(II) analogue, bis(diethyldithiocarbamato)tin(II)[158] a gain in weight at 91°C in air was explained by incomplete oxidation of the complex to give $OSn(Et_2DTC)_2$, with further oxidation occurring at 160°C. It was suggested that decomposition followed one of two mechanisms, depending on the temperature. At temperatures between 200 and 300°C the following primary mechanism

was proposed:

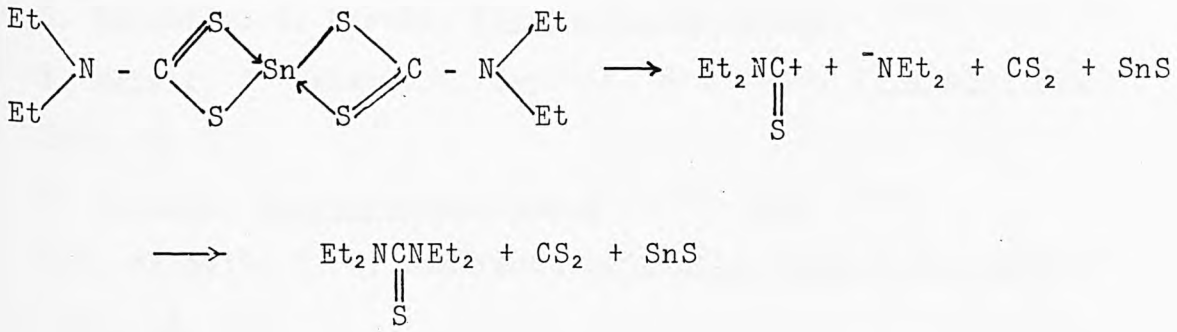

At higher temperatures, the primary mechanism was claimed to be:

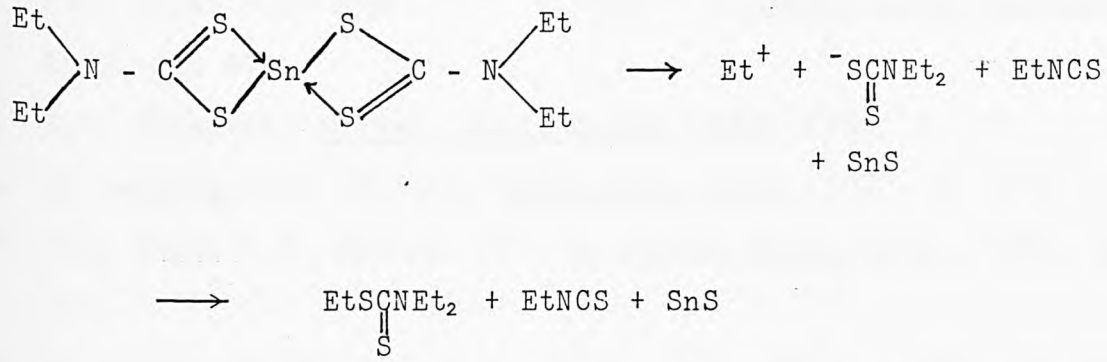

Other decomposition products, not explained by either of the above mechanisms were also recorded, some of these from reactive intermediates said to be produced in the primary reaction, and others due to cyclisation and dehydrogenation reactions, eg. pyridine and 1-ethyl pyrol.

1.4. References

1. S. Shishido, Y. Masuda, Nippon Kagaku Kaishi, 1973, (1), 185.
2. T. Meisel, Z. Halmos, K. Seybold, E. Pungor, J. Therm. Anal., 1975, 7, 73.
3. P. Baraldi, Spectrochim. Acta A, 1979, 35A, 1003.
4. S.K. Patnaik, P, K. Maharana, Radiochim. Radioanal. Lett., 1981, 46, 271.
5. B.M. Nirsha, Yu.A. Velikodnyi, B.V. Zhadanov, V.A. Olikova, N.I. Pirtskhalava, Zh. Obshch. Khim., 1981. 51, 1441.
6. K.O. Hartman, I.C. Hisatsune, J. Phys. Chem., 1965, 69, 583.
7. M.D. Judd, M.I. Pope, C.G. Wintrell, J. Appl. Chem.Biotechnol., 1972, 22, 679.
8. Y.S. Osinavik, Vestsi. Akad. Navuk. BSSR, 1965, 3, 47.
9. R. Canning, M.A. Hughes, Thermochim. Acta, 1973, 6, 399.
10. E.L. Head, C.E. Holley, Jr., J. Inorg. Nucl. Chem., 1964, 26, 525.
11. Y. Masuda, S. Shishido, J. Inorg. Nucl. Chem., 1980, 42, 299.
12. Y. Masuda. Thermochim.Acta, 1982, 53, 215.
13. J. Fenerty, P.G. Humphries, J. Pearce, Thermochim. Acta, 1983, 61, 319.
14. J. Charles, P.W. Kopf, S. Toby, J. Phys. Chem., 1966, 70, 1478.
15. P. Baraldi, Spectrochim. Acta A, 1981, 37A, 99.
16. B.M. Nirsha, V.I. Bogomolov, R.V. Kuznetsova, S.I. Samolyuk, Zh. Obshch. Khim., 1979, 49, 13.
17. K.A. Nadzharyan, S.M. Portnova, V.F. Ryurikov, Zh. Neorg. Khim., 1982, 27, 316.
18. P. Ravindranathan, K.C. Patil, Thermochim. Acta. 1983, 71, 53.
19. K. Muraishi, T. Takano, N. Kenzo, N. Tanaka, J. Inorg. Nucl. Chem., 1981, 43, 2293.

20. R. Shuffenecker, Y. Trambouze, M. Prettre, Ann. Chim., 1962, 7, 127.

21. R. Shuffenecker, Y. Trambouze, M. Prettre, Ann. Chim, 1962, 7, 136.

22. G.R. Rao, K.C. Patil, C.N.R. Rao, Inorg. Chim. Acta, 1970, 4, 215.

23. A.K. Galwey, D.M. Jamieson, M.E. Brown, J. Phys. Chem., 1974, 78, 2664.

24. D. Dollimore, K.H. Tonge, J. Inorg. Nucl. Chem., 1967, 29, 621.

25. G. Djega-Mariadassou, A. Marques, G. Panretier, Bull. Soc. Chim. Fr., 1971, 3166.

26. G.Ya. Berezin, V.M. Fomin, V.V. Zueva, Deposit. Doc., 1977, VINITI, 1350.

27. M. Dabkowska. Ann. Univ. Mariae Curie-Sklodowska, Sect. AA: Phys. Chem., 1976-77,(pub. 1980), 31.

28. S.R. Dharwadkar, M.S. Kumbhar, M.S. Chandrasekharaiah, M.D. Karkhanavala, J. Inorg. Nucl. Chem., 1980, 42, 1621.

29. Y. Masuda, Thermochim. Acta, 1983, 67, 271.

30. Y. Masuda, Thermochim. Acta, 1983, 60, 203.

31. B. Mentzen, Ann. Chim., 1968, 3, 367.

32. G.D. Buttress, M.A. Hughes, J. Chem. Soc., A, 1968, 64, 1272.

33. E.R. Russell, M.L. Hyder, Inorg. Nucl. Chem. Lett., 1976, 12, 247.

34. A.V. Dubrovin, A.I. Zhirov, K.M. Dunaeva, V.V. Aleksandrov, V.G. Morozov, V.N. Agafanov, V.V. Boldyrev, V.I. Spitsyn, Zh. Neorg. Khim., 1978, 23, 3072.

35. M. Bideau, B. Claudel, Thermochim. Acta, 1978, 27, 285.

36. V.V. Kolesnik, A.I. Zhirov, K.M. Dunaeva, V.I. Spetsyn, Zh. Neorg. Khim., 1980, 25, 1329.

37. V.I. Spitsyn, V.V. Kolesnik, K.M. Dunaeva, A.I. Zhirov, Dokl. Akad. Nauk SSSR, 1981, 257, 122.

38. I.C. Hisatsune, E.C. Beahm, R.J. Kempf, J. Phys. Chem., 1970, 74, 3444.

39. E.G. Nadirov, Deposit. Doc., 1977, VINITI 4370.

40. ibid , Deposit. Doc., 1977, VINITI 4369.

41. ibid , Deposit. Doc., 1977, VINITI,4372.

42. T.S. Oakwood, M.R. Miller, J. Am. Chem. Soc., 1950, 72, 1849.

43. P. Baraldi, Spectrochim. Acta A, 1982, 38A, 51.

44. B.M. Nirsha, A.D. Chubinidze, Yu.A. Velikodnyi, B.V. Zhadanov, V.A. Olikova, Zh. Obshch. Khim., 1983, 53, 1466.

45. M.A. Bernard, F.Busnot, Bull. Soc. Chim., Fr., 1968,2000.

46. N.R. Chaudhuri, S. Mitra, G.K. Pathak, J. Therm. Anal., 1979, 16, 13.

47. A.I. Grigor'ev, N.V. Donchenko, Yu.S. Nekrasov, Zh. Neorg. Khim., 1983, 28, 1355.

48. K. Manabe, T. Kubo, Kogyo Kagaku Zasshi, 1966, 69, 1733.

49. R. Leibold, F. Huber, J. Therm. Anal., 1980, 18, 493.

50. K.C. Patil, G.V. Chandrashekhar, M.V. George, C.N.R. Rao, Can. J. Chem., 1968,46, 257.

51. J. Leicester, M.J. Redman, J. Appl. Chem., 1962, 12, 357.

52. X. Wang, X. Xin, A. Dai, Nanjing Daxue Xuebao Ziran Kexue, 1983, (2), 261.

53. K. Manabe, T. Kubo, Kogyo Kagaku Zasshi, 1966, 69, 1727,

54. J.-L. Dorémieux, Bull. Soc, Chim., Fr., 1967, 4586.

55. H.G. M^{c}Adie, J. Inorg. Nucl. Chem., 1966, 28, 2801.

56. V.V. Panevchik, V.M. Goryaev, Izv. Vyssh. Uchebn. Zaved, Khim. Khim. Technol., 1979, 22, 1303.

57. K. Manabe, M. Ogawa, Nippon Kagaku Kaishi, 1979, (8), 1013.

58. I.S. Shaplygin, V.P. Komarov, V.B. Lazarev, J. Therm. Anal., 1979, 15, 215.

59. K. Manabe, M. Ogawa, Nippon Kagaku Kaishi, 1983, (7), 1092.

60. P.S. Clough, D. Dollimore, P. Grundy, J. Inorg. Nucl. Chem., 1969, 31, 361.

61. A.V. Dubrovin, V.V. Boldyrev, V.G. Morozov, Thermochim. Acta, 1978, 27, 299.

62. V.S. Schmidt, V.G. Andryushin, Radiokhymia, 1982, 24, 601.

63. A.V. Dubrovin, K.M. Dunaeva. V.N. Agafonov, Radiokhymia, 1979, 21, 584.

64. H.A. Papazian, P.J. Pizzolato. J.A. Patrick, J. Am. Ceram. Soc., 1971, 54, 250.

65. G. Fabbri, P. Baraldi, Atti Soc. Nat. Mat., 1975, 106, 57.

66. G. Fabbri, P. Baraldi, Atti Soc. Nat. Mat., 1975, 106,81.

67. N.B. Fialko, L.N. Usherenko, Tezisy Dokl. Soveshch, Kinet. Mekh. Khim. Reakts. Tverd Tela, 7th., 1977, 1, 129.

68. J.E. House, Jr., D.D. Dunlap, Thermochim. Acta, 1980, 42, 377.

69. K. Habersberger, V. Balek, J. Sramek, Radiochim.Radioanal. Lett., 1977, 28, 301.

70. S. Tsutai, Akita Kogyo Koto Semmon Gakko Kenkyu Kiyo, 1977, 12, 55.

71. K.N. Ninan, C.G.R. Nair, Thermochim. Acta, 1979, 30, 25.

72. K. Nagase, K. Sato, N. Tanaka, Bull. Chim. Soc. Jpn., 1975, 48, 439.

73. E.G. Derouane, Z. Gabelica, R. Hubin, M.J. Hubin-Franskin, Thermochim. Acta, 1975, 11, 287.

74. J.-J. Gardet, B. Guilhot, M. Soustelle, Bull. Soc. Chim., Fr., 1976, 1413.

75. L.L. Bircumshaw, I. Harris, J. Chem. Soc., 1948, 1898.

76. L.L. Bircumshaw, I. Harris, J. Chem. Soc., 1939, 1637.

77. P.E. Yankwich, J.L. Copeland, J. Am. Chem. Soc., 1957, 79, 2081.

78. E.D. Macklen, J. Inorg. Nucl. Chem., 1968, 30, 2689.

79. P.W.M. Jacobs, A.R.T. Kureishy, Trans. Faraday Soc., 1962, 58, 551.

80. J.A. Allen, D.E. Scaife, J. Phys. Chem., 1954, 58, 667.

81. D. Krug, W. Haedrich, Experientia Suppl., 1979, 37, (Angew. Chem. Thermodyn. Thermoanal.), 54.

82. E.D. Macklen, J. Inorg. Nucl. Chem., 1967, 29, 1229.

83. V. Rao, A.L. Shashimohan, A.B. Biswas, J. Mater. Sci., 1974, 9, 430.

84. H. Hashimoto, Kenkyu Hokoku-Asahi Garasu Kogyo Gijutsu Shoreikai, 1980, 37, 15.

85. X. Wang, P. Wu, X. Xin, A. Dai, Y. Zhang, Fenzi Kexue Yu Huaxue Yanjiu, 1983, 3, 39.

86. R.A. Brown, S.C. Bevan, J. Inorg. Nucl. Chem., 1966, 28, 387.

87. Z. Gabelica, R. Hubin, E.G. Derouane, Thermochim. Acta, 1978, 24, 315.

88. E. Wisgerchof, J.W. Geus, Mater. Res. Bull., 1983, 18, 993.

89. W.W. Wendland, Anal. Chem., 1958, 30, 58.

90. A.W. Wylie, J. Chem. Soc., 1947, 1687.

91. V.Sharov, G.V. Bezdenezhnykh, Usp. Khim., 1981, 50, 1197.

92. V.M. Padmanabhan, S.C. Saraiya, A.K. Sundaram, J. Inorg. Nucl. Chem., 1960, 12, 356.

93. K.G. Nair, V.V. Sreerajan, V.S.V. Nayar, C.G.R. Nair, Thermochim. Acta, 1980, 39, 253

94. A. Glasner, M. Steinberg, J. Inorg. Nucl. Chem., 1960, 16, 279.

95. A. Glasner, E. Levy, M. Steinberg, W. Bodenheimer, Talanta, 1964, 11, 405.

96. A. Glasner, E. Levy, M. Steinberg, J. Inorg, Nucl. Chem.; 1963, 25, 1415.

97. G.L. Jeyaraj, J.E. House, Jr., Thermochim. Acta, 1983, 71, 345.

98. W.W. Wendlandt, Anal. Chem., 1959, 31, 408.

99. W.W. Wendlandt, T.D. George, G.R. Horton, J. Inorg. Nucl. Chem., 1961, 17, 273.

100. A. Glasner, M. Steinberg, J. Inorg. Nucl. Chem., 1961, 22, 39.

101. Y. Saito, S. Sasaki, Netsu Sokutei, 1980, 7, 67.

102. E. Yatabe, L.I. Pollock, At. Energy Canada Ltd., 1952, CEI-49.

103. G.D. Buttress, M.A. Hughes, J. Chem. Soc., A, 1968, 1985.

104. P.L. Günther, H. Rehäag, Ber., 1938, 71B, 1771.

105. W.W. Wendlandt, Tex. J. Sci., 1958, 10, 271.

106. W.W. Wendlandt, E.L. Simmons, J. Inorg Nucl. Chem., 1965, 27, 2317.

107. E.L. Simmons, W.W. Wendlandt, Thermochim. Acta, 1971, 2, 217.

108. J.E. House, Jr., T.G. Blunthal, Thermochim. Acta, 1980, 36, 79.

109. J.E. House, Jr., A.M. Learnard, Thermochim. Acta, 1977, 18, 295.

110. E.L. Simmons, W.W. Wendlandt, J. Inorg. Nucl. Chem., 1965, 27, 2325.

111. W.W. Wendlandt, T.D. George, K.V. Krishnamurty, J. Inorg. Nucl. Chem., 1961, 21, 69.

112. U.B. Ceipidor, G. D'Ascenzo, M. Tomassetti, E. Cardarelli, Thermochim. Acta, 1979, 30, 15.

113. J.B. Holden, Jr., Diss. Abstr., 1962, 23, 62.

114. S.P. Goel, P.N. Mehrotra, Thermochim. Acta, 1983, 68, 137.

115. J. Gopalakrishnan, B. Viswanathan, V. Scrinivasan, J. Inorg. Nucl. Chem., 1970, 32, 2565.

116. S.P. Goel, P.N. Mehrotra, Thermochim. Acta, 1983, 70, 201.

117. H. Langfelderova, J. Mikovic, J. Garaj, J. Gazo, Thermochim.

Acta, 1973, 5, 303.

118.G.L. Jeyaraj, J.E. House. Jr., Thermochim. Acta, 1983, 68, 201.

119.A.H. Verdonk, Thermochim. Acta, 1972, 4, 25.

120.S.R. Sagi, K.V. Ramana, M.S.P. Rao, Thermochim. Acta, 1979, 31, 285.

121.E. Wenda, J. Therm. Anal., 1981, 20, 153.

122.P.K. Gallagher, Inorg. Chem., 1965, 4, 965.

123.P.K. Gallagher, C.R. Kirkjian, Inorg. Chem., 1966, 5, 214.

124.M.G. Usha, M.S. Rao, T.R.N. Kutty, Thermochim. Acta, 1981, 43, 35.

125.K. Muraishi, K. Nagase, N. Tanaka, Themochim. Acta, 1978, 23, 125.

126.K.A. Jones, R.J. Acheson, B.R. Wheeler, A.K. Galwey, Trans. Faraday Soc., 1968, 64, 1887 .

127.S. Shishido, K. Ogasawára, Sci. Rep. Niigata Univ., Ser. C, 1971, 3, 23.

128.J.A. Herrero, J. Bermudez, E.G. Rios, An. Quim., 1977, 73, 1271.

129.C.A. Waring, W.S. Horton, J. Amer. Chem. Soc., 1945, 67, 540.

130.L.H. Long, J. Chem. Soc., 1956, 3410.

131.R.P. Johnson, S.J.W. Price, Can. J. Chem., 1972, 50, 50.

132.T.S. Milazzo, Diss. Abstr. Int. B, 1978, 39, 736.

133.G.G. Devyatykh, Izv. Akad. Nauk, SSSR, Ser. Khim., 1972, 2472.

134.G.A. Razuvaev, N.S. Vyankin, O.A. Shchepetkova, Tetrahed., 1962, 18, 667.

135.M.C. Daly, Diss. Abstr., Int. B, 1978, 38, 4827.

136.G. Razuaev, N.S. Vyazankin, Yu.I. Dergunov, N.N. Vyshinskii, Zh. Obshch. Khim., 1961, 3, 1712.

137.W.P. Neumann, E. Petersen, R. Sommer, Angew. Chem., 1965, 338, 1.

138.H. Gilman, J. Eisch, J. Org. Chem., 1955, 20, 763.

139. E. Amberger, Angew. Chem., 1960, 72, 78.

140. Cahours, Ann., 1860, 114, 377.

141. C.A.Kraus, R.H. Bullard, J. Amer. Chem. Soc., 1929, 51, 3605.

142. R.F. Chambers, R.C. Sherer, J. Amer. Chem. Soc., 1926, 48, 1054.

143. O. Schmitz-Dumont, H. Meyer, Z. Anorg. Allgem. Chem., 1941, 248, 289.

144. W.T. Reichle, J. Polym. Sci., 1961, 49, 521.

145. R.L. Dannley, W.A. Aue, J. Org. Chem., 1965, 30, 3845.

146. A.N. Bryukhanov, Zh. Obshch. Khim., 1975, 45, 2692.

147. M.A. Mesubi, G.A. Olatunji, Thermochim. Acta, 1983, 67, 307.

148. P.J. Shapiro, E.I. Becker, J. Org. Chem., 1962, 27, 4668.

150. W.B. Simpson, Chem. Ind., 1966, 21, 854.

151. A.N. Fester, Diss. Abstr., B, 1968, 29, 103.

152. K.Shisido, S. Kozima, J. Org. Chem., 1964, 29, 907.

153. D. Perry, R.A. Geanangel, Inorg. Chim. Acta, 1975, 13, 185.

154. G.K. Bratspies, J.F. Smith, J.O. Hill, T.J. Magee, Thermochim. Acta, 1977, 19, 349.

155. G.K. Bratspies, J.F. Smith, J.O. Hill, R.J. Magee, Thermochim. Acta, 1977, 19, 335.

156. G.K. Bratspies, J.F. Smith, J.O. Hill, R.J. Magee, Thermochim. Acta, 1977, 19, 361.

157. G.K. Bratspies, J.F. Smith, J.O. Hill, Thermochim. Acta, 1977, 19, 373.

158. G.K. Bratspies, J.F. Smith, J.O. Hill, R.J. Magee, Thermochim. Acta, 1978, 27, 307.

Index - Chapter 2.

2.1. Introduction.

In this chapter the preparation of the compounds on which thermal analyses were carried out in this work is described. The compounds prepared were mono- and di-carboxylato tin(II) complexes, and organotin nitrates and sulphates. The Sn(II) oxalate and malonate complexes were originally prepared by Filmore[1], the acetates by Knifton[2], and the formates by Arifin[3], and are described in previous theses by the group. Each of these researchers carried out partial studies on some aspects of the thermal bahaviour of complexes including some product analysis but no in-depth study has been performed on any of them to determine the exact nature of intermediates from the decomposition reactions and the volatile products evolved at each stage. To this end an apparatus for the study of thermal decompositions has been designed and built and in which gas, liquid and solid volatile products and solid residues can be collected and analysed. The details and operation of this apparatus are also described in this chapter.

2.2. Tin(II) carboxylate complexes.

The preparation of these complexes is, in many cases, very sensitive to changes in the nature of the counter cation, acid strength, and metal carbonate concentration. For these reasons, emphasis has been placed on careful monitoring of reaction conditions.

Throughout this course of study, all reactions involving tin(II) have been carried out under an atmosphere of oxygen-free nitrogen to prevent oxidation of Sn(II) to Sn(IV). The starting material for all the preparations is the blue-black tetragonal tin(II) oxide which is easily made from stannous sulphate solutions[4], and is stable to oxidation and hydrolysis. The products obtained were dried in vacuo over KOH for several days, then stored in well-stoppered containers in a desiccator to minimise water absorption.

Table 2.1. Elemental Analysis Results for Transition metal tin (II) formates.

	Complex	Mn	Co	Ni	Zn
Sn(%)	Calc.	33.58	33.29	33.31	32.85
	Found	32.90	32.63	32.85	32.11
C(%)	Calc.	11.89	11.79	11.80	11.63
	Found	11.74	11.75	11.55	11.72
H(%)	Calc.	2.12	2.12	2.13	2.08
	Found	2.40	1.95	2.21	2.27

Table 2.2: X-Ray Diffraction data for Transition metal Tin(II) Formates, $|M_3Sn_4(CHOO)_{14}.8H_2O|$.

Mn		Co		Ni		Zn	
d(Å)	I(%)	d(Å)	I(%)	d(Å)	I(%)	d(Å)	I(%)
11.94	100	11.70	30.6	11.63	100	11.63	100
7.89	26.3	7.76	3.6	7.69	13.0	7.73	11.5
7.55	45.0	7.31	13.2	7.26	11.1	7.29	8.3
6.92	60.0	6.97	100	6.94	99.4	6.92	89.8
6.70	14.0	6.71	3.0	6.71	5.3	6.69	7.3
6.34	10.2	6.42	2.6	6.45	3.5	6.40	3.8
		6.12	5.6	6.08	5.1	6.11	6.4
		5.98	6.2				
5.68	10.8	5.70	6.4	5.68	7.1	5.67	7.3
5.39	20.8	5.39	4.7	5.40	2.5	5.40	5.8
5.04	9.0	5.37	4.8	5.02	2.7	5.04	4.1
4.90	15.8	4.90	6.8	4.90	27.4	4.90	25.9
4.66	47.5	4.76	4.4	4.76	11.8	4.76	3.7
4.43	13.0	4.60	25.4	4.55	4.6	4.58	3.8

Table 2.2. Cont..

4.38	10.8	4.50	13.9	4.45	5.5	4.42	3.7
4.35	8.8	3.95	5.9				
3.97	6.5	3.93	6.1	3.79	40.8		
3.78	6.2	3.78	8.1	3.78	42.8	3.78	33.4
		3.71	20.1	3.63	3.1		
		3.69	19.7				
		3.29	5.7				
		3.19	57.4	3.10	6.4		
3.10	6.0	3.18	57.4	3.06	5.1	3.10	7.1
3.06	5.5	3.02	2.9			3.06	4.5
		2.96	8.9	2.96	2.7		
		2.95	8.7	2.72	2.2		

2.2.1. Complex tin (II) formates.

The Mn, Co, Ni, and Zn complex derivatives of stannous formate were prepared according to the following method.

0.02 mole of blue-black stannous oxide was refluxed under nitrogen with 60ml. of 60%w/v formic acid until all the stannous oxide had been taken into solution. To the stannous formate solution was added 0.02 mole of the relevant metal carbonate and the mixture refluxed for a further hour. The hot solution was then filtered and a product allowed to crystallise out. The crystals first formed were filtered off and discarded bacause they were found to consist of the excess of unreacted tin(II) formate. The liquor was concentrated down slightly on a rotary evaporator and the final products allowed to crystallise out. Elemental analyses of the products are in table 1, and these taken with the thermogravimetric data (Ch.3), show that the complexes obtained have the formula $M_3Sn_4(CHOO)_{14}\cdot 8H_2O$.

2.2.2. Complex tin (II) acetates.

The Na, K, Ca, and NH_4^+ Complexes of stannous acetate were prepared by refluxing 0.02 mole of blue-black stannous oxide under nitrogen with 50ml. of 50w/v% acetic acid solution for 1-1½ hours, until most of the stannous oxide had been taken into solution. To this solution was added 0.01 mole of the metal or ammonium carbonate and the solution was refluxed again for approximately 30mins.. For the calcium complex, the solution was filtered while hot, and the product allowed to crystallise out without evaporating down the liquor. For the Na, K, and NH_4^+ complexes, after filtering, the solutions were evaporated down on the rotary evaporator until the excess of acetic acid had been removed. The K and NH_4^+ complexes precipated out immediately on cooling the mother liquor from the rotary evaporator, but for the Na complex a viscous oil was obtained, which, when stood for a few days gave square, colourless crystals of the complex sodium tin acetate. The products obtained were washed with acetone and ether and dried in vacuo over KOH. Elemental analysis results are in table 3. From these analyses and from thermogravimetric studies, the Ca salt is found to be

Table 2.3: Elemental Analyses for Complex Tin(II) Acetates.

	C(%)		H(%)		N(%)	
	Calc.	Found	Calc.	Found	Calc.	Found
$(NH_4)Sn(CH_3COO)_3$	22.95	22.42	4.17	3.91	4.46	4.31
$NaSn(CH_3COO)_3.H_2O$	21.38	21.29	3.29	3.21	-	-
$KSn(CH_3COO)_3$	21.50	21.48	2.71	2.63	-	-
$CaSn_2(CH_3COO)_6$	22.80	22.72	2.87	2.83	-	-

Table 2.5: Elemental Analyses for Complex Tin(II) Oxalates.

	C(%)		H(%)	
	Calc.	Found	Calc.	Found
$Na_2Sn(C_2O_4)_2$	14.09	14.45	0	0
$K_2Sn(C_2O_4)_2.H_2O$	12.28	12.17	0.51	0.47
$CaSn(C_2O_4)_2.H_2O$	13.61	13.52	0.57	0.72

Table 2,7: Elemental Analyses for Complex Tin(II) Malonates.

	C(%)		H(%)		N(%)	
	Calc.	Found	Calc.	Found	Calc.	Found
$(NH_4)_2Sn_2(CH_2C_2O_4)_3$	18.65	18.68	2.43	2.43	4.83	4.66
$Na_2Sn_2(CH_2C_2O_4)_32H_2O$	17.27	17.47	1.61	1.59	-	-
$K_2Sn_2(CH_2C_2O_4)_3.H_2O$	16.90	17.01	1.26	1.21	-	-
$CaSn_2(CH_2C_2O_4)_33H_2O$	16.95	16.92	1.90	1.89	-	-

Table 2.4: X-Ray Diffraction Data for Complex Tin(II) Acetates.

Ammonium		Sodium		Potassium		Calcium	
d(Å)	I(%)	d(Å)	I(%)	d(Å)	I(%)	d(Å)	I(%)
11.83	33.7			11.65	17.6	11.57	100
		11.00	100				
10.59	100			10.41	100		
9.95	86.7			9.97	20.8		
				9.34	13.2		
8.76	27.6	8.75	28.2				
7.93	64.3			7.93	14.7		
7.67	30.6	7.73	6.5	7.60	9.7		
				7.52	11.5		
7.21	23.5						
		7.08	10.8				
6.97	36.7	6.91	3.7	6.86	13.0	6.91	5.9
		6.80	4.4				
		6.59	4.8				
		6.45	18.5				
6.34	57.1	6.28	9.7				
6.07	65.3			6.07	6.8	6.12	9.1
5.97	44.9	5.97	5.6	5.97	14.5		
		5.84	10.5	5.87	20.8		
				5.82	29.4		
		5.72	9.2				
		5.62	3.9				
		5.52	13.4	5.54	7.3		
		5.36	5.3	5.45	5.5		
				5.09	7.1		
				4.97	13.2		
		4.79	20.3				
		4.62	4.2			4.60	4.8
4.25	28.6	4.26	10.5	4.24	17.7		
		4.22	7.6	4.21	7.8		
4.15	27.6						
		3.84	13.1	3.81	5.9		
		3.58	13.9				

Table 2.6: X-Ray Diffraction Data for Complex Tin(II) Oxalates.

Sodium		Potassium		Calcium	
d(Å)	I(%)	d(Å)	I(%)	d(Å)	I(%)
		9.44	11.0		
				8.90	23.3
		8.81	17.7	8.75	13.4
		8.65	14.0		
		8.23	18.5		
		7.87	20.0		
7.71	60.1				
7.60	100				
7.43	33.2				
				7.31	100
				7.20	48.3
6.97	34.0				
				6.81	13.4
				6.48	39.7
		6.35	7.7		
		5.91	12.7	5.99	32.8
5.86	15.4	5.86	12.7		
5.72	10.7				
				5.62	32.8
5.41	16.6	5.40	18.2	5.47	33.6
		5.30	19.8		
5.11	41.5	5.12	39.8		
		5.06	100	5.05	17.2
4.98	36.0	4.90	6.8	4.94	10.8
4.84	12.6			4.84	13.4
4.73	41.1				
		4.55	8.2		
4.50	24.1	4.50	7.7	4.48	11.2
		4.39	9.8	4.42	37.9
4.29	56.9			4.23	53.0
4.14	26.5			4.17	19.8
4.10	22.5			4.11	14.2
4.01	11.9	4.00	9.0	4.07	11.6

Table 2.6: Cont..

Sodium		Potassium		Calcium	
d(Å)	I(%)	d(Å)	I(%)	d(Å)	I(%)
3.95	16.2				
3.79	14.6				
3.73	19.8	3.68	10.8	3.74	9.9
3.48	17.8	3.50	10.2		
3.43	31.2			3.43	26.7
3.39	13.8				
3.29	12.6	3.28	11.8		
3.24	13.0				
3.22	14.6	3.22	8.8		
3.19	27.3			3.18	55.2
				3.10	16.4
3.02	11.9			3.01	12.9
2.88	8.3				

$CaSn_2(CH_3COO)_6$, while the K and NH_4^+ complexes have the formula $K/NH_4Sn(CH_3COO)_3$, and the Na complex is $NaSn(CH_3COO)_3.H_2O$.

2.2.3. Complex tin(II) oxalates.

Tin(II) oxalate cannot be prepared directly from stannous oxide and oxalic acid solution in the same way as the formates and acetates, and was therefore prepared first as follows: 0.02 mole of stannous oxide was refluxed under nitrogen with approximately 30ml. of 50% acetic acid solution, until all the oxide had dissolved. Boiling 40% oxalic acid solution was added to the stannous acetate solution and creamy-white stannous oxalate precipitated out of solution immediately. The solid product was filtered off from the cooled solution, dried and analysed to make sure that pure SnC_2O_4had been obtained.

To prepare Na, K, and Ca complexes 0.02 mole of stannous oxalate was then added to the oxalate solution and the mixture refluxed again until all the stannous oxalate had been taken into solution. The complex oxalate products crystallised out from the cooled solution without further concentration of the mother liquor. The K complex was found to have the formula $K_2Sn(C_2O_4)_2.H_2O$. Elemantal analysis results on the complexes are presented in table 5, and thermogravimetric traces shown in Chapter 3.

2.2.4. Complex tin (II) malonates.

To prepare the sodium, potassium and ammonium complexes, 0.01 mole of stannous oxide was refluxed under nitrogen with the minimum of 40w/v% malonic acid solution required to take all the stannous oxide into solution. 0.01 mole of the metal or ammonium oxalate was then added and the reactants refluxed for 1 hour. The resultant solution was filtered while hot and left to allow products to crystallise out slowly over several days, (except the case of the sodium complex which precipitated out rapidly from the cooled solution. Due to the very high solubility of the complexes in the malonic acid liquors, it was essential to keep the liquor concentration to a minimun, because no product precipitated out of

Table 2.8: X-Ray Diffraction Data for Complex Tin(II) Malonates.

Ammonium		Sodium		Potassium		Calcium	
d(Å)	I(%)	d(Å)	I(%)	d(Å)	I(%)	d(Å)	I(%)
						14.51	43.6
13.54	3.7						
				13.70	16.0		
13.27	3.5			12.36	11.3		
12.14	9.2	12.19	11.2				
		11.95	10.8				
10.61	37.1			10.63	60.6		
		10.09	21.5			10.07	10.3
		9.59	7.5				
				9.21	46.8		
						9.06	100
		8.64	20.4	8.60	44.2		
8.47	9.6	8.47	8.4				
8.29	21.2					8.32	24.0
8.20	16.0	8.18	23.7				
		7.96	37.0				
				7.83	10.0		
7.68	8.0						
		7.51	19.0	7.46	58.4		
				7.19	42.0		
						6.93	27.3
6.67	12.0			6.75	32.9		
				6.54	21.2		
		6.37	15.9	6.30	21.6	6.28	21.1
6.17	42.5	6.20	100	6.21	10.4		
6.03	2.4	5.98	35.4	6.02	8.7		
5.86	2.4	5.98	35.4	5.95	9.5		
		5.89	10.8	5.83	38.5		
		5.76	27.4	5.74	29.4		
5.61	7.1	5.71	24.6	5.65	8.7	5.63	34.8
		5.49	14.3	5.50	100		
5.39	9.0	5.35	15.2	5.30	16.0	5.33	14.2
5,17	9.1	5.14	8.7	5.16	15.6		

Table 2.8: Cont..

d(Å)	I(%)	d(Å)	I(%)	d(Å)	I(%)	d(Å)	I(%)
				5.00	24.7	5.01	26.3
		4.88	15.0	4.91	7.8	4.88	11.1
				4.87	8.7		
4.67	7.2	4.72	15.2	4.72	9.1		
4.64	7.2						
4.59	6.2			4.59	10.8		
4.56	8.1	4.57	12.9	4.53	14.7		
		4.47	16.4			4.47	18.6
4.34	100	4.39	11.0				
4.25	5.0	4.28	9.1	4.26	13.4		
		4.19	24.6	4.21	22.5	4.14	7.5
4.02	5.3	4.02	15.0			4.08	21.1
3.96	7.3	3.90	6.3	3.95	12.6	3.95	9.5
				3.92	13.4		
				3.86	10.4		
3.80	8.6	3.79	8.0	3.83	21.2		
				3.73	15.2		
		3.67	7.0			3.66	53.1
				3.62	26.4	3.62	12.4
3.56	7.4	3.58	6.8			3.57	13.7
3.54	7.2			3.54	16.5		
		3.50	11.5	3.48	13.9	3.48	11.9
		3.43	12.2	3.43	14.3		
				3.38	8.7	3.40	5.9
3.33	6.3	3.35	9.6	3.34	13.0		
				3.27	9.5	3.28	14.9
		3.21	18.0	3.23	10.0		
				3.14	13.4		
		3.05	8.2	3.10	10.0	3.08	12.6
						2.94	8.2
2.84	5.3	2.82	8.7				

solution in the presence of excess liquor.

Elemental analyses and thermogravimetric studies show that the formula for these complexes is $M_2Sn_2(CH_2C_2O_4)_3.xH_2O$, (for Na, x=2, K, x=1, NH_4, x=0). Elemental analyses are given in table 7 and thermogravimetric data in Chapter 3.

A Ca complex tin (II) malonate was prepared by a method similar to that used for the alkali metal complexes except that, due to the very low solubility of the Ca complex in the malonic acid liquor, larger volumes of malonic acid were used. 0.01 mole of stannous oxide was refluxed with 50ml. of 40w/v% malonic acid solution until all the stannous oxide was in solution. To this solution was added 0.005 mole of calcium carbonate and the mixture refluxed for a further 30mins.. The microcrystalline product, $CaSn_2(CH_2C_2O_4)_3.3H_2O$ precipated out of solution almost immediately after filtering. The solution was allowed to cool slowly, then left at room temperature to complete the crystallisation. The crystals were filtered off, washed with methanol, then dried in vacuo over KOH. The elemental analyses results are in table 7, and the thermogravimetry trace in Chapter 3.

2.3. Preparation of organotin nitrates and sulphates.

2.3.1. Organotin (IV) nitrates.

The diorganotin (IV) nitrates, $R_2Sn(NO_3)_2$, (where R=ethyl, propyl, and phenyl), and R_3SnNO_3, (where R=phenyl), were prepared from the corresponding organotin oxide and nitric acid, according to the reaction schemes:

$$R_3SnOH + HNO_3 \longrightarrow R_3SnNO_3 + H_2O$$

$$R_2SnO + 2HNO_3 \longrightarrow R_2Sn(NO_3)_2 + H_2O$$

The stoichiometric amounts of the oxides or hydroxide were

Table 2.9: Elemental Analyses for di-alkyl and di-aryl tin Dinitrates.

	C(%)		H(%)		N(%)	
	Calc.	Found	Calc.	Found	Calc.	Found
$Et_2Sn(NO_3)_2$	16.51	16.26	3.47	3.81	9.63	9.06
$Ph_2Sn(NO_3)_2$	36.29	36.23	2.54	2.56	3.94	3.59

Table 2.10: X-Ray Diffraction Data for di- alkyl and aryl Tin Dinitrates.

Ethyl		Phenyl	
d(Å)	I(%)	d(Å)	I(%)
		11.59	32.7
10.84	24.0		
10.63	19.0		
		10.41	62.4
10.12	100		
		9.07	44.6
7.60	7.4		
		7.24	100
		7.08	80.2
		6.83	39.6
6.72	7.1		
		6.44	29.7
		6.05	70.3
		5.52	57.4
		4.85	55.5
		4.77	29.7
		4.40	33.7
		4.26	62.4
		3.96	32.7
		3.79	61.4

refulxed for approximately 1 hour with concentrated HNO_3 diluted to 10ml. with distilled water. The solution obtained was evaporated down on a rotary evaporator to between 1 and 2ml., and the product allowed to crystallise out slowly over several days. The products were filtered off without washing and dried in vacuo over silica gel. Elemental analyses results for the organotin nitrates are in table 9, and thermogravimetry traces shown in Chapter 4.

2.3.2. Organotin (IV) sulphates.

The organotin (IV)sulphates, R_2SnSO_4, R = methyl, ethyl and propyl, were prepared according to the following reaction:

$$R_2SnO + H_2SO_4 \longrightarrow R_2SnSO_4 + H_2O$$

The organotin oxide was refluxed for approximately 1 hour with the stoichiometric amount of H_2SO_4 diluted to 10ml. with distilled water. The resultant solutions were evaporated down on a rotary evaporator until the first evidence of crystallisation was seen. The solutions were then left to allow the products to crystallise out. The products were filtered off, washed with acetone, and dried in vacuo over silica gel.

For dipropyltin sulphate, it was necessary to evaporate the solution to dryness and to place the product in a desiccator immediately, due to the extremely deliquescent nature of this material.

All the organotin sulphates are deliquescent and can absorb moisture even in a desiccator under vacuum.

2.4. Thermal Decomposition Studies.

The preliminary studies on the complexes and organotin compounds prepared in this work were carried out under an

atmosphere of nitrogen using a STA 790 thermal analyser. Use of this technique provided accurate information on the temperatures ($\pm 1^{\circ}C$) at which decomposition, or phase changes occurred, and the approximate extent of decomposition. From these preliminary studies a tentative assignment could be made of the decomposition pathways. This method is not, however, capable of providing information on the nature of either the volatile products or the solid residues at the various stages of decomposition. It was, therefore, necessary to design and build equipment which would meet the needs of the research project. Namely, to have a controlled means of heating larger amounts of samples to the required temperatures and a means of collecting solid, liquid and gaseous products in sufficient quantities to be able to carry out all the analytical tests required, including Mass Spectrometry, infra-red, X-Ray Diffraction, Mössbauer Spectroscopy, and elemental analysis where appropriate.

The equipment designed and built for these studies is shown in figure 1. It consists of nitrogen entering the apparatus from the right, passing through a gas bubbler at a flow rate controlled by Tap W. A second Tap X, is situated immediately after the gas bubbler to prevent evolved gases flowing back towards the bubbler, and to prevent seepage of nitrogen into the evacuated section of the equipment.

A known weight of sample is placed in a weighed Pyrex cup, C, which fits inside the furnace, (F), at the centre of the heating element, (E), (the furnace arrangement is shown diagramatically in figure 2). The furnace chamber is Pyrex and has a platform, (P), at the centre of the heating coil on which the sample cup C is situated. On the opposite side of the platform is a NiCr/NiAl thermocouple, (N), which is connected to a temperature controller, (T), that can operate over the temperature range ambient to $400^{\circ}C$. The accuracy of the controller is $\pm 5^{\circ}C$ at $400^{\circ}C$, and $\pm 1^{\circ}C$ at $100^{\circ}C$. The Nichrome wire heating element is connected to a variac to permit alteration of the rate of heating. The furnace is surrounded by an insulating jacket, (J), of alumina cement of average thickness 1". A water cooled cold probe, (CP), is fitted in the neck of the furnace for collecting volatile products which

Figure 2.1: Thermal Decomposition Apparatus.

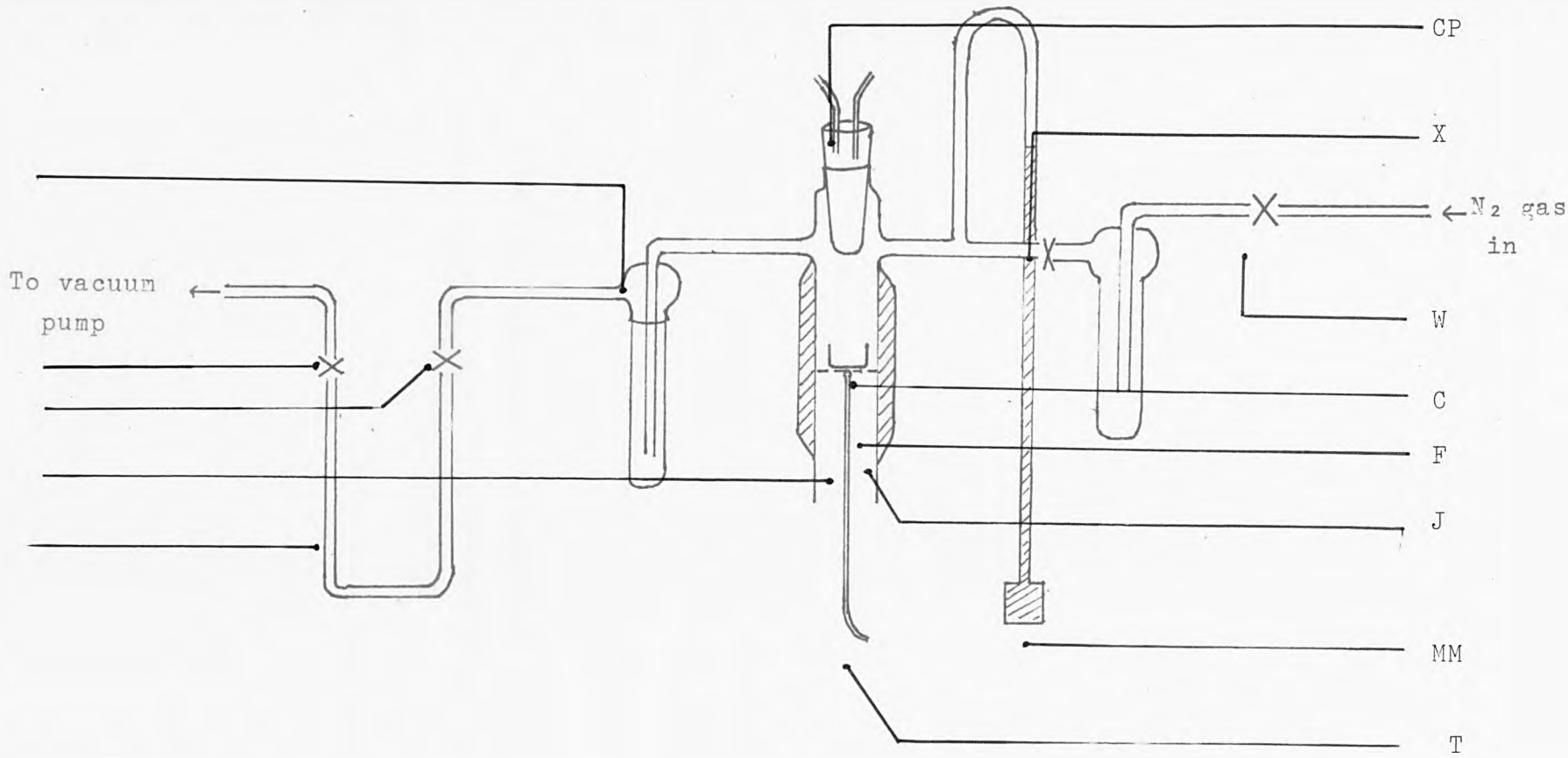

Figure 2.1: Thermal Decomposition Apparatus.

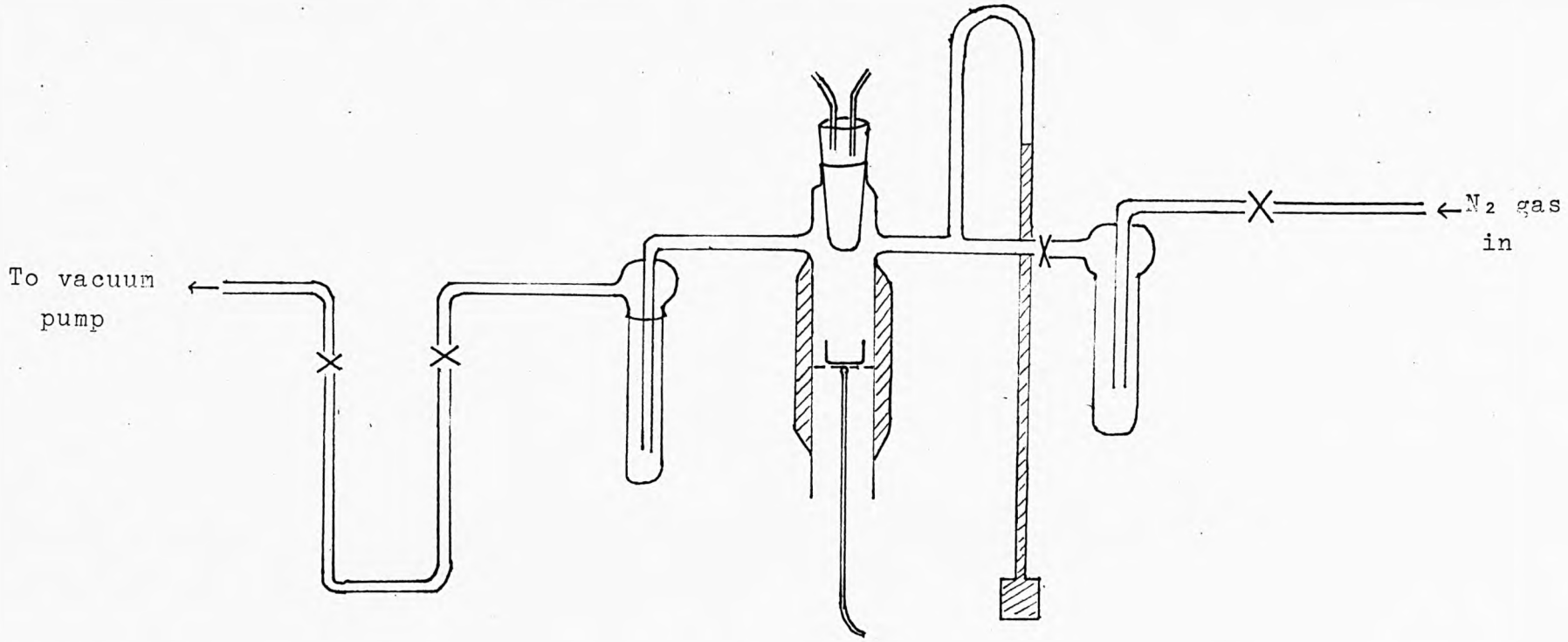

Figure 2.2: Diagramatic Representation of Furnace Arrangement.

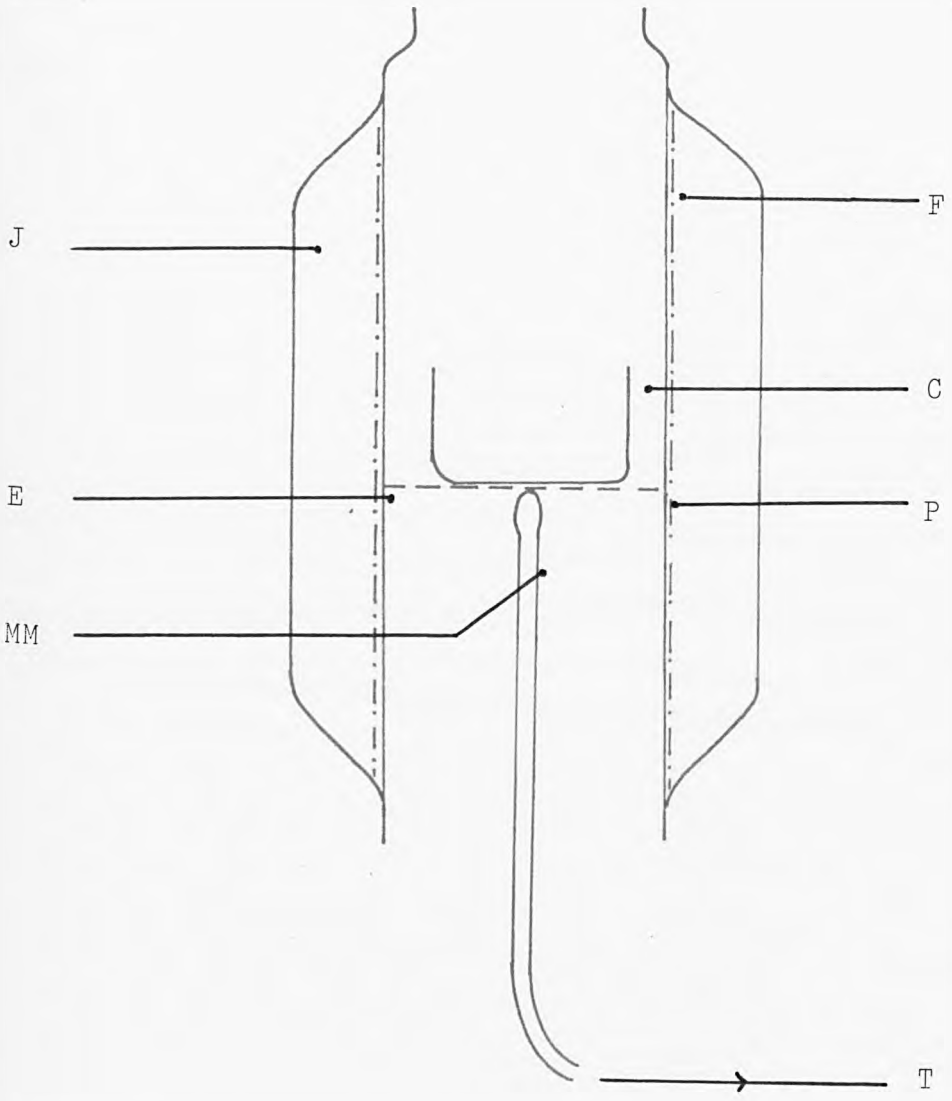

Figure 2.2: Diagramatic Representation of Furnace Arrangement.

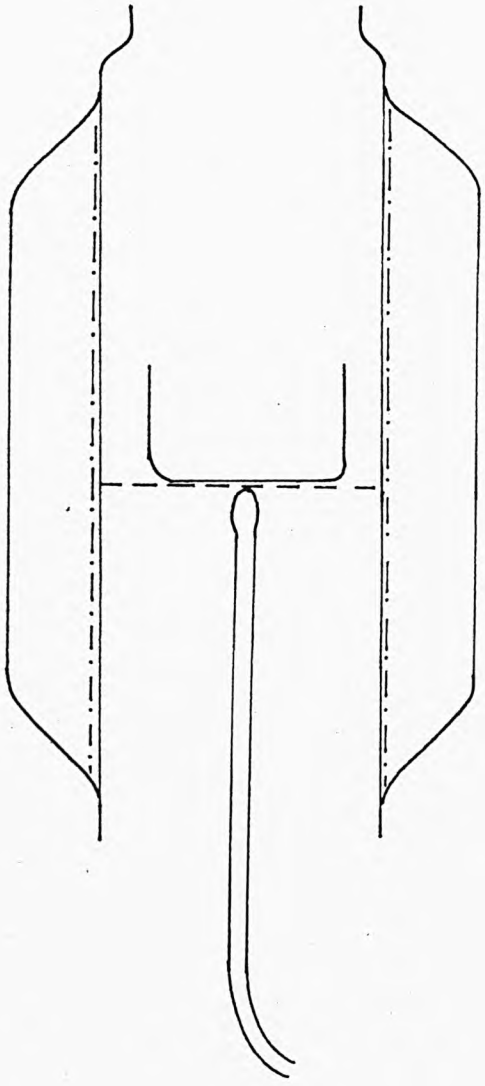

are solid at room temperature. Those components of the evolved gases which are not solid at ca. 12°C pass across the cold probe to a U-tube, (U), which is opened and closed using taps Y and Z. For products which are liquid at room temperature, the cold probe is replaced by a ground glass stopper and the cold finger, (CF), cooled with ice or cardice. The liquid products are collected at the bottom of the cold finger and taken for analysis.

For each decomposition, the known weight of sample is placed inside the furnace and the furnace stoppered. All the junctions are greased and made airtight, and air flushed out of the system with oxygen-free nitrogen, leaving taps W,X,Y, and Z open. Taps W and X are then closed and the nitrogen evacuated. The gas pressure in the system is monitored using a mercury manometer, (MM), situated between tap X and the furnace. When all the nitrogen has been removed, tap Z is closed and nitrogen re-admitted to give atomspheric pressure in the system. This process is repeated twice and the system finally evacuated and pumped off for ca. 10mins. to remove as much of the residual nitrogen as possible. Taps W,X, and Z are then closed to seal off the furnace, the cold finger, and the U-tube from the atmosphere. The sample is then heated to the required temperature and maintained at this temperature until no more gases are evolved, (indicated by manometer level), or no more liquid or solid products are collected. At this point, the heater is turned off and the U-tube isolated from the rest of the apparatus by closing tap Y. Nitrogen is re-admitted into the system at a slow rate to maintain a positive pressure. When atmospheric pressure has been reached, the U-tube is disconnected by unfastening the ball and socket joints II and III, and the contents of the U-tube taken for gas analysis by Mass spectroscopy. Once the residue in the cup has cooled down, it is removed from the furnace and taken for various analytical tests.

A further refinement to these thermal investigations is in the form of a modified pyrolysis head attachment for the Gas Chromatrography-Mass Spectrometer. The heating rate of the pyrolysis head can be varied using a variac and in all cases small amounts of sample are taken and heated up to ca. 700°C in an atmosphere of argon, passing the volatile products directly

into the Mass Spectrometer through a gas chromatography column. This facility enables a complete breakdown of the decomposition to be observed as it happens, in a shorter time than usually taken using the large scale apparatus with sample collection. This method also minimises the chances of gas-phase reactions taking place prior to Mass Spectroscopic analysis, which may occur in the time taken in conveying the U-tube to the Mass Spectrometer.

2.5. References.

1. E.J. Filmore, Ph.D. Thesis, 1972.
2. J.F. Knifton, Ph.D. Thesis, 1965.
3. Z.B. Arifin, Ph.D. Thesis, 1981.
4. J.D. Donaldson, W. Moser, W.B. Simpson, J. Chem. Soc., 1964, 5942.

Index - Chapter 3.

3.1. Introduction.

In this chapter the thermal behaviour of four groups of tin (II) carboxylate complexes is discussed. The four series studied are: (i) Transition metal tin formate complexes of the type $M_3Sn_4(CHOO)_{14}.8H_2O$, (where M = Mn, Zn, Ni, and Co). (ii) Tin acetate complexes, $XSn(CH_3COO)_3.nH_2O$, (for X = NH_4,K, n = 0, for X = Na, n = 1), and $Ca_2Sn_2(CH_3COO)_6$. (iii) complex tin oxalates, $X_2Sn(C_2O_4)_2.H_2O$, (for X = Na, n = 0, for X = K, n = 1), and $CaSn(C_2O_4)_2.H_2O$. (iv) Complex tin malonates, $X_2Sn_2(CH_2C_2O_4)_3.nH_2O$, (for X = NH_4, n = 0, for Na, n = 3, for X = K, n = 1), and $CaSn_2(CH_2C_2O_4)_3.3H_2O$.

3.2. Complex Tin(II) Formates.

The thermal analytical data for the complex tin(ii) formates, $M_3Sn_4(CHOO)_{14}.8H_2O$, (where M = Mn, Zn, Ni, and Co), and the data used to characterise the products are discussed in the following section, and the likely mechanisms of the decompositions described in section 3.3.

3.2.1. $Mn_3Sn_4(CHOO)_{14}.8H_2O$.

From the TG/DTA data (Fig. 3.1.), this complex undergoes a three-stage thermal decomposition under an atmosphere of nitrogen to leave a residue of 53.3% based on the starting material:

Figure 3.1: TG/DTA data for $Mn_3Sn_4(CHOO)_{14}.8H_2O$.

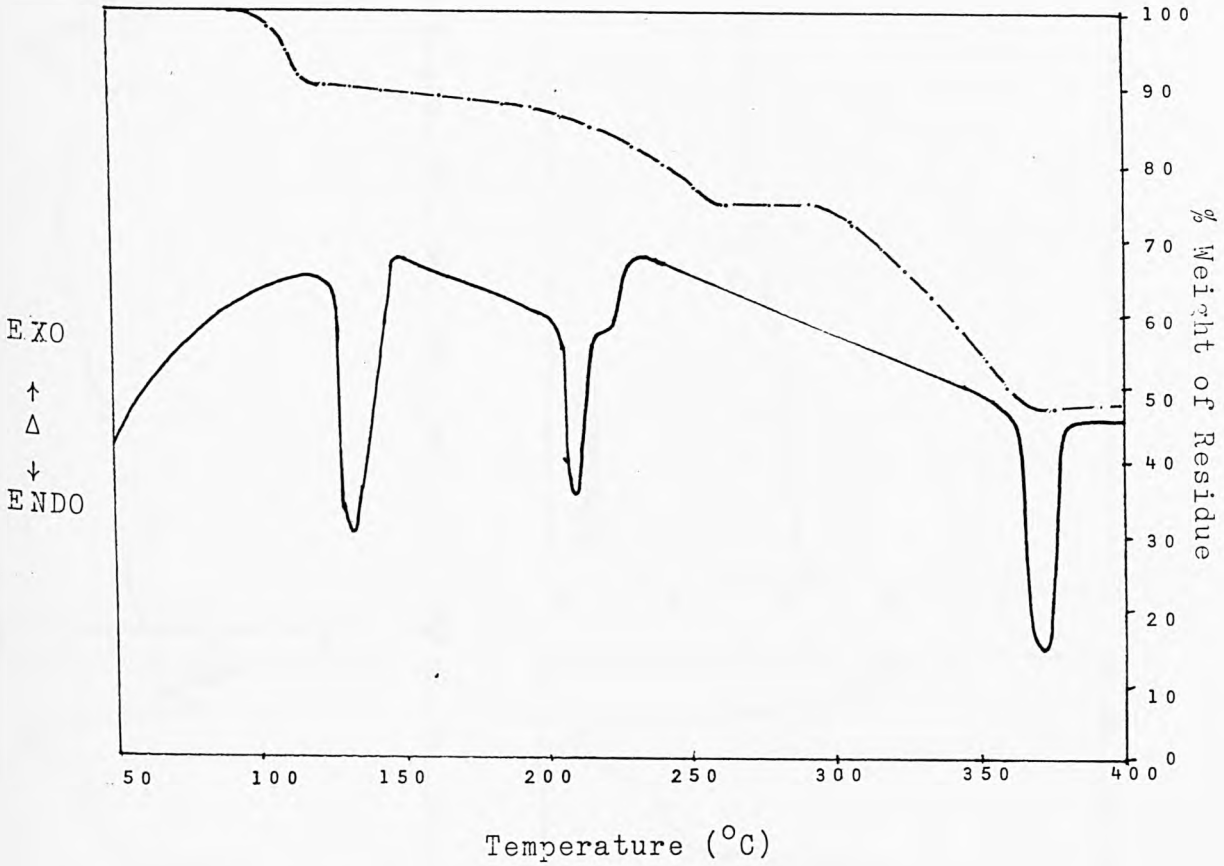

First Stage, (119°C).

The first weight loss is 9.8%, which is found to be due to loss of all eight molecules of water of crystallisation, (q.v. elemental analyses and i.r. spectrum, Table 3.2 and Fig. 3.2, respectively).

The X-ray data, (Table 3.1), for the intermediate differ from those of the starting material.

The i.r. spectrum has no peak at ca. 3300cm^{-1} due to bonded water, and the elemental analyses show the carbon and hydrogen concentrations to be consistent with the anhydrous complex.

Figure 3.2. I.R. Spectra for $Mn_3Sn_4(CHO_2)_{14}.8H_2O$ Decomposition Products.

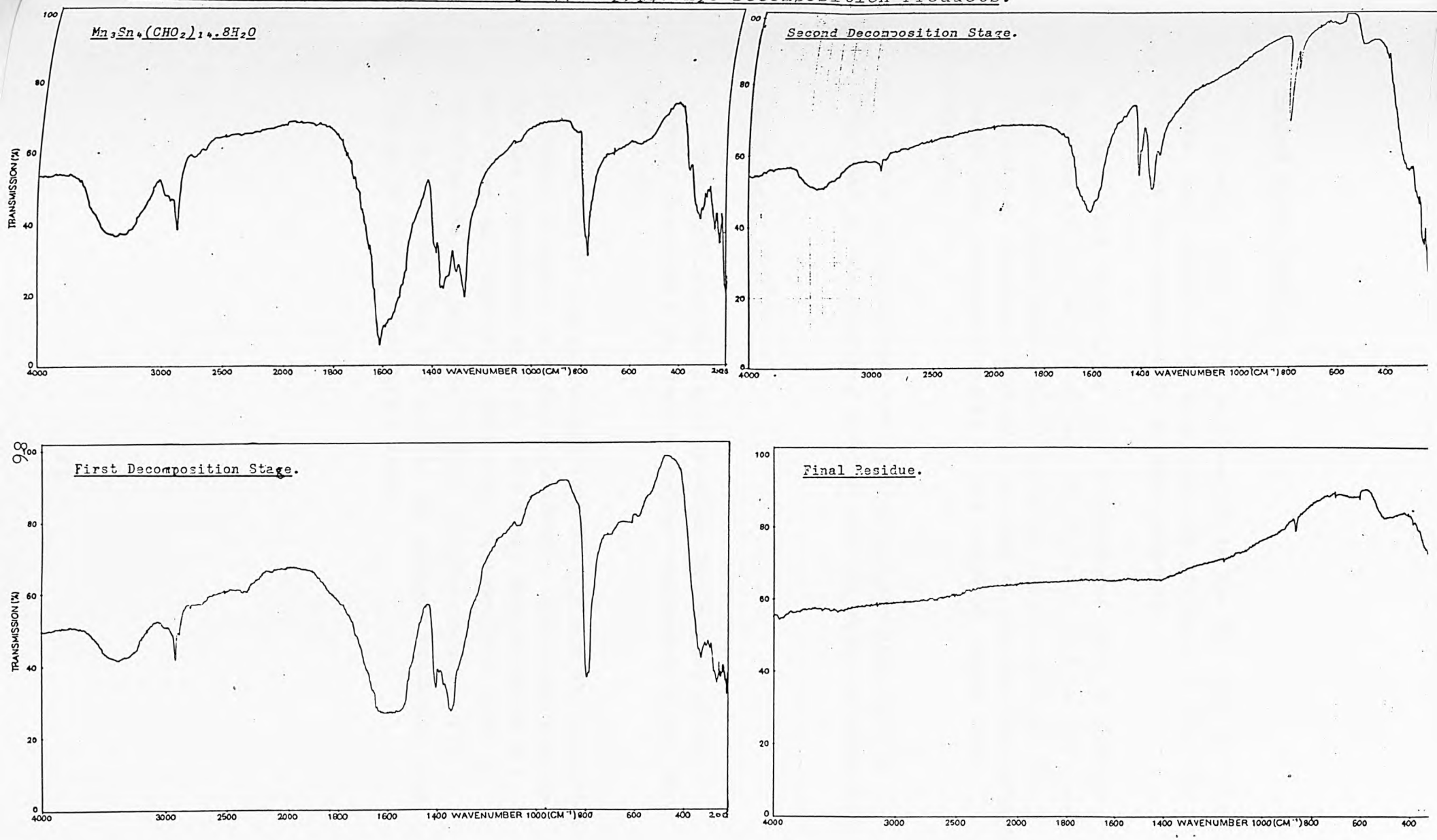

Second Stage (204°C).

A weight loss of 16% is observed in the TG trace for this stage. Mass spectrometry data show the presence of CO_2, CO, and O_2 as the identifiable gaseous products.

Elemental analyses on this intermediate imply a product with the stoichiometric formula $Mn_3Sn_4C_8H_8O_{19}$. From the i.r. data, this intermediate still contains formate groups. The vibrational spectrum is similar to that of the starting material except that additional peaks in the carbonyl region have appeared.

The X-ray powder pattern of this intermediate differs from that of the starting material and the first intermediate.

Third Stage (352°C).

This final decomposition involves the removal of all organic components to yield a residue consisting of Mn, Sn, and O only.

From the TG trace, (weight loss 19.7%), and the elemental analyses, (absence of organic residues), this final residue has the composition $Mn_3Sn_4O_7$. The X-ray data in Table 3.1 show that the product at this stage differs from those in previous stages. Mass spectrometry results indicate the presence of CO, CO_2, and MeOH in the gaseous products, plus traces of acetone and formic acid.

Table 3.1. X-Ray Diffraction data for $Mn_3Sn_4(CHOO)_{14}.8H_2O$ Decomposition Products.

First Stage		Second Stage		Residue	
d(Å)	I(%)	d(Å)	I(%)	d(Å)	I(%)
		14.03	7.6		
		13.29	9.3		
11.63	100	12.08	12.7		
8.92	42.8	8.92	20.8		
		7.62	13.0		
6.91	59.3	6.75	12.5		
6.73	19.5				
6.67	20.9				
5.57	12.1				
4.91	26.9	5.11	100	5.11	97.2
				4.99	100
				4.81	84.6
4.58	25.3	4.64	29.2	4.65	31.6
				4.45	24.4
		4.23	22.5	4.22	18.7
3.94	11.8			3.91	36.2
3.78	37.0			3.65	37.0
				3.57	64.6
3.33	14.5	3.38	18.9	3.39	20.4
3.29	11.8	3.21	31.9	3.21	27.8
3.09	12.8			2.97	14.2
		2.87	33.1	2.87	26.9
				2.81	16.8
				2.66	35.6
		2.60	13.7	2.65	32.0
		2.59	13.7		

Table 3.2. Elemental Analyses for $Mn_3Sn_4(CHOO)_{14}.8H_2O$ Decomposition Products.

	C(%)		H(%)	
	Calc.	Found	Calc.	Found
$Mn_3Sn_4(CHOO)_{14}$	13.23	12.95	1.11	0.92
$Mn_3Sn_4C_8H_8O_{19}$	9.15	8.89	0.77	0.72
$Mn_3Sn_4O_7$	0	0.99	0	0.04

Table 3.4. Elemental Analyses for $Zn_3Sn_4(CHOO)_{14}.8H_2O$ Decomposition Products.

	C(%)		H(%)	
	Calc.	Found	Calc.	Found
$Zn_3Sn_4(CHOO)_{14}$	13.52	13.14	1.14	1.20
$Zn_3Sn_4C_8H_8O_{19}$	8.97	9.24	0.75	0.66
$Zn_3Sn_4O_7$	0	0	0	0

3.2.2. $Zn_3Sn_4(CHOO)_{14}.8H_2O$.

I.R.,X-ray diffraction, and elemental analysis results, (Fig. 3.4 and Tables 3.3 and 3.4, respectively), verify the above structure. The TG/DTA traces, (Fig. 3.3), show that a three stage decomposition occurs, leaving a final residue of 52.5%.

Figure 3.3: TG/DTA traces for $Zn_3Sn_4(CHOO)_{14}.8H_2O$.

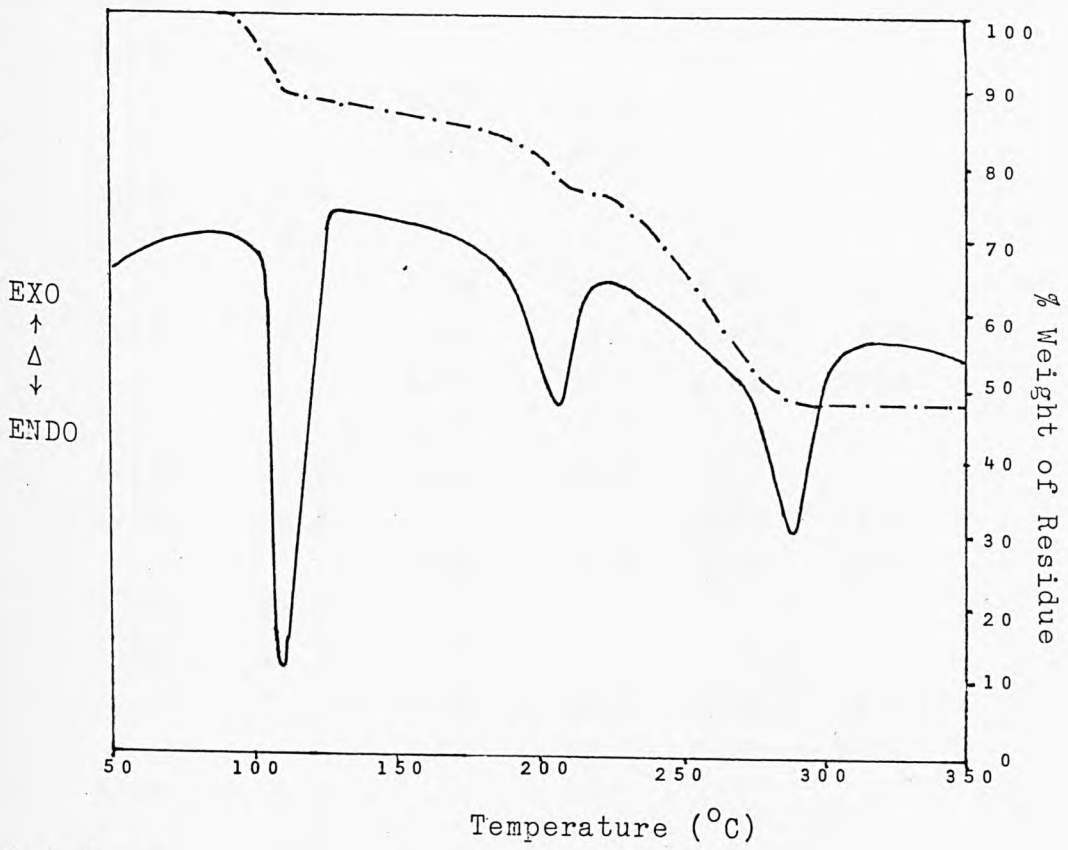

First Stage.

TG/DTA, i.r., X-ray diffraction, and elemental analyses were performed on this first intermediate and show it to be the anhydrous form of the starting material.

Table 3.3. X-Ray Diffraction data for $Zn_3Sn_4(CHOO)_{14}.8H_2O$ Decomposition Products.

First Stage		Second Stage		Residue	
d(Å)	I(%)	d(Å)	I(%)	d(Å)	I(%)
11.62	100				
9.17	33.1	9.19	13.6		
8.97	45.7	8.96	35.8		
8.16	9.9				
				7.63	8.9
6.91	49.4				
6.69	18.5				
		6.25	14.4		
		6.03	10.3		
5.68	8.9				
5.33	8.6				
		5.08	100	5.10	100
4.89	14.1	4.95	7.5	4.85	9.6
		4.65	38.3	4.64	28.9
		4.53	7.2		
4.41	21.0	4.42	10.0		
4.32	14.8			4.33	8.6
		4.24	11.9	4.24	10.6
3.77	26.7				
3.76	19.3				
		3.37	20.0	3.38	16.6
		3.21	29.2	3.21	29.6
3.10	8.1				
3.04	8.6				
		2.87	39.4	2.87	28.7
		2.68	16.4		
		2.67	15.3	2.66	14.4

Figure 3.4. I.R. Spectra for $Zn_3Sn_4(CHO_2)_{14}.8H_2O$ Decomposition Products.

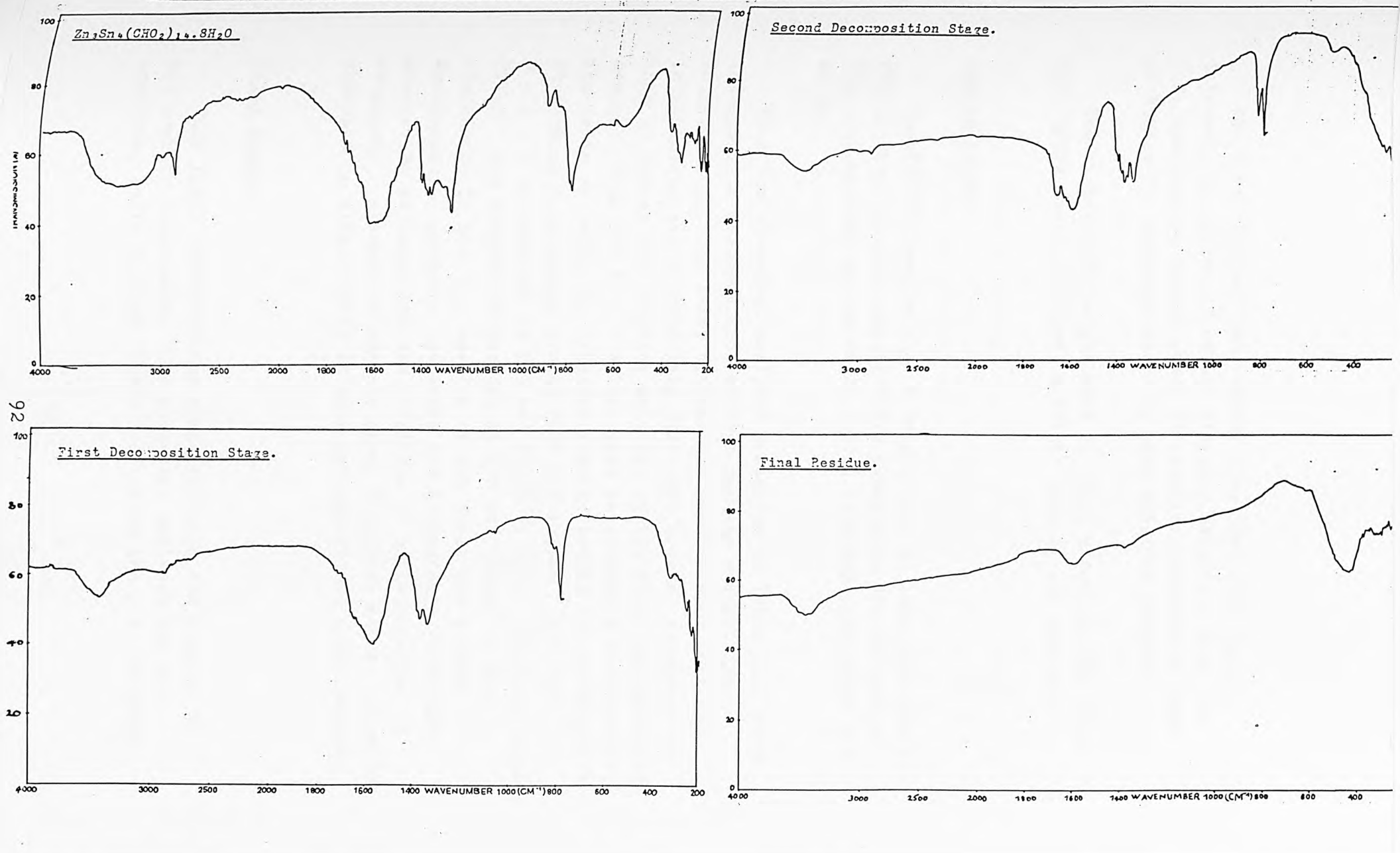

The X-ray diffraction results show that this first intermediate differs from the starting material. From the i.r. spectra, no bonded water is visible, (absence of peak at 3300cm^{-1}), although there is some moisture present.

The theoretical weight loss for this stage is 10%, from the TG/DTA trace obtained, a weight loss of 12% was seen.

Second Stage.

The TG/DTA results show a weight loss of 14%, (202.32g), which, from the mass spectrometry results is due to loss of CO_2, O_2, and CO, in the ratio 1:1:4, with hydrogen given off as H_2.

From the elemental analyses presented in Table 3.4, this intermediate decomposition product has the composition $Zn_3Sn_4C_8H_8O_{19}$. The X-ray diffraction results show that the intermediate has a completely different crystal structure to that of either the starting material or the first decomposition product. From the i.r. results, this intermediate would still appear to resemble the original formate having the carboxylate stretching frequencies around 1600 and 1350cm^{-1} and the O - C - O deformation at 807 and 782cm^{-1}, (q.v. original complex 772cm^{-1} and dehydrated complex at 808 and 781cm^{-1}). The similarity in the i.r. spectra of the first and second decomposition products indicates the persistence of formate groups. No evidence for the existence of oxalate groups is obtained, (absence of oxalate group frequency at ca. 380cm^{-1}) observed in alkali metal formate decompositions under vacuum.

Third Stage.

This final decomposition stage involves the removal of all organic components, (see elemental analyses and i.r. spectrum, Table 3.4 and Figure 3.4). From the i.r. spectrum,

only one peak due to metal oxide is present, ($433cm^{-1}$).

This final decomposition stage removes 8XC, 8XH, and 12XO, (20.5% weight loss on starting material). Only CO and O_2 are identified by mass spectrometry, the major product being CO. The gaseous products, therefore, consist of 8XCO, $2XO_2$ and $4XH_2$.

From elemental analysis and the weight losses, the final residue is found to be $Zn_3Sn_4O_7$. Mössbauer analysis on the residue shows the majority of the Sn to be present as Sn(II) with a small amount of Sn(IV). The X-ray diffraction pattern is different to all the previous intermediates, however, seven lines coincide with lines for the product of the previous decomposition stage.

3.2.3. $Ni_3Sn_4(CHOO)_{14}.8H_2O$.

A four stage decomposition process is seen in the TG/DTA analysis of this complex, (Fig. 3.5), to leave a final residue of 61%.

Figure 3.5: TG/DTA traces for $Ni_3Sn_4(CHOO)_{14}.8H_2O$.

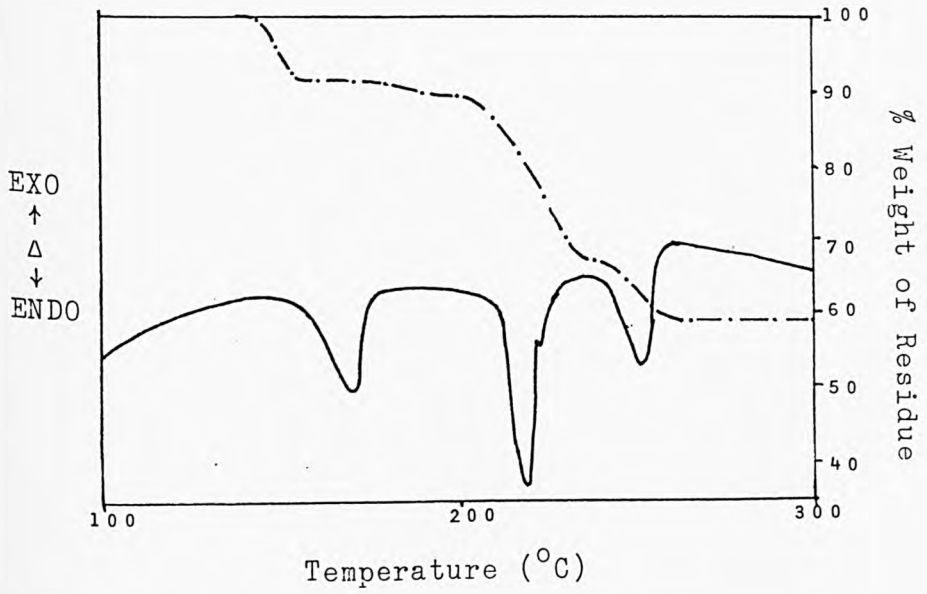

Figure 3.6. I.R. Data for $Ni_3Sn_4(CHO_2)_{14}.8H_2O$ Decomposition Products.

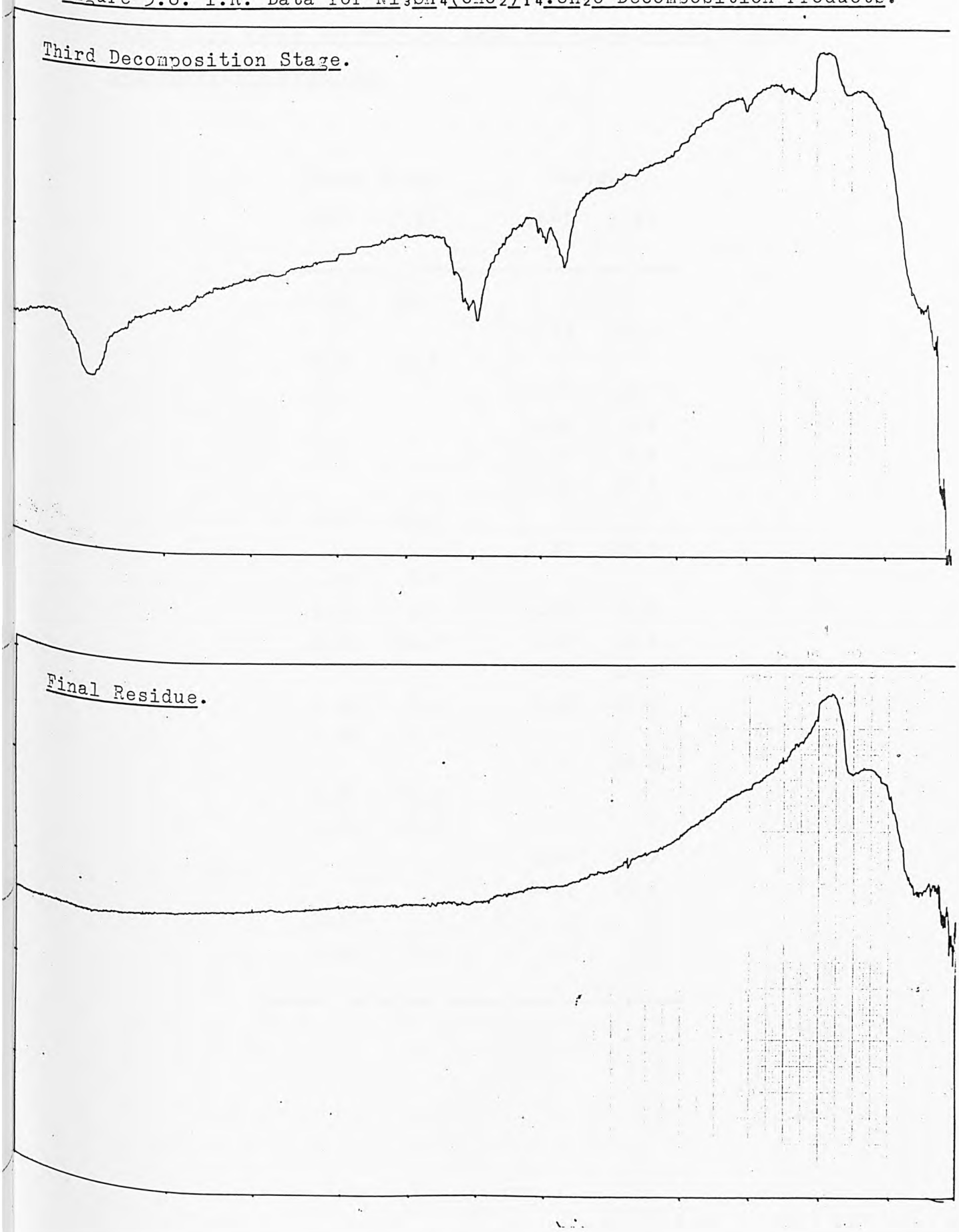

Table 3.5. X-Ray Diffraction data for $Ni_3Sn_4(CHOO)_{14}.8H_2O$ Decomposition Products.

Third Stage		Residue	
d(Å)	I(%)	d(Å)	I(%)
11.62	100		
		7.63	10.4
6.91	59.1		
		5.09	100
		4.85	5.2
		4.83	6.8
		4.64	38.9
4.52	15.3		
		4.22	15.3
4.10	6.8		
3.96	4.5	4.01	6.8
3.69	24.0	3.68	10.4
		3.60	11.8
3.41	9.0	3.38	20.4
3.36	5.8		
		3.21	33.9
3.02	38.3		
3.00	16.5		
		2.87	17.0
		2.65	20.1
2.58	7.3		
2.54	6.5		

First Two Stages. (144°C)

These first two stages involve dehydration of the starting material. The first stage is a weight loss of 7%, which on a weight basis corresponds to loss of five water molecules. This is verified by the elemental analysis results.

The second decomposition results in complete dehydration of the complex, giving a weight loss of 10% for removal of all water molecules, (theoretical weight loss 10.1%).

Third Stage. (215°C)

A weight loss of 23.5% is seen on the TG trace, which from the elemental analyses is due to loss of 8 X C, 8 X H, and 12 X O. The mass spectrometry results show only the presence of methanol and CO_2 in the volatile products from this decomposition.

The composition of the intermediate formed in this decomposition is $Ni_3Sn_4C_6H_6O_{16}$. The X-ray data for this intermediate are not the same as those for either the equivalent stages in the other complexes, or for the original Ni complex.

Fourth Stage. (246°C)

A weight loss of 15.8% is found in the TG trace for this decomposition, this is associated with loss of 6 X C, 6 X H, and 9 X O, which from the mass spectrometric analysis are lost as CO_2 and MeOH. From the weight loss and the elemental analyses, this ratio of CO_2:MeOH is 3:3.

The X-ray data on the residue are different to either the starting material or the previous intermediate.

Table 3.6. Elemental Analyses for $Ni_3Sn_4(CHOO)_{14}.8H_2O$ Decomposition Products.

	C(%)		H(%)	
	Calc.	Found	Calc.	Found
$Ni_3Sn_4(CHOO)_{14}.3H_2O$	12.58	12.62	1.51	1.22
$Ni_3Sn_4C_6O_{16}H_6$	7.31	7.47	0.61	0.35
$Ni_3Sn_4O_7$	0	0	0	0

Table 3.8. Elemental Analyses for $Co_3Sn_4(CHOO)_{14}.8H_2O$ Decomposition Products.

	C(%)		H(%)	
	Calc.	Found	Calc.	Found
$Co_3Sn_4(CHOO)_{14}$	13.11	12.96	1.10	1.27
$Co_3Sn_4C_6H_6O_{16}$	7.30	6.31	0.61	0.49
$Co_3Sn_4O_7$	0	0.50	0	0.03

3.2.4. $Co_3Sn_4(CHOO)_{14}.8H_2O$.

From the TG/DTA traces, (Fig. 3.7), this complex is seen to undergo a three stage decomposition to give a final residue of 56.5%.

Figure 3.7: TG/DTA traces for $Co_3Sn_4(CHOO)_{14}.8H_2O$.

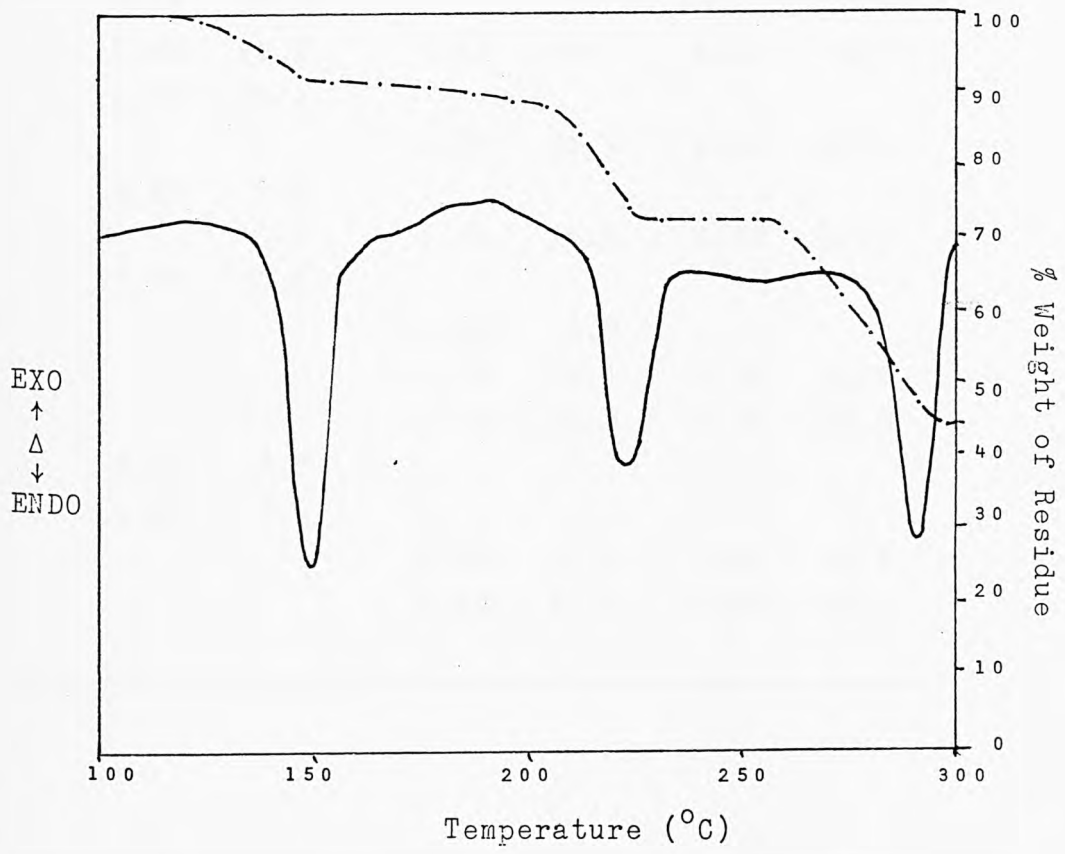

First Stage. (124°C).

A weight loss of 10% corresponding to the first decomposition step is seen in the TG trace. From the i.r. spectrum and carbon and hydrogen analysis results, (Fig. 3.8 and Table 3.8) this intermediate would appear to be the anhydrous starting material.

The X-ray data for this first intermediate are different

Table 3.7. X-Ray Diffraction data for $Co_3Sn_4(CHOO)_{14}.8H_2O$ Decomposition Products.

First Stage		Second Stage		Residue	
d(Å)	I(%)	d(Å)	I(%)	d(Å)	I(%)
11.62	100				
6.93	57.5				
6.68	10.9	5.11	100	5.11	100
4.89	29.1				
		4.65	36.5	4.64	28.4
4.43	7.5				
		4.24	16.8	4.23	12.9
3.77	37.5				
		3.49	8.9		
		3.38	15.1	3.38	14.0
		3.21	34.2	3.21	29.0
3.09	8.7				
3.05	7.8				
		2.87	35.9	2.87	26.9
		2.67	15.5	2.67	12.1

Figure 3.8. I.R. Spectra for $Co_3Sn_4(CHO_2)_{14}.8H_2O$ Decomposition Products.

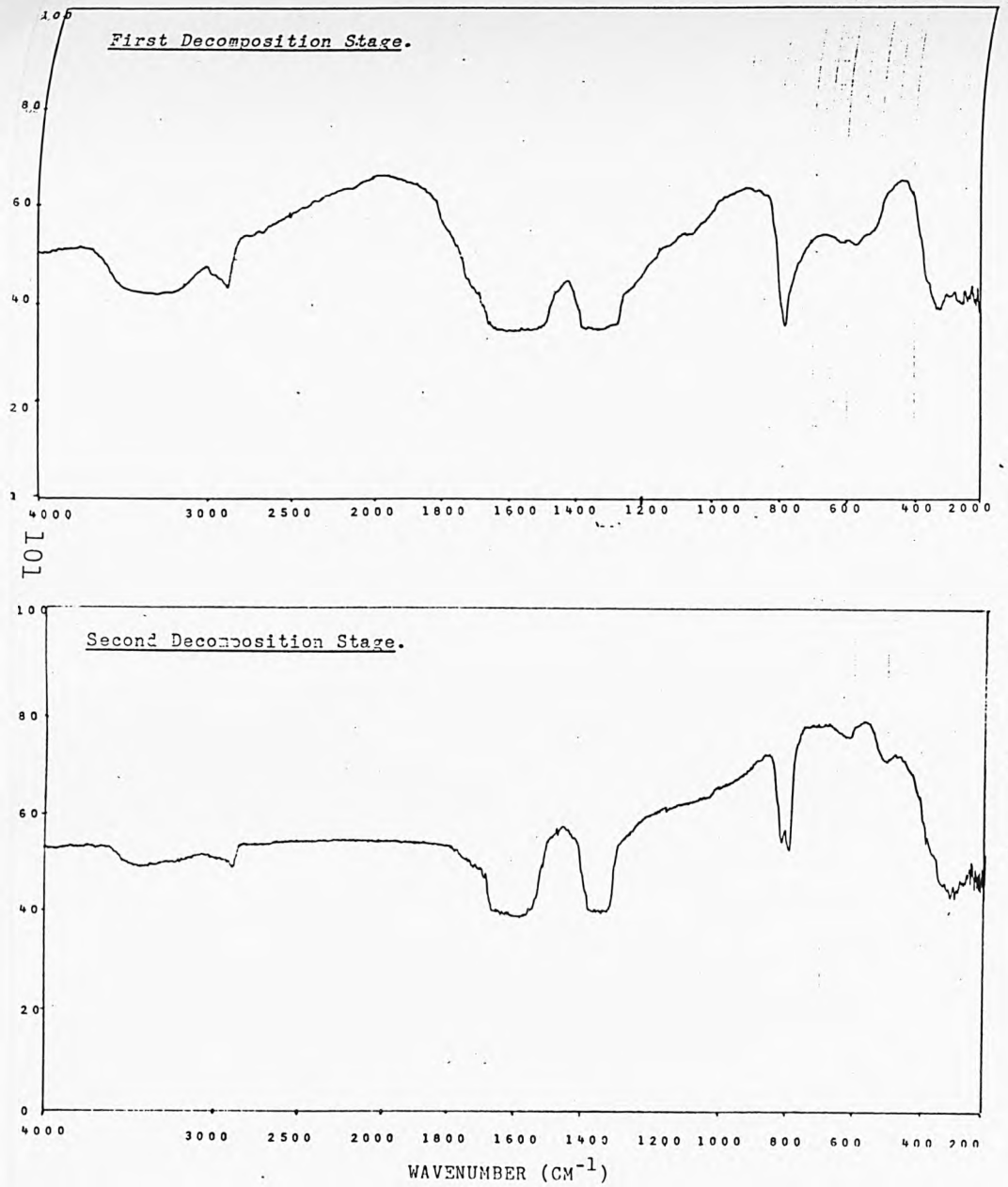

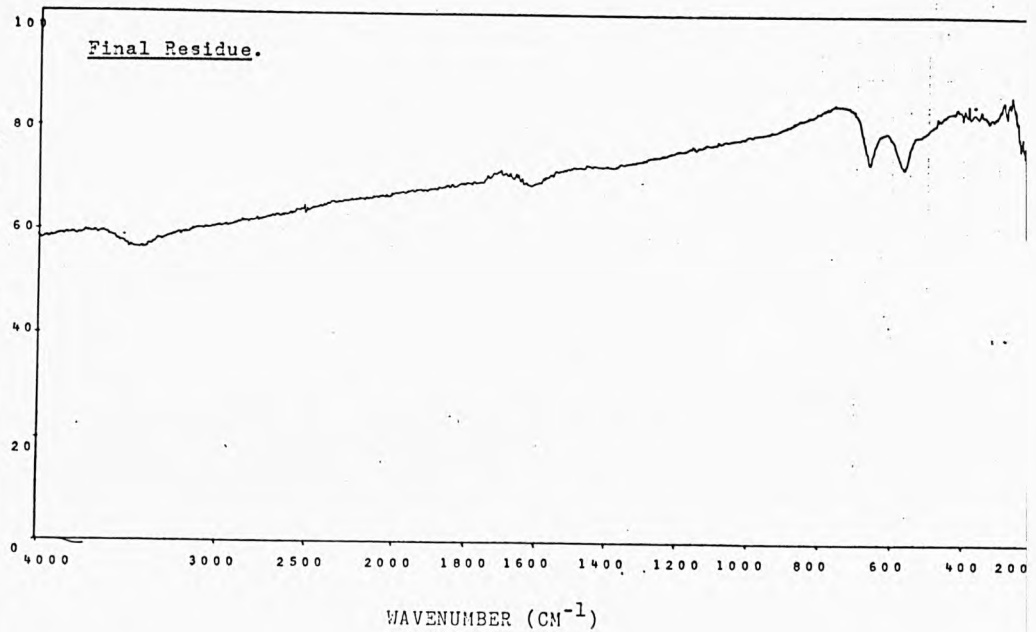

to those of the parent complex, although some lines do coincide, (Table 3.7).

Second Stage. (215°C)

A weight loss of 18% is found from the TG trace. Mass spectrometric analysis of the gaseous components of this decomposition show that the major product is acetone, with minor products acetic acid and O_2, traces of CO_2 and MeOH are also identified.

From the weight loss, and the elemental analyses, this intermediate is believed to have the following composition: $Co_3Sn_4C_6H_6O_{16}$, (theoretical weight loss 20.7%). The i.r. spectrum, (Fig. 3.8), of this intermediate again shows the presence of formate groups.

The X-ray data is distinct from the previous intermediate and also from the starting material.

Third Stage. (286°C).

This decomposition involves a weight loss of 16% and the removal of all organic components, (see elemental analyses), to leave a residue weight of 56%.

The mass spectrometry results show the gaseous products to comprise of CO and CO_2, (hydrogen is evolved as H_2 gas, 2.5 molecules produced).

The X-ray data has lines which are the same as in the other transition metal tin formate complexes, and virtually identical to those of the previous intermediate. However, the

pattern is different to both the starting material and the first intermediate. The final residue has the composition $Co_3Sn_4O_7$, (theoretical weight loss 15.5%), equivalent to 53.5% weight of the starting material.

3.3. Discussion.

The complex tin(ii) formates - $M_3Sn_4(CHOO)_{14}.8H_2O$, (M = Mn, Co, Ni, Zn) decompose thermally in three stages viz. (1) dehydration; (2) breakdown of all or part of the formate associated with the tin, and (3) decomposition of the remaining formate groups to give oxides. The gaseous products obtained from the pyrolyses do differ but this can be explained in terms of the different mechanisms of the formate decomposition and different gas phase reactions due to the presence of different oxide phases.

The first stage in the decomposition of all of the complex formates is dehydration. The Zn, Mn and Co derivatives lose water in one stage but differences in the strengths of the transition metal to water ligand bonds are reflected in the dehydration temperatures which are 100, 119 and 134°C, respectively, (published values, 90, 80 and 90°C) - TG traces Figs. 3.3, 3.1 and 3.7. The Ni complex loses water in two stages giving first a trihydrate at 144°C and then the anhydrous formate at about 190°C, (Fig. 3.5). The weight losses, product elemental analyses, (Tables 3.2, 3.6 and 3.8) all confirm that the final product of the first stage is the anhydrous complex formate - $M_3Sn_4(CHOO)_{14}$.

The x-ray diffractogramme powder patterns of the hydrated $M_3Sn_4(CHOO)_{14}.8H_2O$ clearly show that the Ni and Co compounds are isostructural and that the Mn and Zn compounds have lattices very similar to those of the Co and Ni derivatives. The powder data for the dehydrated materials also show that the anhydrous compounds $M_3Sn_4(CHOO)_{14}$ are isostructural for

M = Co and Ni, and that again the Zn and Mn derivatives have lattices closely related to those of the Ni and Co compounds.

The second decomposition stage involves breakdown of some of the formate groups present to metal leaving a formate as part of the solid residue. The number of formates decomposing and the metal to which they are attached do differ for the complexes and three distinct processes are found:

1) loss of six formate groups attached to tin atoms,
2) loss of eight formate groups attached to the transition metal
3) loss of eight formate groups attached to tin.

For the Mn and Zn complexes this decomposition step takes place at 204 and 195°C, respectively, with weight losses equivalent to decomposition of six formate groups to give metal oxides and gaseous products. Powder x-ray analysis of the residue at this stage clearly shows the presence of lines assignable to blue-black stannous oxide, and no lines assignable to Mn and Zn oxides. These results suggest that six of the eight formate groups associated with Sn breakdown in this decomposition step (q.v. decomposition temperature for $Sn(CHOO)_2$ between 195 and 200°C).

These results are explained in terms of two types of formate bonding in the Mn and Zn complexes - (1) six formate groups which are bonded to Sn only, and (2) eight formate groups which are bonded to the transition metal only and/or transition metal and tin. In the latter type the formate groups must be more strongly bound to the transition metal and hence remain undecomposed in the solid residue.

In the case where M = Ni, eight of the formate groups present brokedown at this stage at 215°C but no lines

assignable to SnO are found in the x-ray data (Table 3.5). This suggests again the presence of two different types of formate in the lattice viz. six formate groups attached to Sn and eight formate groups attached to transition metal and/or the transition metal and Sn, but in this case the formate groups bonded to the transition metal or the transition metal and tin decompose before those bonded only to tin. The presence of x-ray diffraction reflections due to NiO in the decomposition product are consistent with this proposed pyrolysis route for $Ni_3Sn_4(CHOO)_{14}.8H_2O$.

In the case of the Co complex, eight formate groups decompose at 211°C leaving six formate groups intact in the solid residue, (i.r. spectrum Fig. 3.8). The x-ray data for this intermediate clearly show the presence of SnO, and only one extra line assignable to the remaining Co species. For the Co complex, therefore the two types of formate present are the eight strongly associated with tin and the six strongly associated with the transition metal.

The different solid phases formed at this stage are found to have a profound effect on the gas-phase reactions taking place. The four complexes can be divided into two groups - (i) the Mn and Zn complexes and (ii) Ni and Co complexes. For the first group, the major gaseous product is CO, with CO_2, O_2 and H_2 identified as minor products. In the second group, no CO is evolved, and extensive gas-phase reactions occur resulting in the formation of more complex organic molecules.

For the Mn and Zn complexes the following two formate group decomposition mechanisms are proposed to take place simultaneously:

1) 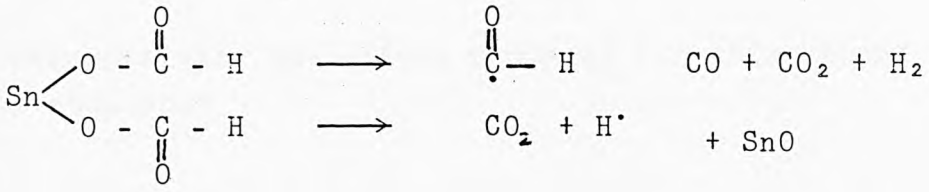

2) 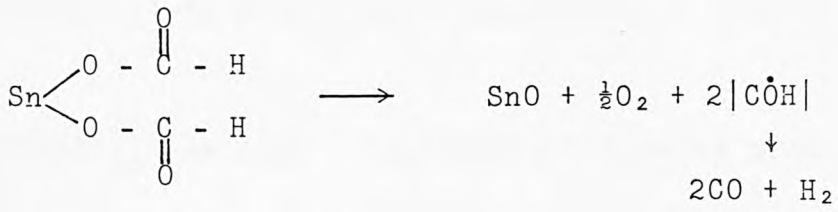

These mechanisms cannot however be used to explain the gaseous decomposition products for either the Ni or the Co complexes. For the Ni derivative the major gaseous products are MeOH and CO_2, and for the Co complex, a number of organic species are identified, (eg. acetone, acetic acid and MeOH). The following mechanism is suggested as the precursor to the reactions leading to all of these larger organic molecules:

3) 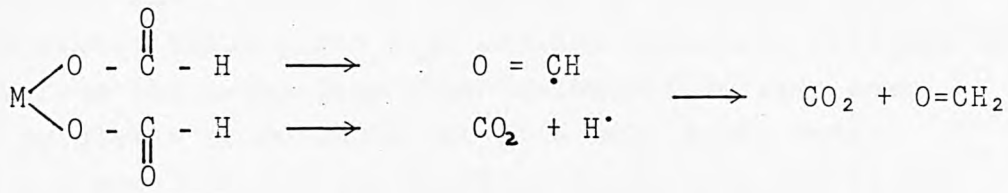

$H^{\cdot}$ radicals present in the vapour phase bring about further

reactions to give MeOH and larger organic molecules.

The decomposition mechanisms proposed for this second pyrolysis step are:

$$M_3Sn_4(CHOO)_{14} \longrightarrow 3SnO + M_3Sn(CHOO)_8 + |5CO + CO_2 + O_2 + 3H_2|$$

$$Ni_3Sn_4(CHOO)_{14} \longrightarrow 3NiO + SnO + Sn_3(CHOO)_6 + |MeOH + CO_2|$$

$$Co_3Sn_4(CHOO)_{14} \longrightarrow 4SnO + Co_3(CHOO)_6 + \text{Gaseous products.}$$

In the final decomposition step for all these complexes, the formate groups remaining from the previous stage are broken down to give a mixture of metal oxides and gaseous volatile products.

In the cases of the Mn, Zn and Co complexes, the decomposition temperatures obtained, (350, 262 and 281°C, respectively), are in good agreement with the pyrolysis temperatures for the corresponding metal formates to give metal oxide residues, (340, 270 and 315°C). The decomposition temperature for the Ni complex is 246°C, which is breakdown of stannous formate, but at a higher temperature than usually observed, (195-200°C). However, from the x-ray data this decomposition step does involve pyrolysis of $Sn(CHOO)_2$ to give SnO. X-ray data (Tables 3.4 and 3.3) for the final products from the Ni and Co complexes show only the presence of SnO and the transition metal oxide as the only major solid phases present, as would be expected from the subsequent breakdown of the suggested products from the second stage of the decomposition. SnO and MO are also the major products for the Zn and Mn systems although in the case of the Mn complex the x-ray

data do not preclude the presence of a distinct Mn-Sn oxide.

The weight losses observed in the TG traces (Figs. 3.1, 3.3, 3.5, and 3.7) are in very good agreement with formation of residues with the analytical composition $M_3Sn_4O_7$. The absence of any organic groups at this stage is verified by both the elemental analyses (Tables 3.2, 3.4, 3.6, and 3.8) and the i.r. spectra, (Figs. 3.2, 3.4, 3.6, and 3.8) and show that the final decomposition steps for these complexes are:

$$M_3Sn(CHOO)_8 + 3SnO \longrightarrow 4SnO + 3MO + \text{Gaseous products.}$$

(M = Mn, Zn)

$$Sn_3(CHOO)_6 + SnO + 3NiO \longrightarrow 4SnO + 3NiO + \text{Gaseous products}$$

$$Co_3(CHOO)_6 + 4SnO \longrightarrow 4SnO + 3CoO + \text{Gaseous products.}$$

An interesting feature of the results from studies on the gaseous products is the information provided on the catalytic activity of the transition metal and tin(II) oxides. The presence of nickel oxide in the second and third stage decomposition products leads to catalytic reactions in the gas-phase products with the production of methanol and other organic molecules. A lack of catalytic activity of tin(II) oxide is indicated by the fact that its presence as a second stage decomposition product in the pyrolyses of the Mn and Zn complexes does not lead to catalysed reactions in the gas-phase. The subsequent formation of MnO or a Mn-Sn oxide in the third stage decomposition of the Mn-containing complex does, however, lead to catalytic activity. The catalytic behaviour of the breakdown products

of $Co_3Sn_4(CHOO)_{14}$ is, however anomalous because the second stage product (SnO) does appear to show catalytic activity while the third stage product (CoO) does not. This observation suggests that the second stage process may not be simple formation of SnO but that probably minor amounts of a CoSn oxide are formed and that these act as catalysts of the gas-phase products of the second stage reaction.

3.4. Complex Tin Acetates.

In this section the thermal behaviour of complex tin acetates of the type $ASn(CH_3COO)_3.xH_2O$, (for A = Na, x = 1, for A = K and NH_4^+, x = 0), and $CaSn_2(CH_3COO)_6$, and thermal analytical techniques used to characterise decomposition products discussed. In section 3.5. the likely decomposition mechanisms are presented.

3.4.1. $NaSn(CH_3COO)_3.H_2O$.

No melting point is observed in the DTA trace of the Na complex, (Fig. 3.9). Decomposition occurs in three stages commencing at 84°C and complete by 500°C to leave a final residue weight of 51.5%.

Figure 3.9. TG/DTA trace for $NaSn(CH_3COO)_3.H_2O$.

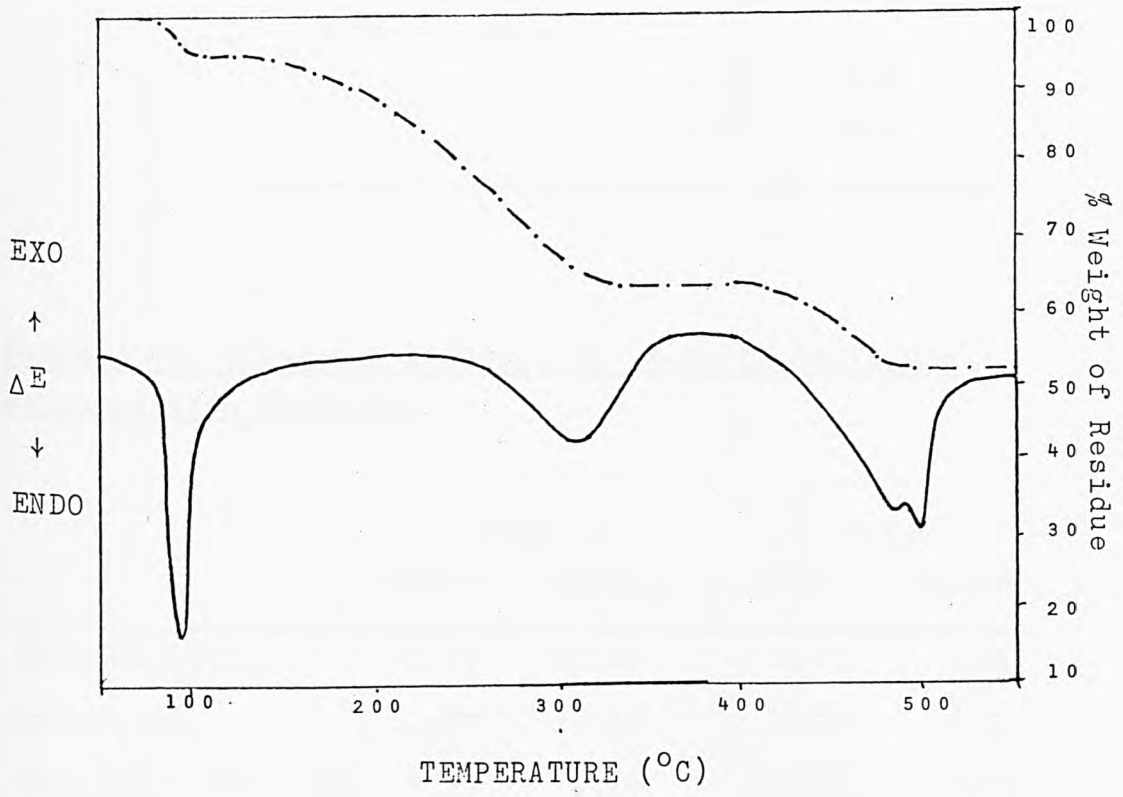

Table 3.9. X-ray Diffraction data for $NaSn(CH_3COO)_3.H_2O$ Decomposition Products.

First Stage		Second Stage	
d(Å)	I(%)	d(Å)	I(%)
		12.87	100
10.84	100		
9.42	37.2		
9.33	37.2		
8.76	46.2		
6.30	32.1		
5.98	39.7		
5.85	39.7		
5.50	37.2	5.59	7.8
		5.11	46.1
4.62	25.6	4.64	23.5
		4.35	7.0
		4.21	4.4
3.58	46.2		
		3.38	9.5
		3.20	12.6

Table 3.10. Elemental Analyses for $NaSn(CH_3COO)_3.H_2O$ Decomposition Products.

	C(%)		H(%)	
	Calc.	Found	Calc.	Found
$NaSn(CH_3COO)_3$	22.59	22.07	2.85	3.01
$NaSnC_2O_3H_3$	11.07	10.89	1.39	1.51
$\frac{1}{2}Na_2CO_3 + SnO + \frac{1}{2}C$	6.59	6.65	zero	zero

Figure 3.10 I.R. Spectra for $NaSn(CH_3COO)_3.H_2O$ Decomposition Products.

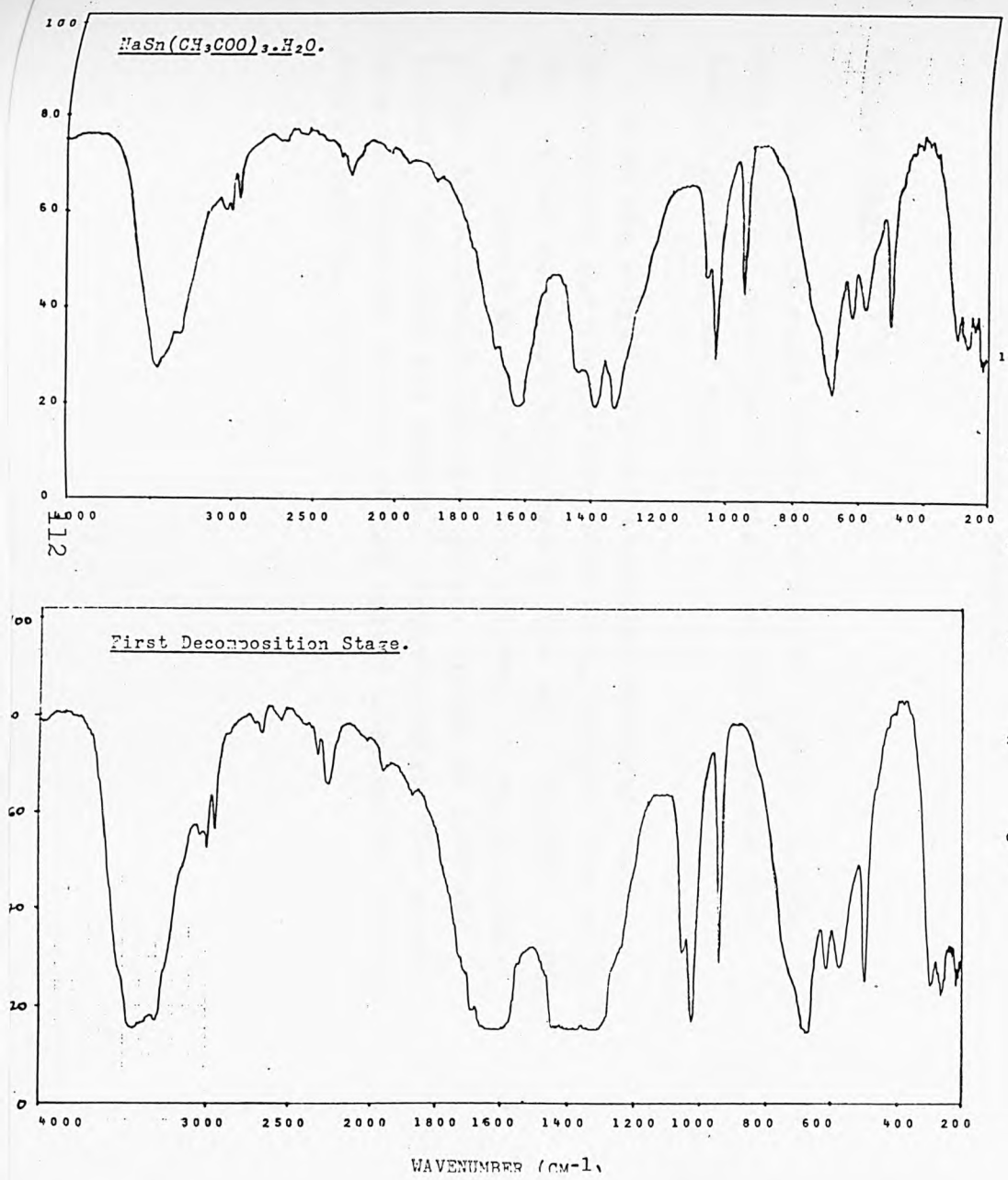

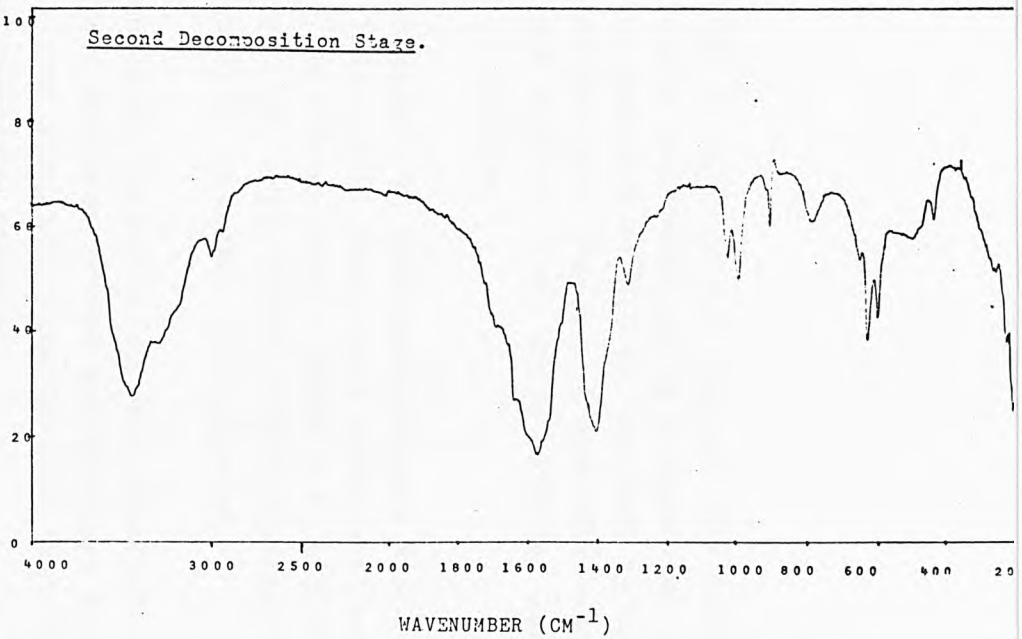

First Stage ($95^{o}C$)

The TG trace shows a 5.25% weight loss at this temperature, which in the large scale decomposition is accompanied by the evolution of H_2O. The presence of H_2O is verified by the use of self-indicating silica gel. Removal of one mole water is equivalent to a weight loss of 5.3%, which compares wery well with the experimental results.

The hygroscopic nature of this intermediate means that the i.r. spectrum, (Fig. 3.10) shows that water has been reabsorbed. However, the x-ray data. (Table 3.9) indicate that a transition from the crystalline complex hydrate to an almost amorphous anhydrous material has occurred.

The elemental analyses (Table 3.10) were obtained immediately after the intermediate had been formed and although a very little moisture has been absorbed, clearly show that this intermediate is the anhydrous complex.

Second Stage ($313^{0}C$)

This second stage involves a weight loss of 31.75%, which from the mass spectrometry results is due to the evolution of CO_2 and acetone.

From the weight loss and elemental analyses, this intermediate has the formula $NaSnC_2O_3H_3$, |weight loss 30.3%|. The evolved gases are therefore in the ratio $CH_3COCH_3 + CO_2$. The i.r. spectrum indicates the presence of carboxylate groups and aliphatic hydrogen atoms, (peaks at 1580 and $1417cm^{-1}$, and 2940 and $3000cm^{-1}$, respectively). The x-ray data is different to that of the parent complex and clearly shows lines due to SnO.

Third Stage (497°C)

In this decomposition a weight loss of 11% is observed, leaving a residue of 52%. The mass spectrometric analysis on volatiles indicates that only acetone is formed. This leaves a final residue with the composition $NaSnCO_{2.5}$, which agrees very well with the elemental analyses.

3.4.2. $KSn(CH_3COO)_3$.

The TG/DTA trace (Fig. 3.11) has a melting endotherm at 177°C, followed by a two stage decomposition to yield a residue weight of 62.7%.

Figure 3.11. TG/DTA Trace for $KSn(CH_3COO)_3$

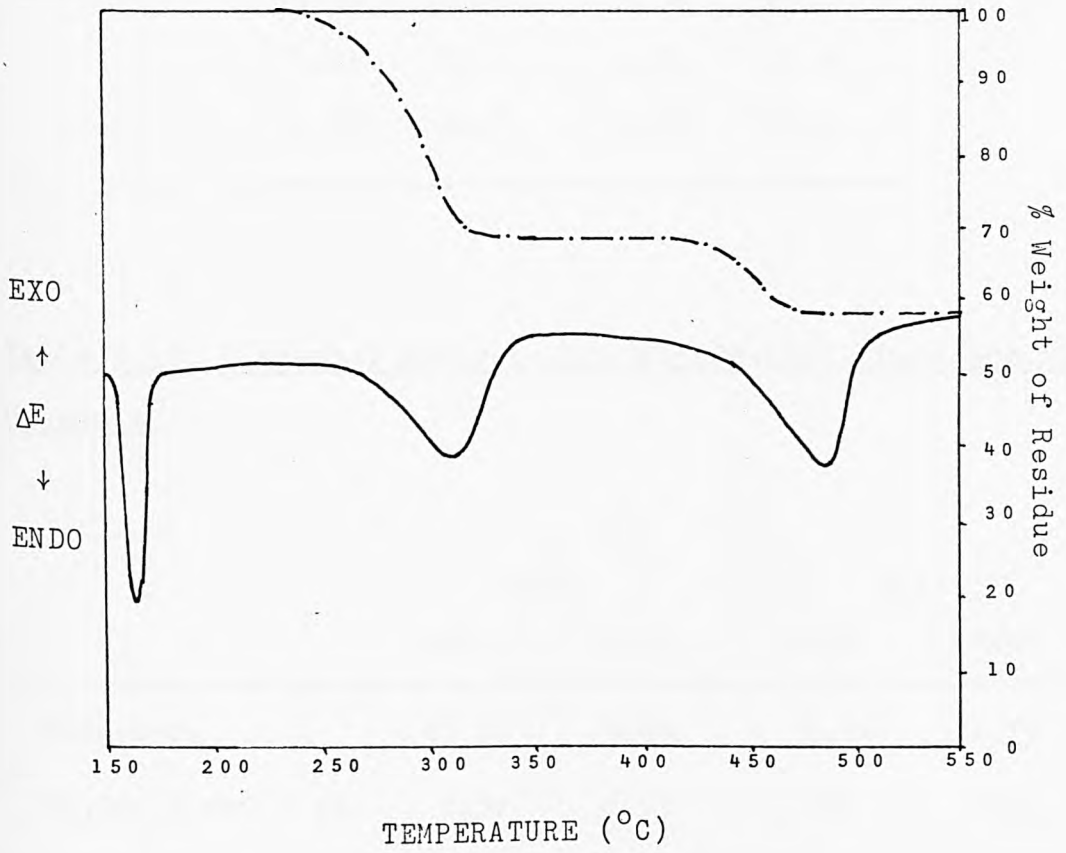

Table 3.11. X-Ray Diffraction data for $KSn(CH_3COO)_3$ Decomposition Products.

First Stage		Residue	
d(Å)	I(%)	d(Å)	I(%)
5.11	100	5.11	100
4.64	60.2	4.64	35.1
4.22	32.5	4.21	27.2
3.38	20.5	3.38	15.7
3.21	32.5	3.21	31.9
2.87	33.7	2.86	32.3

Table 3.12. Elemental Analyses for $KSn(CH_3COO)_3$ Decomposition Products.

	C(%)		H(%)	
	Calc.	Found	Calc.	Found
$KSnC_2O_3H_3$	10.31	9.96	1.30	1.57
$\frac{1}{2}K_2CO_3 + SnO + \frac{1}{2}C$	6.31	6.13	0	0.44

Figure 3.12: I.R. Spectra for $KSn(CH_3COO)_3$ Decomposition Products.

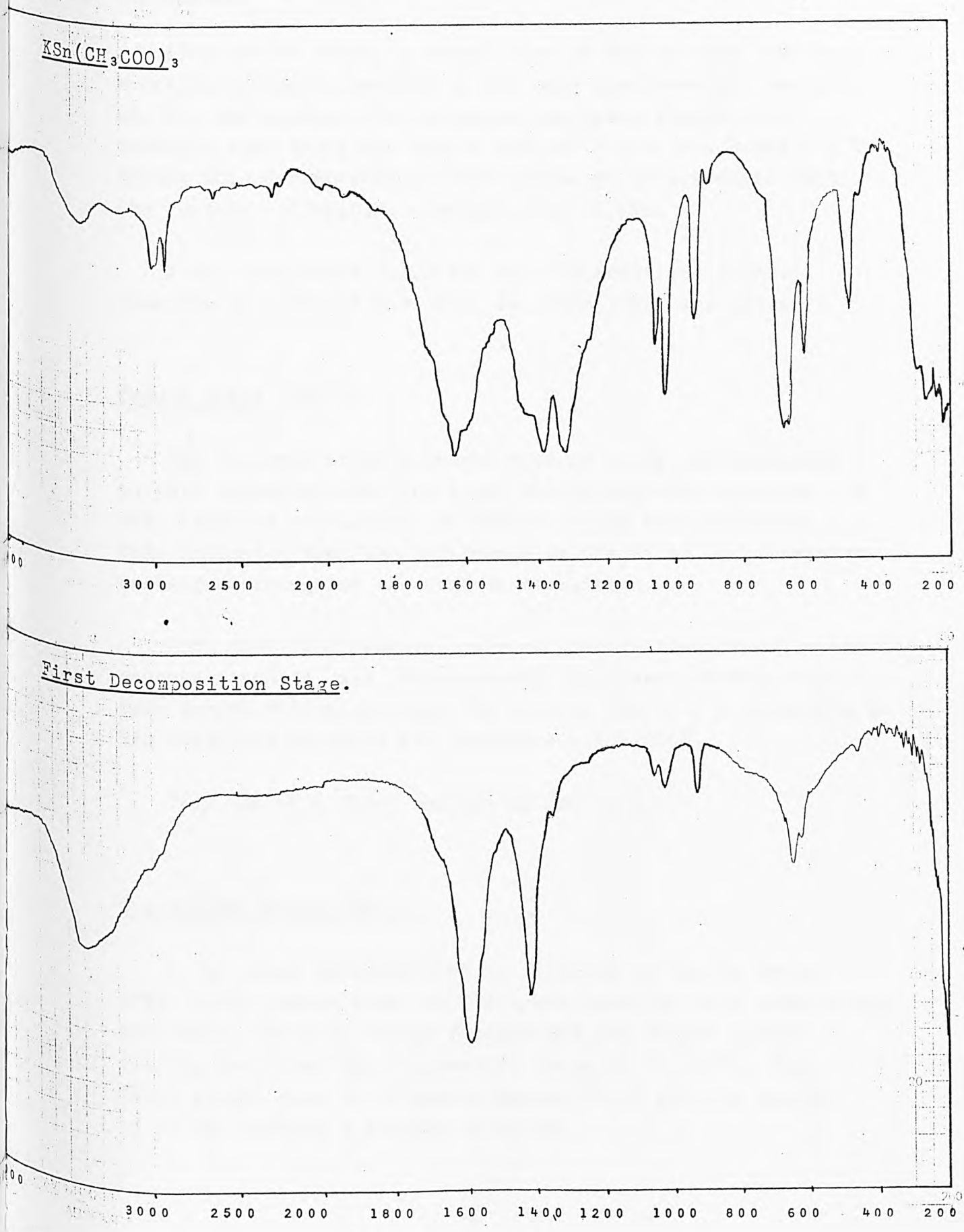

First Stage (320°C).

From the TG trace, a weight loss of 31% is seen, the only volatile products observed in the mass spectrometric analysis are CO_2 and acetone. The elemental analyses (Table 3.12) indicate that there has been a loss of 4 x C, 6 x H and 3 x O during this decomposition. This leaves an intermediate with the formula - $KSnC_2O_3H_3$ (weight loss 29.8%).

X-ray data(Table 3.11) for this intermediate clearly show the presence of SnO only, no other lines are present.

Second Stage (489°C)

The TG trace shows a weight loss of 10.5% corresponding to this decomposition. The x-ray diffractogramme contains the same lines as previously, no further lines have appeared. This indicates that the SnO formed in the first stage remains unchanged throughout the next decomposition.

From mass spectrometry, only acetone is identified in the gaseous products, and from elemental analyses, (Table 3.12) this decomposition involves the loss of $1\frac{1}{2}$x C, 3 x H and $\frac{1}{2}$ x O. The volatiles productd are therefore - $\frac{1}{2}CH_3COCH_3$.

This leaves a final residue of $SnKCO_{2.5}$.

3.4.3. $(NH_4)Sn(CH_3COO)_3$

A two stage decomposition is observed in the TG trace (Fig. 3.13), which from the DTA trace involves four endothermic processes. The four energy changes and two weight losses overlap and cover the temperature range 89 to 250°C. The first weight loss is of approximately 24.5% and the second of 33.7%, leaving a residue of 41.8%.

Figure 3.13. TG/DTA Trace for $(NH_4)Sn(CH_3COO)_3$

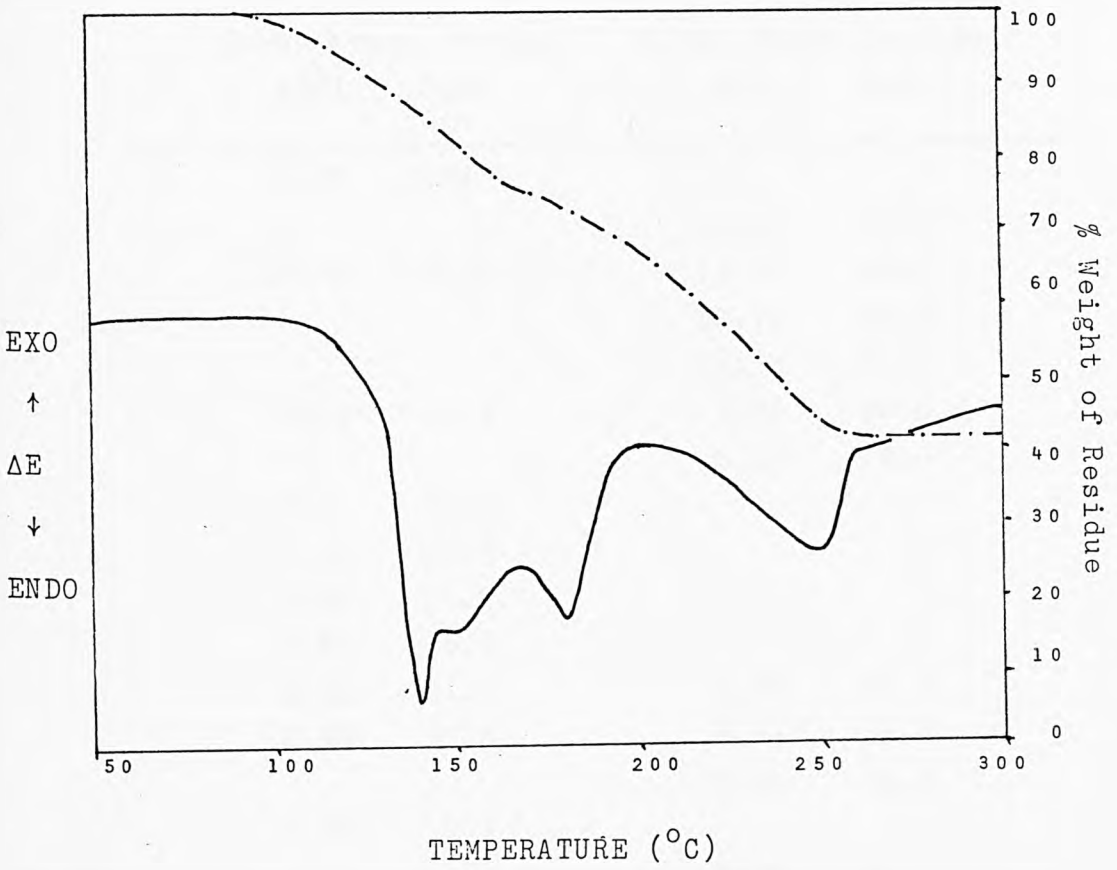

The mass spectrometry data on the volatile products show the presence of acetone, CO_2 and acetic acid. Using chemical means, evolution of NH_3 is observed. A gas chromatographic method was also employed to determine whether H_2 or CH_4 gases were being formed in the decomposition. No H_2 or CH_4 were identified.

The final residue collected was amorphous, so that no x-ray data could be obtained. Elemental analyses on the residue show that no organic groups remain. From the weight of the residue and the i.r. spectrum, (Fig. 3.14) however, this would appear to be SnO, (calculated weight of residue 42.9%, found 41.8%).

Table 3.13. X-Ray Data for $CaSn_2(CH_3COO)_6$ Decomposition Products.

First Stage (Probe)		First Stage (Residue)	
d(Å)	I(%)	d(Å)	I(%)
14.05	100		
		13.57	70.1
13.23	33.2	13.15	100
		12.72	94.8
		12.34	22.7
9.29	11.9	9.36	20.6
		8.43	18.6
8.12	34.6		
7.28	25.9		
6.59	14.2		
5.86	46.7		
5.81	44.9	5.82	25.8
5.60	37.5	5.61	16.0
		5.52	18.6
5.26	7.1		
		5.09	73.7
5.04	8.7		
4.97	9.0		
4.76	20.1		
		4.64	26.3
4.57	9.5		
4.31	11.9		
		4.20	15.5
4.04	13.2		
3.62	9.2		
3.57	22.7		
3.37	13.2		
3.21	6.1	3.20	19.6
3.16	6.6		
		2.96	18.6
		2.75	11.3

Figure 3.14: I.R. Spectra for $(NH_4)\ Sn(CH_3COO)_3$ Decomposition Products.

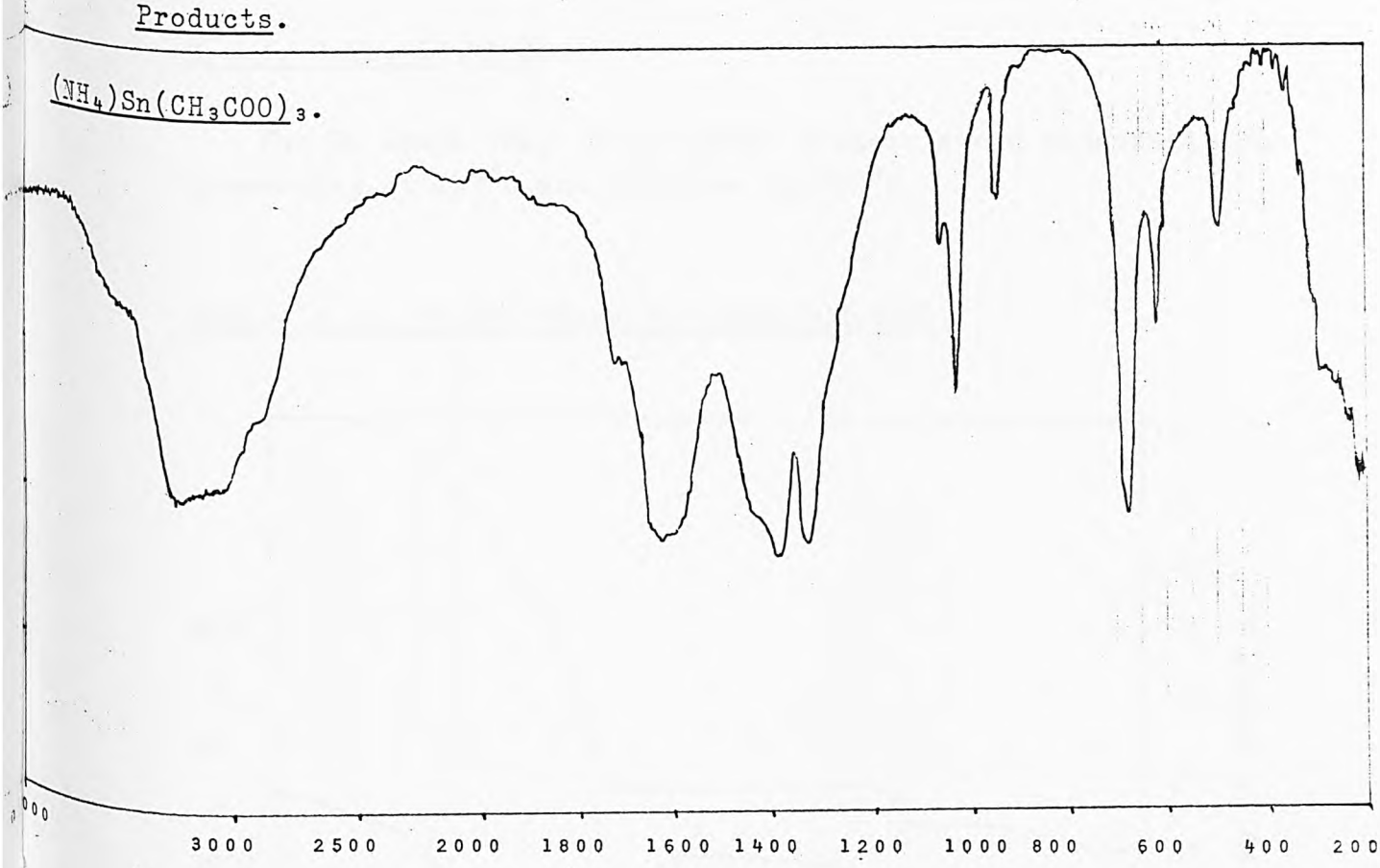

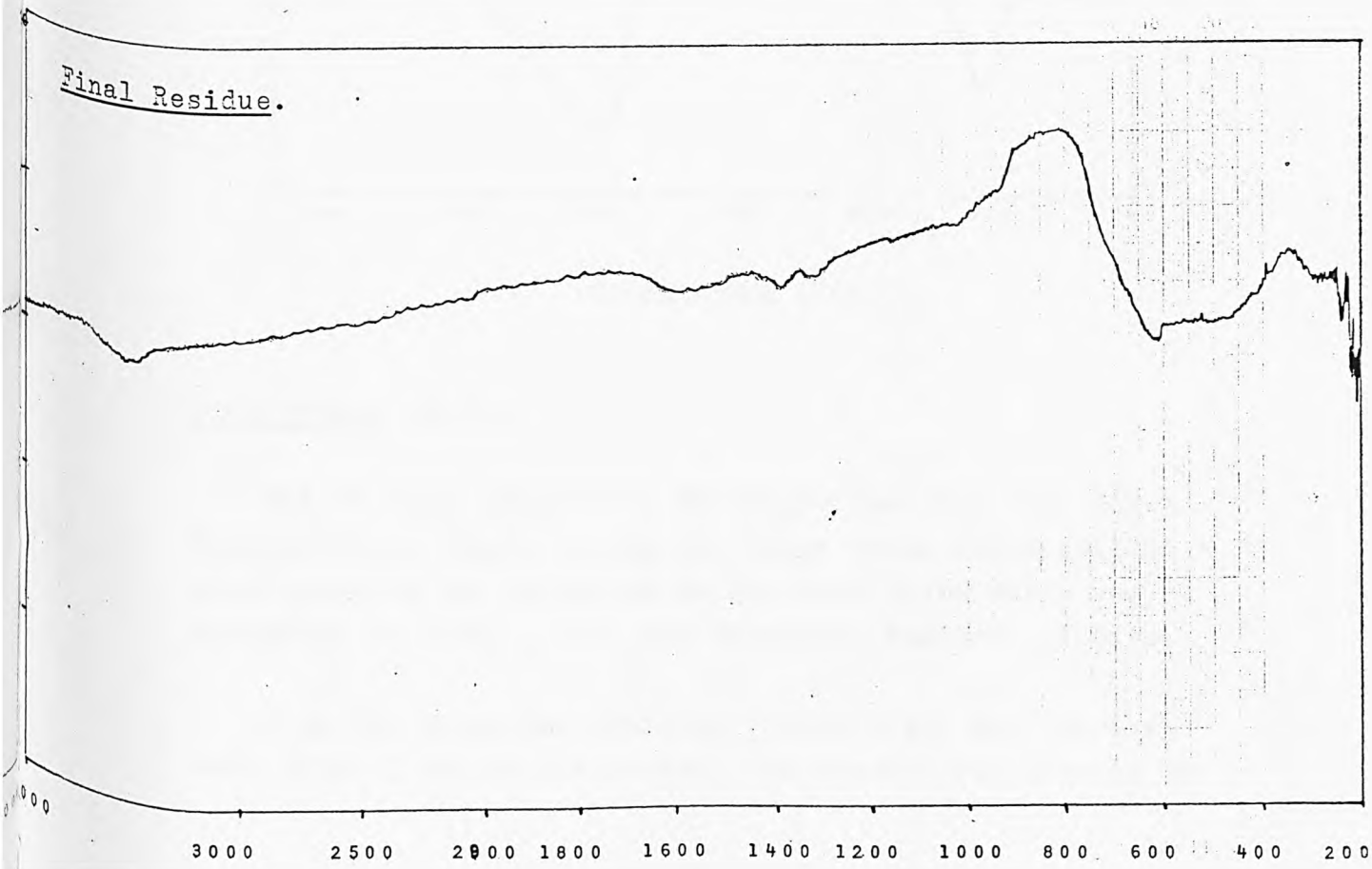

3.4.4. $CaSn_2(CH_3COO)_6$

The TG trace (Fig. 3.15) shows a three stage decomposition commencing at 217°C and complete by 500°C.

Figure 3.15. TG/DTA Trace for $CaSn_2(CH_3COO)_6$

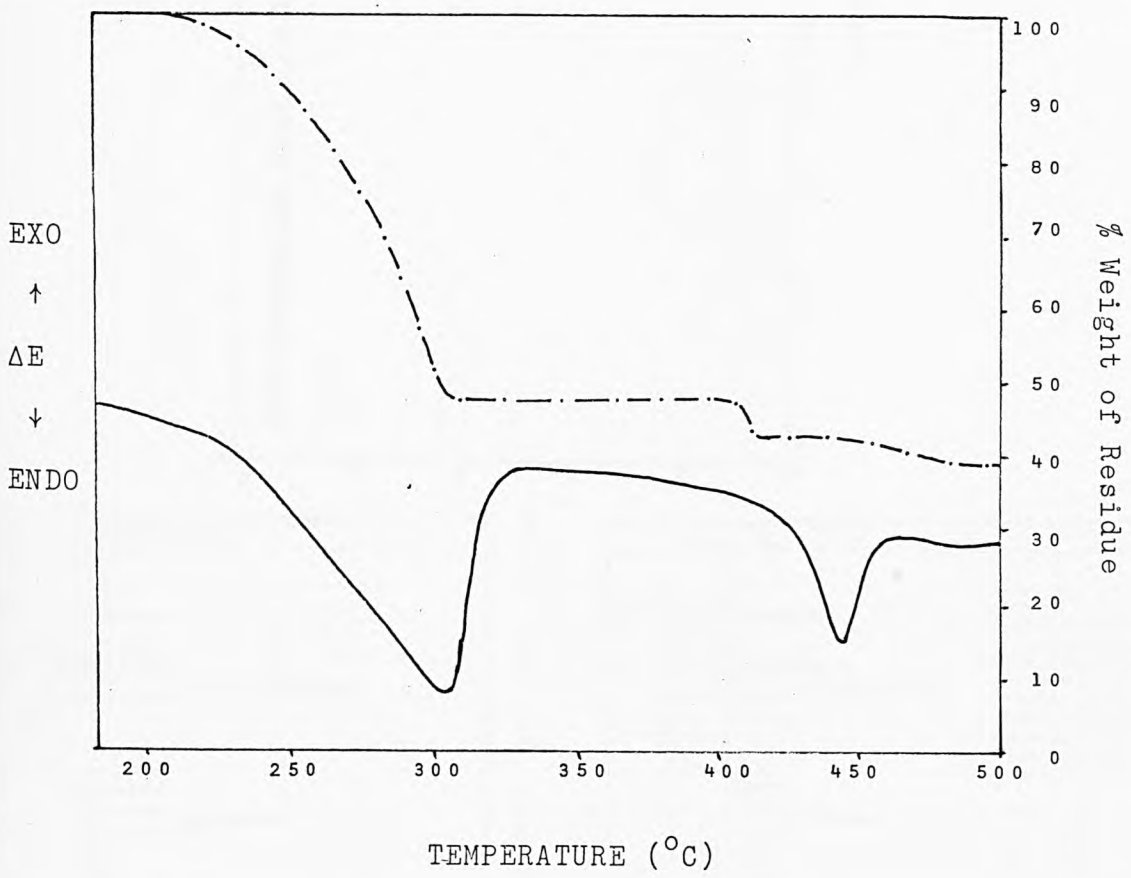

First Stage (316°C)

The TG trace shows a 51.8% weight loss for this first decomposition stage. During the large scale decomposition a solid product was collected on the cold probe which was subjected to x-ray , i.r. and elemental analyses studies.

From the elemental analyses (Table 3.14) and the i.r. data (Fig. 3.16) in particular, the product can clearly be

Figure 3.16. I.R. Spectra for $CaSn_2(CH_3COO)_6$ Decomposition Products.

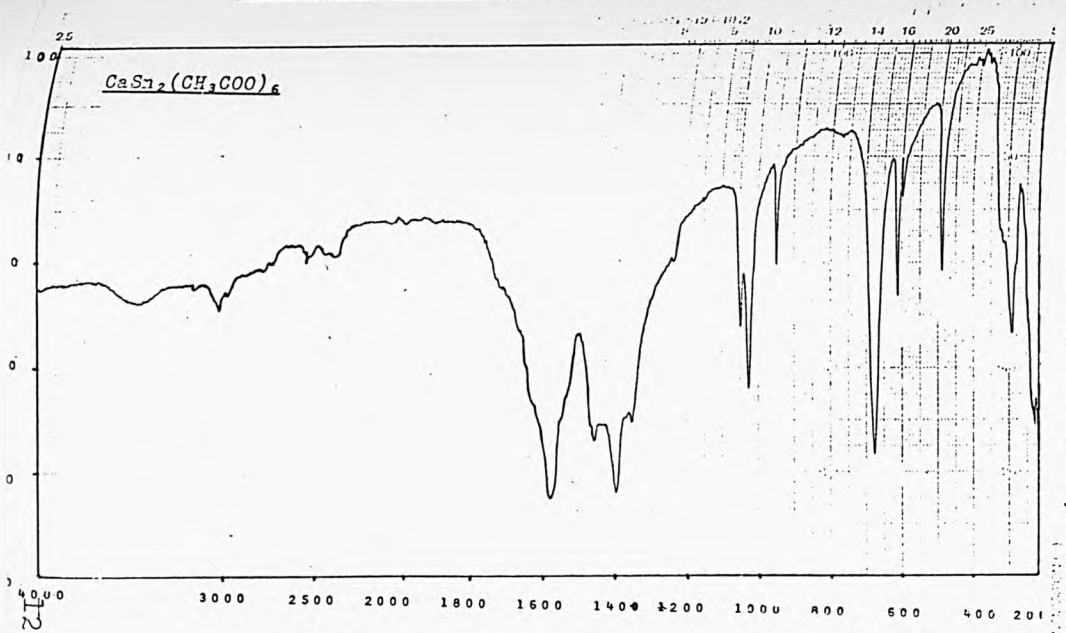

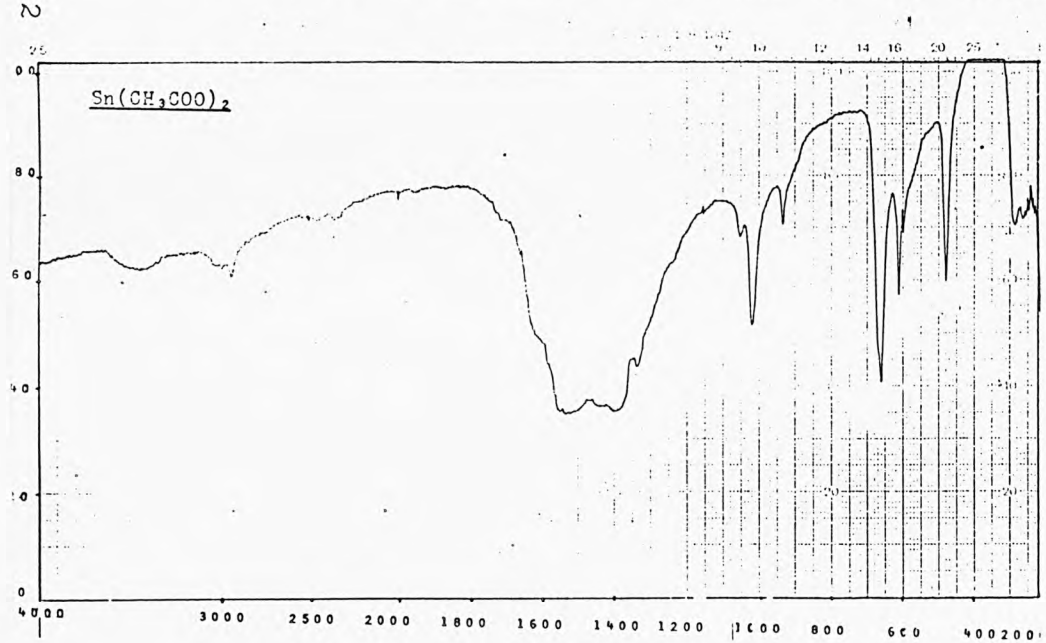

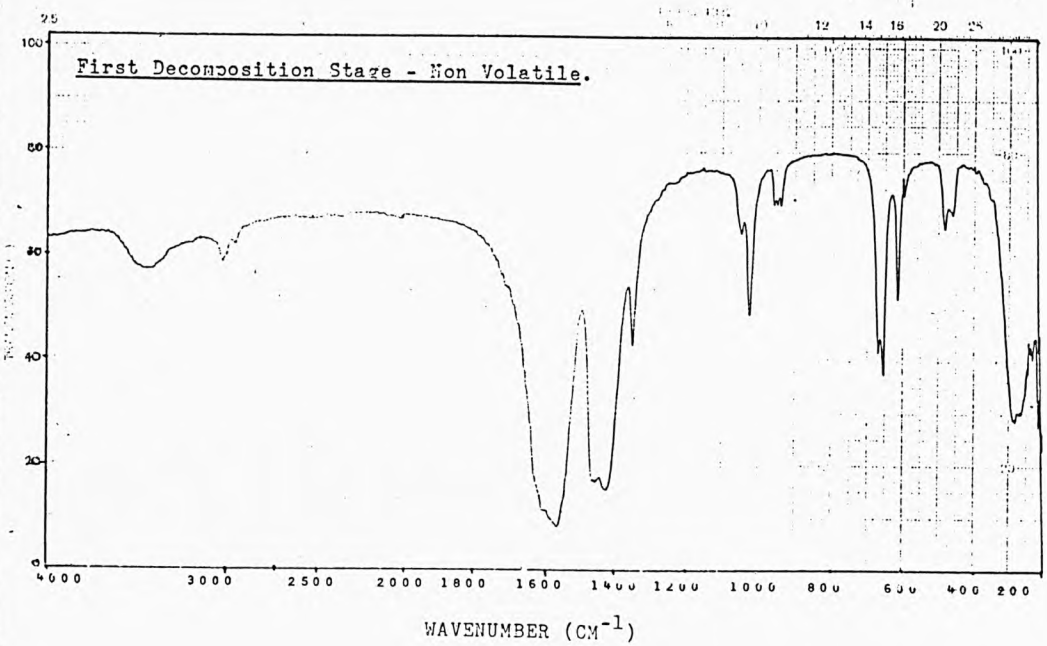

seen to be $Sn(CH_3COO)_2$. The i.r. spectra of the complex, the decomposition product, and $Sn(CH_3COO)_2$ are all very similar, however, the peaks at ca. 1050 and 1020cm^{-1} have a characteristic size relative to the other lines present. In both the decomposition product and $Sn(CH_3COO)_2$, the peak at 1050cm^{-1} is very small compared to the peak at 1020cm^{-1}. However, in the complex the peak at 1050cm^{-1} is 75% of the size of the other peak, due to the two CH_3 environments in the complex.

The residue remaining after loss of $Sn(CH_3COO)_2$ still has carboxylate group vibrational frequencies, although shifted slightly and of a different shape to those in the parent complex. Three overlapping peaks due to C - C stretching modes in the region of 950cm^{-1} have appeared, compared to the one, sharp peak in the parent complex at 950cm^{-1}.

The x-ray pattern at this stage (Table 3.13) is different to that of the parent complex and is seen to contain lines for blue-black stannous oxide.

The mass spectrometry data shows the presence of CO_2 and acetone. Based on the elemental analysis results and the TG trace, the first intermediate is believed to have the general formula - $CaSnC_4H_6O_5$. To form this intermediate the loss of $SnC_4H_{12}O_7$ has occurred, (calculated weight loss 53.6%).

Second Stage (439°C)

A weight loss of 6% is recorded in the TG trace, but the only gaseous product identified in the mass spectrometric analysis was C_2H_6.

The weight loss and elemental analyses indicate the loss of 2 x C and 6 x H to leave a residue of $CaSnC_2O_5$, which is equivalent to a weight loss of 4.8%.

Third Stage (456°C)

A weight loss of 3% is seen in the TG trace. The elemental analysis results show that there is 1.5 mole carbon in the residue and no hydrogen. These results are in good agreement with the formation of $CaCO_3$ + SnO + 0.5C in the final decomposition stage. The gaseous products are then $\frac{1}{2}$C and 1 x O, which is identified in the mass spectrometric analysis of the volatile decomposition prodcuts as CO_2.

Table 3.14. Elemental Analyses for $CaSn_2(CH_3COO)_6$ Decomposition Products.

	C(%)		H(%)	
	Calc.	Found	Calc.	Found
$Sn(CH_3COO)_2$	20.28	19.87	2.55	2.53
$CaSnC_4H_6O_5$	16.39	16.71	2.06	2.03
$CaCO_3$ + SnO + $\frac{1}{2}$C	7.48	7.70	zero	0.76

3.5. Discussion.

For the complex tin(II) acetates - $ASn(CH_3COO)_3$, (A = Na, K, and NH_4^+) and $CaSn_2(CH_3COO)_6$, only the Na salt $NaSn(CH_3COO)_3.H_2O$ is hydrated at room temperature. Dehydration of the Na complex takes place in a single step at 93°C, showing that water is weakly held in the lattice. The anhydrous species formed is extremely deliquescent and rapidly re-absorbs moisture from the atmosphere. The x-ray data for the anhydrous product are in Table 3.9. The x-ray patterns for the anhydrous Na, K and NH_4^+ derivatives - $ASn(CH_3COO)_3$, (A = Na, K, and NH_4^+) show that the compounds are not isostructural. Some lines in the x-ray patterns for each of the complexes do coincide, but no two of the complexes have very closely related parameters showing that the lattices of all three are different.

For the anhydrous Na, K and Ca compounds the first pyrolysis step involves breakdown of acetate groups associated with tin at 313, 320 and 316°C, respectively, followed by decomposition of the acetates associated with the alkali metal. The similarity in the decomposition temperatures of the first pyrolysis step for the Na, K, and Ca complexes implies very similar tin - acetate bond strengths.

In the case of the Ca complex, only one of the tin - acetate groups decomposes to give SnO and gaseous products in the first decomposition stage, the other tin - acetate group volatilises intact and the solid sample collected on the cold probe is identified as $Sn(CH_3COO)_2$, (elemental analyses Table 3.14). This implies that two different types of stannous acetate group are present in the complex - one which is bonded only to the Sn, the other which is bonded to both the Ca and Sn, but more strongly to the tin.

The x-ray patterns for the solid residues from this

decomposition stage show, in all cases, the presence of blue-black SnO. For the potassium derivative the only x-ray lines seen are those of SnO, showing that the K species present is amorphous. Both the Na and Ca decomposition products contain lines for SnO and other lines which are not related to any of the original lines for the parent conplexes, but are identified as being due to the presence of alkali metal and alkaline earth metal acetates in the residue. The presence of these acetates is also confirmed by their i.r. spectra, (Figs. 3.10, 3.12 and 3.16) and the elemental analyses, (Tables 3.10, 3.12 and 3.16).

The mass spectrometric analysis of the gaseous products from this decomposition stage identified $CH_3COCH_3 + CO_2$ as the gaseous products in all three cases. This suggests that the same pyrolysis mechanism is taking place for all three complexes and that the different solid residues have the same effect on gas-phase reaction. The mechanism for breakdown of the $Sn(CH_3COO)_2$ group in each case is:

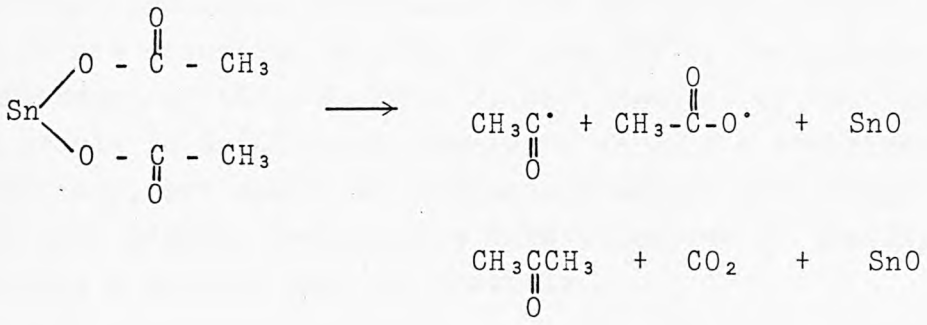

This gives an overall decomposition reaction for the anhydrous Na and K complexes of:

$$ASn(CH_3COO)_3 \longrightarrow CH_3COOA + SnO + CH_3COCH_3 + CO_2$$

(A = Na and K)

and for the Ca derivative:

$$CaSn_2(CH_3COO)_6 \longrightarrow Ca(CH_3COO)_2 + SnO + Sn(CH_3COO)_2\uparrow + CH_3COCH_3 + CO_2$$

In the case of the ammonium complex, the tin - acetate portion does not decompose first, but follows after the breakdown of the ammonium acetate present. In the TG trace (Fig. 3.13) the two pyrolysis steps cannot be separated, however the percentage weight losses for the two processes show that the ammonium acetate group decomposes first at 139°C. The DTA trace for this stage shows that three endothermic processes associated with the single weight loss of 24.5% are occurring at 139, 151 and 179°C, (calculated for breakdown of $(NH_4)CH_3COO$ - 24.6%). Removal of CH_3COONH_4 would result in $Sn(CH_3COO)_2$ remaining as only a transient intermediate, but since the subsequent weight loss stage occurs at a similar temperature identification of tin(II) acetate as a product was not possible.

The gaseous products observed at this stage are ammonia and acetic acid and these result from pyrolysis of the ammonium acetate group via the mechanism:

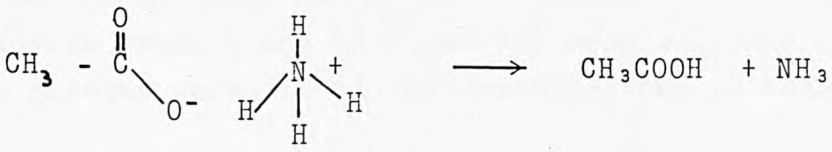

$$\longrightarrow CH_3COOH + NH_3$$

The final decomposition stage for the Na, K and NH_4^+ complexes and the second stage for the Ca complex involve decomposition of the remaining acetate groups associated with the alkali and alkaline earth metal. These processes take place at higher temperatures, (490, 489 and 439°C, respectively), that are similar to the published values for thermal decomposition of the acetates, viz. 500, 495 and 420°C for CH_3COONa, CH_3COOK and $Ca(CH_3COO)_2$, respectively. Breakdown of the transient intermediate product for the ammonium complex occurs at low temperature (248°C) as would be expected if the intermediate was $Sn(CH_3COO)_2$. Elemental analyses were obtained on the Na and K residues, and together with the weight losses are in good agreement with formation of only 1 mole Na and K carbonate, and ½ mole carbon. The mass spectrometric analysis of volatile products show only the presence of small amounts of acetone.

For the ammonium derivative, a weight loss of 33.7% is obtained in this final stage and this agrees well with breakdown of $Sn(CH_3COO)_2$ to give SnO (calculated weight loss 32.5%). The gaseous products observed during this decomposition - CH_3COCH_3 and CO_2, are the same as those observed in the pyrolysis reactions for the other acetates, which were assigned to decomposition of the acetate groups associated with Sn. The final solid product did not show any x-ray diffraction lines consistent with the formation of amorphous SnO.

The weight loss at this third stage for the Ca complex (6%) is too small to be explained in terms of a mechanism involving formation of $CaCO_3$ (calculated weight loss 11.6%). In agreement with the reported decomposition of pure $Ca(CH_3COO)_2$, a mechanism must involve formation of CaC_2O_4, C and H (weight loss 4.8%). It is significant that the two stage mechanism would result in the release of ethane as the gaseous product and this was the only molecule identified in the gaseous products of the decomposition at this stage.

The final stage in the decomposition of $CaSn_2(CH_3COO)_6$ occurs at 460°C, (published value for decomposition of CaC_2O_4 - 460°C), with a weight loss of 3%. The final residue collected has the formula $SnCaC_{1.5}O_4$, (calculated weight loss 3.5%, elemental analyses Table 3.14), which is a mixture of SnO, $CaCO_3$, and C. The mass spectrometric analysis of volatile gases shows only the presence of CO_2, in agreement with the following disproportionation reaction:

$$CO \longrightarrow \tfrac{1}{2}CO_2 + \tfrac{1}{2}C\downarrow$$

ie. the final decomposition reaction for $CaSn_2(CH_3COO)_6$ is:

$$SnO + CaC_2O_4 \longrightarrow SnO + CaCO_3 + \tfrac{1}{2}C + \tfrac{1}{2}CO_2$$

For the anhydrous Na and K compounds, thermal decomposition follows the same route to give an overall decomposition sequence of :

$$ASn(CH_3COO)_2 \longrightarrow SnO + CH_3COOA \longrightarrow SnO + \tfrac{1}{2}A_2CO_3 + \tfrac{1}{2}C$$
$$+ CH_3COCH_3 + CO_2 \qquad + \delta\text{acetone}$$

(for A = Na, K)

For the ammonium derivative the decomposition scheme proposed is:

$$(NH_4)Sn(CH_3COO)_3 \longrightarrow Sn(CH_3COO)_2 \longrightarrow SnO + CH_3COCH_3 + CO_2$$
$$+ NH_3 + CH_3COOH$$

and for the Ca complex:

$$CaSn_2(CH_3COO)_6 \longrightarrow Ca(CH_3COO)_2 + SnO \longrightarrow CaC_2O_4 + SnO + Sn(CH_3COO)_2\uparrow + CH_3COCH_3 + C_2H_6 + CO_2$$

$$\longrightarrow CaCO_3 + SnO + \tfrac{1}{2}CO_2$$

3.6. Complex Tin Oxalates.

In this section results of the thermal decomposition of complex tin oxalates of the type - $A_2Sn(C_2O_4)_2.xH_2O$, (for A = Na, x = 0, for A = K, x = 1), and $CaSn(C_2O_4)_2.H_2O$ are presented. The analytical techniques used to characterise the products are discussed in this section and the mechanisms proposed for the decomposition pathways presented in section 3.7.

3.6.1. $Na_2Sn(C_2O_4)_2$

The TG/DTA studies (Fig. 3.17) show that decomposition of the sodium complex commences at 307°C and terminates at 536°C with a residue weight of 28.5%. Decomposition takes place in three stages, with weight losses of 59.5, 6 and 6% for first, second and third stages, respectively.

Figure 3.17. TG/DTA Trace for $Na_2Sn(C_2O_4)_2$

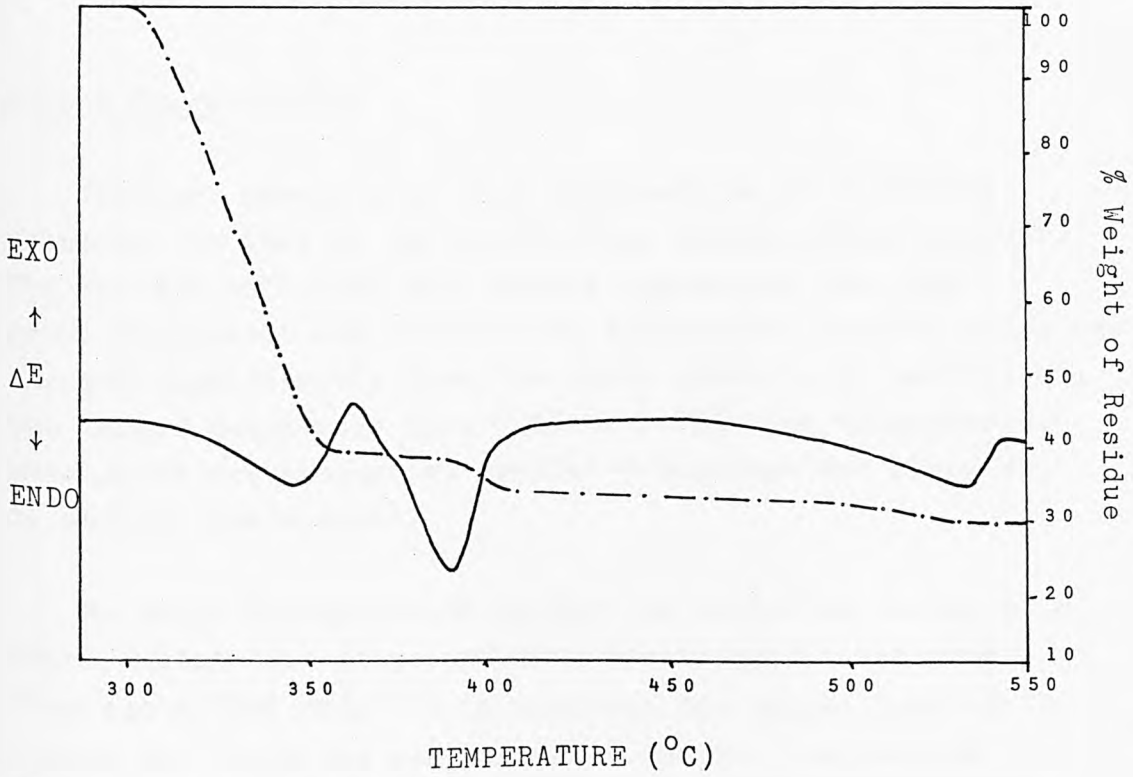

First Stage (323°C)

The i.r. spectrum of this first intermediate (Fig. 3.18) shows little change from that of the starting material, except that the oxalate group frequency at 382cm^{-1} is less distinct.

The residue collected at the end of this decomposition shows a marked colour change from white in the parent complex to orange-red at this stage. The x-ray data (Table 3.15) is a little different, several of the weaker bands are missing and there is a slight shift in the d-spacings.

From the mass spectromteric analysis, the only evolved gas which could be identified was CO_2. Together with the CO_2, a small quantity of a solid product was collected on the cold probe and subsequent tin analysis of the residue showed that most of the tin had volatilised. The tin analyses agree that only 0.25 mole Sn is present in the residue, to give a composition of $Na_2Sn_{0.25}C_{1.5}O_{2.75}$, (calculated weight loss 59.6%, weight loss found 59.5%).

Second Stage (378°C)

The i.r. spectrum of this intermediate is virtually identical to that of the first stage decomposition product. The residue collected is a darker orange-red than the previous product and has a x-ray diffraction pattern which has changed significantly from the first product. In particular, the larger d-spacings from 7.65 to 5.75Å have disappeared, more lines are present at smaller d-spacings and lines due to SnO are now present.

No solid decomposition product is collected on the cold probe during this stage and mass spectrometric analyses show again that only CO_2 is evolved. The weight loss of 7% agrees well with the removal of $\frac{1}{2}C$ and $\frac{3}{4}O$, (calculated

Figure 3.18. I.R. Spectra for $Na_2Sn(C_2O_4)_2$ Decomposition Prosucts.

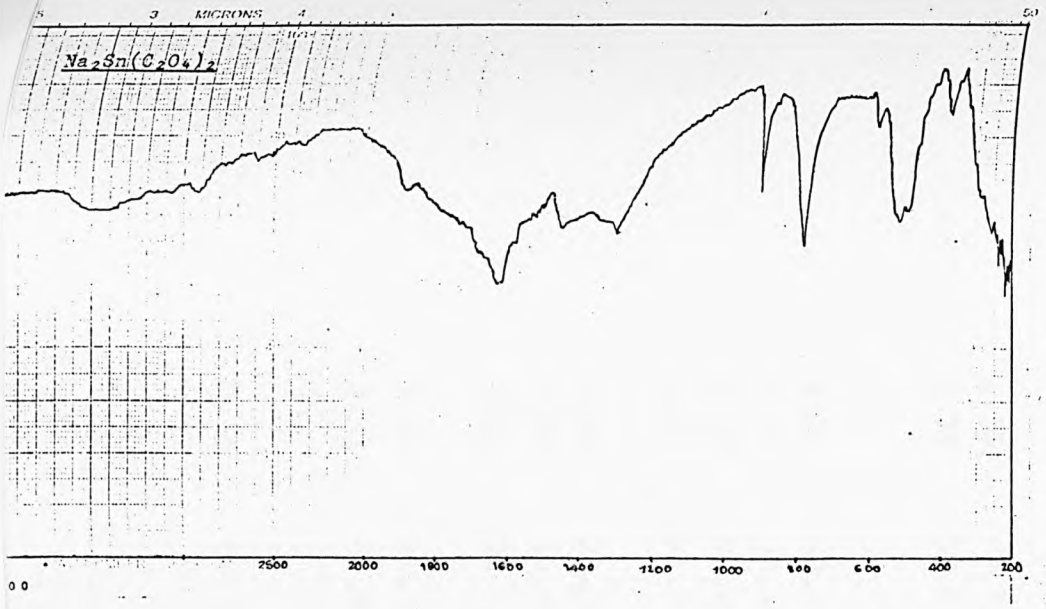

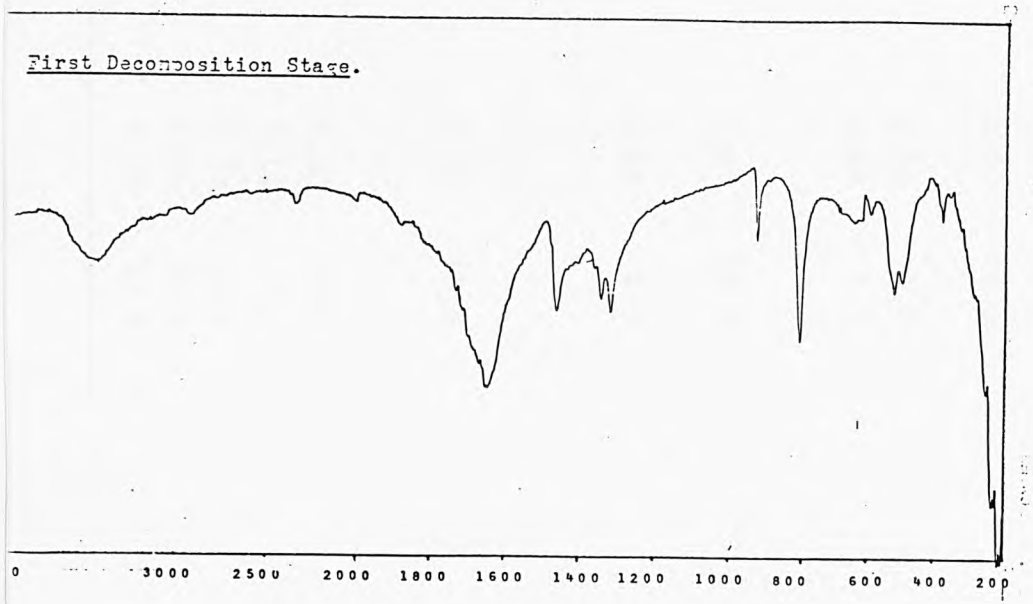

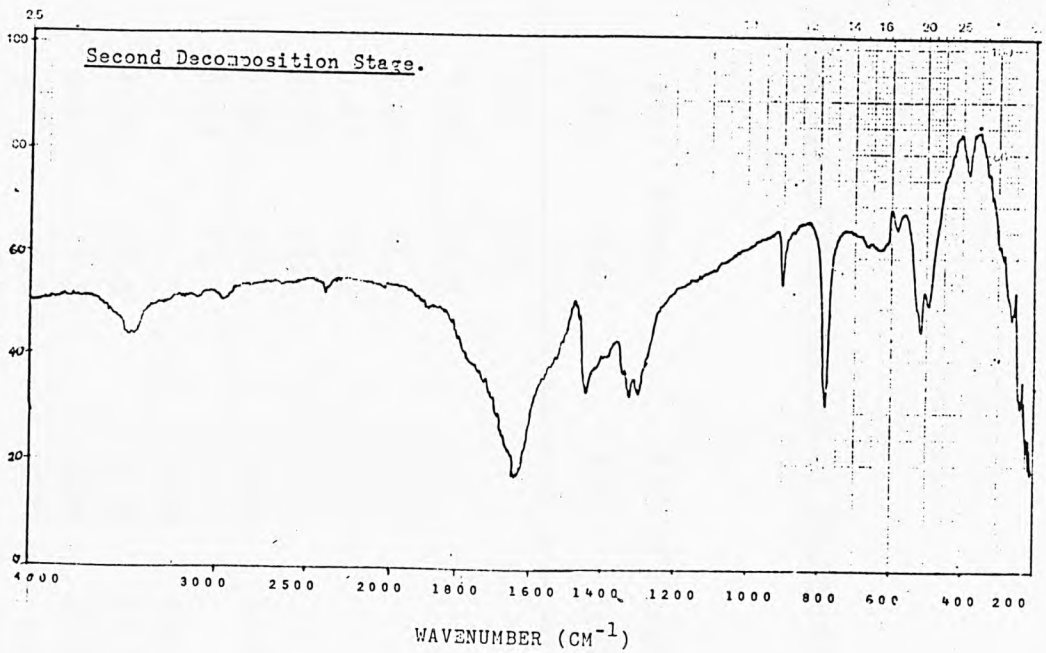

Table 3.15. X-Ray Data for $Na_2Sn(C_2O_4)_2$ Decomposition Products

First Stage		Second Stage	
d(Å)	I(%)	d(Å)	I(%)
7.65	100		
7.49	33.9		
7.04	55.0		
5.88	52.3		
5.75	28.4		
5.52	20.2	5.52	12.0
5.13	77.1		
		5.08	100
5.00	50.5	4.96	13.3
4.87	27.5	4.85	27.8
4.75	46.8	4.74	7.0
		4.66	33.5
4.51	59.6	4.50	10.4
4.31	57.8		
		4.24	6.6
		4.21	8.9
4.15	50.5		
4.11	30.3		
4.03	28.4	4.07	10.8
3.95	27.5		
		3.83	8.9
3.75	27.5		
3.55	19.3		
3.44	54.1		
		3.37	10.8
3.32	26.7		
3.24	26.6		
		3.20	23.1
		3.14	9.2
2.95	28.4	2.95	5.4
		2.86	31.3
		2.67	13.6

weight loss 5.3%), which is verified by the elemental analyses (Table 3.16). This leaves a residue with the formula $Na_2Sn_{0.25}CO_2$.

Third Stage (390°C).

The weight loss during this final decomposition would again agree with the loss of $\frac{1}{2}C$ and $\frac{3}{4}O$, which is also verified by the elemental analyses which indicate a final residue of $Na_2Sn_{0.25}O_{1.25}C_{0.5}$.

Table 3.16. Elemental Analyses for $Na_2Sn(C_2O_4)_2$ Decomposition Products.

	C(%)		H(%)		Sn(%)	
	Calc.	Found	Calc.	Found	Calc.	Found
Probe Sample	11.61	11.39	0	0.18	57.42	57.28
$Na_2Sn_{0.25}C_{1.5}O_{2.75}$	13.07	13.57	0	0.44	21.55	21.33
$Na_2Sn_{0.25}CO_2$	10.20	9.90	0	0.10	25.15	24.98
$Na_2Sn_{0.25}C_{0.5}O_{1.25}$	6.02	6.24	0	0.24	29.77	29.64

Figure 3.20. I.R. Spectra for $K_2Sn(C_2O_4)_2.H_2O$ Decomposition Products.

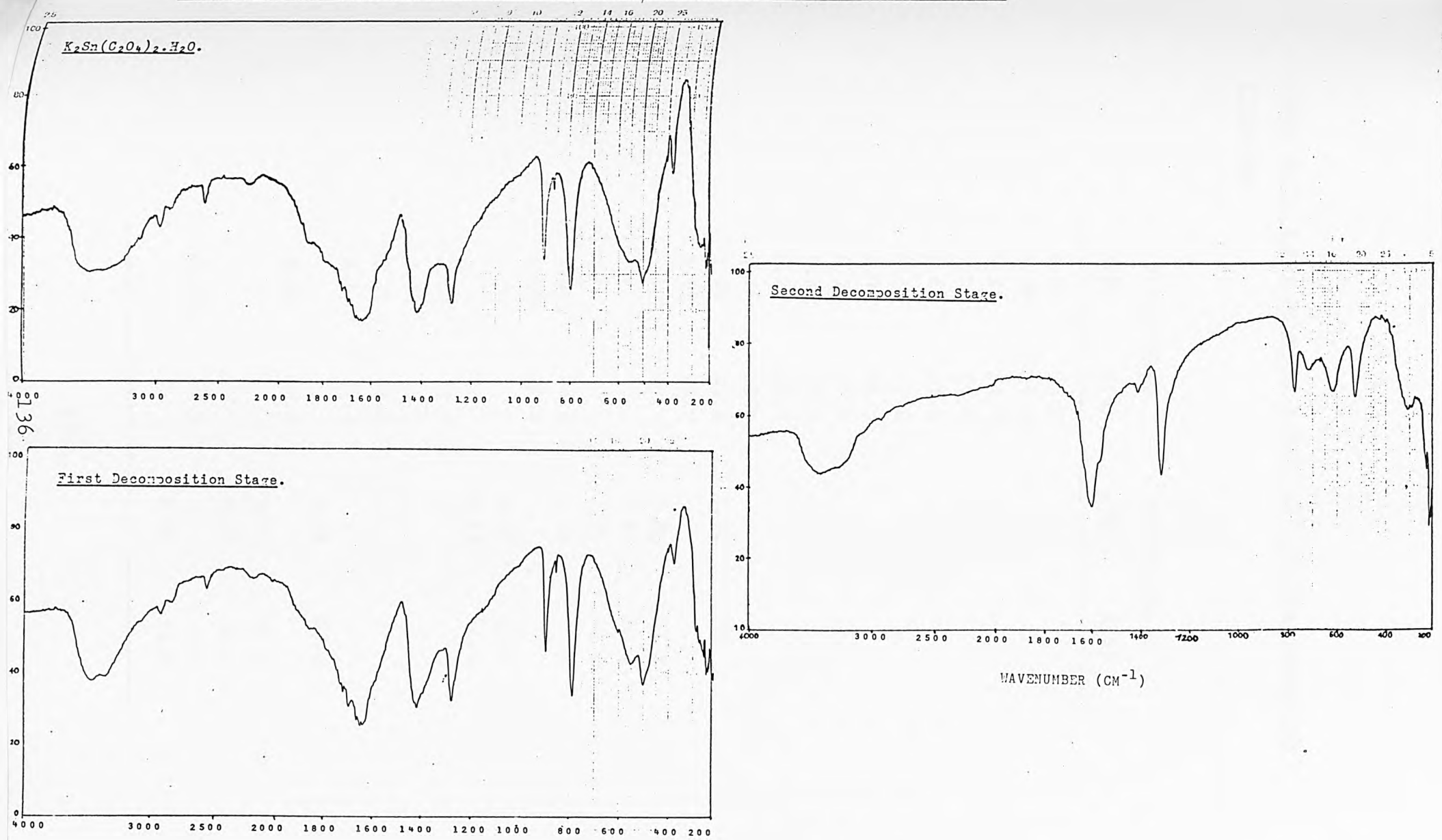

Table 3.17. X-Ray Data for $K_2Sn(C_2O_4)_2.H_2O$ Decomposition Products.

First Stage		Second Stage	
d(Å)	I(%)	d(Å)	I(%)
8.87	35.2		
8.70	49.5		
8.26	54.3		
7.89	49.5		
6.66	23.8		
6.38	51.4		
5.92	54.3		
5.76	25.7		
5.43	58.1		
5.29	46.7		
5.17	100		
5.08	84.8	5.10	100
4.91	41.9		
		4.82	10.8
		4.62	38.2
		4.51	6.2
4.40	43.8	4.44	5.2
4.33	32.4		
		4.27	17.8
		4.23	14.5
4.02	33.3		
3.51	41.9		
3.45	36.2		
3.41	33.3		
		3.38	18.5
3.30	40.0		
		3.21	32.9
		2.87	39.4
2.68	27.6		
		2.66	14.8

3.6.2. $K_2Sn(C_2O_4)_2.H_2O$

A three stage decomposition is indicated in the TG trace for this complex (Fig. 3.19), commencing at 190°C and complete by 570°C. A final residue weight of 69%, based on the original complex is obtained.

Figure 3.19. TG/DTA Trace for $K_2Sn(C_2O_4)_2.H_2O$

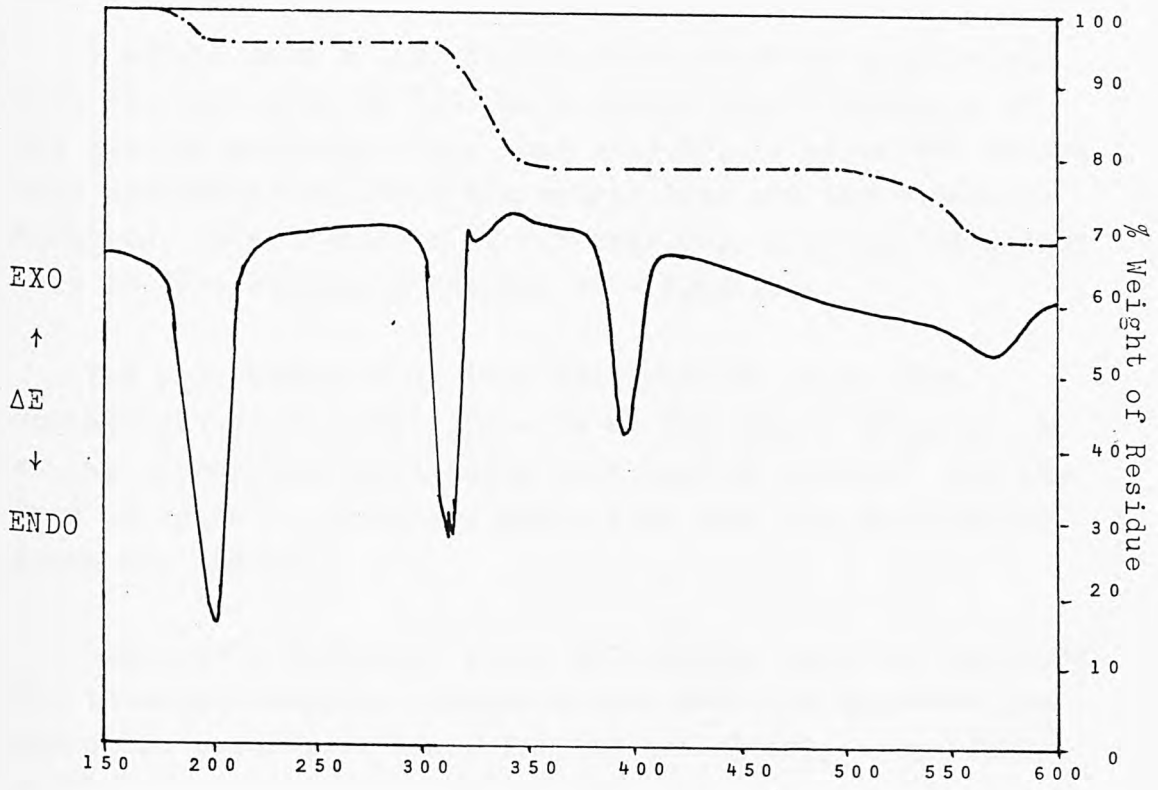

First Stage

The first stage involves a weight loss of 4%, which from the elemental analyses, (Table 3.18) is found to be due to loss of one mole water per formula weight of complex, (calculated weight loss 4.6%).

Due to the extremely hygroscopic nature of this anhydrous material, it very rapidly reabsorbed water, giving an i.r. spectrum in which water is again found to be present, (Fig. 3.20).

The x-ray data (Table 3.17) is similar to that of the parent complex but some lines are missing and there is a shift in the d-spacings of the remaining lines.

Second Stage.

A weight loss of 18% is observed, which is associated with the evolution of CO_2. Mass spectrometric analysis of the gaseous products shows that only CO_2 is given off during this decomposition. From the weight loss and the elemental analyses, this is a loss of 1.5 mole CO_2, (calculated weight loss 18.4%), leaving a residue of - $K_2SnC_2O_5$.

The i.r. spectrum of this intermediate shows that oxalate groups are still present at this time. Although the strong carboxylate stretching mode band at 1416cm^{-1} and the band at 555cm^{-1}, which are associated with the carboxylate group are absent.

Completely different x-ray diffraction data are obtained for this intermediate, compared with both the hydrated and anhydrous complexes. Lines for SnO are clearly seen (Table 3.17).

Third Stage.

The final stage involves a weight loss of 9% to give a residue which appears to have the formula K_2SnCO_4. This agrees very well with the elemental analyses and the weight loss based on the TG trace.

Mass spectrometry again identified only CO_2 in the gaseous products, implying that in the final stage $\frac{1}{2}CO_2$ + $\frac{1}{2}C$ are evolved.

Table 3.18. Elemental Analyses for $K_2Sn(C_2O_4)_2.H_2O$ Decomposition Products.

	C(%)		H(%)	
	Calc.	Found	Calc.	Found
$K_2Sn(C_2O_4)_2$	12.87	12.99	0	0.04
$K_2SnC_2O_5$	7.98	8.45	0	0.03
K_2CO_3 + SnO	4.40	4.91	0	0

3.6.3. $CaSn(C_2O_4)_2.H_2O$

The TG trace (Fig. 3.21) shows a three stage decomposition commencing at 130°C and finishing at 500°C.

First Stage (175°C)

The first decomposition stage involves evolution of H_2O, which is verified by the elemental analyses (Table 3.20). Very little change is observed in the i.r. spectrum of this first intermediate, (Fig. 3.22), however, the x-ray diffraction data show a number of new lines, together with the lines originally present in the parent complex (Table 3.19).

The i.r. spectrum shows that the oxalate group is still present, (two peaks at 426 and 399cm^{-1}), which agrees with the 5% weight loss in the TG trace and the elemental analyses.

Second Stage (394°C)

The TG trace shows a weight loss of 20% which, from the mass spectrometry data is due to loss of CO_2. No other gaseous products are identified and no solid products are collected during the large scale decomposition. In the i.r. spectrum, although very similar in many features to the previous two spectra, the oxalate bands at 427 and 400cm^{-1} are greatly reduced and the three bands also associated with carboxylate vibration modes at 521, 502 and 489cm^{-1} are resolved into a single peak at 521cm^{-1}.

From the weight loss and the elemental analyses the intermediate appears to be of the general formula $CaSnC_2O_5$, and still contains an oxalate group. The formation of this intermediate involves the evolution of CO_2. The x-ray data are different to both the parent complex and the intermediate and show the presence of SnO.

Figure 3.21. $CaSn(C_2O_4)_2.H_2O$ TG/DTA Trace.

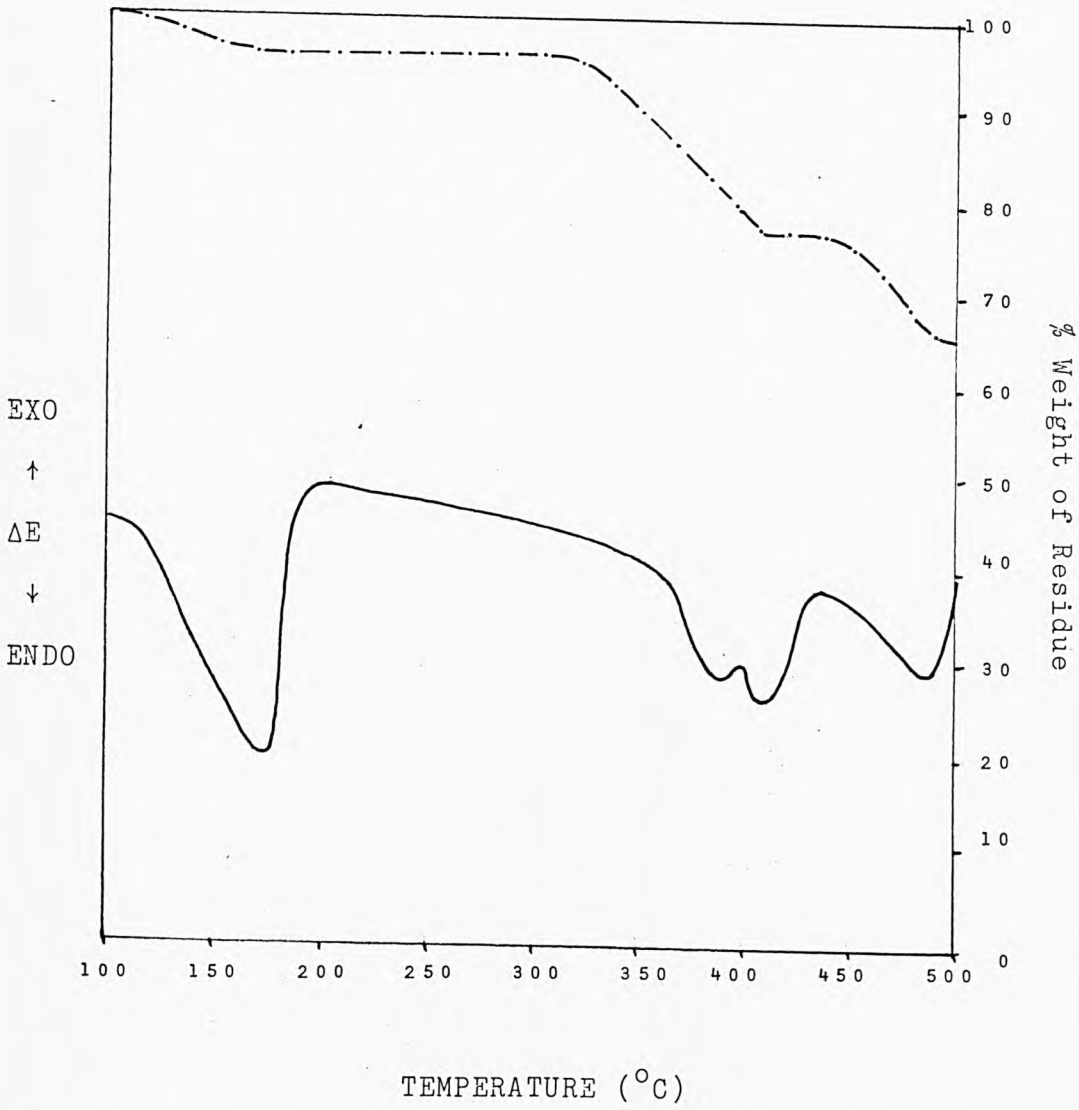

Figure 3.22. I.R. Spectra for $CaSn(C_2O_4)_2.H_2O$ Decomposition Products.

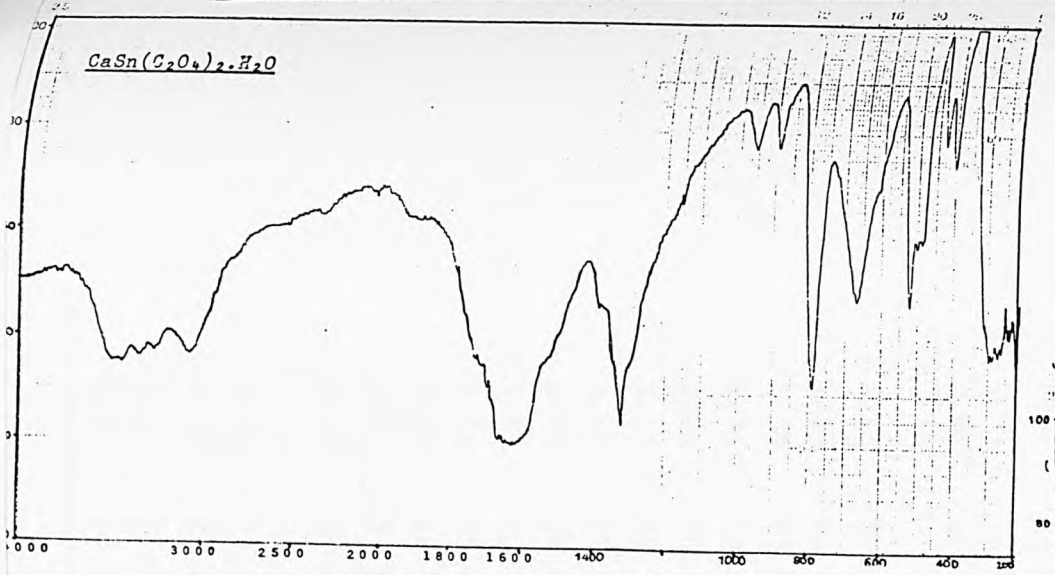

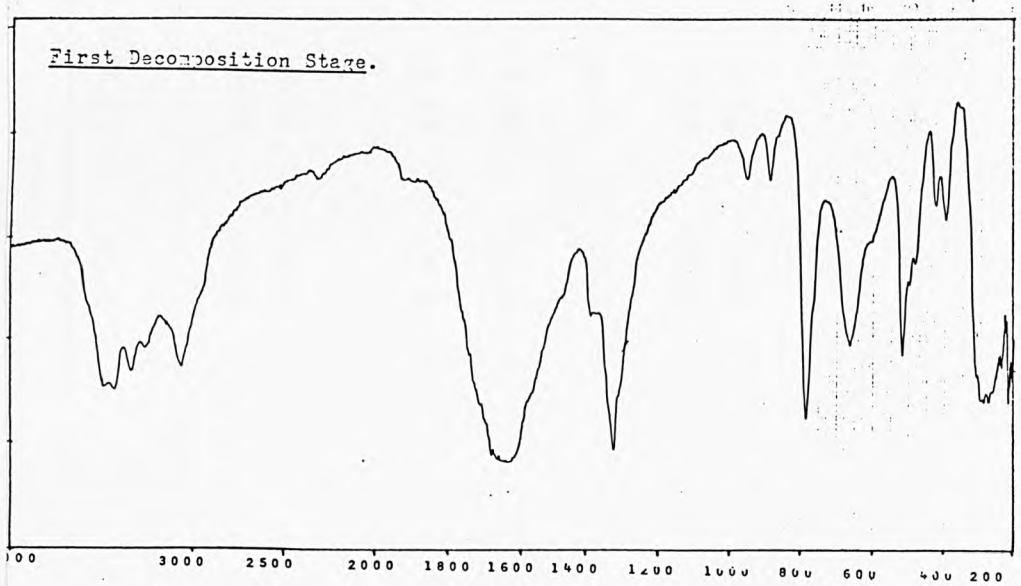

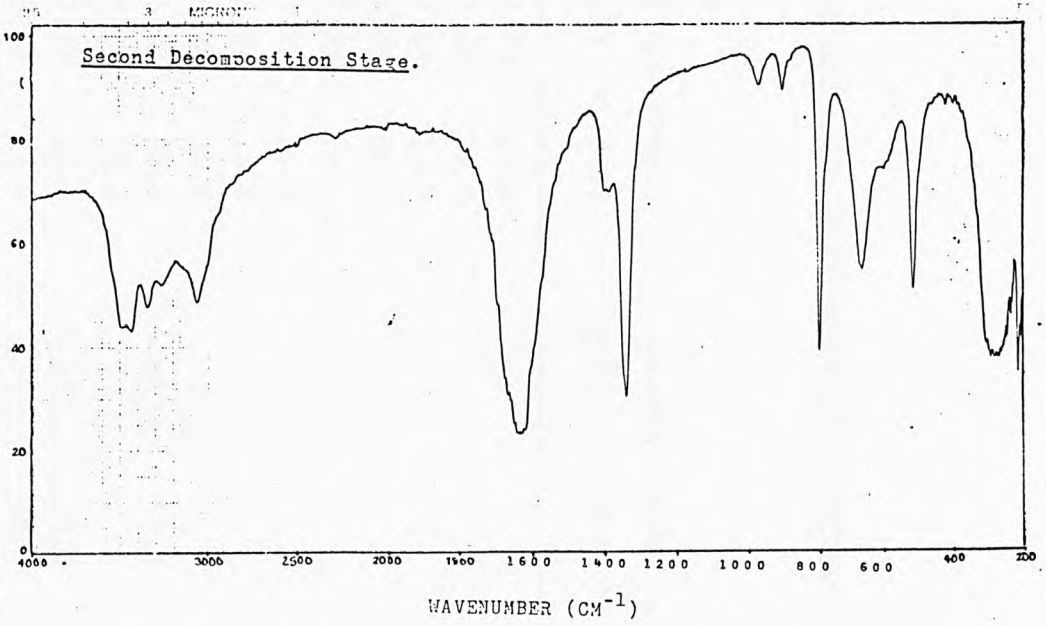

Table 3.19. X-Ray Data for $CaSn(C_2O_4)_2.H_2O$ Decomposition Products.

First Stage		Second Stage	
d(Å)	I(%)	d(Å)	I(%)
13.19	12.2		
12.18	20.9		
9.95	13.3		
8.91	30.6		
7.33	100		
7.22	35.7		
6.84	16.8		
6.49	37.8		
6.04	38.8	6.04	19.5
5.63	38.8		
5.47	46.4	5.47	7.9
5.06	23.0	5.10	100
4.94	12.8		
4.86	10.7		
		4.65	35.3
4.48	41.8		
4.42	61.2		
4.38	25.5		
4.34	19.4	4.34	7.6
4.24	56.1	4.22	12.9
4.15	38.3		
4.12	29.1	4.11	12.2
4.07	30.6		
3.97	15.8	3.96	5.3
3.74	25.0		
3.66	10.7	3.67	7.6
3.55	25.5		
3.44	42.3		
		3.38	24.4
3.19	74.0	3.20	41.6
3.10	21.4		
3.03	11.7		
2.89	11.2	2.87	43.9

Third Stage (500°C)

From the TG study, a residue of 65% remains at the end of this final decomposition. This has the composition $CaSnCO_4$, (calculated residue weight 66.5%). In the final decomposition stage CO_2 was identified as the only gaseous product by the mass spectrometry study. The weight loss of 10.5% and the elemental analyses indicate that 1 x C and 1 x O are evolved at this time. These form the gaseous product CO_2.

Table 3.20. Elemental Analyses for $CaSn(C_2O_4)_2.H_2O$

	C(%)		H(%)	
	Calc.	Found	Calc.	Found
$CaSnC_4O_8$	14.34	14.06	0	0.22
$CaSnC_2O_5$	9.13	9.59	0	0.49
$CaCO_3 + SnO$	5.11	4.96	0	0.10

3.7. Discussion.

For the hydrated oxalate complexes - $K_2Sn(C_2O_4)_2.H_2O$ and $CaSn(C_2O_4)_2.H_2O$, decomposition takes place in three stages, viz. (1) dehydration, (2) decomposition of the oxalate group associated with tin, and (3) decomposition of the oxalate group associated with alkali or alkaline earth

metal. The Na complex is the only derivative which is anhydrous at room temperature, but it still undergoes a three stage decomposition process, involving (1) volatilisation of part of the stannous oxalate portion, (2) decomposition of the remaining, undecomposed, stannous oxalate, and (3) breakdown of the remaining Na oxalate.

Powder x-ray data for the hydrated K and Ca compounds (Tables 3.17 and 3.19) show that the two complexes are not isostructural and have very different lattice parameters. The x-ray patterns for the anhydrous materials also show that all three complexes (Na, K and Ca) have different crystal structures and lattice parameters.

The first stage in the decomposition of the K and Ca complex oxalates is dehydration, which occurs at high temperatures - 198 and 174°C, respectively, (TG traces Figs. 3.19 and 3.21), and is in very good agreement with the dehydration temperatures of K and Ca oxalates at ca. 190 and 170°C, respectively. The weight losses and the elemental analysis results (Tables 3.18 and 3.20) confirm that the final residues from this first decomposition stage are the anhydrous complexes - $K_2Sn(C_2O_4)_2$ and $CaSn(C_2O_4)_2$.

The first stage in the decomposition of the Na derivative occurs at 323°C with volatilisation of part of the complex - SnC_2O_4, and CO_2. From the weight losses and elemental analyses (Table 3.16) only 0.75mole SnC_2O_4 appears to have been removed with the formation of 0.75mole Na_2O. This leaves 0.25mole $Na_2Sn(C_2O_4)_2$ undecomposed in the residue at this temperature. The absence of any lines for SnO in the x-ray pattern (Table 3.15) is further evidence for the presence of 0.25mole of $Na_2Sn(C_2O_4)_2$. The i.r. spectrum also shows that the product of this first decomposition is identical to that of the starting material. The only noticeable change in the product from this first pyrolysis step is a colour change from white to orange-red.

The anhydrous K and Ca complexes decompose at 316 and 382°C with breakdown of the oxalate groups associated with Sn (decomposition temperature for stannous oxalate >280°C). This is reflected in the x-ray data which clearly show the presence of blue-black stannous oxide. Several other lines are also present, which can be assigned to Ca and K oxalate.

The i.r. spectra (Figs. 3.20 and 3.22) are also consistent with decomposition of the stannous oxalate portion of the complexes. The carboxylate stretching frequencies ca. 1600 and 1400cm^{-1} show marked shifts and are resolved into the single, sharper peaks which would be expected if only one oxalate specie were present.

Mass spectrometric analysis of volatile products identified only CO_2, implying the pyrolysis reaction of the oxalate is:

$$C_2O_4^{2-} \longrightarrow CO_2 + |CO| \downarrow \tfrac{1}{2}CO_2 + \tfrac{1}{2}C.$$

The decomposition reactions for all three complexes are:

$$Na_2Sn(C_2O_4)_2 \longrightarrow 0.75Na_2O + 0.25|NaSn(C_2O_4)_2| + 0.75SnC_2O_4\uparrow + CO_2 + \tfrac{1}{4}O$$

$$K_2Sn(C_2O_4)_2 \longrightarrow SnO + K_2C_2O_4 + 1\tfrac{1}{2}CO_2 + \tfrac{1}{2}C$$

$$CaSn(C_2O_4)_2 \longrightarrow SnO + CaC_2O_4 + 1\tfrac{1}{2}CO_2 + \tfrac{1}{2}C$$

After volatilisation of the stannous oxalate portion of the Na complex, a reaction analagous to those for the K and Ca reactions above takes place with breakdown of the stannous oxalate portion of the remaining complex to give SnO and 0.25mole $Na_2C_2O_4$. This decomposition step occurs with a weight loss of 6% at 390°C, a temperature that is too low for breakdown of the oxalate group associated with Na (ca. 530°C).

The x-ray data clearly show the presence of blue-black SnO, Na_2O and $Na_2C_2O_4$, (Table 3.15). The i.r. spectra of the products at this stage are very similar to those of the parent complex and the first decomposition product, showing that oxalate groups are still present. Mass spectrometric analysis again identifies only the presence of CO_2 in the gaseous products, suggesting the reaction:

$$0.75Na_2O + 0.25|Na_2Sn(C_2O_4)_2| \longrightarrow 0.75Na_2O + 0.25SnO + \\ + 0.25Na_2C_2O_4 + \delta CO_2$$

The final decomposition stage for the three complexes occurs at high temperatures - 536, 566 and 495°C, for the Na, K and Ca complexes respectively, and involve breakdown of the alkali or alkaline earth metal oxalates. The decomposition temperatures agree well with the published values for breakdown of the corresponding alkali and alkaline earth oxalates at 530, 560 and 490°C, respectively.

Weight losses, elemental analyses, and mass spectrometric data suggest that the final residues have the compositions (based on the starting materials): Na_2O + 0.25SnO; K_2CO_3 + SnO: and $CaCO_3$ + SnO, which are formed by the reactions:

$$0.75Na_2O + 0.25SnO + 0.25Na_2C_2O_4 \longrightarrow Na_2O + 0.25SnO + 0.5C + 0.75O$$

$$SnO + K_2C_2O_4 \longrightarrow SnO + K_2CO_3 + |CO| \downarrow \tfrac{1}{2}CO_2 + \tfrac{1}{2}C$$

$$SnO + CaC_2O_4 \longrightarrow SnO + CaCO_3 + |CO| \downarrow \tfrac{1}{2}CO_2 + \tfrac{1}{2}C$$

3.8. Complex Tin Malonates.

In this section the thermal decomposition of complex tin malonates of the type - $A_2Sn_2(CH_2C_2O_4)_3.xH_2O$, (for A = Na, x = 2, for A = K, x = 1, for A = NH_4^+, x = 0) and $CaSn_2(CH_2C_2O_4)_3.3H_2O$ is presented. The techniques used to obtain the results are outlined and the pyrolysis mechanisms presented in section 3.9.

3.8.1. $Na_2Sn_2(CH_2C_2O_4)_3.2H_2O$

A three stage decomposition is observed for the Na complex over the temperature range 177 to 386°C, (TG trace Fig. 3.23).

Figure 3.23. TG/DTA Trace for $Na_2Sn_2(CH_2C_2O_4)_3.2H_2O$

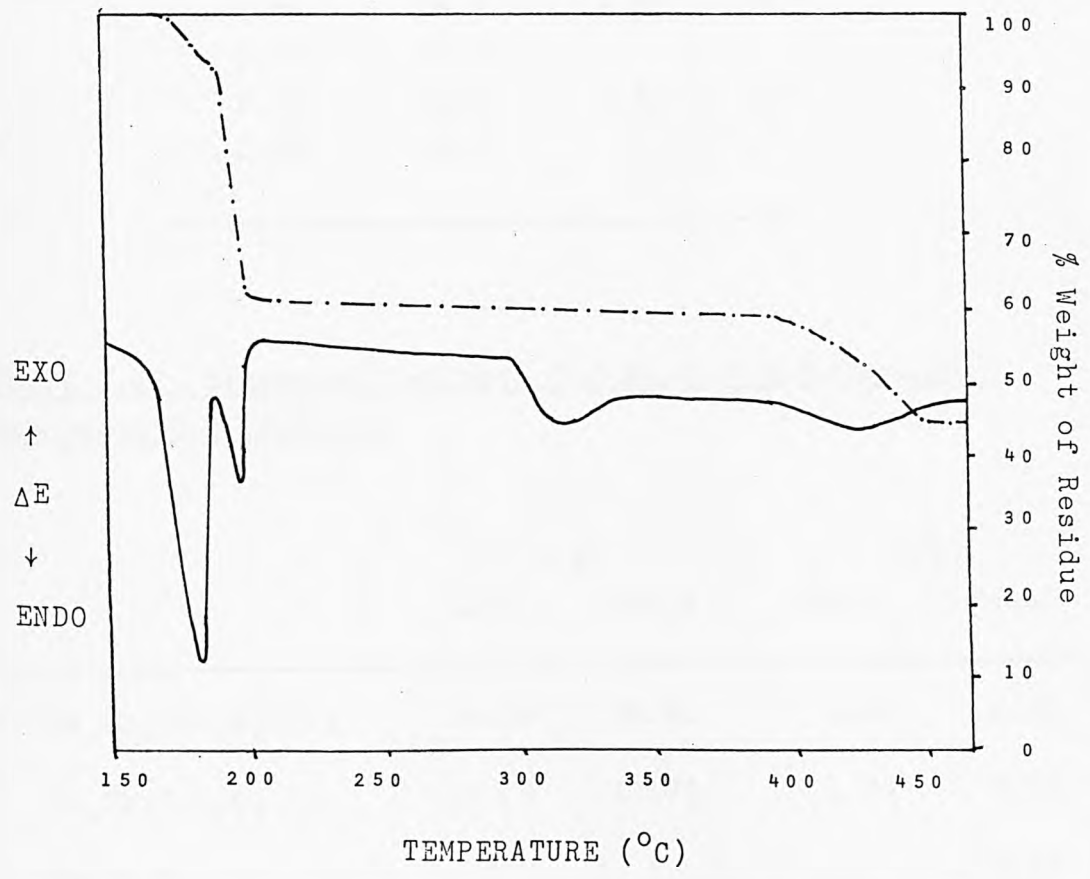

Table 3.21. X-Ray Data for $Na_2Sn_2(CH_2C_2O_4)_3 .2H_2O$ Decompositon Products.

Second Stage		Residue	
d(Å)	I(%)	d(Å)	I(%)
12.80	87.1		
5.10	86.0	5.10	100
		5.02	23.9
		4.79	19.1
		4.64	39.9
4.45	100		
		4.22	9.8
		3.64	7.0
		3.57	16.3
		3.37	16.0
3.20	35.5	3.21	31.5
2.86	28.9	2.87	33.7
2.73	37.7		
2.65	21.4	2.66	13.5
2.36	10.5		

Table 3.22. Elemental Analyses for $Na_2Sn_2(CH_2C_2O_4)_3.2H_2O$ Decomposition Products.

	C(%)		H(%)	
	Calc.	Found	Calc.	Found
$Na_2Sn_2(CH_2C_2O_4)_3$	18.32	18.01	1.02	1.22
$Na_2Sn_2C_4H_6O_6$	11.08	11.63	1.39	0.98
$Na_2Sn_2O_3$	0	0	0	0.28

Figure 3.24. I.R. Spectra for $Na_2Sn_2(CH_2C_2O_4)_3.2H_2O$ Decomposition Products.

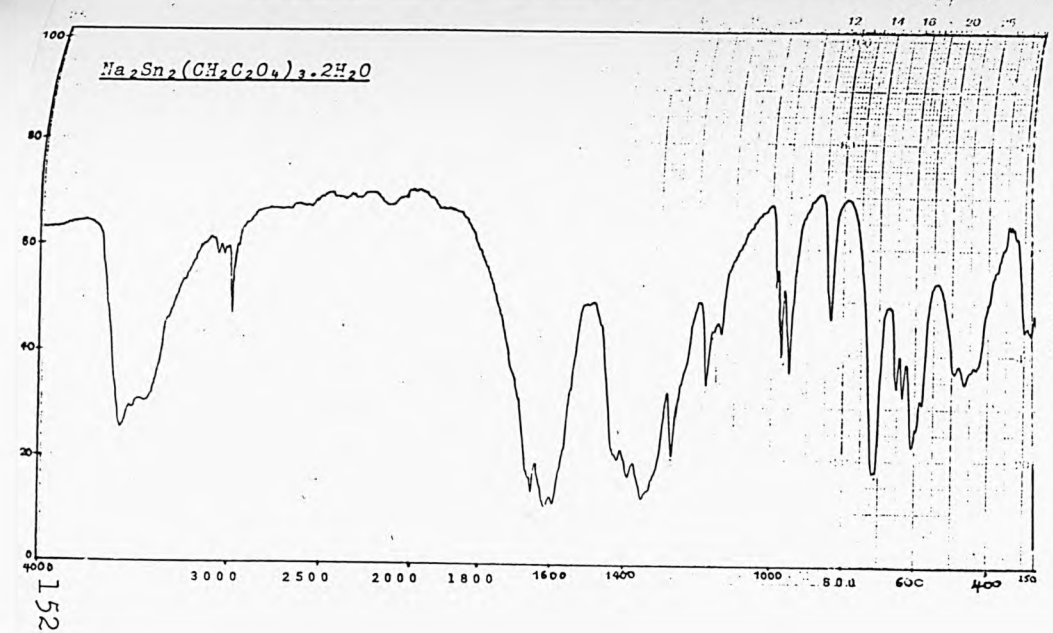

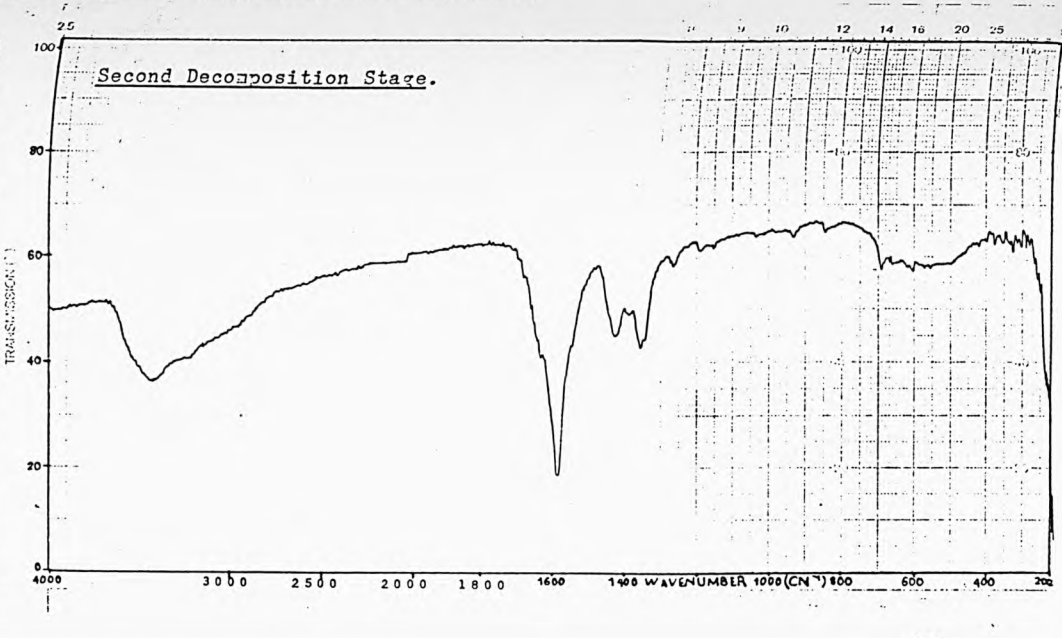

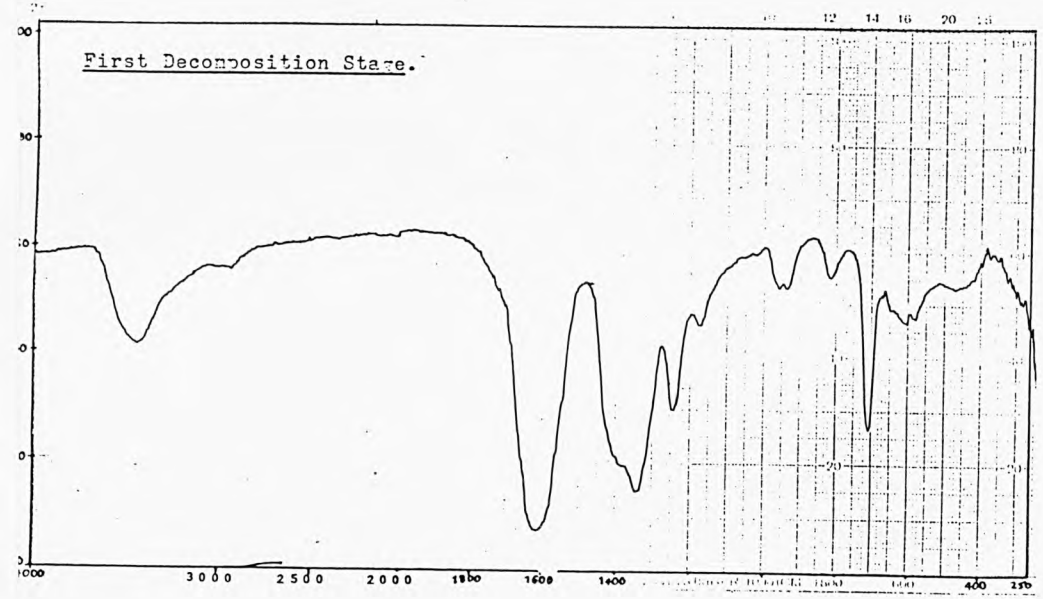

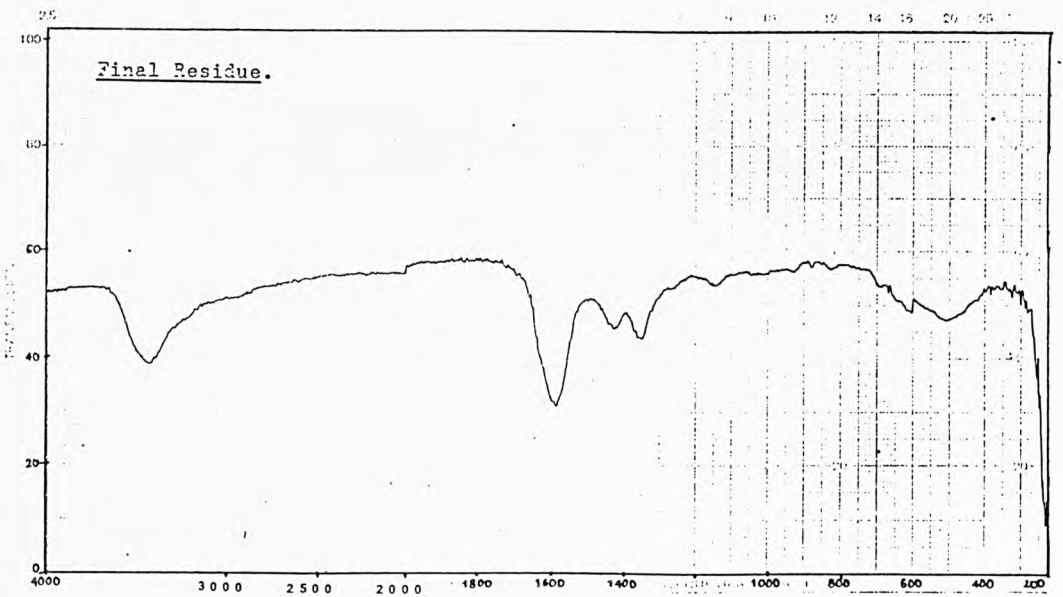

First Stage (184°C)

This first decomposition step involves dehydration of the starting material to give an amorphous intermediate for which no x-ray data could be obtained.

A weight loss of 6.4% is obtained (calculated 5.8%), which is in very good agreement with the calculated value and the elemental analyses support these results (Table 3.22). The i.r. spectrum (Fig. 3.24) has no peak at ca. 3575cm^{-1} associated with coordinated water or at 1650cm^{-1}, the deformation mode for H_2O.

Water was demonstrated to be evolved during the large scale decomposition using self-indicating silica gel, where a colour change from blue to pink was observed.

Second Stage (199°C)

A weight loss of 32.75% is seen at this stage. A more crystalline product is obtained, which has x-ray parameters different to the starting material, with lines corresponding to SnO (Table 3.21).

The i.r. spectrum shows only the presence of carboxylate groups in the region 1600 - 1350cm^{-1} (three peaks at 1585, 1425 and 1350cm^{-1}). From elemental analysis, the composition of the intermediate is found to be $Na_2Sn_2C_4H_6O_6$. This is a weight loss of 30.7%, which from mass spectrometry is found to be due to evolution of CO and CO_2.

Third Stage (386°C)

A 16% weight loss is seen at this stage. The final residue has x-ray data very similar to those for the final residue of the K complex. The lines found in both residues are assigned to SnO.

Table 3.23. X-Ray Data for $K_2Sn_2(CH_2C_2O_4)_3.H_2O$ Decomposition Products.

First Stage		Residue	
d(Å)	I(%)	d(Å)	I(%)
5.10	100	5.09	100
		4.89	53.2
		4.80	49.8
4.64	34.2	4.63	30.0
		4.22	9.5
		3.64	20.5
		3.57	34.6
3.38	16.8	3.38	13.3
3.21	34.2	3.20	27.0
2.86	37.8	2.87	26.2
2.66	16.8	2.67	22.8

The i.r. spectrum has one peak in the carboxylate frequency region, which could be due to a very small amount of the previous intermediate remaining.

From the mass spectrometric study the gaseous products were found to comprise of acetone and CO_2. This agrees with evolution of 4 x C, 6 x H and 3 x O from the previous intermediate, (calculated weight loss 16.3%) to leave a residue of composition $Na_2Sn_2O_3$ (residue weight 53.5%).

3.8.2. $K_2Sn_2(CH_2C_2O_4)_3H_2O$

The potassium complex undergoes a two stage decomposition commencing at 199°C. The coordinated water is not evolved in the initial decomposition but is involved in the first decomposition reaction.

Figure 3.25. TG/DTA Trace for $K_2Sn_2(CH_2C_2O_4)_3.H_2O$

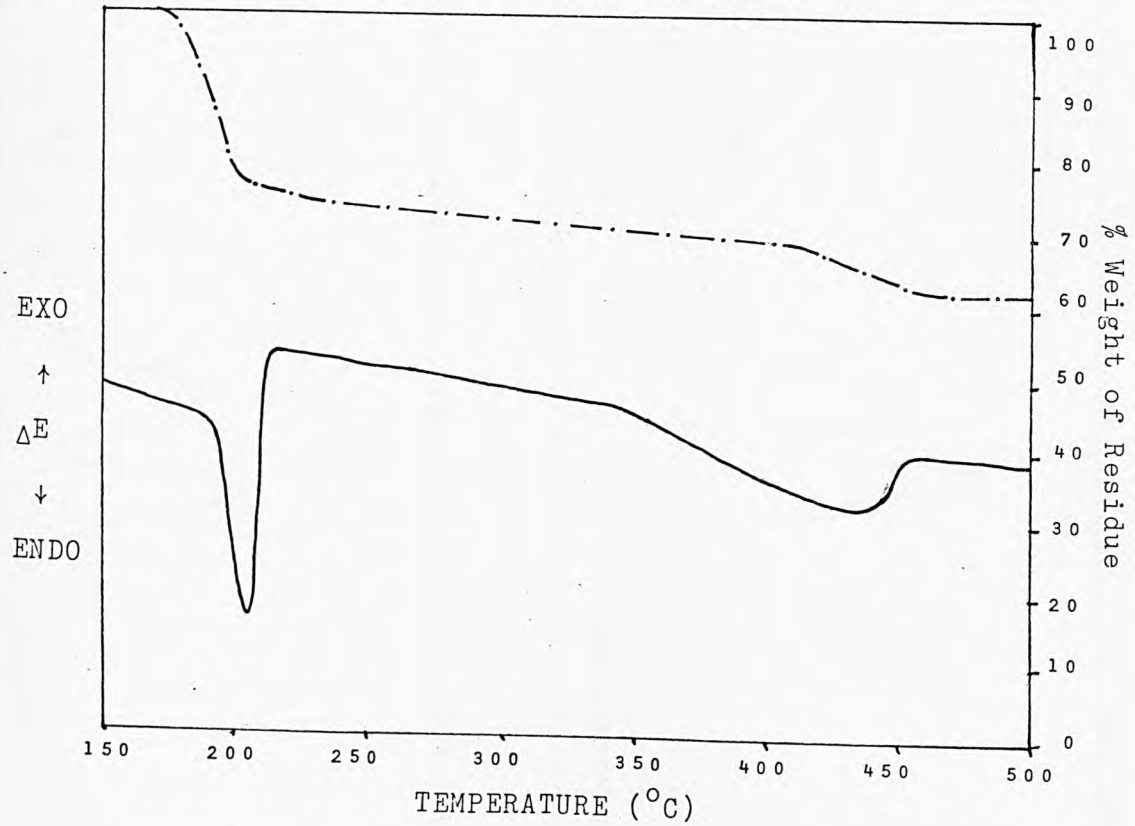

Figure 3.26. I.R. Spectra for $K_2Sn_2(CH_2C_2O_4)_3.H_2O$ Decomposition Products.

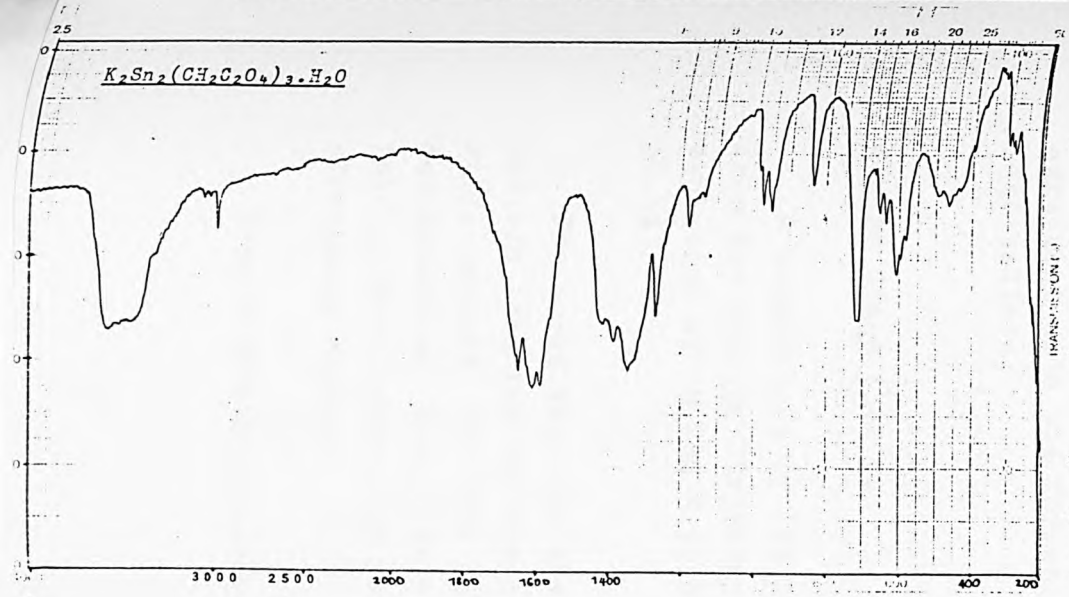

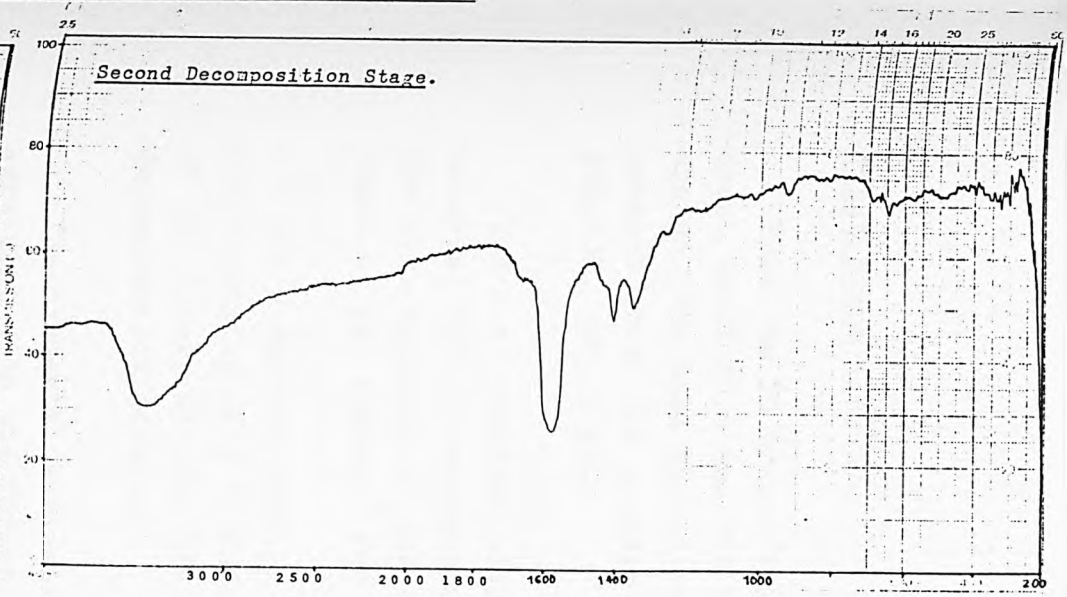

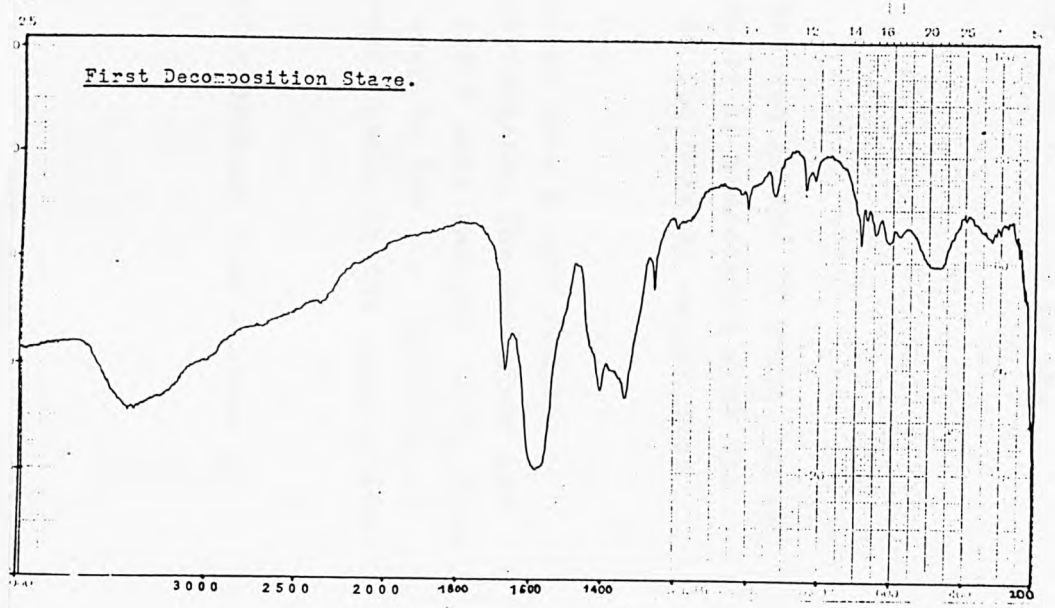

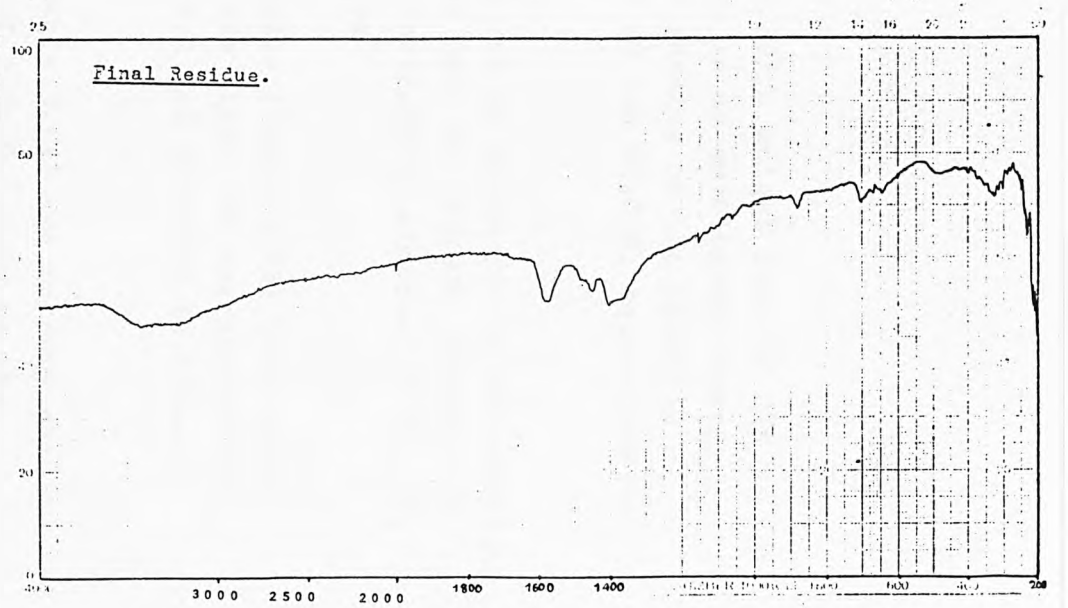

First Stage (199°C).

From the TG trace (Fig. 3.25) a weight loss of 27% is seen, which from the DTA trace is an endothermic energy change. The mass spectrometry results on the volatile product show the presence of CO_2 and CH_3COH, equivalent to $\frac{1}{2}CH_3COH$, $3CO_2 + \frac{1}{4}O_2$.

The i.r. spectrum (Fig. 3.26) is different to the starting material and corresponds quite well to CH_3COOK. Notable in the i.r. spectrum of the intermediate is absence of the CH_2 peaks at ca. 2960cm^{-1} and 714cm^{-1}.

The x-ray diffraction results (Table 3.23) have lines corresponding only to SnO, these lines are characteristic of the finely divided blue-black SnO produced in these decomposition studies.

The elemental analyses (Table 3.24) are in very good agreement with the formation of $K_2Sn_2C_{4.5}H_6O_6$ as the intermediate.

Second Stage (382°C)

A weight loss of 11% is observed in the TG trace, which from the mass spectrometry results is associated with the evolution of $CH_3COH + \frac{1}{2}C_2H_4 + \frac{1}{2}C$ (calculated weight loss 10.1%).

The x-ray data for the residue show a more complex pattern than for the first intermediate. The SnO lines are still present, but four other lines have emerged during this decomposition. Very little is seen in the i.r. spectrum of this product except for some small peaks in the carboxylate stretching region.

From elemental analyses and Mössbauer data - where a

singlet is seen at δ = 2.60±0.01mms^{-1}, the final residue is believed to be 2SnO + K_2CO_3.

Table 3.24. Elemental Analyses for $K_2Sn_2(CH_2C_2O_4)_3.H_2O$

	C(%)		H(%)	
	Calc.	Found	Calc.	Found
$K_2Sn_2C_{4.5}H_6O_6$	11.45	11.22	1.28	1.50
K_2CO_3 + 2SnO + ½C	4.30	4.11	0	0

3.8.3. $(NH_4)_2Sn_2(CH_2C_2O_4)_3$

The ammonium salt undergoes a two stage decomposition but the two stages are so close together that they cannot be separated. The TG trace shows a change in gradient at ca. 57.5% followed by a further weight loss of 21.5% to leave a residue of ca. 21%, (TG trace Fig. 3.27).

Figure 3.27. TG/DTA Trace for $(NH_4)_2Sn_2(CH_2C_2O_4)_3$.

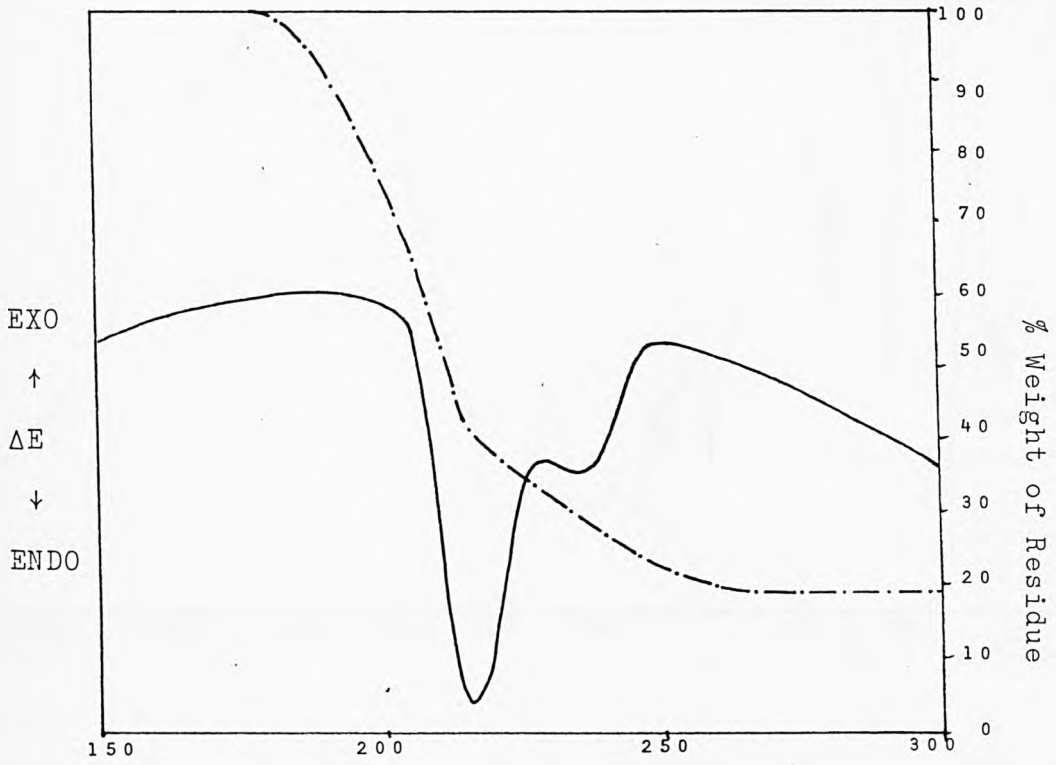

During the large scale decomposition a small amount of a white product was collected on the cold probe which, when analysed for carbon and hydrogen (Table 3.26) and an i.r. spectrum obtained (Fig. 3.28), is in good agreement with the formation of $Sn(CH_3COO)_2$.

The mass spectrometric analysis of volatiles shows the presence of CO_2, MeCN and O_2 , with smaller amounts of acetone and acetic acid.

Only one of the nitrogen atoms is involved in the formation of MeCN, the other is evolved as NH_3 which was identified in the volatile gases by chemical means.

Figure 3.28: $(NH_4)_2Sn_2(CH_2C_2O_4)_3$ Decomposition Products.

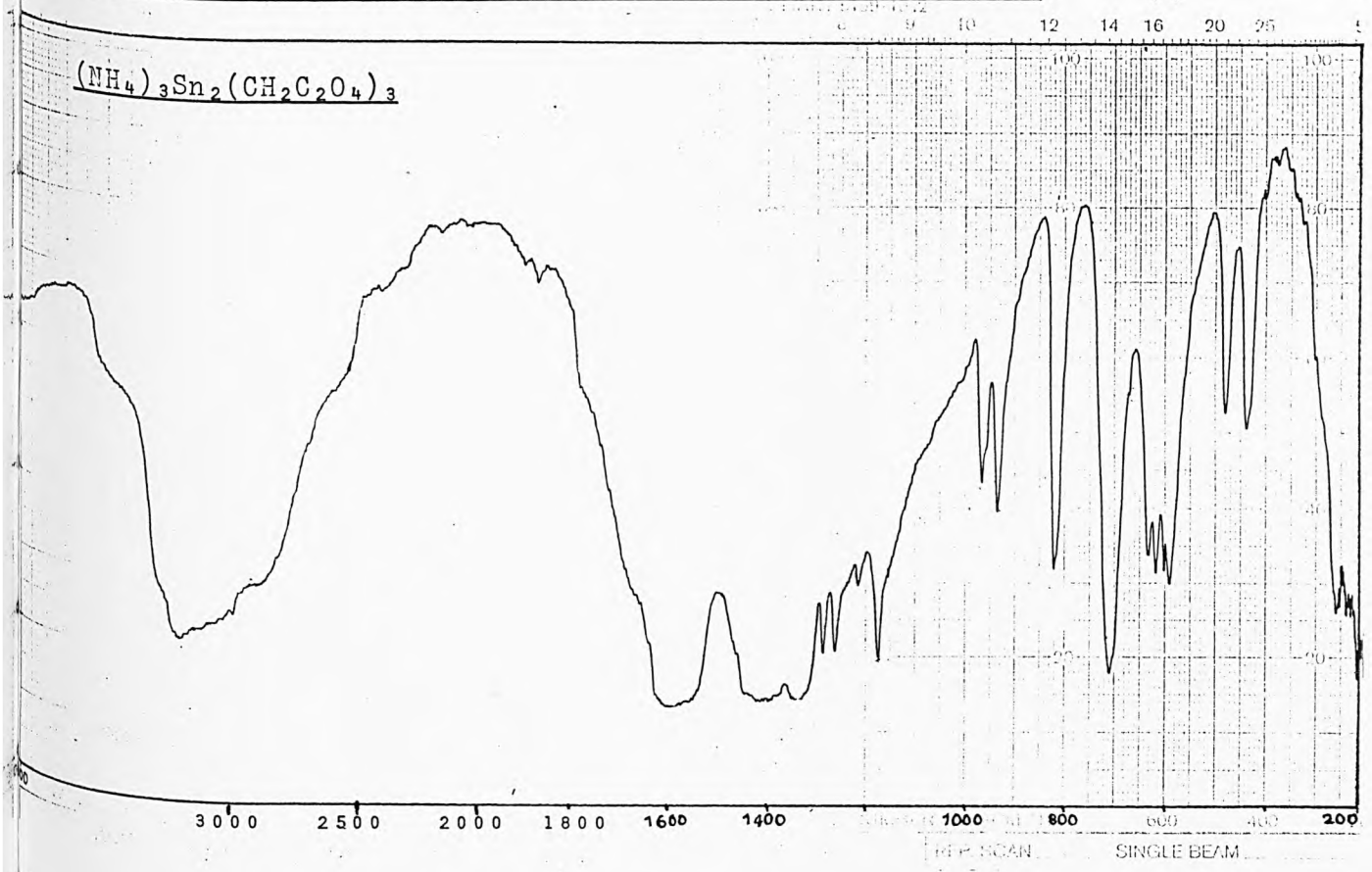

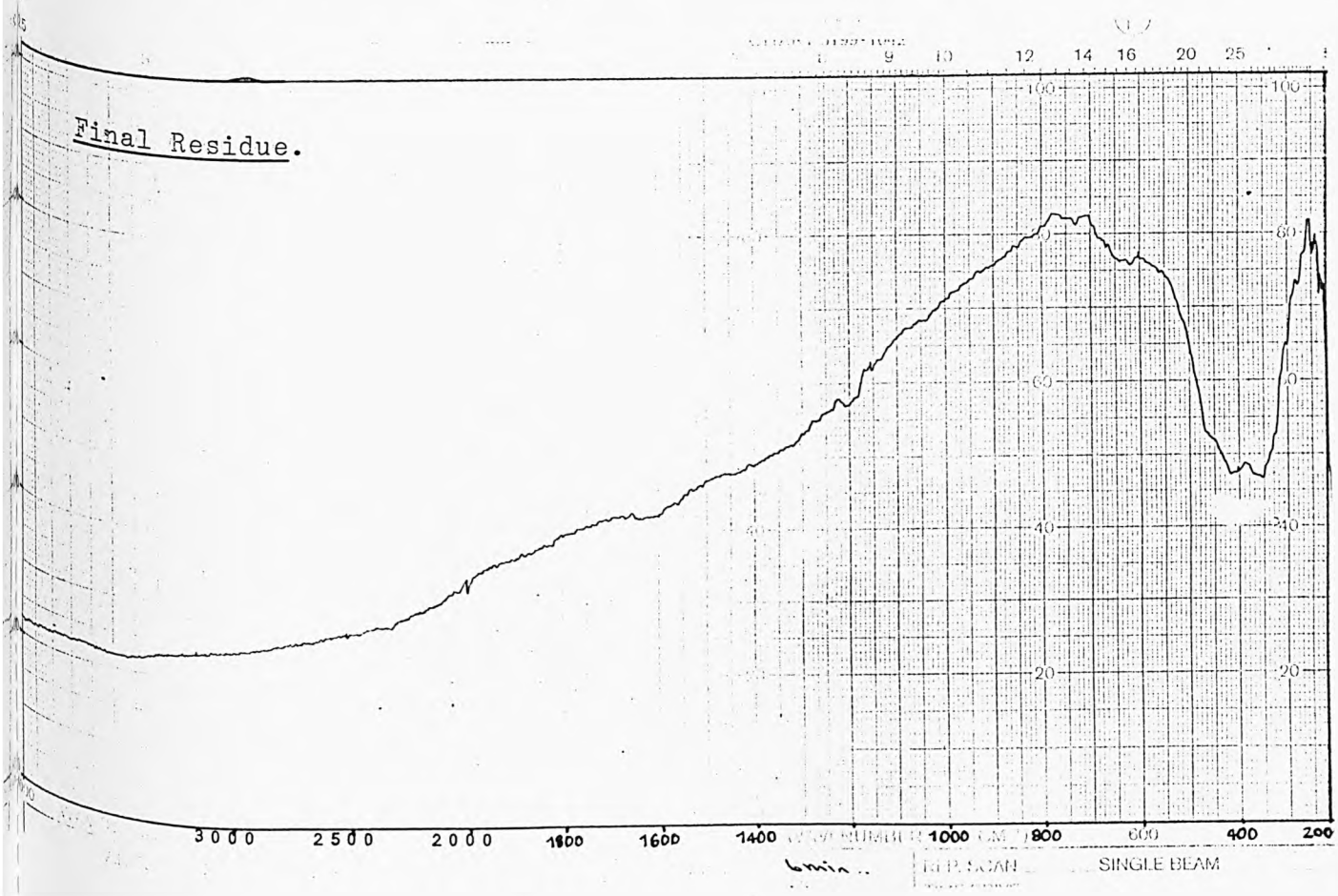

Table 3.25. X-Ray Data for $(NH_4)_2Sn_2(CH_2C_2O_4)_3$ Decomposition Product .

d(Å)	I(%)
5.09	100
4.60	36.1
4.23	8.6
3.37	10.8
3.20	24.7
2.86	21.3

Table 3.26. Elemental Analyses for $(NH_4)_2Sn_2(CH_2C_2O_4)_3$ Products

	C(%)		H(%)	
	Calc.	Found	Calc.	Found
$(CH_3COO)_2Sn$	20.28	19.90	2.55	2.51
SnO	0	0.90	0	0.06

The i.r. spectrum and the x-ray diffraction data (Table 3.25) suggest that the final residue is SnO. The i.r. spectrum has one peak at ca. 400cm^{-1} and no organic constituents are observed.

3.8.4. $CaSn_2(CH_2C_2O_4)_3.3H_2O$

The calcium malonate complex undergoes a three-stage decomposition over the temperature range 155 to 460°C to leave a residue of 59%.

Figure 3.29. TG/DTA Trace for $CaSn_2(CH_2C_2O_4)_3.3H_2O$

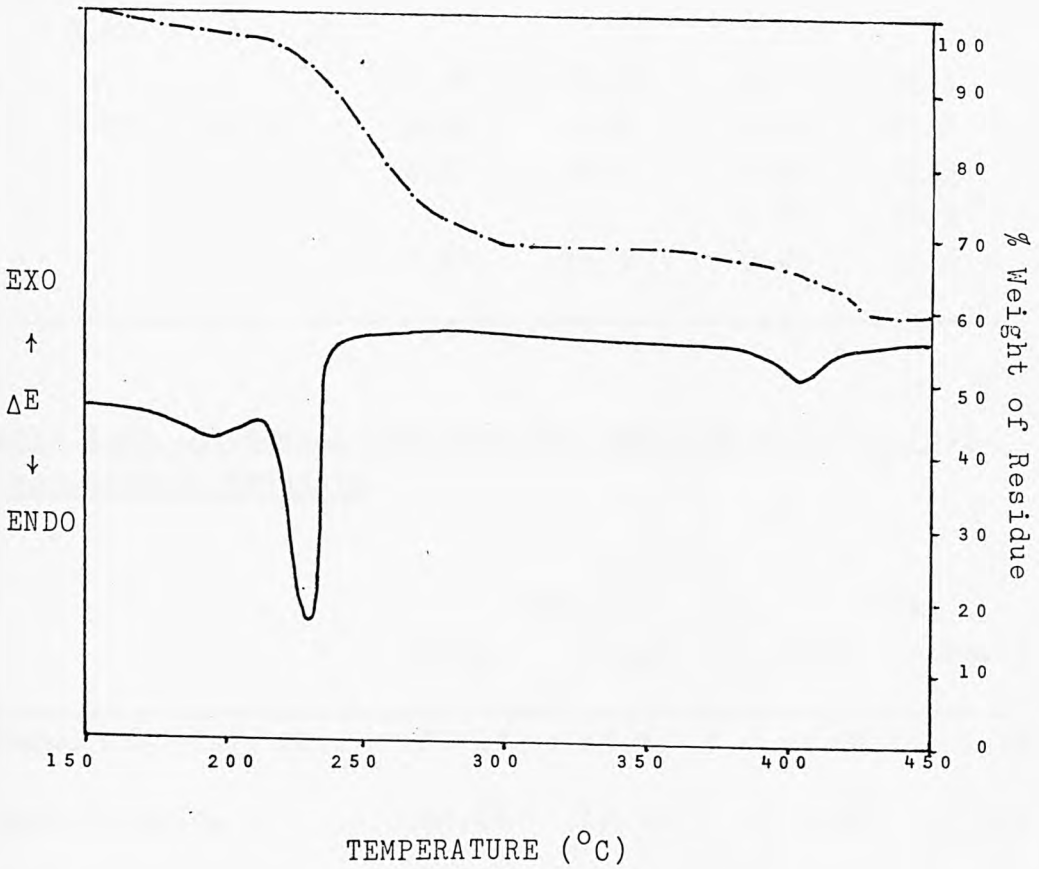

Table 3.27. X-Ray Data for $CaSn_2(CH_2C_2O_4)_3.3H_2O$ Decomposition Products.

First Stage		Second Stage		Residue	
d(Å)	I(%)	d(Å)	I(%)	d(Å)	I(%)
14.47	35.4				
9.04	100				
8.29	13.3				
6.56	43.5				
5.63	17.7				
5.02	10.7	5.10	100	5.09	100
4.65	5.5	4.64	30.3	4.64	35.8
4.47	6.7				
4.07	11.6	4.23	9.3	4.23	8.6
3.66	7.0				
3.62	6.1				
		3.38	17.0	3.37	15.4
3.28	10.4	3.21	27.8	3.21	28.6
		2.87	31.1	2.87	31.3
				2.68	10.9
		2.67	11.5	2.67	12.2

Table 3.28. Elemental Analyses for $CaSn_2(CH_2C_2O_4)_3.3H_2O$ Decomposition Products.

	C(%)		H(%)	
	Calc.	Found	Calc.	Found
$CaSn_2(CH_2C_2O_4)_3.2H_2O$	17.43	17.36	1.90	1.82
$CaSn_2C_{4.5}H_6O_6$	12.46	12.95	1.39	1.43
$CaSn_2C_{1.5}O_5$	4.79	4.83	0	0

Figure 3.30: $CaSn_2(CH_2C_2O_4)_3.3H_2O$ Decomposition Products - I.R. Spectra

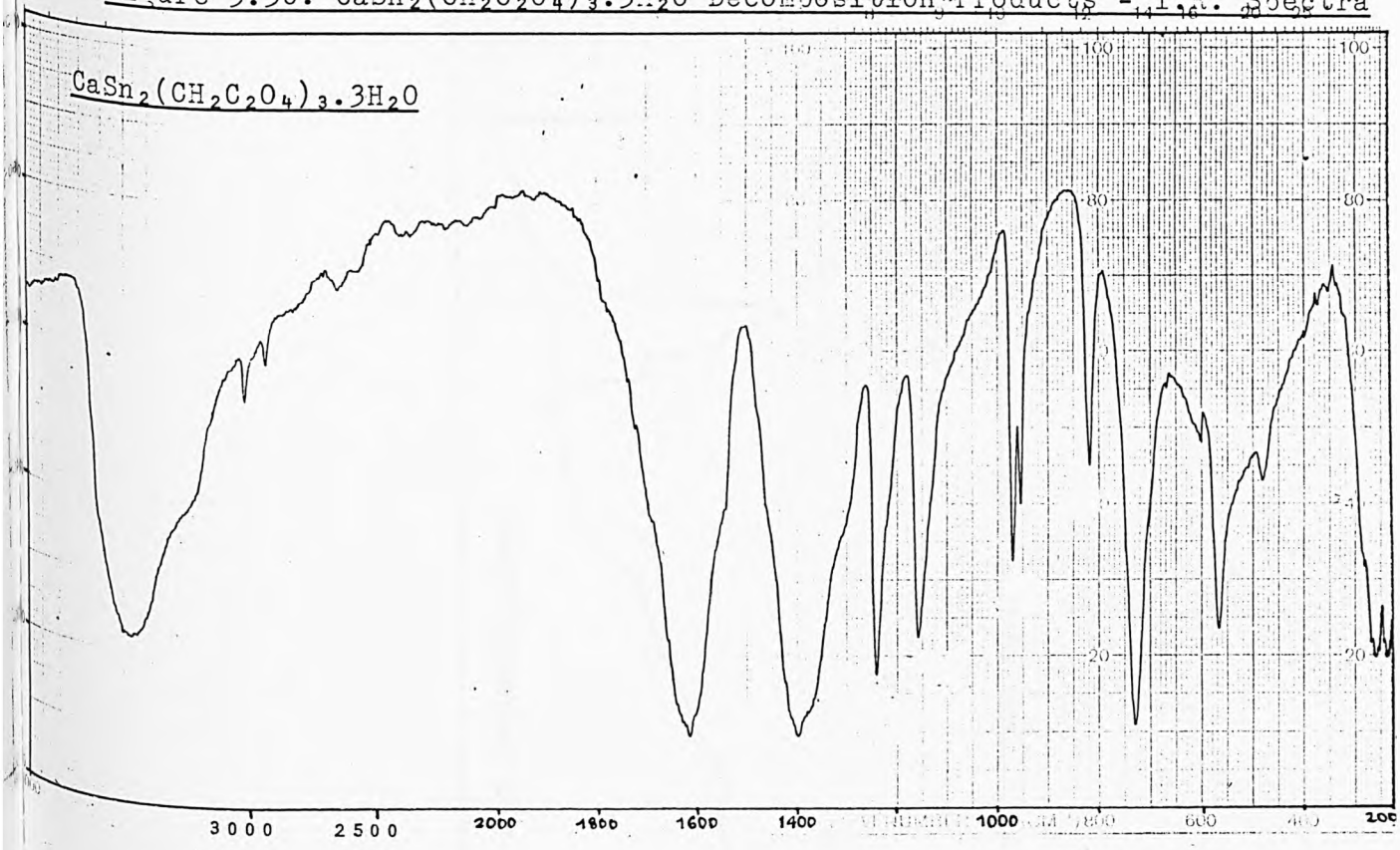

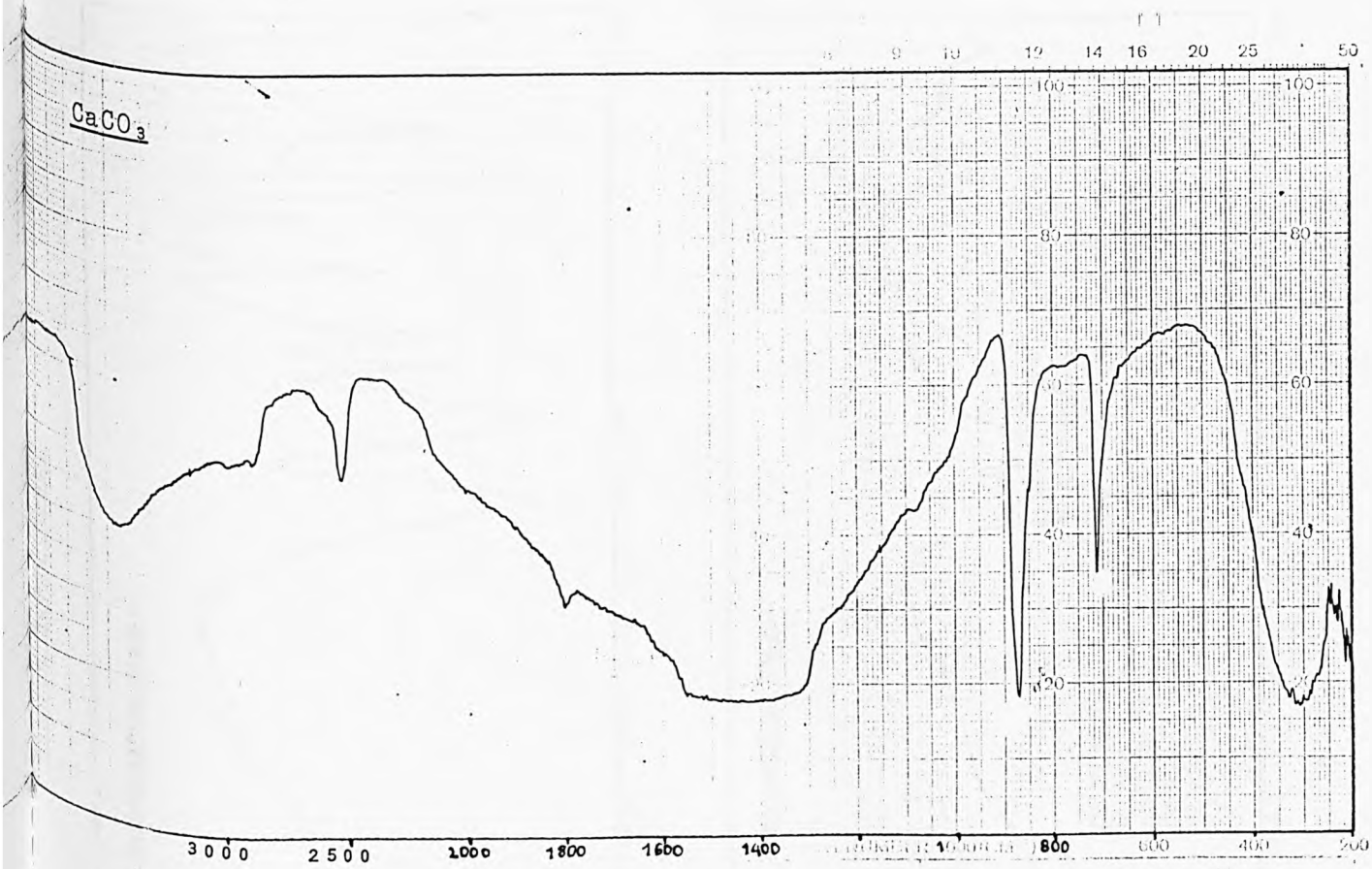

Figure 3.30. Cont.

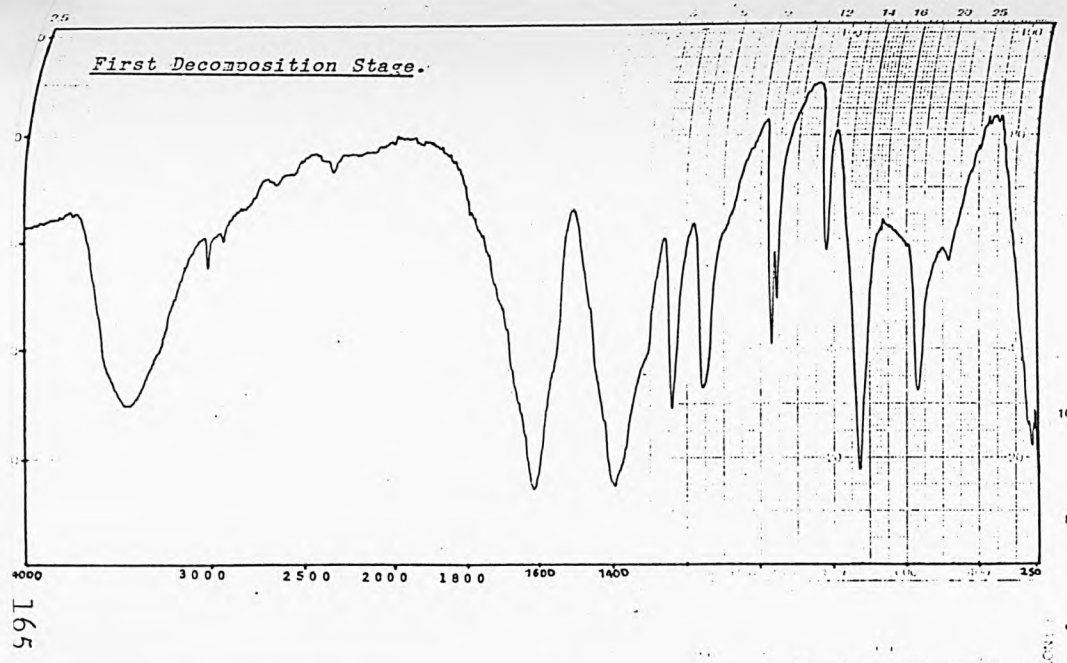

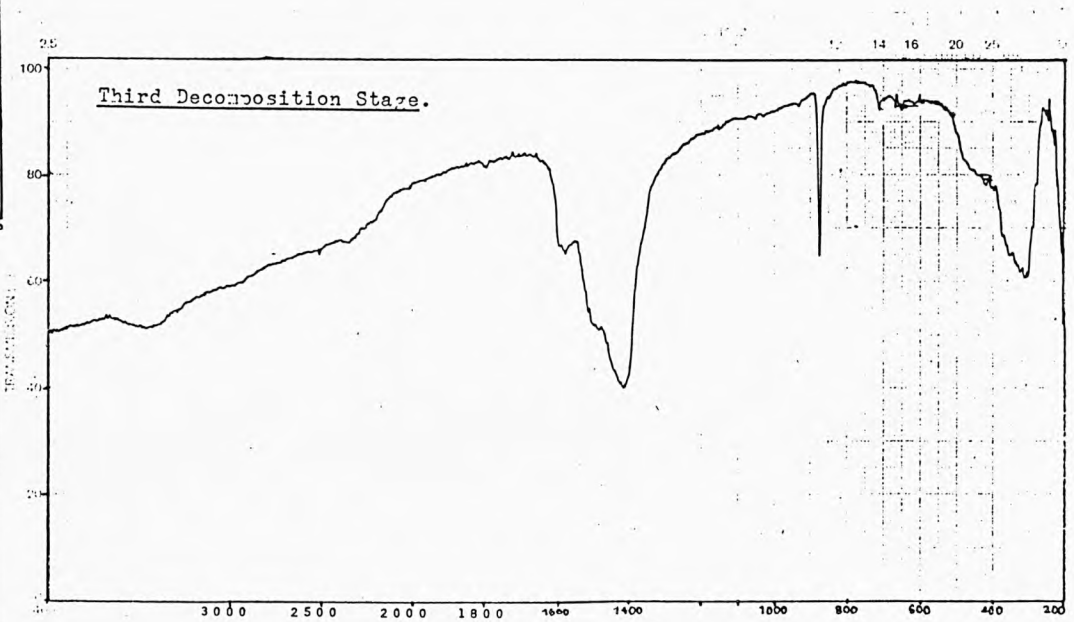

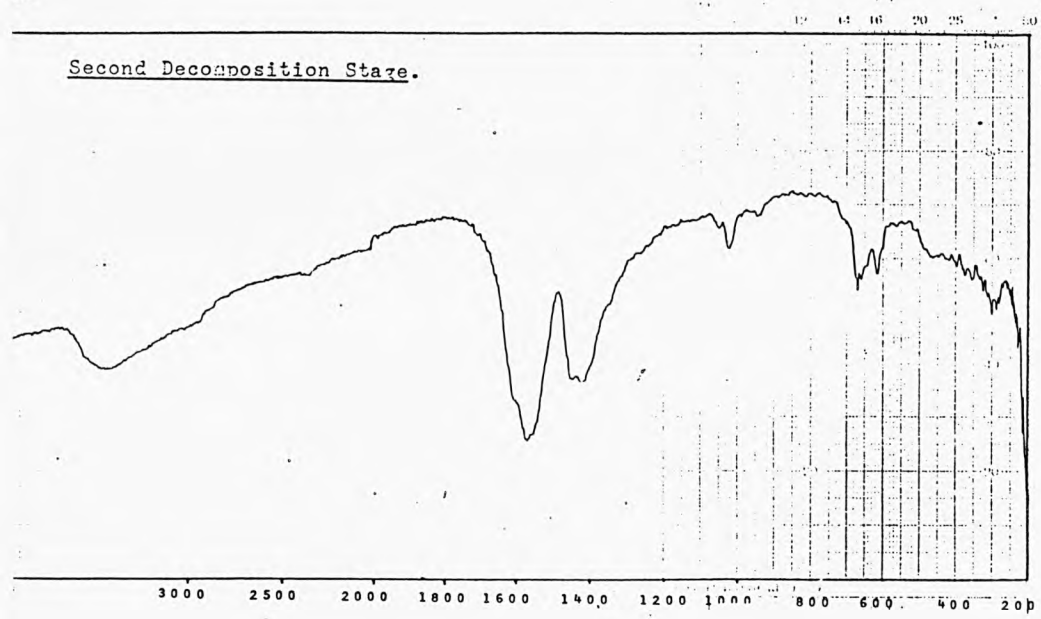

First Stage (192°C)

The TG trace (Fig. 3.29) shows a 3.5% weight loss corresponding to this first decomposition step. The i.r. spectrum (Fig. 3.30) is identical to that of the starting material, showing that no structural changes have taken place.

From the elemental analyses (Table 3.28) this first intermediate appears to be the dihydrate, ie. one water molecule eliminated initially, (calculated weight loss 2.8%). The x-ray data (Table 3.27) show that the unit cell has contracted compared with the trihydrate.

Second Stage (231°C)

A 28% weight loss is seen in the TG trace for this decomposition, which from the i.r. spectrum is associated with complete breakdown of the malonate structure. The i.r. spectrum shows the presence of carboxylate units, and comparing the spectrum with metal acetates, gives very good correlation. In particular, the intermediate has two peaks at 1022 and 1050cm^{-1}, q.v. CH_3COOK 1018 and 1049cm^{-1} (CH_3 rocking modes) and composite peaks in the region 680 - 615cm^{-1} (CH_3COOK - 670 to 620cm^{-1}).

From the elemental analyses it is proposed that this intermediate has the composition $CaSn_2C_{4.5}H_6O_6$. The x-ray data are consistent with the presence of SnO in the form previously observed in these decomposition studies.

During decomposition gaseous products are evolved, these were analysed by mass spectrometry which showed that acetone and CO_2 were produced.

Third Stage (377°C)

A weight loss of 9.5% is observed, which from mass spectrometric analysis is due to the evolution of acetone, this has a calculated weight loss of 9.1%.

The i.r. spectrum is different to that of either the malonate or the second intermediate, and by comparison with the i.r. spectrum of $CaCO_3$ is found to be in good agreement. The x-ray data are virtually identical to those of the second intermediate, showing that SnO is still present.

Based on these findings and the elemental analyses, the final residue has the formula $CaSn_2C_{1.5}O_5$ and comprises of $CaCO_3 + 2SnO + \frac{1}{2}C$.

3.9. Discussion.

The complex tin(II) malonates - $A_2Sn_2(CH_2C_2O_4)_3.xH_2O$, (for A = Na, x = 2, for A = K, x = 1, for A = NH_4^+, x = 0), and $CaSn_2(CH_2C_2O_4)_3.3H_2O$ decompose via slightly different processes. For the Na complex, decomposition occurs in three stages: (1) loss of both water molecules, (2) breakdown of the malonate groups associated with Sn to give SnO and partial breakdown of the malonate groups associated with Na to give CH_3COONa, and (3) pyrolysis of CH_3COONa to give Na_2CO_3. In the case of the K derivative the decomposition is by a two stage process, the water molecule is not evolved in a first pyrolysis step but is involved in the breakdown of the stannous malonate groups, with the formation of SnO and CH_3COOK. The second pyrolysis step is equivalent to the third stage in the Na complex, being breakdown of the alkali metal acetate to give K_2CO_3. The Ca malonate complex

behaves in a way which is intermediate between the Na and K derivatives, ie. decomposition takes place in three stages, the first stage being partial dehydration and the second stage being decomposition involving the remaining water molecules to give SnO and $Ca(CH_3COO)_2$. The final step is again breakdown of acetate to carbonate giving $CaCO_3$. For the ammonium complex, no clear decomposition stages can be identified but there appear to be two overlapping processes with SnO as the final product.

For the Na and Ca complexes, $Na_2Sn_2(CH_2C_2O_4)_3.2H_2O$ and $CaSn_2(CH_2C_2O_4)_3.3H_2O$, where dehydration is the first pyrolysis reaction, the water is evolved at relatively high temperatures (184 and 192°C respectively, see TG traces in Figs. 3.23 and 3.29). Although the dehydration temperatures are high they are consistent with those of known alkali and alkaline earth malonates, eg. $Na_2(CH_2C_2O_4).H_2O$ (185°) and $Ba(CH_2C_2O_4).H_2O$(170°). The weight losses, product elemental analyses, (Tables 3.22 and 3.28), and i.r. spectra (Figs. 3.24 and 3.30) all confirm that the final products of this first decomposition stage for the Na and Ca complexes are the anhydrous complex malonate, $Na_2Sn_2(CH_2C_2O_4)_3$ and the dihydrate $CaSn_2(CH_2C_2O_4)_3.2H_2O$, respectively. The anhydrous Na complex was found to be amorphous but the dihydrated Ca complex is crystalline with a simpler x-ray diffraction powder pattern (Table 3.27) than the parent material.

The next stage in the decomposition of the complexes involves the complete breakdown of the malonate groups associated with tin to give SnO plus the first step of the breakdown of the malonate groups associated with the s-block elements. Two step decompositions have been reported for the simple alkali and alkaline earth elements with the first step being evolution of CO and formation of acetates[11]. The acetate formation step in the complex tin malonates occur at 202, 199 and 231°C for the Na, K and Ca derivatives respectively and these temperatures are lower than the first step in the decomposition of the simple malonates at

341, 341 and 400°C, respectively. The decomposition of the malonate groups associated with the tin clearly catalyse the first step breakdown of the remaining malonate groups to give acetate.

Two different decomposition mechanisms are proposed for this decomposition stage. For the Na derivative, the anhydrous complex is brokendown to give $2SnO + 2CH_3COONa$ with evolution of CO_2 and CO. In the cases of the K and Ca derivatives, decomposition proceeds directly from the hydrated complexes to SnO and metal acetates, but with evolution of methanol and CO_2, showing that the coordinated water has been involved in the pyrolysis mechanism. The mechanism for the anhydrous Na complex, $Na_2Sn_2(CH_2C_2O_4)_3$ involves proton dissociation from an active methylene group to an adjacent carboxylic oxygen atom followed by ion-exchange and breakdown of the malonate groups, as in the alkali metal malonates[11], ie.

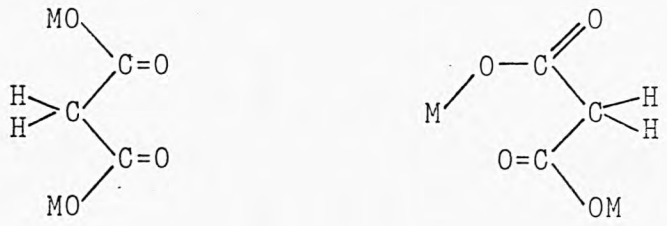

PROTON ↓ DISSOCIATION

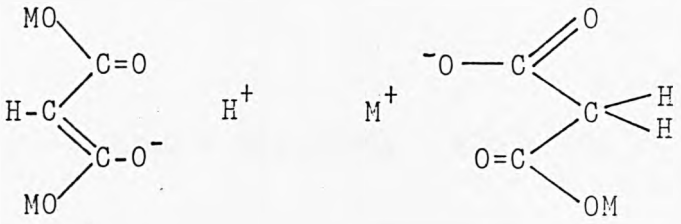

ION ↓ EXCHANGE

DECOMPOSITION

↓

MO

DECARBOXYLATION

↓

$CH_3COOM + CO_2$

However, with the hydrated complexes, ($K_2Sn_2(CH_2C_2O_4)_3.H_2O$ and $CaSn_2(CH_2C_2O_4)_3.2H_2O$) decomposition must proceed via a combination of the above mechanism and attack by H_2O on the active CH_2 groups to give methanol:

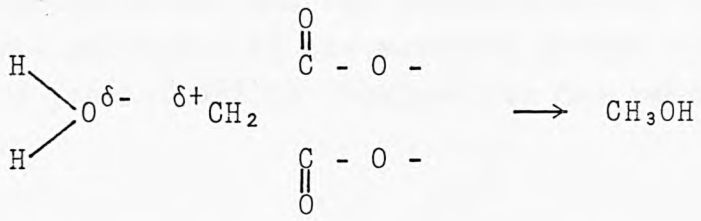

The decomposition reactions taking place are:

$$Na_2Sn_2(CH_2C_2O_4)_3 \longrightarrow 2SnO + 2CH_3COONa + 4CO + CO_2$$

$$K_2Sn_2(CH_2C_2O_4)_3.2H_2O \longrightarrow 2SnO + 2CH_3COOK + \tfrac{1}{2}C + CH_3OH + 2CO + 2CO_2 + \tfrac{1}{2}O$$

$$CaSn_2(CH_2C_2O_4)_3.2H_2O \longrightarrow 2SnO + Ca(CH_3COO)_2 + \tfrac{1}{2}C + CH_3OH + 3\tfrac{1}{2}CO_2$$

For all three complexes the final pyrolysis reaction involves breakdown of the acetate groups to give metal carbonates with evolution of acetone, (Na and K), and ethane + CO (Ca). The final decomposition reactions take place at 435, 451 and 403°C, respectively in the correct order for breakdown of the alkali metal and alkaline earth metal acetates, although at slightly lower temperatures than the 490, 489 and 439°C, respectively found for the acetates formed from simple malonates.

For the ammonium complex, $(NH_4)_2Sn_2(CH_2C_2O_4)_3$, decomposition takes place in two closely overlapping and inseparable steps to leave a residue equivalent to one mole SnO, (calculated residue weight 23%, obtained 21%). Decomposition commences ca. 200°C which is very similar to the temperature for breakdown of the malonate groups associated with Sn. During the course of the decomposition a solid product was collected on the cold probe which from the elemental analyses was found to be stannous acetate, $Sn(CH_3COO)_2$. The temperature of decomposition and the weight loss are in agreement with the pyrolysis of the malonate groups associated with Sn. A weight loss of 58% is obtained for the reaction:

$$(NH_4)_2Sn_2(CH_2C_2O_4)_3 \longrightarrow (NH_4)_2C_2O_4 + SnO + Sn(CH_3COO)_2\uparrow + CO_2 + 2CO$$

From the mass spectrometric analysis both CO_2 and CO are identified in the gaseous products. Ammonia from a second step breakdown of ammonium oxalate is also found in the gaseous products. Complete decomposition of ammonium oxalate is equivalent to a weight loss of 21.4% which is in good agreement with the experimental weight loss of ca. 23% and the observed

gaseous products:

$$(NH_4)_2C_2O_4 \longrightarrow 2NH_3 + 2CO_2 + H_2$$

The x-ray data on the solid residue show only the presence of blue-black SnO.

The decomposition reactions of the acetates formed in this step are single stage processes for the Na and K complexes, and acetone is the only gaseous decomposition product:

$$2CH_3COOA \longrightarrow A_2CO_3 + CH_3COCH_3 \qquad (A = Na, K)$$

For the Ca complex this step involves the two overlapping processes involved with the conversion of acetate to oxalate and the subsequent decomposition of Ca oxalate. The total weight loss of 9.7% at this stage is thus made up of two weight losses of ca. 6.1 and 3.6%, respectively. These results are similar to those described for $CaSn_2(CH_3COO)_6$ in section 3.5, the presence of ethane and CO_2 rather than acetone in the gaseous products of the decomposition of the Ca compound is also consistent with observations made on the decomposition of $CaSn_2(CH_3COO)_6$ and can be explained in terms of formation of calcium oxalate as a transient intermediate with evolution of C_2H_6, (calculated weight loss 4.7%), which is unstable at the temperature formed (405°C). This would then be followed by rapid decomposition to give the final, stable product $CaCO_3$ with evolution of CO, which disproportionates to give CO_2 (4.4% weight loss). This would give a total weight loss of 9.1%, which is in good agreement with the experimental value.

The x-ray data on these final residues still show the presence of SnO and in the case of the Na and K systems, lines due to carbonates.

3.10. References.

1. Ref. 127 Chapter 1.

Index - Chapter 4.

4.1. Introduction.

In this chapter the thermal behaviour of a number of compounds containing Sn - C bonds is recorded, Four different types of organotin compound have been studied: (i) those containing oxide or hydroxide groups; (ii) organotin nitrates; (iii) organotin sulphates; and (iv) organotin carboxylates.

4.2. Triphenyltin hydroxide, $|Ph_3SnOH|$.

The thermal gravimetry/differential thermal analysis data, (TG/DTA), show that Ph_3SnOH decomposes in three stages as detailed in Table 4.1 and Fig. 4.1.

Decomposition Reaction	Temperature (°C)	Weight Loss (%)	DTA Feature
1	75	2.5	Endothermic
2	290	59.5	Endothermic
3	362	16.5	Endothermic

TABLE 4.1.

From the percentage weight loss data, the first decomposition corresponds to the reaction:

$$2Ph_3SnOH \xrightarrow{75^{\circ}C} Ph_3SnOSnPh_3 + H_2O \quad .....(1)$$

and the second to:

$$nPh_3SnOSnPh_3 \xrightarrow{290^{\circ}C} (Ph_2SnO)_n + nPh_4Sn \quad .....(2)$$

Fig. 4.1.

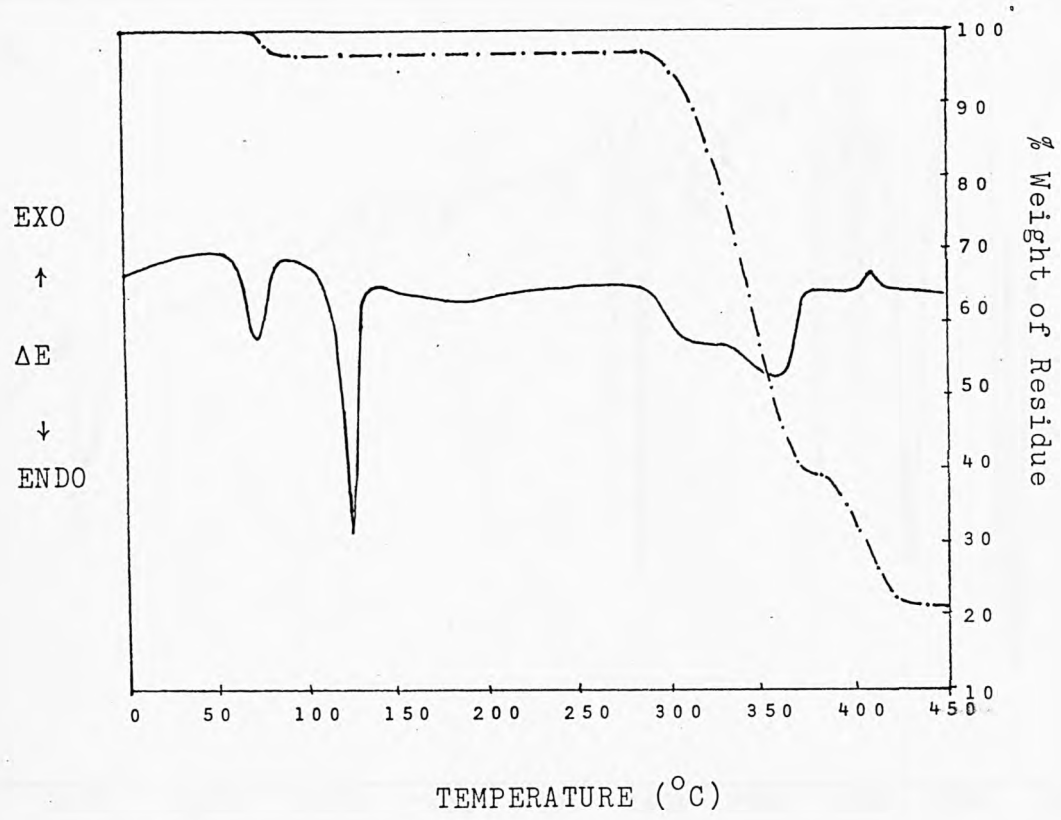

However, no simple decomposition reaction can be inferred from the percentage weight loss recorded in the third decomposition, and to confirm the products postulated in the reactions (1) and (2), (also proposed by other workers[1-3]), the pyrolysis of approximately 0.2g Ph_3SnOH was carried out stepwise at temperatures slightly in excess of those recorded in Table 4.1, with product isolation and characterisation at each stage.

The volatile product on the probe was collected and a sample of the non-volatile product removed for analysis. The compounds identified are in Table 4.2, and their i.r. spectra presented in Fig. 4.2.

Figure 4.2: I.R. Spectra of Ph_3SnOH Decomposition Products.

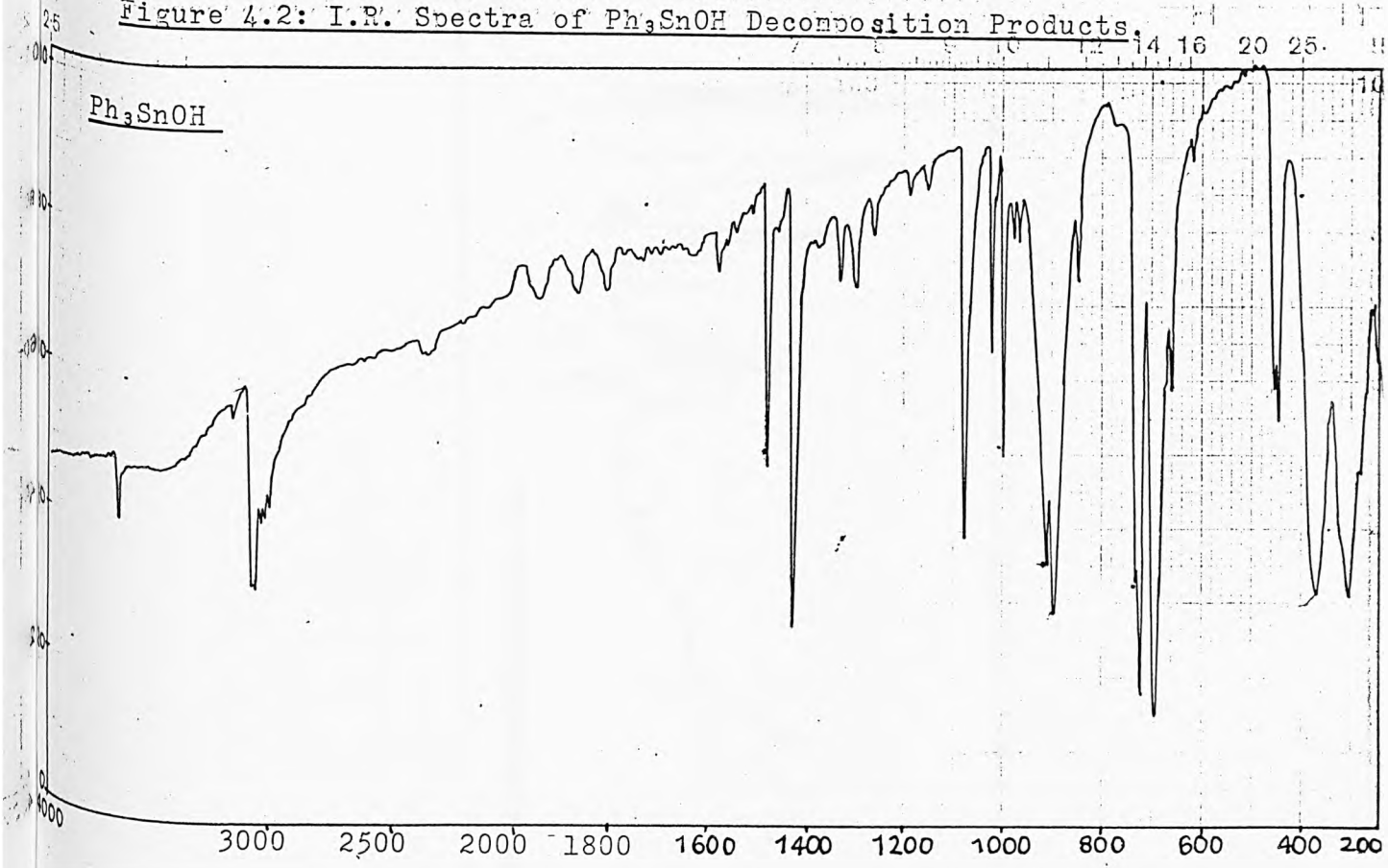

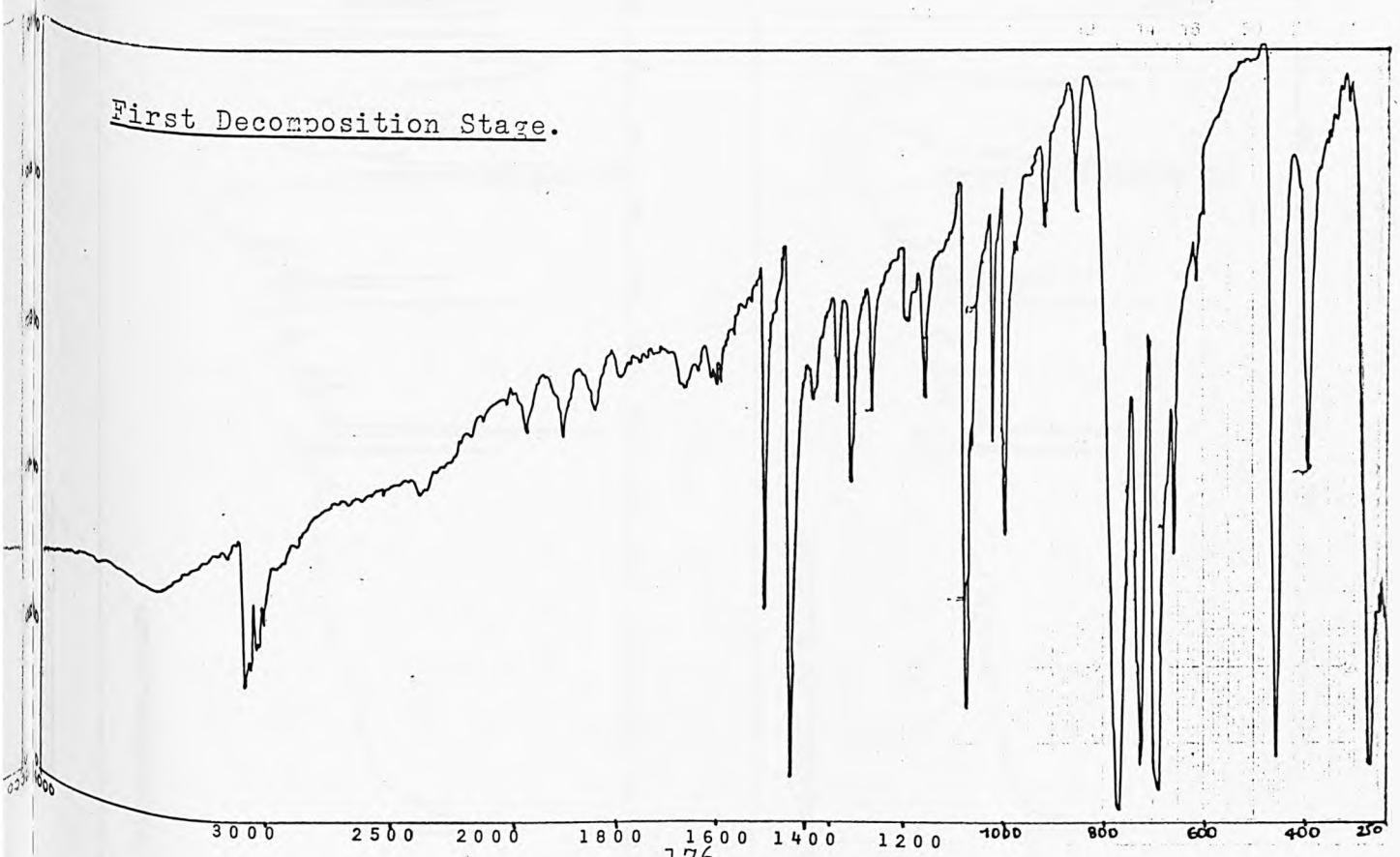

Figure 4.2. Cont..

Second Decomposition Stage.

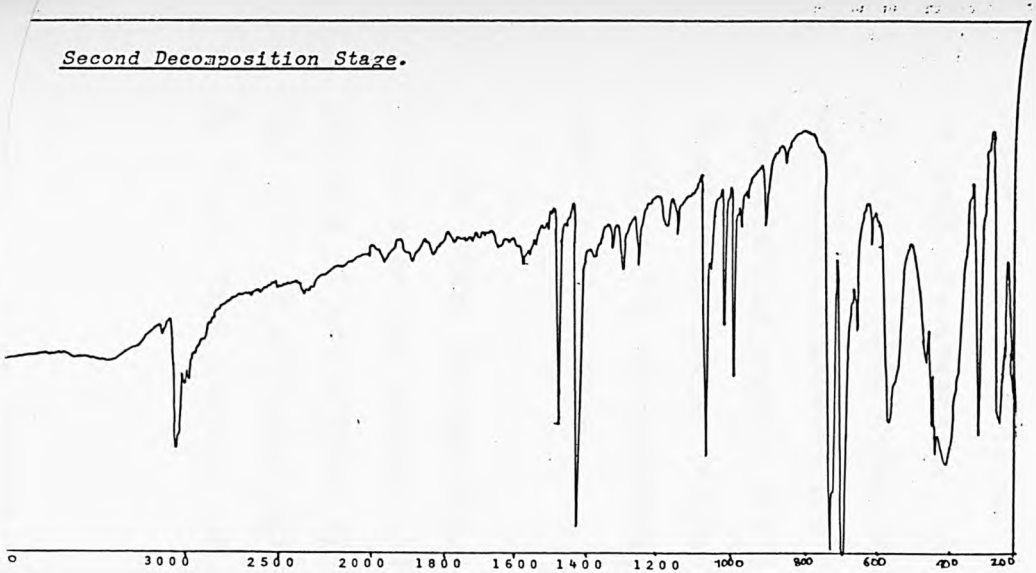

Third Decomposition Stage - Ph_2

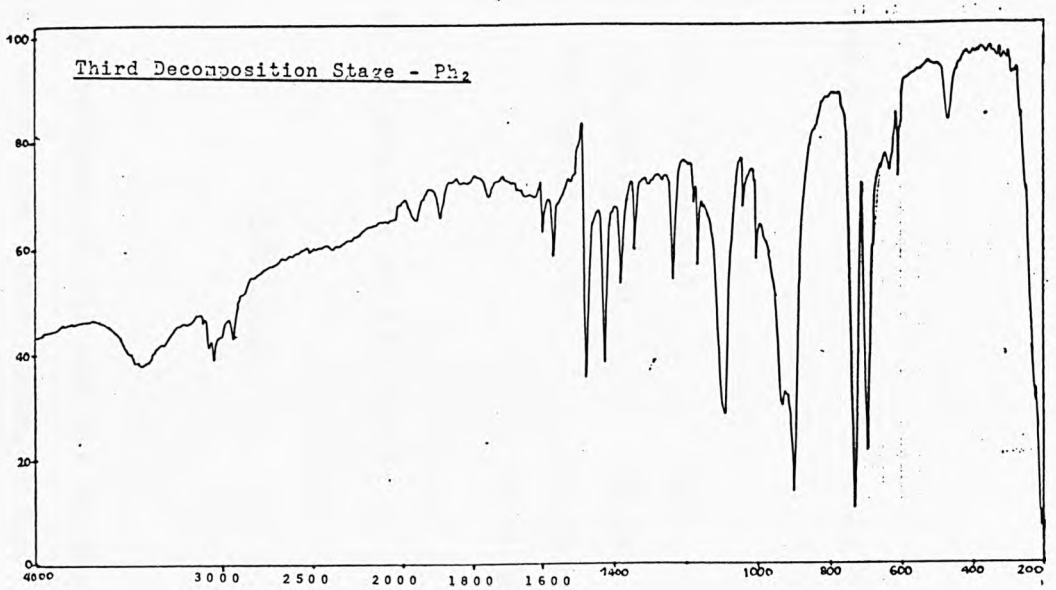

Third Decomposition Stage - Ph_4Sn

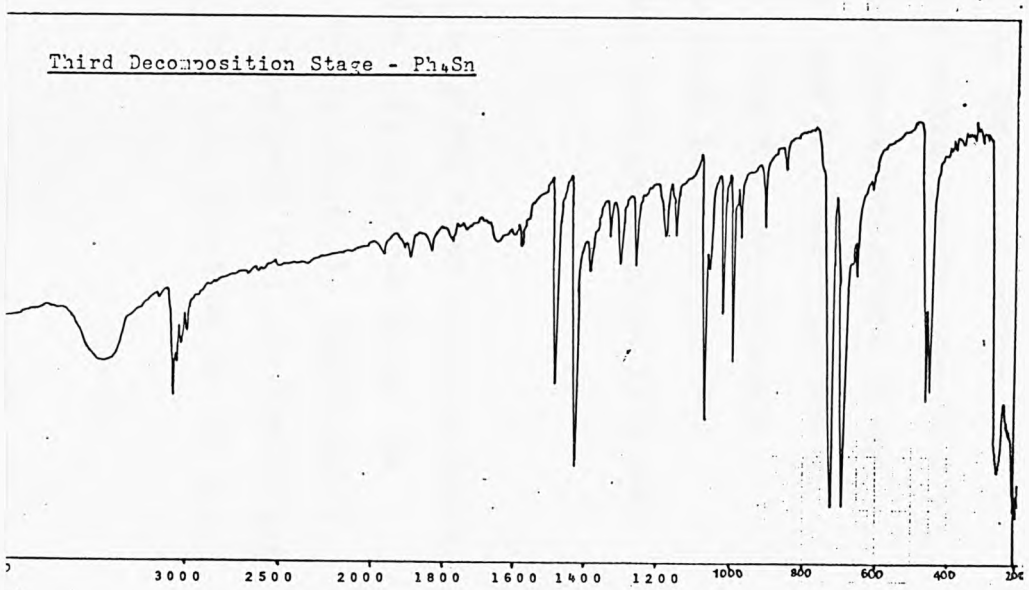

Temperature (°C)	Non-volatile Product		Volatile Product	
85	$(Ph_3Sn)_2O$	(I)	H_2O	
310	$(Ph_2SnO)_n$	(II)	Ph_4Sn	(III)
400	Tin Oxide	(IV)	Ph-Ph*:Ph_4Sn	(V)
			Ph-Ph:Ph_4Sn*	(VI)

*major component; volatility of (V) >(VI)

TABLE 4.2.

The i.r. and C, H analysis of (I) and the TG data are consistent with reaction (1) being the first decomposition step. The O - H bands at 3610 and 895cm^{-1} in the i.r. spectrum of Ph_3SnOH are absent in (I); the percentage weight loss of 2.5 is close to that required, (2.45). Characterisation of the non-volatile product (II) by i.r. and C, H analysis, and of the volatile product (III) by i.r. and U.V. spectroscopy identified them as $(Ph_2SnO)_n$ and Ph_4Sn respectively. For reaction (2) the percentage weight loss required is 59.3 and that found is 59.5.

The third decomposition reaction gives three final products, a non-volatile residue (IV), whose i.r. spectrum shows the absence of any organic species, and two volatile fractions(V) and (VI) of different volatility. Component (VI) was identified as Ph_4Sn from its i.r. spectrum. The i.r. spectrum of (V) was

similar to that of (VI), but with one extra band at 749cm^{-1}. The absorption band λ_{max} 250nm in the U.V. spectrum of (V) suggested the presence of Ph-Ph. A TLC study using a 100:50:5 mixture of n-butanol:water:acetic acid[4,5] showed that (V) consisted of Ph-Ph with a small amount of Ph_4Sn whereas (VI) consisted mostly of Ph_4Sn with a small amount of Ph-Ph, (Ph-Ph, R_f 1.00, Ph_4Sn, R_f 0.00).

^{119}Sn Mössbauer spectroscopy on the non-volatile residue (IV) gave the following data: a Sn(II) doublet, [δ=2.76mms^{-1}, Δ=1.41mms^{-1},(±0.02mms^{-1})], assignable to SnO and a Sn(IV) singlet (δ = 0.12±0.01mms^{-1}) assignable to SnO

The volumetric determination of Sn(II) in the residue using ceric sulphate showed that the Sn(II):Sn(IV) ratio was approximately 1:5.

When a sample of Ph_3SnOH was heated directly to 400°C more Ph-Ph and SnO were produced than when it was heated stepwise to the same temperature. By titrimetry the Sn(II):Sn(IV) ratio in the residue in this case was approximately 5:1.

Thus for the third decomposition reaction, the contribution of the reductive elimination reaction:

$$(Ph_2SnO)_n \longrightarrow n(Ph\text{-}Ph) + SnO$$

to the overall decomposition of $(Ph_2SnO)_n$ when Ph_3SnOH is heated stepwise to 400°C is less than when it is heated directly to the same temperature.

The results show that the thermal decomposition of Ph_3SnOH by the two modes of heating are as follows:

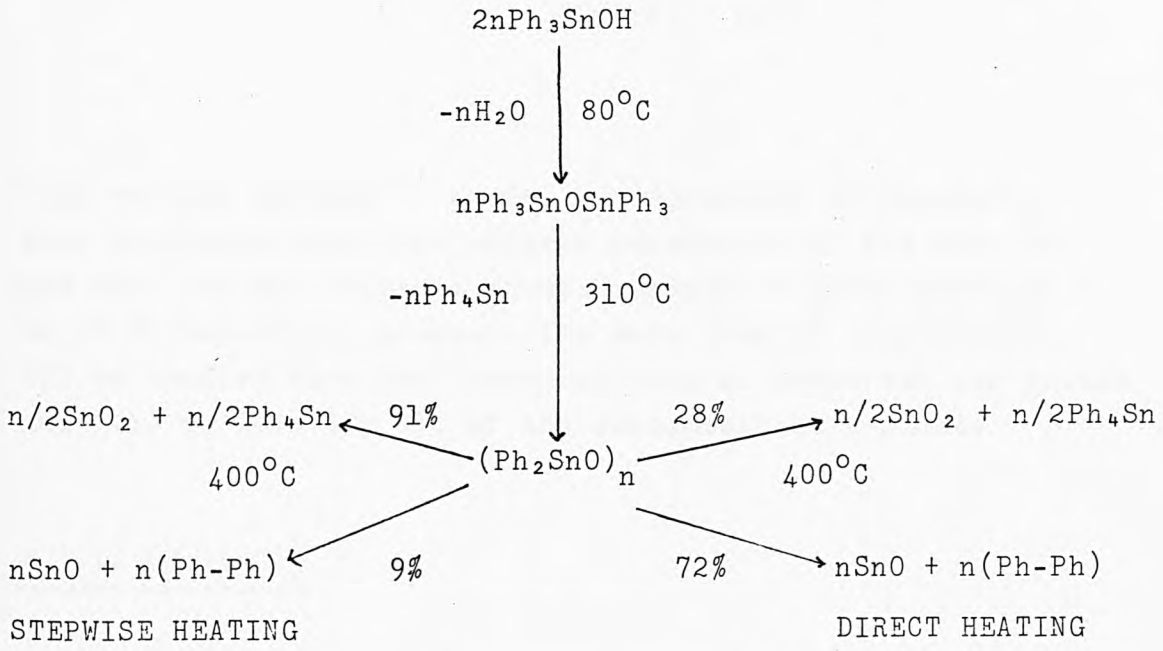

4.3. Alkyl Tin Oxide Polymers.

Since one of the decomposition steps of the pyrolysis of Ph_3SnOH leads to the polymer $(Ph_2SnO)_n$ it was decided to study the thermal decompositions of the compounds $|R_2SnO|_n$, (R= Me, Et, Pr). The decomposition of the polymer intermediate from Ph_3SnOH suggested that two decomposition reactions occurred simultaneously, viz.

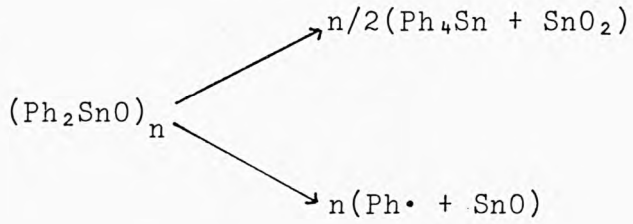

Some earlier workers[1] on the decomposition of $(Me_2SnO)_n$ also suggested that this polymer decomposed in the same way and that the Me• radicals formed reacted to give ethane as a major decomposition product. The main aims of this work are (i) to confirm that the decompositions do occur via two routes and (ii) to identify all of the decomposition products.

4.3.1. $(Me_2SnO)_n$

The TG/DTA data for $(Me_2SnO)_n$, (see Fig. 4.2), show that it melts at 127°C and decomposes in one stage at 390°C with a weight loss of 39%.

Fig. 4.2.

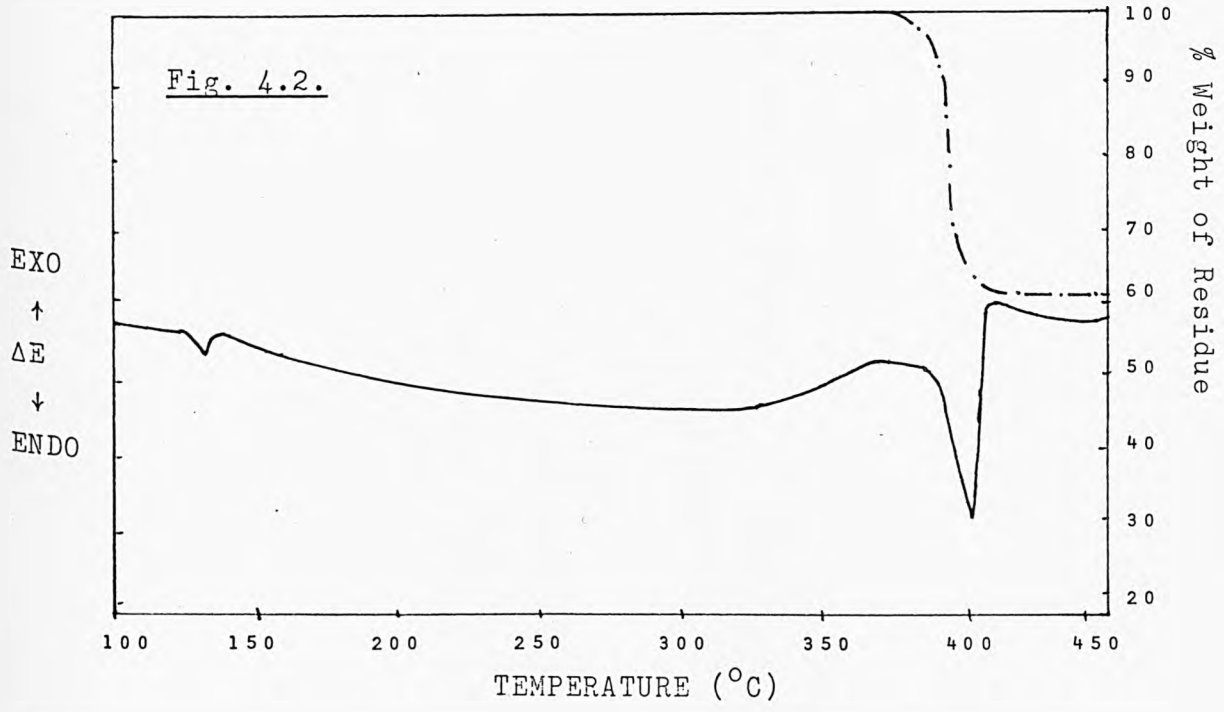

Table 4.3. Mössbauer data for Alkyl Tin Oxide Residues.

Compound	Heating Rate $^{o}min^{-1}$	Sn(II) $\delta(mms^{-1})$	Sn(II) $\Delta(mms^{-1})$	Sn(IV)
$(Me_2SnO)_n$	19 + 47	2.84±0.05	1.96±0.05	Singlet δ 0.18±0.02
	96	2.89±0.02	1.92±0.02	Singlet δ 0.10±0.01
$(Et_2SnO)_n$	19 + 47	2.97±0.10	1.90±0.10	Singlet δ 0.24±0.02
	96	2.90±0.01	1.87±0.01	Doublet δ 0.14±0.03 Δ 0.67±0.03
$(nPr_2SnO)_n$	19	2.86±0.01	1.93±0.01	Doublet δ 0.12±0.03 Δ 0.64±0.03
	47 + 96	2.87±0.01	1.93±0.01	Doublet δ 0.10±0.03 Δ 0.67±0.03
SnO	-	1.71	1.45	-
SnO_2	-	-	-	δ=0, Δ=0

The decomposition pattern was found to be the same at the different heating rates 19, 47, and 96°min^{-1}. Tin(II) analyses of the solid products gave 37% Sn(IV) and 45.7% Sn(II) at these heating rates and show that Sn(II) and Sn(IV) are present in the solid products in the ratio 1:0.83, (Sn(II): Sn(IV)), and this is consistent with decomposition occurring by the two reactions:

$$(Me_2SnO)_n \longrightarrow n/2(Me_4Sn + SnO_2)$$

and

$$(Me_2SnO)_n \longrightarrow n(2Me\cdot + SnO)$$

in the ratio 1.66:1 at all heating rates.

The Mössbauer data for the solid residue, (Table 4.3), confirm the presence of both Sn(IV) and Sn(II) products.

The gaseous products of the pyrolysis were identified by mass spectrometry the main products being Me_4Sn and CH_4. The methane accounted for 93% of the light organic vapours in the products with ethane, ethene and ethyne being minor products at heating rates of 19 and 47°min^{-1} and ethane and ethene being minor products at a heating rate of 96°min^{-1}. The cracking pattern that identifies Me_4Sn as a gaseous product is shown:

Strongest Me_4Sn lines:

	$Me_4{}^{120}Sn$	$\xrightarrow{-Me}$	$Me_3{}^{120}Sn$	$\xrightarrow{-Me}$	$Me_2{}^{120}Sn$
m/e	180.00		164.95		149.93
% Intensity	1.1		100		32.9

	$\xrightarrow{-Me}$	$Me_1{}^{120}Sn$	$\xrightarrow{-Me}$	^{120}Sn
		134.91		120
		35.8		17.6

Lines for the other isotopes of Sn, (^{122}Sn, ^{119}Sn, ^{118}Sn, and ^{117}Sn), following the same cracking pattern, are also present.

4.3.2. $(Et_2SnO)_n$

From the TG/DTA trace, (Fig. 4.3), the polymer $(Et_2SnO)_n$ melts at 137°C and decomposes in a single stage at 359°C with a weight loss of 55.8%. The same decomposition pattern was found at the three heating rates: 19, 47, and 96°min^{-1}, as in the case of the methyl analogue.

Fig. 4.3.

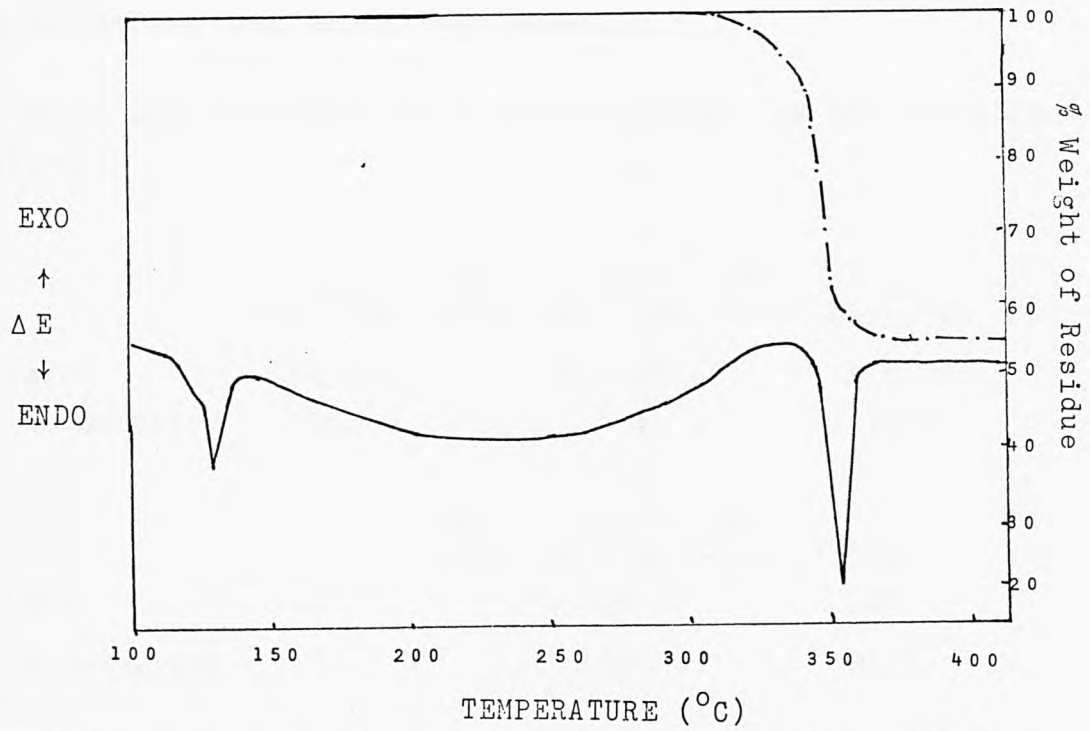

Tin (II) analysis of the solid products gave 28.25% Sn(IV) and 56.5% Sn(II) at these heating rates. This shows that Sn(IV) and Sn(II) are present in the solid products in the ratio 0.5:1, which is consistent with decomposition taking place by the two reactions:

$$(Et_2SnO)_n \longrightarrow n/2(Et_4Sn + SnO_2)$$

and

$$(Et_2SnO)_n \longrightarrow n(2Et\cdot + SnO)$$

in the ratio 1:1 at all heating rates.

The presence of Sn(II) and Sn(IV) in the solid residue is confirmed by the Mössbauer data presented in Table 4.3.

Mass spectrometry was used for analysis of gaseous decomposition products and identified Et_4Sn and butane, (C_4H_{10}) as the major volatile components. At 19 and 47°min^{-1}, the light organic vapours consisted solely of butane. At 96°min^{-1} butane was the major light organic vapour, with minor contributions from ethane and hexane.

Et_4Sn was identified as a gaseous product by the cracking pattern:

	$Et_4{}^{120}Sn$	$\xrightarrow{-Et}$	$Et_3{}^{120}Sn$	$\xrightarrow{-Et}$	$Et_2{}^{120}Sn$
m/e	236.16		207.01		178.00
% Intensity	0.2		3.3		50.0

		$\xrightarrow{-Et}$	$Et{}^{120}Sn$	$\xrightarrow{-Et}$	^{120}Sn
m/e			149		120
% Intensity			100		32.5

The same cracking pattern for the other isotopes, (^{122}Sn, ^{119}Sn, ^{118}Sn, and ^{117}Sn), was also observed.

4.3.3. $(nPr_2SnO)_n$

From the TG/DTA trace, (Fig. 4.4), two endotherms associated with melting are seen at 87 and 116°C, followed by decomposition in a single step at 322°C with a weight loss of 56%. The three heating rates: 19, 47 and 96°min^{-1} all show the same decomposition pattern also found with the methyl and ethyl analogues.

Fig. 4.4.

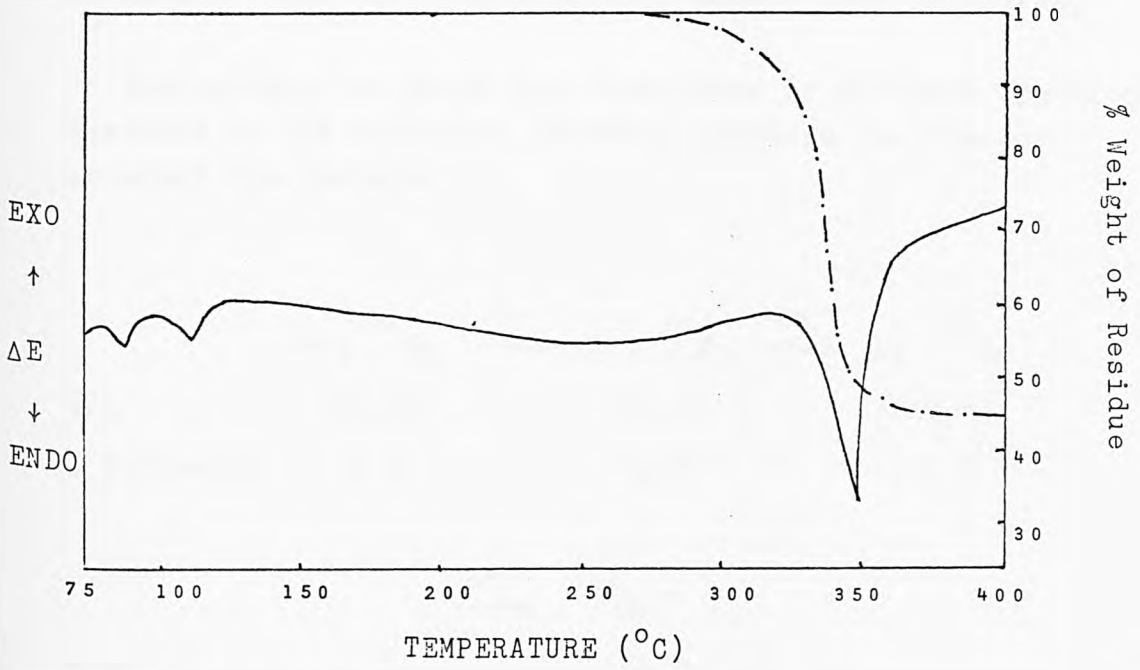

Tin(II) analysis of solid products at these heating rates gave 30% Sn(IV) and 54.3% Sn(II), which gives a ratio of 0.56:1 for Sn(IV):Sn(II) in the solid residue, and is consistent with decomposition taking place by the two reactions;

$$(nPr_2SnO)_n \longrightarrow n/2(Pr_4Sn + SnO_2)$$

and

$$(nPr_2SnO)_n \longrightarrow n(2Pr\cdot + SnO)$$

in the ratio 1:0.9 at all heating rates.

The Mössbauer data in Table 4.3 show that both Sn(II) and Sn(IV) are present in the solid residue.

Pr_4Sn and hexane were identified by mass spectrometry as the major gaseous pyrolysis products at all heating rates. At $19^{o}min^{-1}$, significant amounts of propane and propene are also identified, together with a trace amount of butane. At $47^{o}min^{-1}$, the major light organic vapour observed is hexane with a minor contribution from propane, propene and butane. At $96^{o}min^{-1}$, the only light organic vapour seen is hexane.

The presence of Pr_4Sn was identified in the mass spectrometric analysis by the following cracking pattern for the most abundant tin isotope:

	$Pr_3{}^{120}Sn$	$\xrightarrow{-Pr}$	$Pr_2{}^{120}Sn$	$\xrightarrow{-Pr}$	$Pr\ {}^{120}Sn$	$\xrightarrow{-Pr}$	${}^{120}Sn$
m/e	249.09		206.01		162.97		119.91
% Intensity	0.5		14.8		43.6		14.6

similar cracking patterns for the other Sn isotopes were also recorded.

4.4. Discussion.

The $|R_2SnO|_n$ polymers (R = Me, Et, n-Pr), melt at fairly low temperatures, (127 and 137°C for R = Me and Et, and two endotherms at 87 and 116°C for R = n-Pr, see Figures 4.2, 4.3, and 4.4.). The molten polymers then decompose at 390, 359, and 322°C, respectively. These single stage decompositions result in the formation of tetraalkyltin, light organic vapours, and a solid residue which is a mixture of amorphous tin(ii) oxide, SnO, and tin(iv) oxide, SnO_2.

Although the Sn(ii):Sn(iv) ratios in the final product can be altered if stepwise heating is carried out (ie. heating and cooling again), the rate at which the polymers are heated up to the decomposition temperatures does have an effect on the composition of the gas phase, but has no effect on the ratios of $SnO:SnO_2$ in the solid residues. For $(Et_2SnO)_n$ and $(n\text{-}Pr_2SnO)_n$, the major light organic vapours at all heating rates are butane (R = Et) and hexane (R = n-Pr), which arises from the following decomposition reaction:

$$(R_2SnO)_n \longrightarrow (2R^{\cdot} + SnO)$$

$$\downarrow$$

$$R_2 \qquad (R = Et, n\text{-}Pr)$$

However, for $(Me_2SnO)_n$, the major light organic vapour is methane, not ethane as would be expected from the above reaction. The large amount of methane observed must be due to thermal decomposition of tetramethyltin, Me_4Sn, which is known to give methane on pyrolysis[6-8].

Since the reactions for formation of SnO involve alkyl radicals, it is possible to envisage formation of other light organic compounds via chain reactions of the radicals in the vapour phase and to account for the minor gaseous products identified by mass spectrometric analysis. For $(Me_2SnO)_n$, the minor gaseous products identified are ethane, ethene, and ethyne; for $(Et_2SnO)_n$, ethane and hexane are produced; and for $(n\text{-}Pr_2SnO)_n$, propane, propene and butane are also identified.

Mössbauer spectroscopic analyses were carried out on the solid residues collected after thermal decomposition, and the hyperfine parameters are in Table 4.3. The results clearly show that both tin(ii) and tin(iv) oxide phases are present in all the residues. For the tin(ii) oxide portion of the residues, the isomer shift values are in good agreement with the known values for amorphous SnO, although larger quadrupole splittings are obtained. The stannic oxide component gives slightly anomalous Mössbauer results, producing a singlet at all heating rates for $(Me_2SnO)_n$ and $(Et_2SnO)_n$ at 19 and $47^{\circ}min.^{-1}$, and a doublet for $(n\text{-}Pr_2SnO)_n$ at all heating rates and for $(Et_2SnO)_n$ at $93^{\circ}min.^{-1}$.

Both the chemical shift and quadrupole splitting of the tin(ii) oxide phase obtained are higher than that for crystalline blue-black tetragonal tin(ii) oxide. These data can be explained in terms of the formation of a defect oxide structure in which the tin(ii) environment is more distorted than in the tetragonal oxide and in which the tin-tin interactions known to exist in the blue-black oxide are reduced because of deviations from tetragonal symmetry.

4.5. Organotin Nitrates.

In this section the thermal decompositions of two organotin(II) nitrates - diethyltin dinitrate, $Et_2Sn(NO_3)_2$ and diphenyltin dinitrate, $Ph_2Sn(NO_3)_2$, are presented. The analytical techniques used to characterise the products at each pyrolysis step are discussed in this section and possible mechanisms for their thermal decompositions presented in Section 4.6.

4.5.1. $Et_2Sn(NO_3)_2$.

The TG/DTA studies (Fig. 4.5) show that decomposition commences at 157 °C and terminates at 227°C with a residue weight of 45%. A two stage decomposition process is observed in the TG trace, with weight losses of 20 and 35% for the first and second stages, respectively, and are associated with exothermic energy changes.

Figure 4.5.

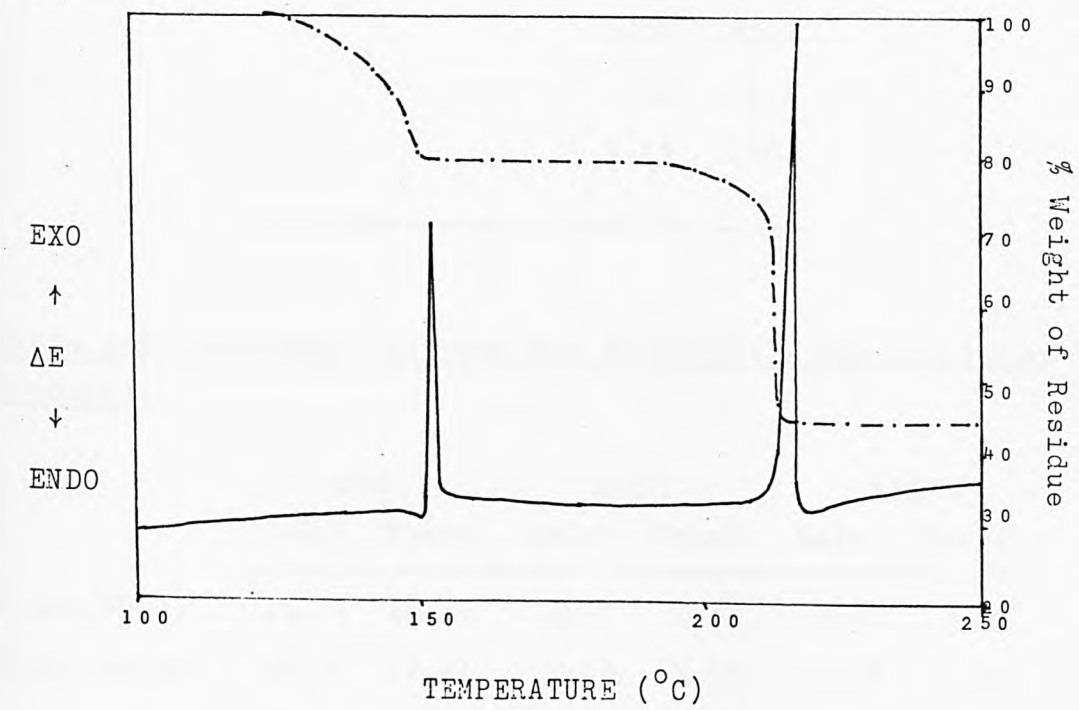

Table 4.4. X-Ray Diffraction Data for $Et_2Sn(NO_3)_2$ Decomposition Products.

First Stage		Residue	
d(Å)	I(%)	d(Å)	I(%)
11.53	60.0		
11.08	100		
10.27	66.7		
9.34	56.7		
9.13	40.0		
8.01	51.7		
7.67	41.7		
5.91	51.7		
		5.62	84.0
5.16	38.3		
		4.57	85.1
		4.14	25.5
		3.15	100

Table 4.5. Elemental Analyses for $Et_2Sn(NO_3)_2$ Decomposition Products.

	C(%)		H(%)		N(%)	
	Calc.	Found	Calc.	Found	Calc.	Found
$Et_2Sn(NO_3)_2$	16.51	16.26	3.47	3.81	9.63	9.06
First Stage	18.77	17.21	2.77	3.57	5.48	5.85
Residue	0	0.50	0	0.23	0	0

Figure 4.6: I.R. Spectra of $Et_2Sn(NO_3)_2$ Decomposition Products.

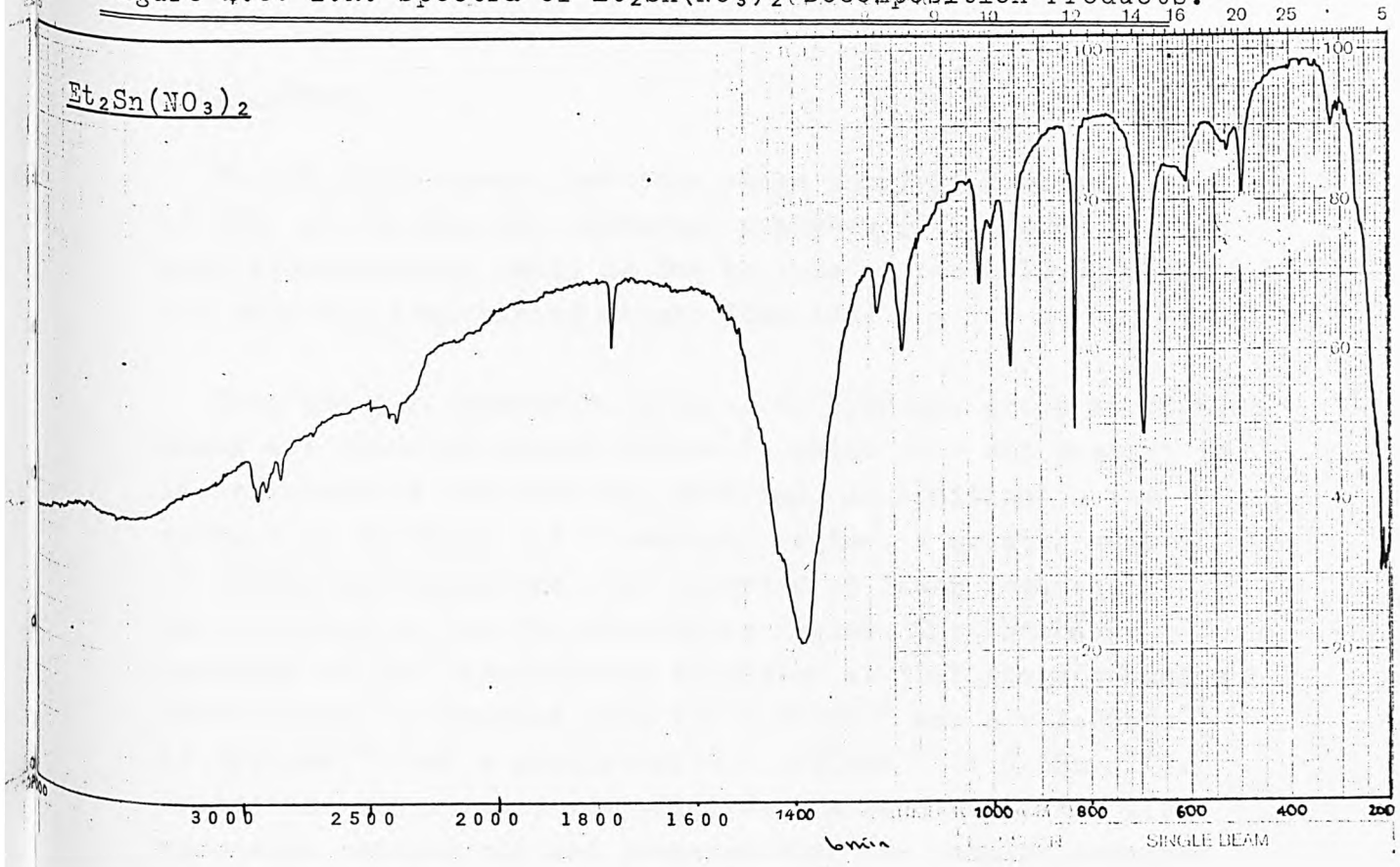

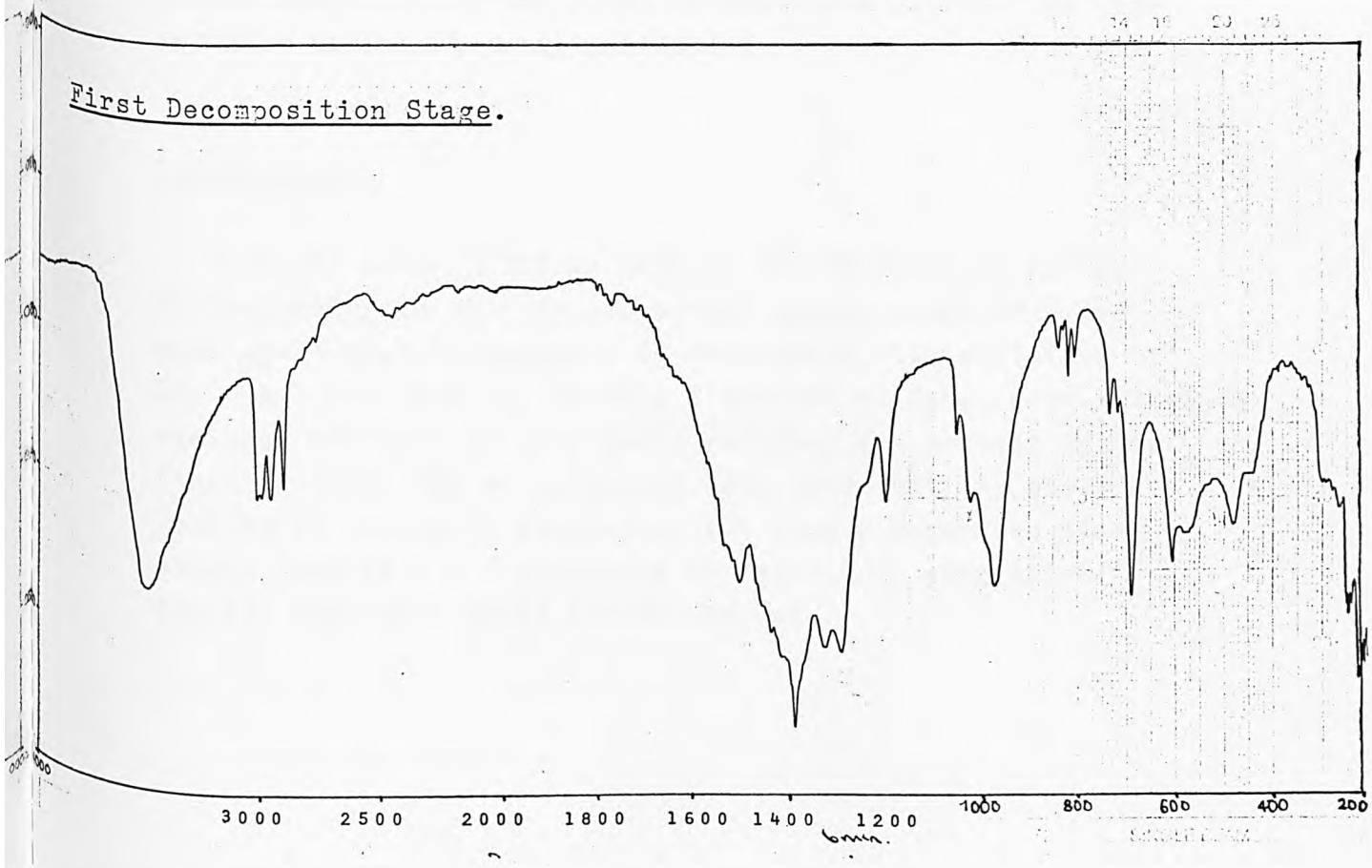

First Stage.

The TG trace shows that this stage involves a weight loss of 20%, which from the elemental analyses (Table 4.5) and the mass spectrometric study is due to loss of one mole NO and one mole O_2, (calculated weight loss 12%).

From the i.r. spectrum, (Fig. 4.6) hydroxyl group stretching modes are observed around 3450cm^{-1}, which were not present in the spectrum of the starting material. In addition to the extra line in the O - H stretching region, a greater number of stretching modes are also observed at lower frequencies particularly in the NO_3 stretching region. The Mössbauer spectrum of the intermediate collected at this stage contains three lines - a doublet with δ = 1.71mms^{-1} and Δ = 4.06mms^{-1} (± 0.02mms^{-1}) and a singlet at δ = 1.75mms^{-1} (± 0.02mms^{-1}). Proton nmr and x-ray powder diffraction studies (Table 4.4) were also carried out and compared with the results obtained for the parent material. The results obtained show that the parent compound and the first intermediate are not the same and have different x-ray parameters.

Second Stage.

A weight loss of 35% is seen in the TG trace at 227°C, corresponding to this decomposition stage, which from the mass spectrometric analysis is associated with evolution of NO, C_2H_6, C_2H_4 and O_2, leaving a residue of SnO_2. From elemental analyses (Table 4.5) no organic residues are present in the final product. The x-ray powder data show that the solid residue is virtually amorphous, but from a Mössbauer study a single line at δ = 0 (relative to $BaSnO_3$) is seen which implies that this final residue is SnO_2.

4.5.2. $Ph_2Sn(NO_3)_2$.

Diphenyltin dinitrate, $Ph_2Sn(NO_3)_2$, decomposes in three stages over the temperature range 101 to 334°C with weight losses of 11.3, 14 and 36.5% for the first, second and third pyrolysis stages, respectively (TG trace Fig. 4.7).

Figure 4.7.

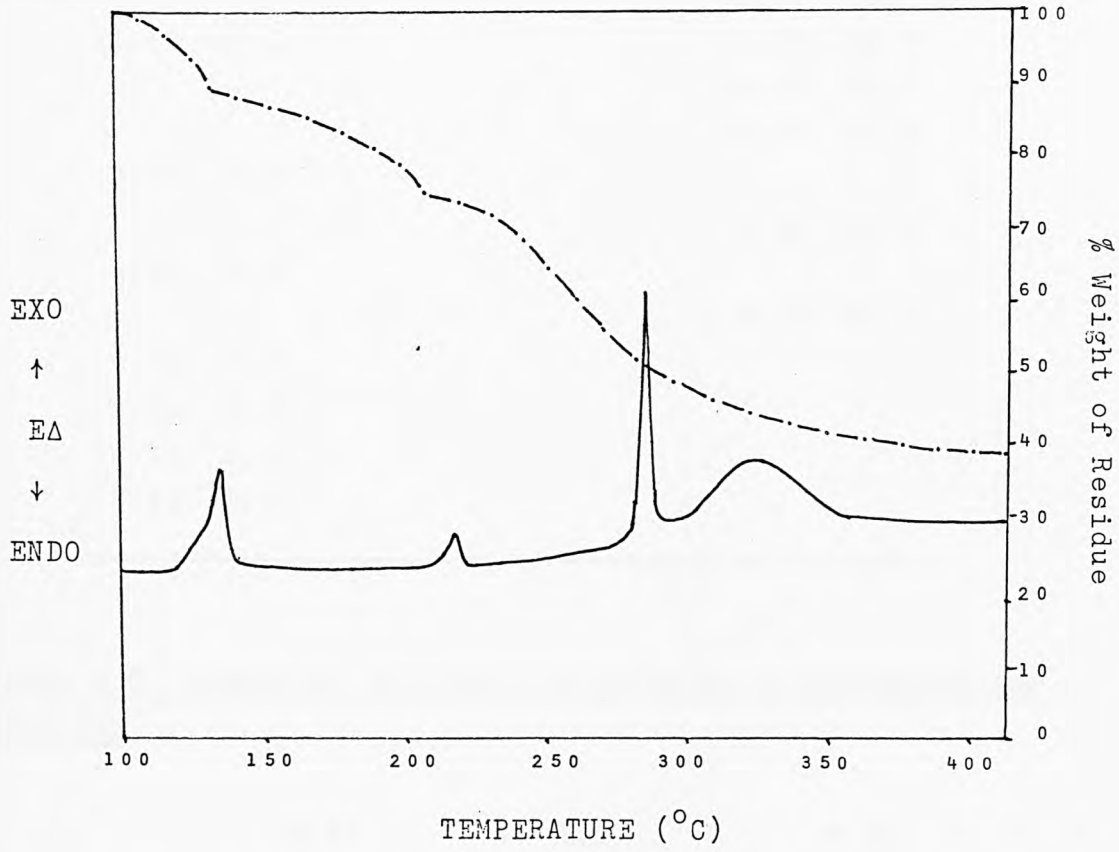

First Stage (101°C).

From the mass spectrometric study and elemental analyses (Table 4.7) the 11.3% weight loss associated with this first pyrolysis reaction involves loss of NO and O_2 as in the case of the ethyl derivative. The i.r. spectrum (Fig. 4.8) still shows the presence of nitrate groups in the region 1550 to 1250cm^{-1} although there are more lines present for the first

Table 4.6. X-Ray Diffraction Data for $Ph_2Sn(NO_3)_2$ Decomposition Products.

First Stage		Second Stage		Residue	
d(Å)	I(%)	d(Å)	I(%)	d(Å)	I(%)
				13.17	61.8
12.85	100	12.85	100		
		12.21	54.2	12.38	86.9
				12.01	100
11.19	45.1			11.18	66.7
				10.67	66.7
				10.27	51.3
8.92	43.6				
				6.45	61.8
6.24	50.0				
				6.13	84.5
6.04	64.5				
5.84	36.6				
4.99	34.5				
4.93	34.5				

Table 4.7. Elemental Analyses for $Ph_2Sn(NO_3)_2$ Decomposition Products.

	C(%)		H(%)		N(%)	
	Calc.	Found	Calc.	Found	Calc.	Found
$Ph_2Sn(NO_3)_2$	36.29	36.23	2.54	2.56	7.06	6.88
First Stage	34.11	33.46	3.15	2.47	3.98	3.50
Second Stage	26.20	26.66	1.84	2.16	5.10	3.60
Residue	4.26	4.32	0	0	0	0

Figure 4.8. I.R. Spectra for $Ph_2Sn(NO_3)_2$ Decomposition Products.

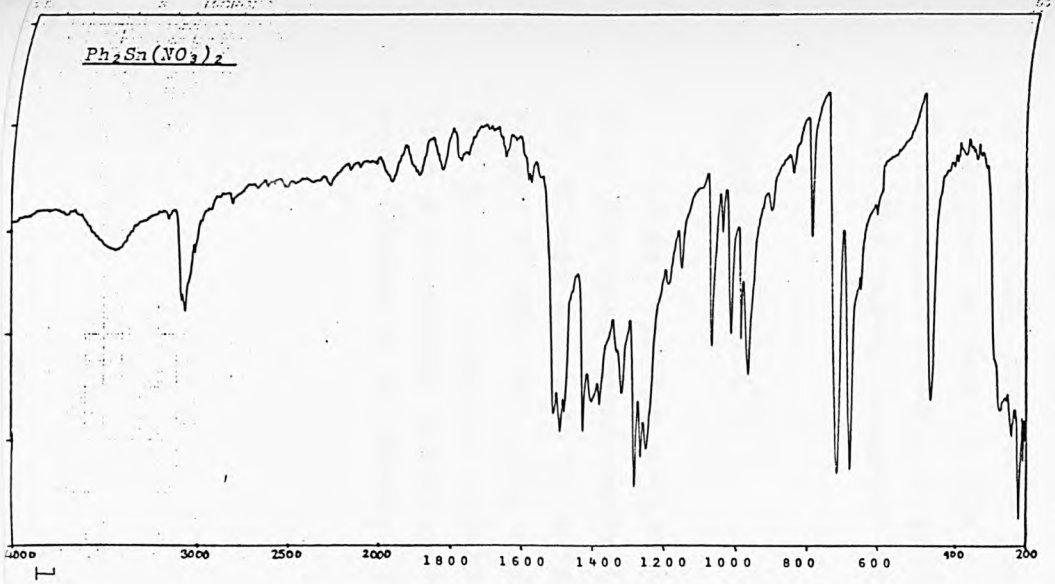

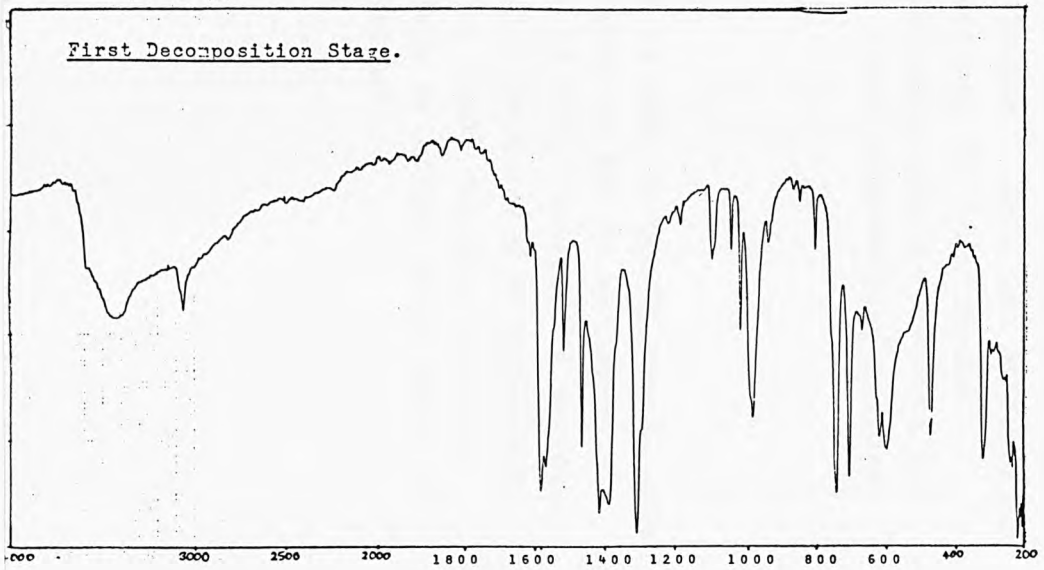

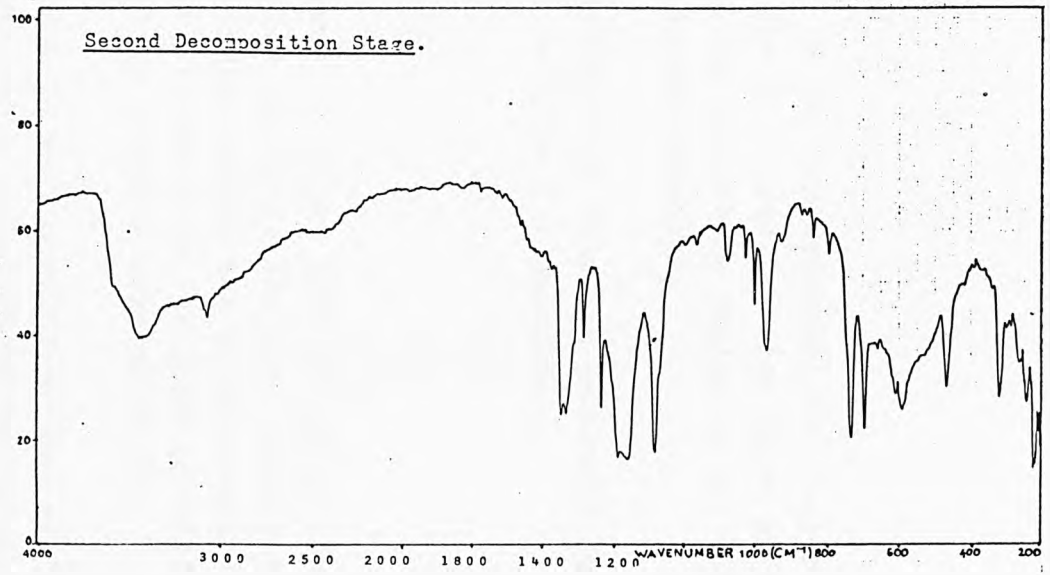

intermediate than in the corresponding NO_3^- region for the parent compound. The i.r. spectrum also shows an extra line in the hydroxyl group stretching region at ca. 3500cm^{-1} not present in the original material.

Powder x-ray diffraction data are presented in Table 4.6 and are different to those for $H_2Sn(NO_3)_2$.

Second Stage (160°C).

From the TG trace, a weight loss of 14% is observed for this second decomposition reaction. The mass spectrometry study and elemental analysis results are in agreement with removal of one mole benzene (C_6H_6) from the first pyrolysis product, this is equivalent to a weight loss of 19.5%.

The i.r. spectrum is very similar to that of the first intermediate except for a reduction in the intensity of the Ph stretching frequency peak at 3062cm^{-1}. Only two diffraction lines can be seen in the x-ray pattern for this second intermediate product compared with more complex patterns for both the parent compound and the first intermediate residue.

Third Stage (334°C)

A final residue weight of 45% is seen in the TG trace, which from the mass spectrometric analysis is due to evolution of NO, Ph and O_2, leaving a residue of SnO_2 (calculated residue weight 51.8%). No x-ray diffraction data could be collected due to the amorphous nature of the final residue, however, from a Mössbauer spectrometry study an isomer shift value of zero (relative to $BaSnO_3$) is obtained.

4.6. Discussion.

The thermal decompositions of diethyltin dinitrate and diphenyltin dinitrate, $Et_2Sn(NO_3)_2$ and $Ph_2Sn(NO_3)_2$, are complicated by their extremely deliquescent nature. The presence of water has the effect of partially hydrolysing the parent compounds during the first decomposition stage resulting in the evolution of NO and O_2 [9-11] to give:

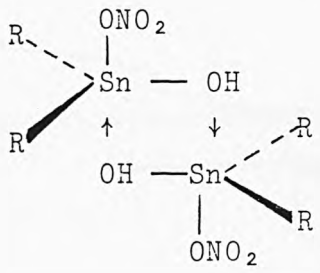

(R = Et, Ph)

These hydrolysis products are formed between 75 and 115°C for the ethyl compound, and between 101 and 146°C for the phenyl derivative and are characterised by elemental analysis (Tables 4.5. and 4.7.), and i.r. and nmr data (Figs. 4.6 and 4.8.). The infra red data show the presence of hydroxyl groups in the hydrolyses products that were not present in the parent organotin nitrates. A proton nmr study was carried out on the decomposition product of the first pyrolysis step for $Et_2Sn(NO_3)_2$ - disturbed triplets for the CH_2 groups, and disturbed doublets for the CH_3 groups are found at 8.2 and 8.6ppm, respectively, showing that there is a down-field shift on the CH_2 frequency of ca. 1ppm relative to the CH_3 groups. The general down-field trend for both the CH_2 and CH_3 group frequencies, and the change-over of frequencies for CH_2 and CH_3 (CH_2 now down-field of CH_3) suggests that strongly electronegative groups are present on an atom adjacent to CH_2. This could be NO_3^-, but the

Figure 4.8. nmr spectrum of $Et_2Sn(NO_3)_2$ - First Decomposition Stage.

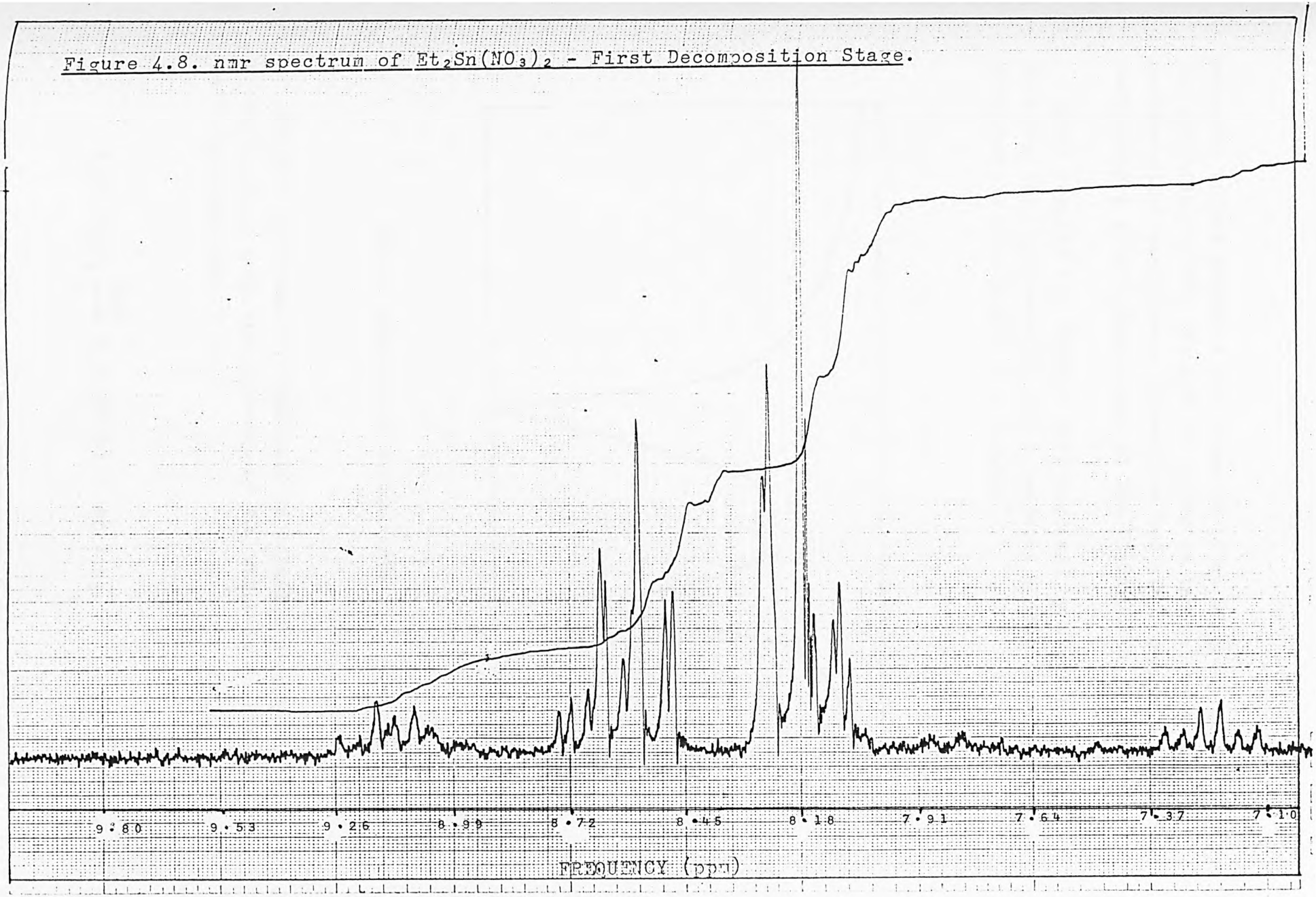

enhanced effect suggests the presence of an OH group as well. The splitting of the CH_2 and CH_3 peaks is indicative of an unsymmetrical environment around the two ethyl groups suggesting a slight distortion in the $Et_2Sn(OH)NO_3$ structure.

These results are further substantiated by the Mössbauer data for this intermediate which contains a doublet with parameters Δ = 3.69 and δ = 1.50mms^{-1}.

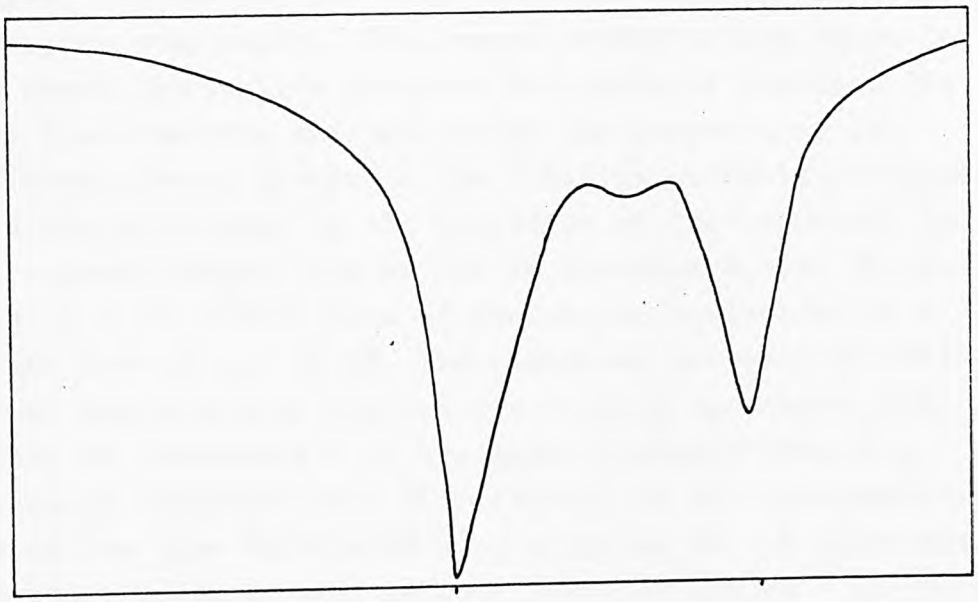

The mass spectrometric analysis on volatile decomposition products shows only the presence of NO, which is consistent with the reaction:

$$R_2Sn(NO_3)_2 \xrightarrow{H_2O} R_2Sn(OH)NO_3 + NO + O_2 \qquad (R = Et,Ph)$$

Giving weight losses of 12 and 11.3% for the ethyl and phenyl derivatives, respectively.

The x-ray data (Tables 4.4 and 4.6) for these first, solid, decomposition products are different to those of the parent compounds, and are not isostructural with each other, (x-ray data also show that the parent nitrates are not isostructural).

For the phenyl derivative there are two further decomposition stages, whereas for the ethyl compound only one further pyrolysis step occurs. The second decomposition stage for the phenyl derivative involves evolution of benzene. The mass spectrometric analysis shows the presence of two different phenyl groups in the volatile products, evolved at different stages in the breakdown of the conpound. An approximate weight loss of 14% is recorded in the TG trace (Fig. 4.7) at 160°C, loss of benzene is equivalent to a weight loss of ca. 19.5%. The elemental analyses on this second decomposition residue are in good agreement with either an intermediate of the type $Ph(H)Sn(OH)NO_3$ or a polymeric structure with Ph-bridging. If the intermediate was of the type $Ph(H)Sn(OH)NO_3$, a strong Sn - H stretching frequency would be seen between 1880 and 1800cm^{-1} in the i.r. spectrum, however, no bands are observed in this region (Fig. 4.8) which suggests that a polymeric intermediate of the the type:

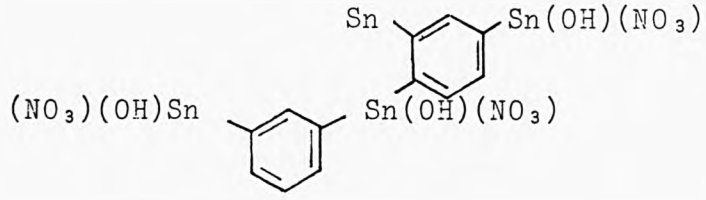

would be more in keeping with the spectroscopic evidence obtained. The i.r. spectrum is virtually identical to that of the first solid decomposition product, except that the phenyl group stretching frequency at 3062cm^{-1} is less distinct, which suggests that a similar compound is formed but with differences in the phenyl groups.

The x-ray data for this intermediate are different to those of both the parent material and the first solid residue, only two lines are visible in the x-ray pattern. It is proposed that this decomposition reaction is:

$$Ph_2Sn(OH)NO_3 \longrightarrow |\tfrac{1}{2}(Ph_2)|Sn(OH)NO_3 + PhH$$

For the ethyl and phenyl derivatives, the final decomposition reactions take place at 227 and 334°C, respectively, and involve breakdown of both the organic and the nitrate groups to give a residue of SnO_2.

The single peaks at $\delta = 0$ in the Mössbauer spectra of the final residue confirm the presence of SnO_2 which, from the elemental analyses is seen to contain some residual carbon in the residue from the phenyl derivative. The x-ray diffraction data show that the SnO_2 is amorphous, some diffuse lines being visible which are due to the carbon.

The mass spectrometric analysis on the gaseous volatile products for the final decomposition step for the ethyl derivative identified - NO, ethane and ethene, which are formed according to the reaction:

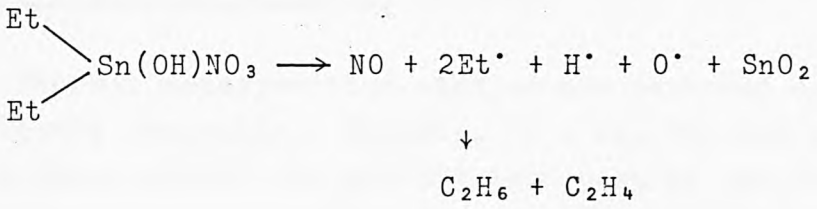

The solid and gaseous products collected at this stage also verify that the partially hydrolysed compound above is the product of the first decomposition reaction. The weight loss for this final decomposition reaction is 36%, (weight loss obtained 35%), leaving a residue of 51.8%.

For the phenyl derivative, the mass spectrometric analysis identified only the presence of NO and Ph, in agreement with the reaction:

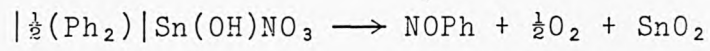

Nitrobenzene has also been identified in the volatile gaseous products of pyrolysis of triphenyltin nitrate (Ph_3SnNO_3), and is substantiated by mass spectrometric analysis which identified two different phenyl groups in the gaseous products.

4.7. Organotin Sulphates $|R_2SnSO_4|$

Thermal decomposition studies are reported on three dialkyltin sulphate compounds - R_2SnSO_4, (R = Me, Et, and n-Pr). The two lower alkyls (Me and Et) decompose in two stages over the temperature ranges 393 - 428 and 380 - 423°C, respectively, without melting . The n-Pr derivative melts endothermically at 129°C prior to decomposing in three stages between 133 and 265°C.

4.7.1. Dimethyltin Sulphate (Me_2SnSO_4)

Figure 4.9.

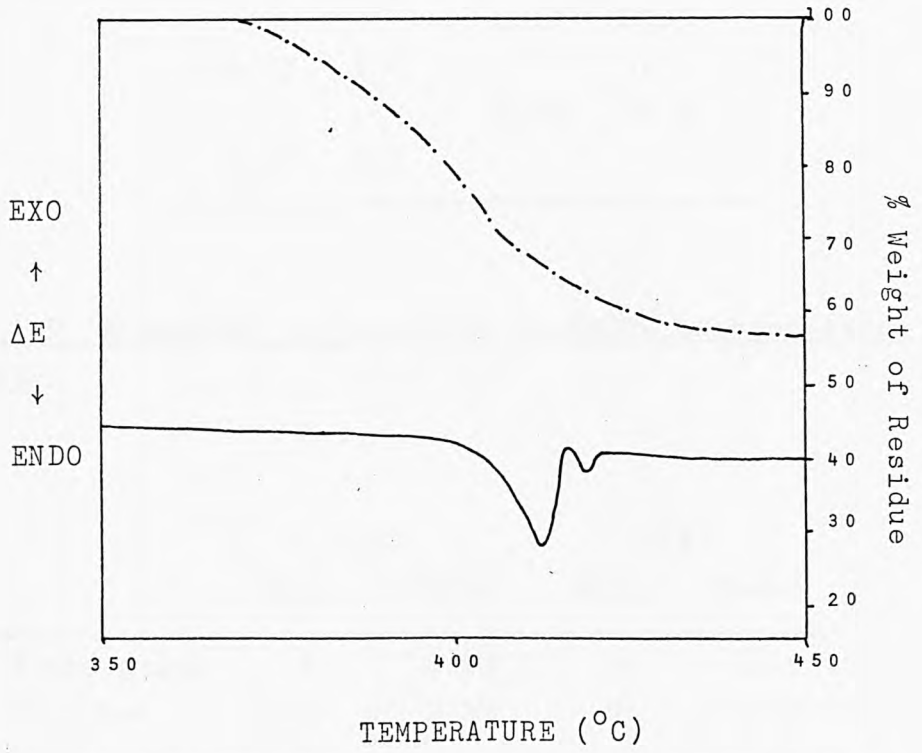

The TG trace (Fig. 4.9) shows that dimethyltin sulphate decomposes in two overlapping stages which are inseparable by the methods available. The mass spectrometric analysis on the volatile gaseous products shows that ethane is evolved

Table 4.8. X-Ray Diffraction Data for Me_2SnSO_4 Decomposition Products.

Me_2SnSO_4		Residue	
d(Å)	I(%)	d(Å)	I(%)
13.02	3.5		
10.90	3.3		
10.69	100		
5.85	8.5		
5.71	4.0		
		5.65	100
5.22	3.2		
		4.59	79.5
		4.17	29.5
4.10	3.6		
		3.16	79.5
3.13	3.3		

Table 4.9. Elemental Analyses for Et_2SnSO_4 Decomposition Products.

	C(%)		H(%)	
	Calc.	Found	Calc.	Found
First Stage	0	0.69	0	0.10
Residue	0	1.29	0	0.14

Table 4.10. X-Ray Diffraction Data for Et_2SnSO_4 Decomposition Products.

First Stage		Residue	
d(Å)	I(%)	d(Å)	I(%)
6.56	5.3		
6.39	10.4		
5.93	100		
5.69	7.5	5.63	87.6
5.56	7.9		
5.54	32.0		
5.09	7.4		
5.06	6.3		
4.86	6.7		
4.50	7.7	4.59	87.6
4.19	6.5	4.15	27.6
3.99	17.0		
3.88	13.9		
3.83	3.6		
3.60	10.9		
3.55	5.6		
3.29	6.0		
3.23	11.2		
		3.16	100
3.05	9.6		
2.98	4.7	3.00	25.7
2.97	4.7		
		2.70	21.0

initially followed by SO_2. X-ray powder data could only be collected on the parent material and the final residue since no stable pyrolysis intermediate could be obtained at the temperature formed. The x-ray data on the final residue (Table 4.8) are the same as those obtained for the final decomposition residue from diethyltin dinitrate.

4.7.2. Diethyltin Sulphate (Et_2SnSO_4)

A two stage decomposition process is observed for Et_2SnSO_4 (TG trace Fig. 4.10) with weight losses of 27 and 24%, leaving a residue weight of 49%.

Figure 4.10.

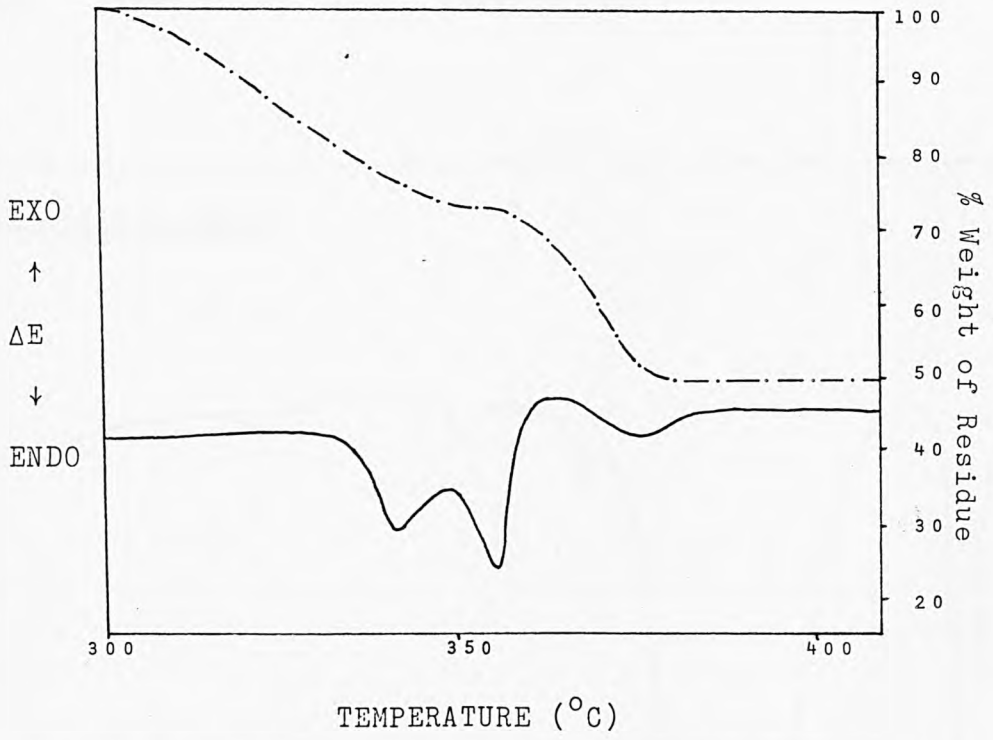

First Stage (380°C)

From the elemental analyses for this first solid intermediate (Table 4.9) all organic groups are removed during this first

Figure 4.11: I.R. Spectra for Et_2SnSO_4 Decomposition Products.

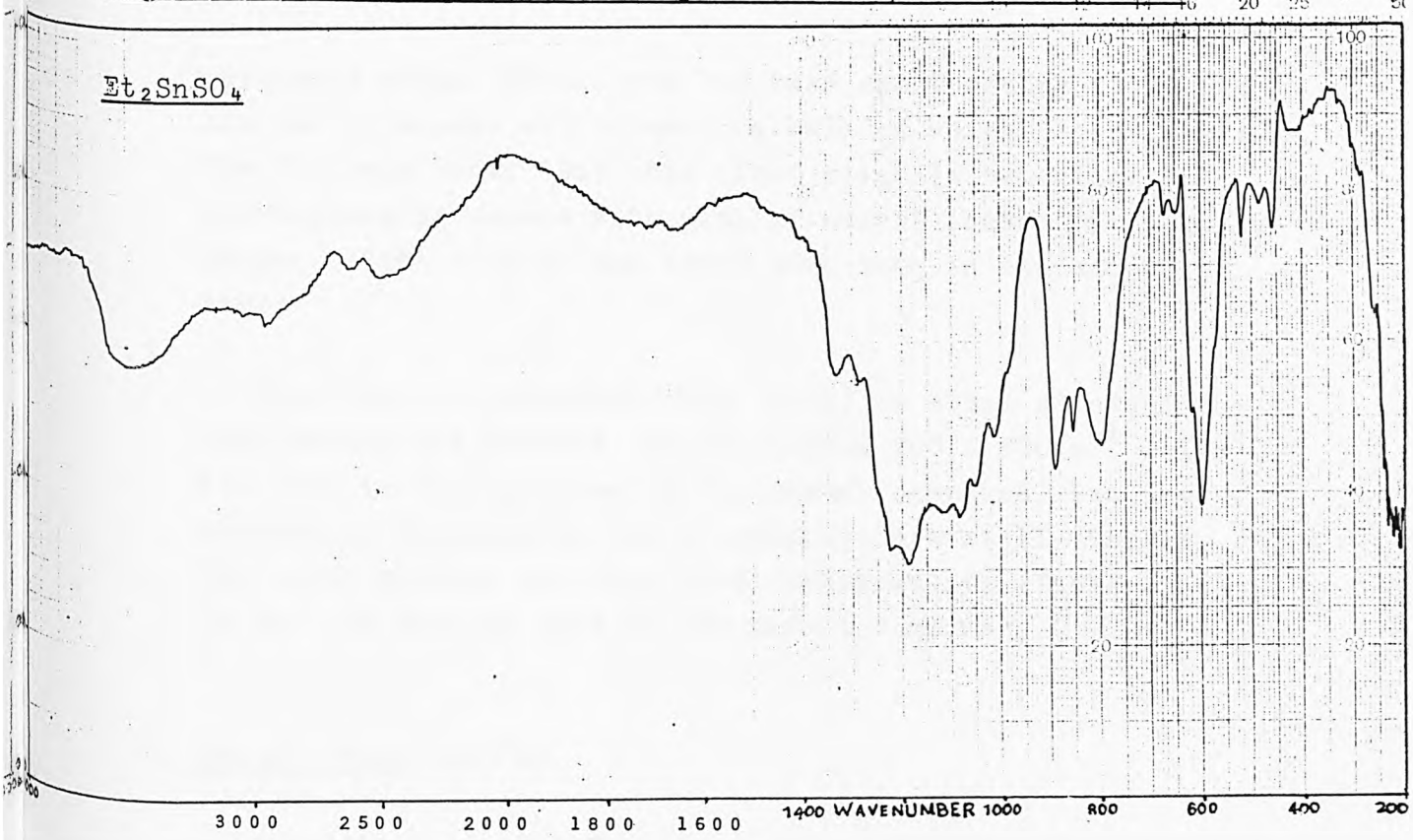

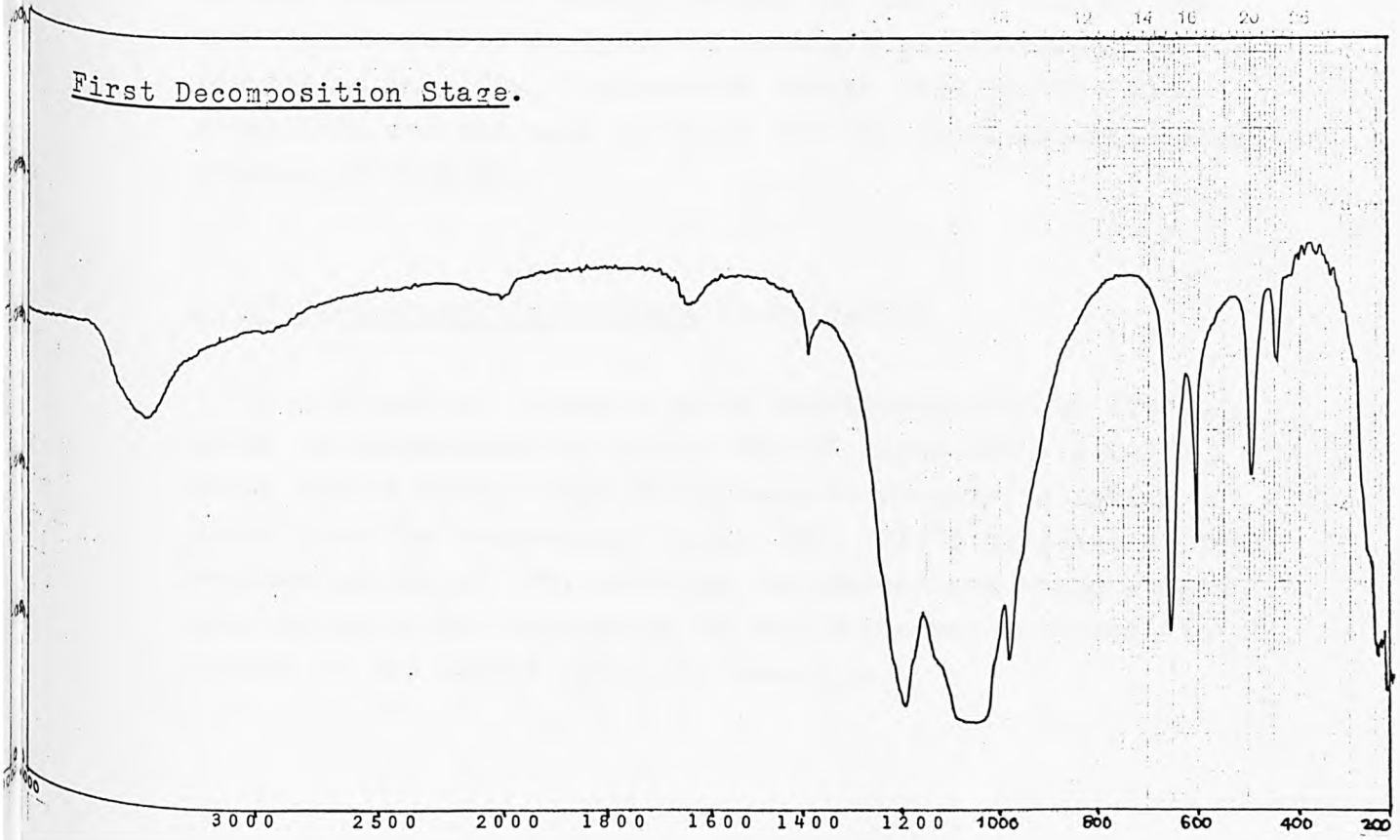

pyrolysis stage, which from the mass spectrometry study are evolved as ethane and ethene (calculated weight loss 21.3%). The TG trace shows that this first stage is two closely overlapping processes with similar weight losses (a slightly larger weight loss in the first step than in the second step).

From the i.r. spectrum (Fig. 4.11) no ethyl stretching frequencies are present in the region 900 - 800cm^{-1} which are seen in the spectrum of the parent compound, but the stretching frequencies due to sulphate are still visible. The x-ray pattern for this first intermediate (Table 4.10) is not the same as that of the parent compound.

Second Stage (423°C).

A weight loss of 24% is seen in the TG trace for this second, final decomposition process, leaving a residue weight of 49%, (calculated residue weight for SnO_2 is 55.2%). The mass spectrometric analysis of volatile gaseous products identified only SO_2, (calculated weight loss 23.5%). The x-ray data are the same as those for the final decomposition product of Me_2SnSO_4.

4.7.3 Di-n-propyltin Sulphate |n-Pr_2SnSO_4|

Di-n-propyltin sulphate melts endothermically at 129°C, prior to decomposing at 133°C. The TG trace (Fig. 4.12) shows that a three stage decomposition process is taking place over the temperature range 133 - 334°C to leave a final residue weight of 52%, although the second and third stages are too close for separation of the transient intermediate formed in the second pyrolysis reaction.

Figure 4.12.

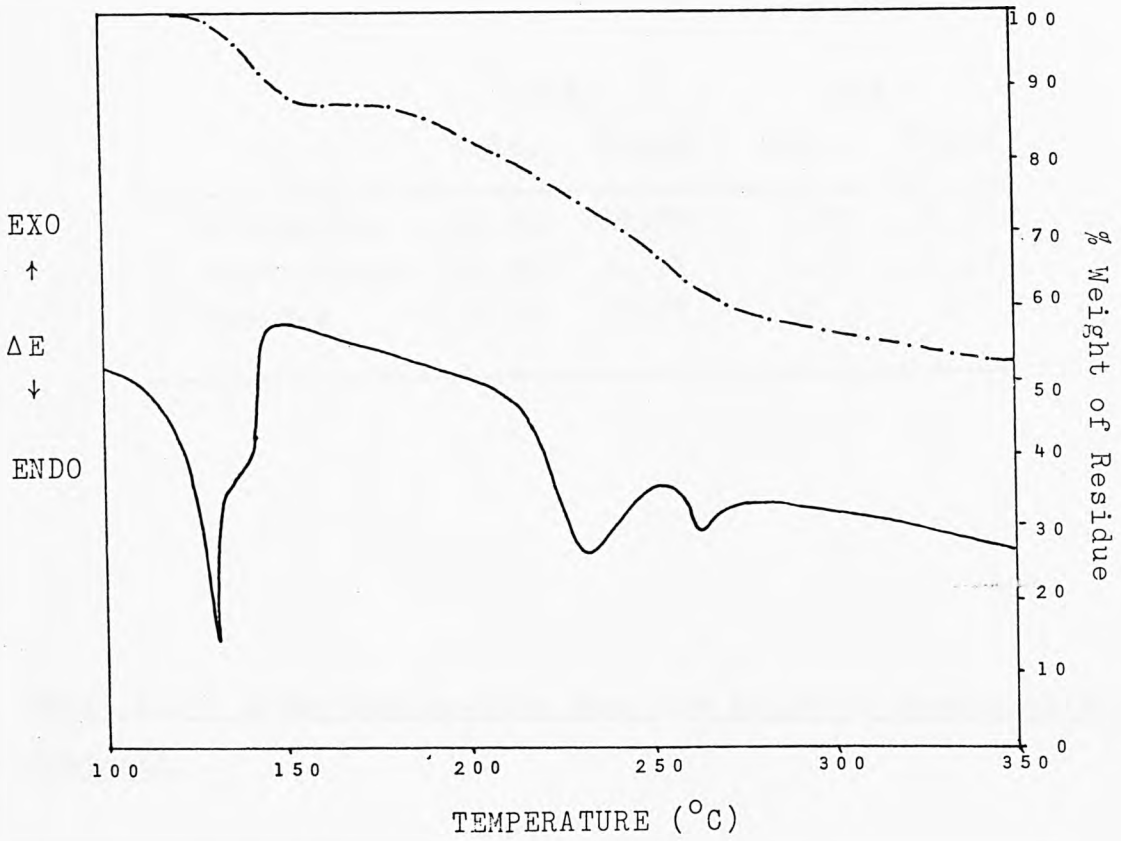

First Stage (133°C)

A weight loss of 12.5% is seen in the TG trace, which, from the mass spectrometric analysis is due to partial breakdown of the nPr groups. The mass spectrometric study identified a number of longer chain alkyl compounds in the evolved vapours from this pyrolysis step.

The i.r. spectrum (Fig. 4.13) shows a diminution in the C - H stretching modes centred around 2950cm^{-1} in the parent compound and broadening of the lower frequency bands associated with the nPr group. No x-ray data could be collected on this product due to its extremely deliquescent nature.

The elemental analysis results (Table 4.11) are in agreement

Table 4.11. Elemental Analyses for n-Pr_2SnSO_4 Decomposition Products.

	C(%)		H(%)	
	Calc.	Found	Calc.	Found
n-Pr_2SnSO_4	23.94	23.00	4.69	5.41
First Stage	13.91	12.11	3.11	3.47
Residue	7.37	7.97	0	0

Table 4.12. X-Ray Diffraction data for Pr_2SnSO_4 Decomposition Products.

First Stage		Residue	
d(Å)	I(%)	d(Å)	I(%)
13.96	100		
8.69	86.6		
6.31	27.4		
		5.95	35.7
5.77	3.4	5.71	46.4
5.63	3.9		
5.57	5.6		
		5.22	100
5.05	5.2		
		4.59	29.8

Figure 4.13: I.R. Spectra for $n\text{-}Pr_2SnSO_4$ Decomposition Products.

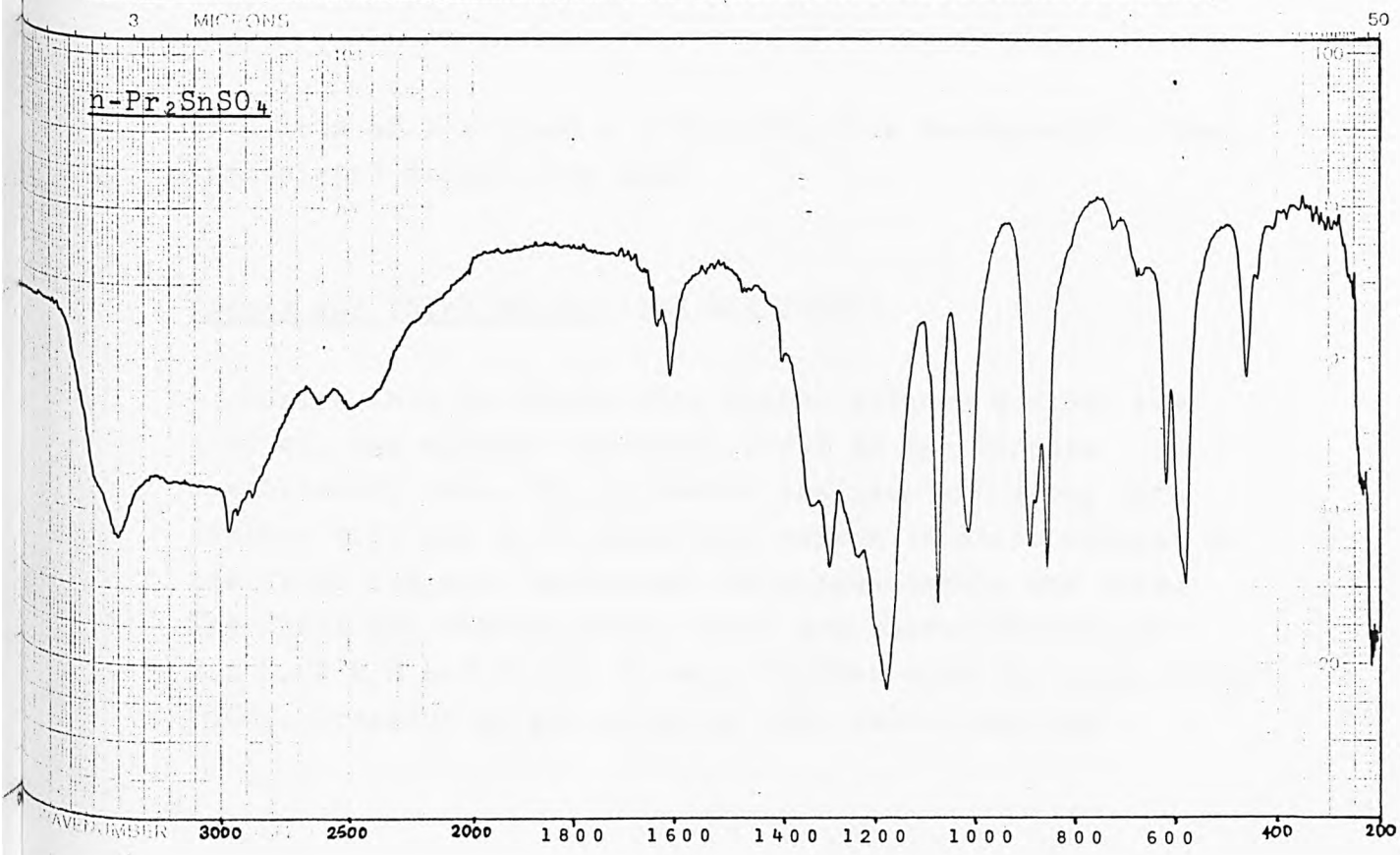

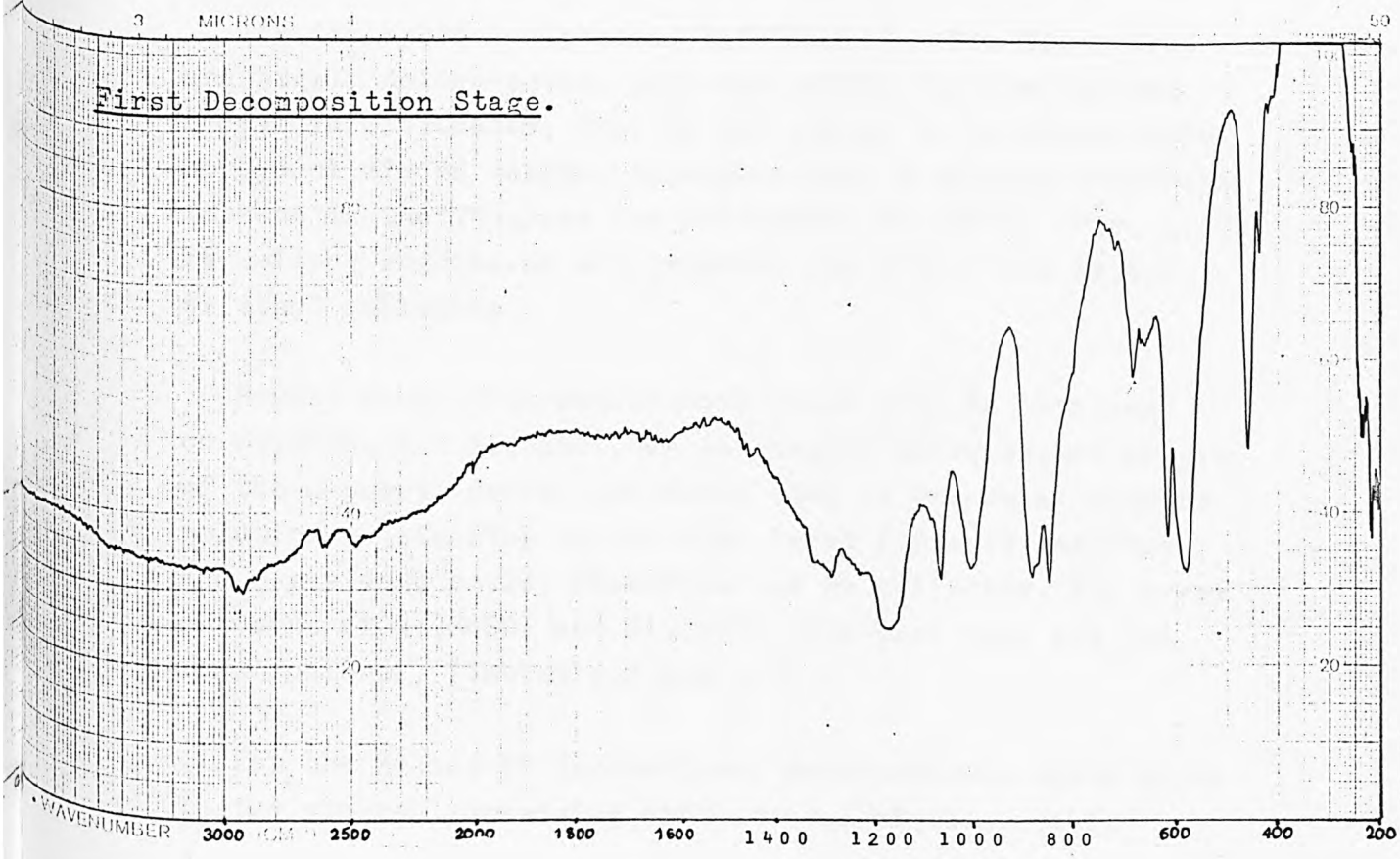

with loss of 3 x C and 6 x H during this decomposition stage (calculated weight loss 14%).

Second and Third Stages (233 and 265°C).

During this pyrolysis step higher alkanes and SO_2 are evolved, the alkanes appearing first in the GC/mass spectrometry scan. The elemental analyses and x-ray data (Tables 4.11 and 4.12) show that carbon is still present in the final residue, equivalent to approximately one mole. The final two decomposition steps are therefore loss of 2 x C, 8 x H and SO_2 to leave a residue with the composition $SnCO_2$, (residue weight obtained 52%, calculated 54%).

4.8. Discussion.

The dialkyltin sulphates, R_2SnSO_4, (R = Me, Et, n-Pr), are highly deliquescent, although unlike the dialkyl and diaryltin dinitrates, they do not appear to be susceptible to hydrolysis on thermal decomposition. A melting endotherm is seen in the TG trace for n-Pr_2SnSO_4 at 129°C, (Fig. 4.12) no melting endotherms are observed for either the methyl or ethyl analogues.

Powder x-ray diffraction data could only be obtained on Me_2SnSO_4 and Et_2SnSO_4, as the highly deliquescent nature of the n-propyl derivative meant that it became an aqueous solution on standing on the open bench for a few minutes, and x-ray data could, therefore not be collected. The x-ray patterns of Me_2SnSO_4 and Et_2SnSO_4 show that they are not isostructural, (Tables 4.8 and 4.10).

For the Me and Et derivatives, decomposition takes place in two stages, commencing with removal of the organic

groups to leave $SnSO_4$, followed by breakdown of stannous sulphate to give SnO_2 and SO_2. In the case of the n-Pr derivative, the longer alkyl chain is less thermally stable and breaksdown in two stages commencing at 133°C. For Me_2SnSO_4 and Et_2SnSO_4, the first decomposition stages are at 410 and 380°C, and the alkyl groups are completely removed. For the methyl compound, the two decomposition stages overlap so that the first intermediate residue could not be collected for analysis.

Di-n-propyltin sulphate decomposes at 133°C with evolution of alkane fragments which, from the mass spectrometric analysis, form long-chain alkanes in the vapour phase. From the weight loss of 13.6% and the elemental analyses on the first solid residue, (Table 4.11), this pyrolysis step involves loss of 3xC and 6xH from each molecule of ~~starting~~ material, to leave an intermediate with the composition $(C_3H_8)SnSO_4$, (calculated weight loss 14%). This can be represented by either n-$PrSn(H)SO_4$ or $MeSn(Et)SO_4$. If this intermediate were the hydride, a strong Sn - H stretching frequency band should be observed at between 1880 and 1800cm^{-1}. However, from the i.r. spectrum (Fig.4.13), it can clearly be seen that no such peak occurs. The most striking difference between the spectra of the parent conpound and that of the first pyrolysis product is the emergence of a peak centred around 676cm^{-1} which was previously observed in the spectrum of $(Et_2SnO)_n$, (Fig. 4.13), associated with rocking modes within the ethyl group. From these considerations it would appear that this first intermediate is in fact $Me(Et)SnSO_4$.

For all three alkyltin sulphates, a tin(ii) sulphate phase is the pyrolysis product formed in the next decomposition step, (first decomposition stage for the methyl and ethyl derivatives, second stage for the n-propyl derivative), although in the cases of the methyl and n-propyl compounds this is inferred from the percentage weight losses,

formation of SnO_2 as the final solid residue, and the results obtained for Et_2SnSO_4. Mass spectrometric analyses on volatile gases produced in this pyrolysis step identified the presence of ethane for Me_2SnSO_4, ethane and ethene for Et_2SnSO_4, and higher alkanes for n-Pr_2SnSO_4, which are consistent with reactions of the type:

$$R_2SnSO_4 \longrightarrow 2R^{\cdot} + SnSO_4 \qquad (R = Me, Et)$$

or for n-Pr_2SnSO_4:

$$(C_3H_8)SnSO_4 \longrightarrow 2xC + 8xH + SnSO_4 + C\downarrow$$

X-ray data could only be collected on the intermediate residue for the ethyl derivative, since this was the only compound to give more than a transient intermediate. The x-ray data for the first decomposition product of Et_2SnSO_4 (Table 4.10) are different to those for the parent compound. The elemental analyses (Table 4.9) confirm that no organic residues are present at this stage. From the i.r spectrum (Fig.4.11) no ethyl group stretching bands are visible between 900 and 800cm^{-1}, however, the sulphate group stretching modes are still present, shifted to slightly lower frequencies.

In all three compounds, the sulphate group breaksdown to give SO_2, with SnO_2 as the final solid residue. Similar decomposition temperatures are observed for Me_2SnSO_4 and Et_2SnSO_4 (428 and 423^{o}C, respectively), whereas for n-Pr_2SnSO_4 the final decomposition step takes place at a

much lower temperature - 265°C. The only volatile product identified in the mass spectrometric analysis is SO_2, no organic or other sulphur-containing compounds are observed.

X-ray and Mössbauer data on the final residue are consistent with the formation of amorphous tin(iv) oxide.

4.9. Organotin Carboxylates.

Two organotin carboxylates are studied - $Ph_3SnOCOPh$ and $BuSn(OAc)_3$. Both of these compounds decompose in four stages (TG traces Figs. 4.14 and 4.16), commencing at 325°C. for $Ph_3SnOCOPh$, and over the temperature range 111 to 364°C for $BuSn(OAc)_3$. A melting endotherm is observed in the DTA trace for $Ph_3SnOCOPh$ at 86°C, in agreement with the published value.

4.9.1. $Ph_3SnOCOPh$.

The four decomposition stages for this compound occur at 325, 363, 400 and 478°C, with weight losses of 50, 8,10 and 10.5%, respectively. From the DTA trace the final pyrolysis step is seen to be exothermic, whereas all other decomposition processes are endothermic.

Due to the amorphous nature of the intermediate decomposition products, no x-ray data could be collected.

Figure 4.14.

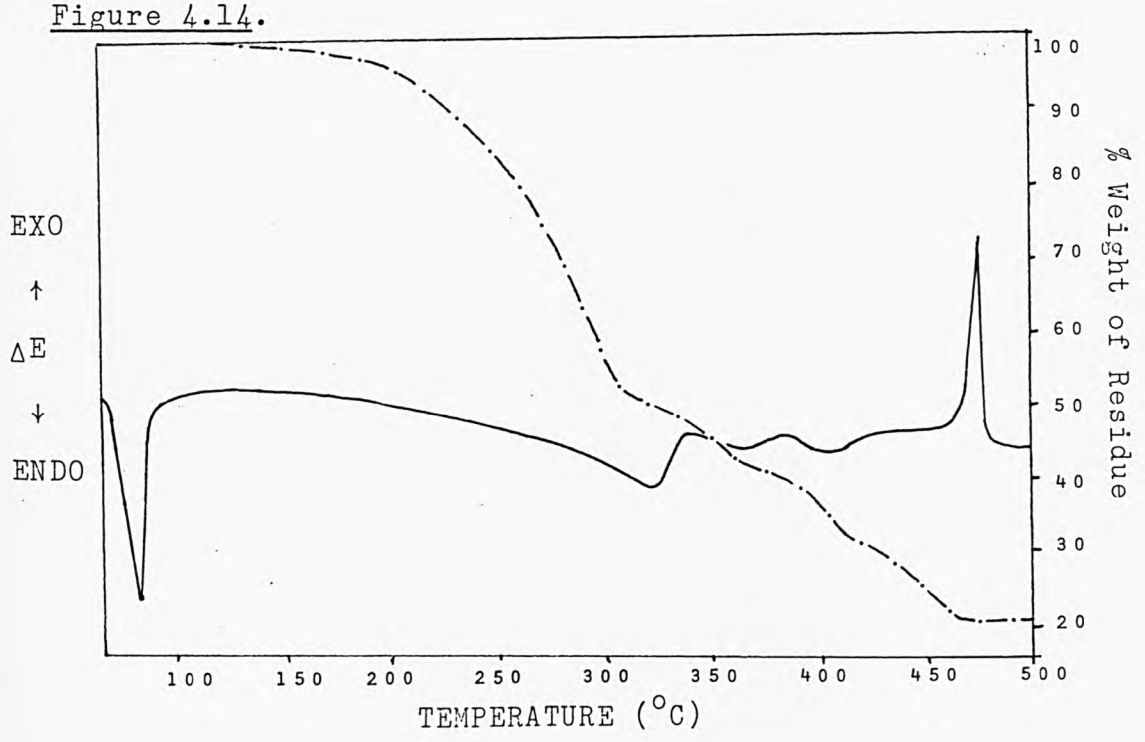

Table 4.13. Elemental Analysis Results for $Ph_3SnOCOPh$ Decomposition Products.

	C(%)		H(%)	
	Calc.	Found	Calc.	Found
First Stage	49.43	48.79	3.44	2.83
Second Stage	43.30	43.83	3.02	2.48
Residue	0	0.32	0	0.53
Probe Sample	64.61	64.80	4.52	4.45

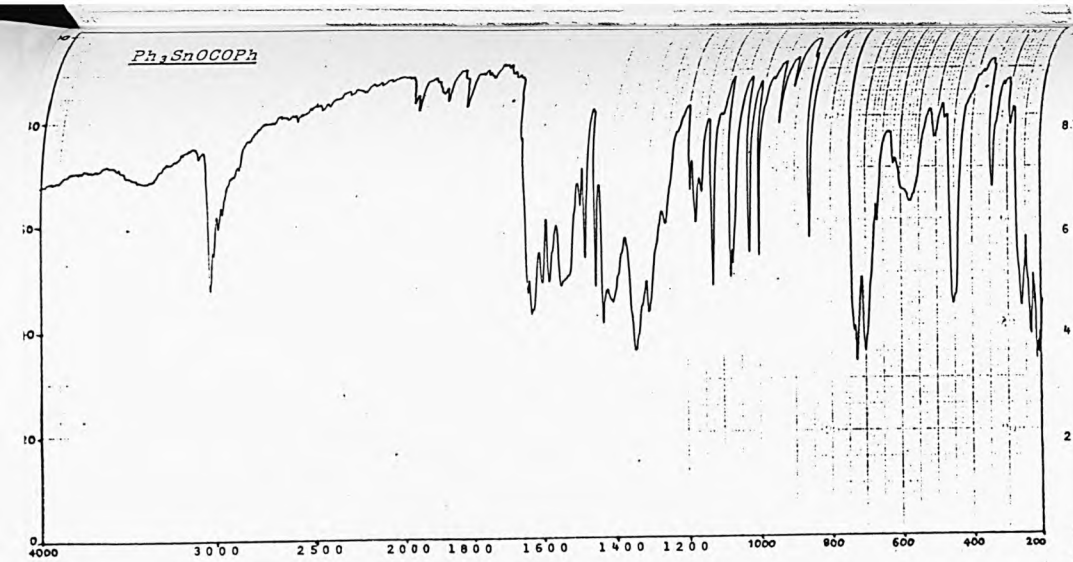
$Ph_3SnOCOPh$
4000 3000 2500 2000 1800 1600 1400 1200 1000 800 600 400 200

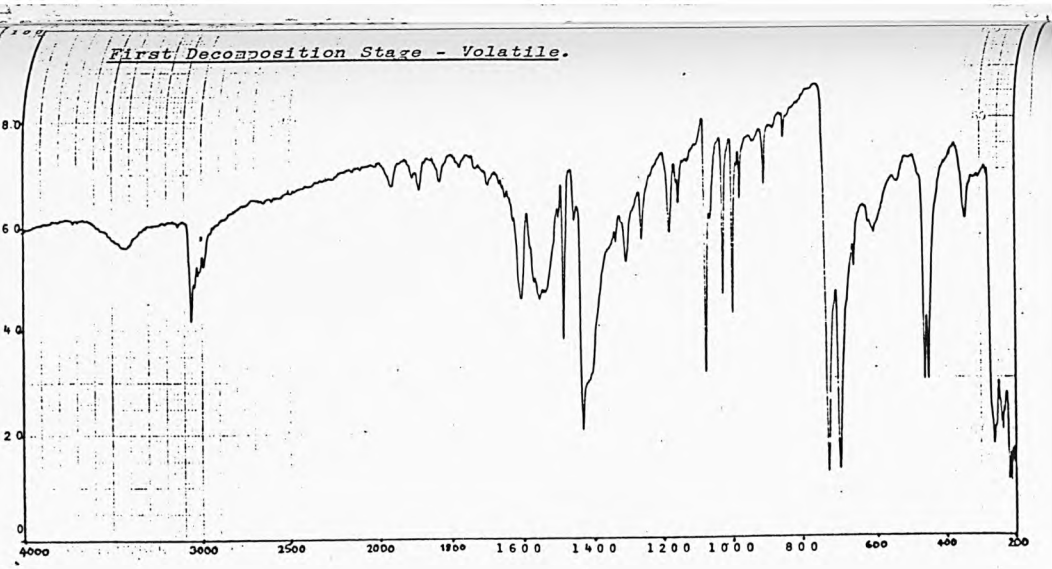
First Decomposition Stage - Volatile.
4000 3000 2500 2000 1800 1600 1400 1200 1000 800 600 400 200

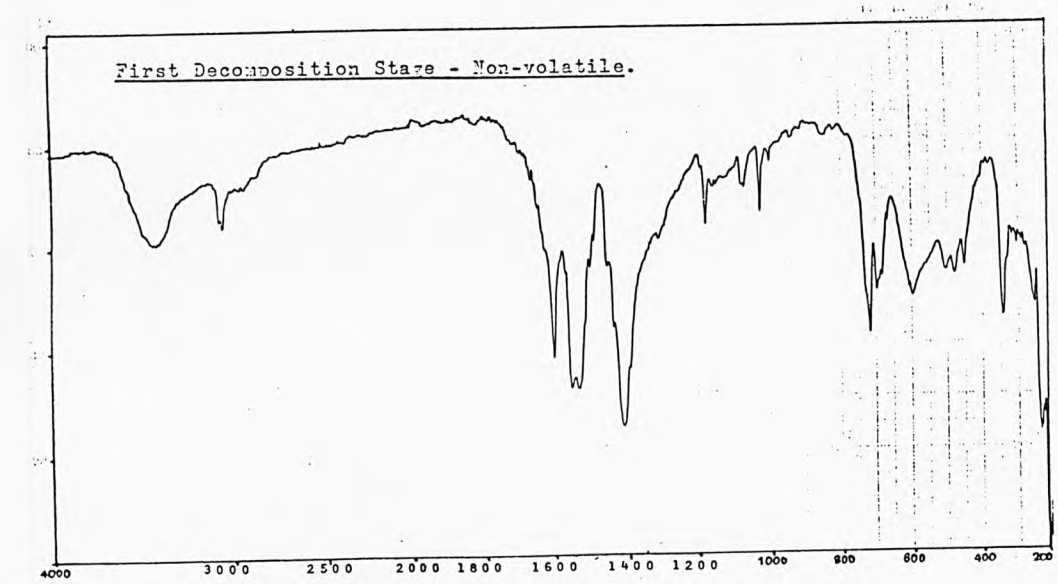
First Decomposition Stage - Non-volatile.
4000 3000 2500 2000 1800 1600 1400 1200 1000 800 600 400 200

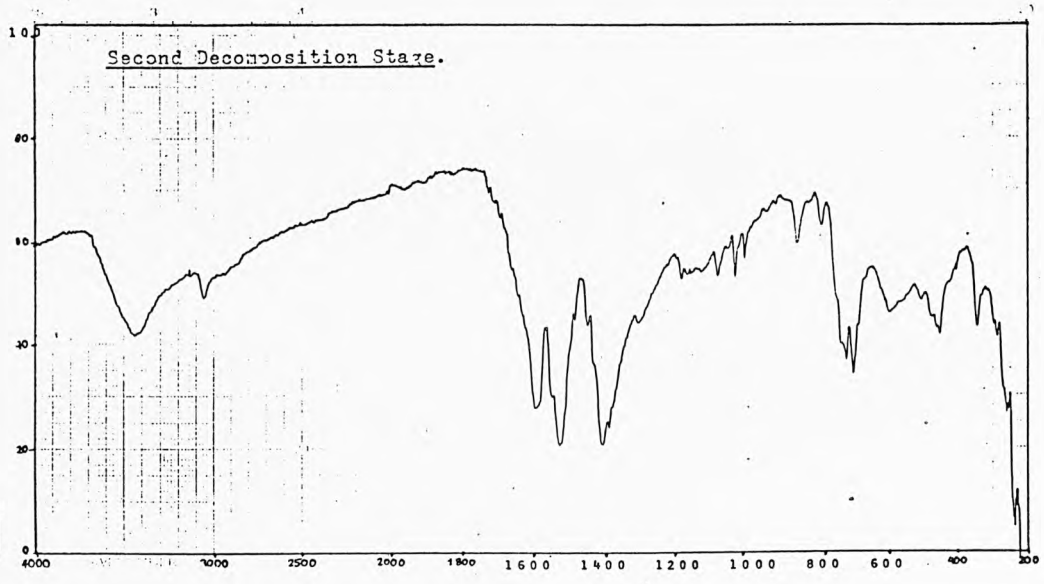
Second Decomposition Stage.
4000 3000 2500 2000 1800 1600 1400 1200 1000 800 600 400 200

First Stage (325°C).

During this decomposition process both solid and gaseous volatile pyrolysis products are collected. The mass spectrometric analysis of volatile gases identified biphenyl. I.R. and elemental analyses (Fig. 4.15 and Table 4.13) were performed on both the solid volatile decomposition product and on the non-volatile solid residue.

The i.r. spectrum of this first intermediate shows that the intensities of the Ph stretching frequency bands at 3068, 3019 and 2998cm^{-1} are greatly reduced and have become two bands at 3070 and 3048cm^{-1}. In addition, the fingerprint region of the spectrum is simplified with a number of bands no longer present, however, the carboxylate stretching modes at ca. 1600 and 1400cm^{-1} can still be seen.

Second and Third Stages (363 and 400°C).

The mass spectrometric analysis on the volatile decomposition products formed during these two stages shows the presence of biphenyl and CO, which are equivalent to a weight loss of 11.4%. The presence of both aryl and carboxylate groups is suggested from the i.r. spectrum, which is very similar to that obtained for the first non-volatile pyrolysis product.

Fourth Stage (478°C).

During this final exothermic decomposition stage all organic components are removed, (elemental analyses Table 4.13) to leave an amorphous solid product.

A Mössbauer spectrometric study carried out on the residue showed a single line with $\delta = 0$ relative to $BaSnO_3$, indicative of SnO_2. Due to the amorphous nature of the final residue no

x-ray diffraction data could be collected.

The mass spectrometric analysis of volatile decomposition products showed the presence of biphenyl and CO as in the previous stage.

4.9.2. n-$BuSn(OAc)_3$.

From the TG/DTA study of n-butyltin triacetate, four decomposition stages are seen, although non-volatile products can only be collected for three processes, the final two processes being too close for product analysis at each stage. The four pyrolysis reactions are seen to occur at 111, 179, 285 and 364°C, with weight losses of 13, 20, 24, and 10%, respectively, (TG/DTA trace Fig. 4.16).

All the decomposition processes for n-$BuSn(OAc)_3$ are endothermic, in contrast with $Ph_3SnOCOPh$ previously mentioned.

Figure 4.16.

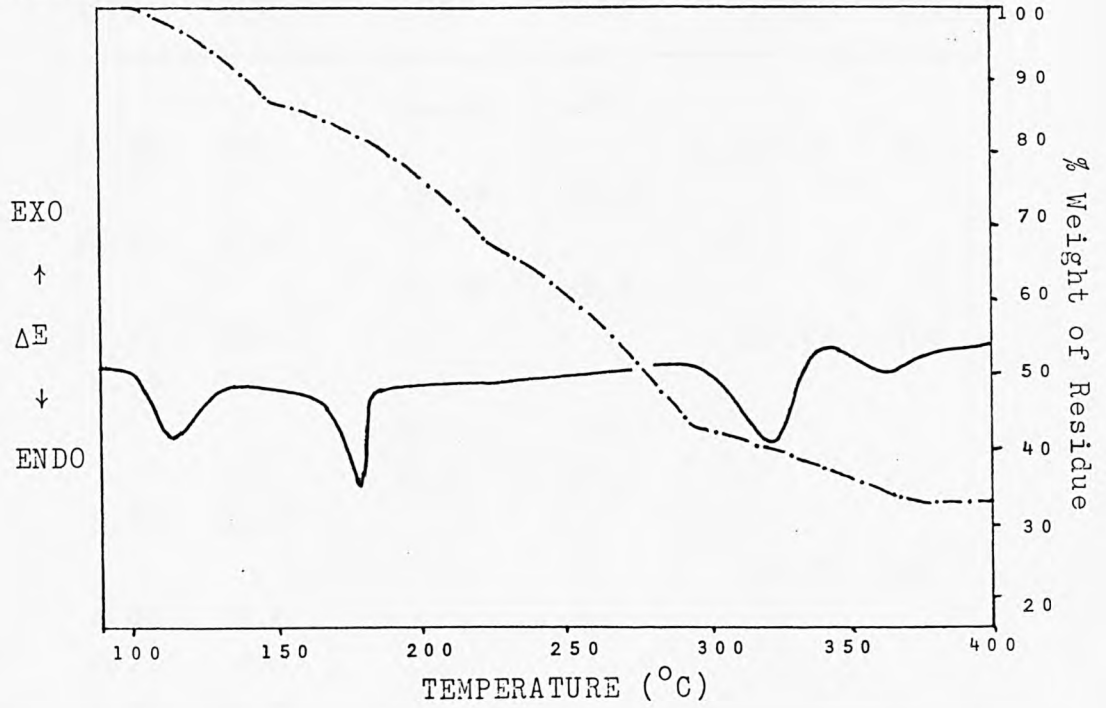

Table 4.14. Elemental Analysis Results for $BuSn(OCOMe)_3$ Decomposition Products.

	C(%)		H(%)	
	Calc.	Found	Calc.	Found
First Stage	31.80	31.20	5.01	4.96
Second Stage	28.70	30.14	4.83	4.90
Residue	0	0	0	0

Table 4.15. X-Ray Diffraction Data for $BuSn(OCOMe)_3$ Decomposition Products.

First Stage		Second Stage		Residue	
d(Å)	I(%)	d(Å)	I(%)	d(Å)	I(%)
		14.44	100		
13.60	100			13.50	95
		13.19	40.02		
12.10	41.0				
		11.88	96.9		
10.80	50.0			10.80	100
9.95	35.5				
		9.72	7.0		
		9.10	18.1		
8.75	81.0				
				6.73	25
4.60	12.0				
4.27	9.0				
3.80	12.5				
3.24	8.0				

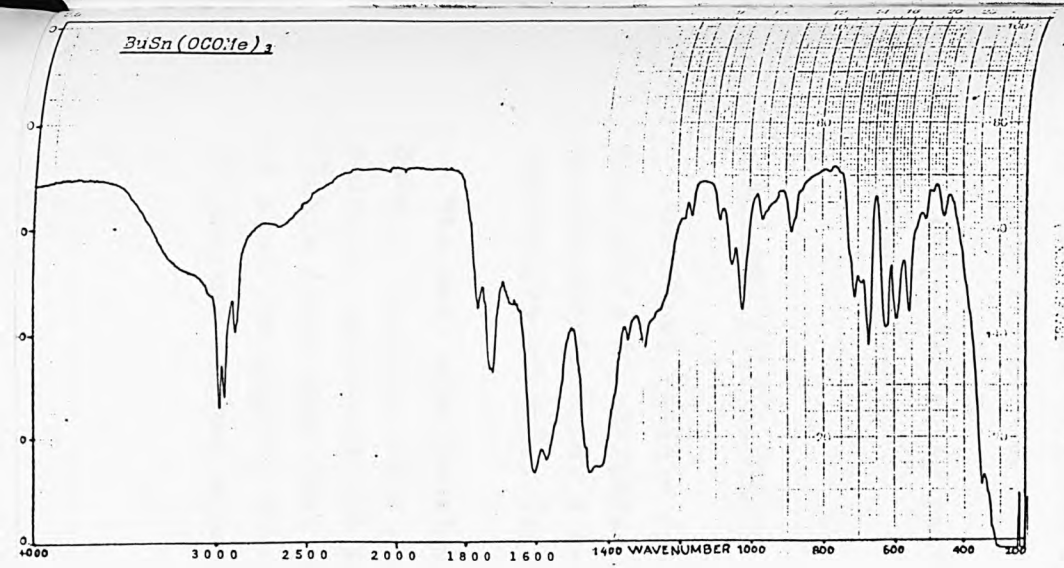
BuSn(OCOMe)3
4000
3000
2500
2000
1800
1600
1400 WAVENUMBER 1000
800
600
400
200

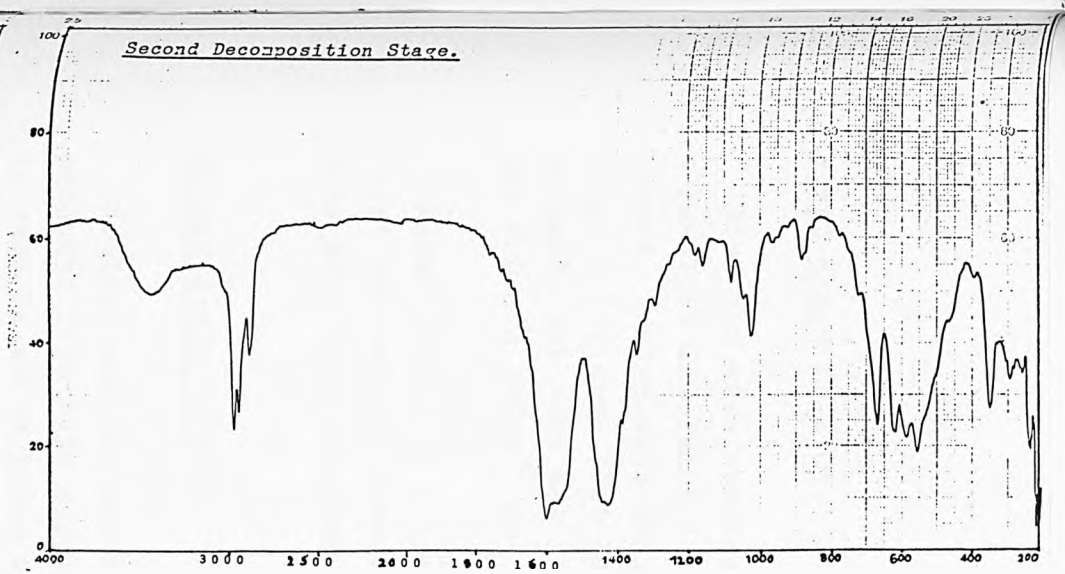
Second Decomposition Stage.
4000
3000
2500
2000
1800
1600
1400
1200
1000
800
600
400
200

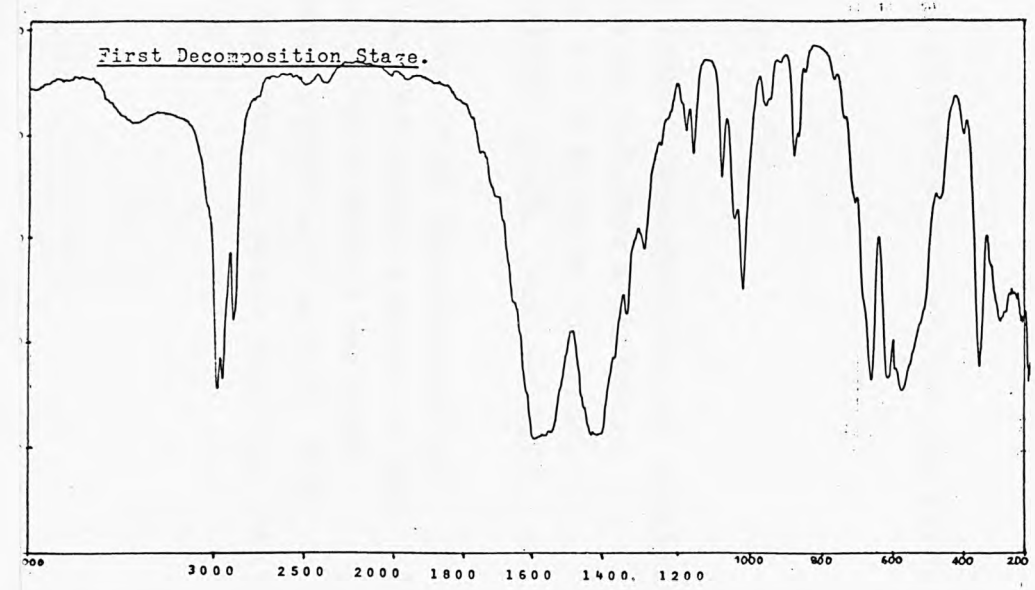
First Decomposition Stage.
3000
2500
2000
1800
1600
1400
1200
1000
800
600
400
200

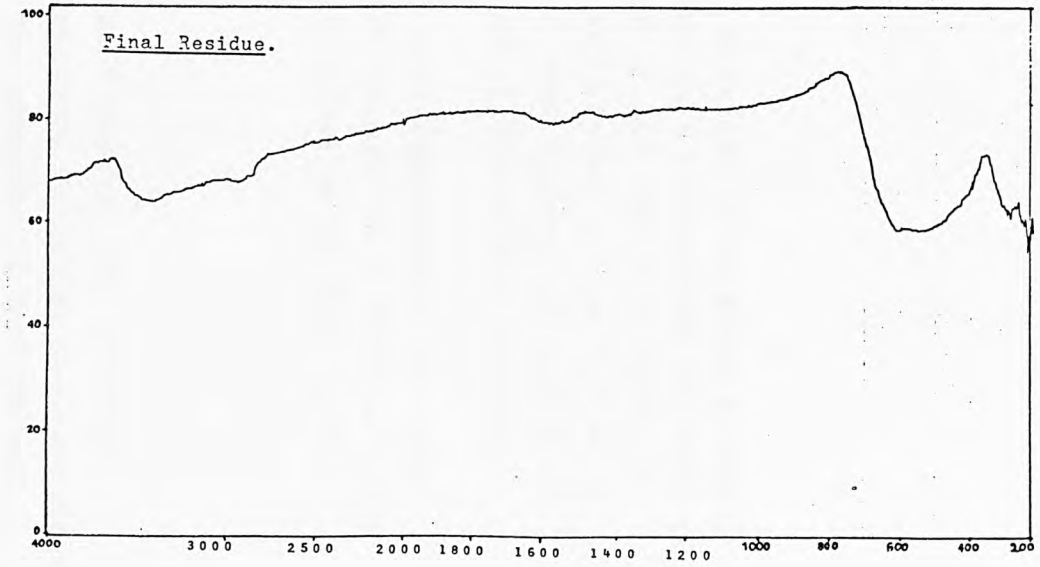
Final Residue.
4000
3000
2500
2000
1800
1600
1400
1200
1000
800
600
400
200

First Stage (111°C).

From the mass spectrometric analysis of volatile products a reaction involving loss of one mole acetone and one mole CO_2 occurs, (calculated weight loss 14.4%). The i.r. spectrum (Fig. 4.17) show that both Bu and acetate groups are still present, but some new lines are seen between 600 and 500cm^{-1} and 400 and 300cm^{-1} not observed in the parent material.

n-BuSn(OAc)$_3$ is a liquid at room temperature, but this first non-volatile decomposition product is a solid — x-ray data have been obtained and are presented in Table 4.15.

Second Stage (179°C).

Acetone and CO_2 are again identified in the volatile products from this pyrolysis reaction. A similar i.r. spectrum is seen in which lines due to the presence of both Bu and acetate groups are seen.

The powder x-ray pattern is different to that for the first intermediate.

Third and Fourth Stages (288 add 364°C)

The final residue from the thermal decomposition of n-butyltin triacetate is amorphous to x-rays, but from a Mössbauer spectrometric study a value of $\delta = 0$ is again obtained, indicative of SnO_2, (residue weight 42.5%, obtained 34%).

The mass spectrometric analysis shows the presence of butane, acetone, CO_2, and a trace of higher alkanes in the volatile decomposition products. The elemental analyses (Table 4.14) show that no organic groups are present. This is also verified by the i.r. spectrum in which only one peak is present centred around 550cm^{-1}.

4.10. Discussion.

The two organotin carboxylates studied - $Ph_3SnOCOPh$ and $BuSn(OCOMe)_3$ both decompose in four stages, (TG traces Figs. 4.14 and 4.16), although in each case only products from three stages can be identified because of overlapping decomposition processes. Butyltin triacetate is a liquid at room temperature, readily decomposing in the presence of oxygen to give the monobutyltin oxyacetate[12]:

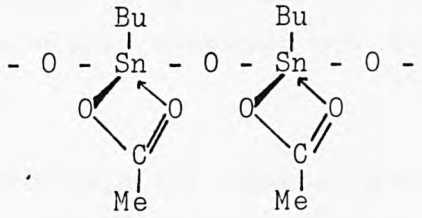

and was therefore stored under an atmosphere of N_2 at all times.

A melting endotherm is observed in the DTA trace of $Ph_3SnOCOPh$ at 86°C, with the first decomposition stage taking place at 325°C. $BuSn(OCOMe)_3$ decomposes at 111°C, in agreement with the lower stability of the tri-carboxylates relative to the mono- and di-carboxylates.

For both compounds the first pyrolysis step involves a condensation reaction with formation of a stannoxane and a stannane for $BuSn(OCOMe)_3$ and $Ph_3SnOCOPh$, respectively. The second stage (two overlapping steps for $Ph_3SnOCOPh$) involves cleavage of the stannoxane/stannane bond with formation of compounds of the type - RSn(O)OCOR'. In the

final stage this is broken down to give a final residue of amorphous SnO_2 (two step process for $BuSn(OCOMe)_3$).

$Ph_3SnOCOPh$ melts and then decomposes at 325°C, with a weight loss of 50%. During this decomposition a solid product was collected on the cold probe which was subjected to i.r. and elemental analyses (Fig. 4.15 and Table 4.13). A comparison of the i.r. spectra of tetraphenyltin, Ph_4Sn, and the solid decomposition product shows that they are similar, although shifts in some lines and the presence of extra lines are seen. The elemental analyses are not in very good agreement with the formation of Ph_4Sn, (analyses obtained - C = 64.81%, H = 4.45%; calculated for Ph_4Sn - C = 67.47%, H = 4.72%). However, a 1:1 mixture of Ph_4Sn and hexaphenylditin, $(Ph_3Sn)_2$, gives C = 64.61%, H = 4.52%, in good agreement with the values obtained and the differences in the i.r. spectra.

Mass spectrometric analysis of volatile gases from the decomposition of $Ph_3SnOCOPh$ identified only biphenyl. The following decomposition reaction is proposed:

$$2Ph_3SnOCOPh \longrightarrow \tfrac{1}{2}\left[Ph - \underset{\underset{OCOPh}{|}}{\overset{\overset{OCOPh}{|}}{Sn}} - \underset{\underset{OCOPh}{|}}{\overset{\overset{OCOPh}{|}}{Sn}} - Ph\right] + Ph_2 + |2Ph + Sn|^*$$

(* as $Ph_4Sn + (Ph_3Sn)_2$).

This is a weight loss of ca. 50% compared with 50% obtained experimentally.

Butyltin triacetate decomposes at 111°C with a weight loss

of ca. 13%, which from the mass spectrometric analysis is evolution of acetone and CO_2, (1 mole CH_3COCH_3 + 1 mole CO_2 are equivalent to weight loss of 14.4%). The condensation reaction believed to be taking place in this decomposition stage is:

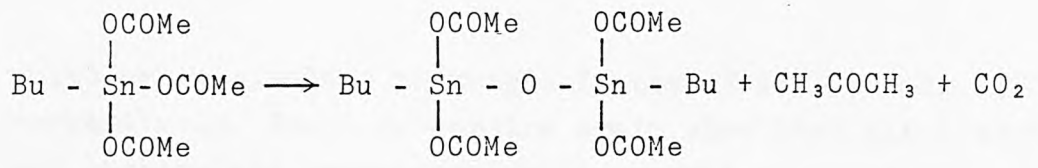

The i.r. spectrum for this first solid residue (Fig. 4.17) shows that both the acetate and the butyl groups are still present, however, extra lines are present at lower frequencies ~600 - 500 and 400 - 300cm^{-1} which are assigned to M - O - M stretching and bending modes. The elemental analyses for this intermediate (Table 4.14) also suggest that the above condensation product has been formed.

A two step process is seen at 363 and 400cm°C for the second decomposition stage of $Ph_3SnOCOPh$ with weight losses of ca. 8 and 10% for the two steps. For $BuSn(OCOMe)_3$, this second stage occurs at a lower temperature - 179°C, and takes place in a single step. The solid products believed to be formed during this decomposition stage are the oxycarboxylates - PhSn(O)OCOPh and BuSn(O)OCOMe.

Mass spectrometric analyses on volatile decomposition products identified biphenyl and CO, and acetone and CO_2 for $Ph_3SnOCOPh$ and $BuSn(OCOMe)_3$, respectively. These results are consistent with the following two pyrolysis reactions:

$$\tfrac{1}{2}\left[\begin{array}{c} \\ \text{Ph - Sn — Sn - Ph} \\ \\ \end{array}\right]\begin{array}{l}\text{OCOPh OCOPh}\\ \text{OCOPh OCOPh}\end{array} \longrightarrow\rightarrow \text{PhSn(O)OCOPh} + \tfrac{1}{2}\text{Ph}_2 + \text{CO}$$

$$\tfrac{1}{2}\left|\text{BuSn(OCOMe)}_2\right|_2\text{O} \longrightarrow \text{BuSn(O)OCOMe} + \tfrac{1}{2}\text{CH}_3\text{COCH}_3 + \tfrac{1}{2}\text{CO}_2$$

which are equivalent to weight losses of 11.4 and 14.4%, respectively. The i.r. spectra again show that alkyl/aryl and carboxylate groups are still present as would be expected from the similar decomposition products which have been formed at each stage. The x-ray diffraction data for the $BuSn(OCOMe)_3$ decomposition product are different to those for the first solid residue (Table 4.15). No lines due to Sn, SnO or SnO_2 are visible in the x-ray pattern for this intermediate. Amorphous pyrolysis products are obtained for all the $Ph_3SnOCOPh$ intermediates.

The elemental analyses are consistent with the intermediate compounds above for both $Ph_3SnOCOPh$ and $BuSn(OCOMe)_3$.

In the final decomposition stage, all organic groups are removed leaving SnO_2, which is identified from the Mössbauer analysis, where an isomer shift value of $0 mms^{-1}$ was obtained relative to $BaSnO_3$. This would be expected from the intermediate products formed in the previous decomposition stage, ie.:

$$\begin{array}{l}\text{R}\\ \\ \text{OCOR}'\end{array}\!\!>\!\text{Sn=O} \longrightarrow \text{SnO}_2 + \text{R}^{\cdot} + {}^{\cdot}\text{COR}'$$

For $BuSn(OCOMe)_3$, butane, butene, acetone, CO_2, and traces of higher alkanes are identified, which is also in agreement with the scheme above where R = Bu and R' = Me, ie.:

$$Bu^{\cdot} + {}^{\cdot}COMe \longrightarrow \tfrac{1}{2}C_4H_{10} + \tfrac{1}{2}C_4H_8 + \tfrac{1}{2}CH_3COCH_3 + \tfrac{1}{2}|CO| + SnO_2$$

$$\text{Disproportionation} \downarrow$$

$$CO_2 + C$$

The i.r. spectrum for the solid residue contains only one broad line centred around $570cm^{-1}$ indicative of Sn - O bonds only.

4.11. References.

1. Ref. 142 Chapter 1.
2. Ref. 143 Chapter 1.
3. Ref. 144 Chapter 1.
4. A.H. Chapman, J.W. Price, Int. Pest. Contr., 1972, 14, 11.
5. Y. Tanaka, T. Morikawa, Japan Analyst, 1964, 13, 753.
6. Ref. 130 Chapter 1.
7. Ref. 131 Chapter 1.
8. Ref. 132 Chapter 1.
9. A.N. Fenster, E.I. Becker, J. Organomet. Chem., 1968, 11, 549.
10. K. Yasuda, H. Matsumoto, R. Okawara, J. Organomet. Chem., 1966, 6, 528.
11. A.M. Domingos, G.M. Sheldrick, J. Chem. Soc., Dalton Trans., 1974, 475.
12. H.H. Anderson, Inorg. Chem., 1964, 3, 912.

5. Conclusions.

The aims of the work described were to determine the decomposition mechanisms of a number of tin containing compounds which could not be elucidated from combined thermogravimetric-defferential thermal analysis alone. A decomposition cell (described in Chapter 2), was developed to permit the stepwise decomposition of sample material with full product analysis. In part of the study the decomposition cell was used in conjunction with pyrolysis-gas chromatography/mass spectrometry to provide a complete breakdown of volatile decomposition products at each step in pyrolysis of the compounds studied.

The thermal decompositions of the following compounds were followed during the course of the work:

(i)Transition metal tin(ii) formate complexes, $M_3Sn_4(CHOO)_{14}.8H_2O$, (M=Mn,Zn,Ni,Co).

(ii)Tin(ii)acetate complexes, $XSn(CH_3COO)_3.nH_2O$, (for $X=NH_4$,K, n=0; for X=Na, n=1), and $Ca_2Sn_2(CH_3COO)_6$.

(iii)Complex tin(ii) oxalates, $X_2Sn(C_2O_4)_2.nH_2O$, (for X=Na, n=0; for X=K, n=1), and $CaSn(C_2O_4)_2.H_2O$.

(iv)Complex tin(ii)malonates, $X_2Sn_2(CH_2C_2O_4)_3.nH_2O$, (for $X=NH_4$, n=0, for X=Na, n=3, for X=K, n=1), and $CaSn_2(CH_2C_2O_4)_3.3H_2O$.

(v) Organotin (iv) oxides and hydroxides, $|R_2SnO|_n$, (R=Me, Et, n-Pr), and Ph_3SnOH.

(vi)Organotin(iv) nitrates, $Et_2Sn(NO_3)_2$ and $Ph_2Sn(NO_3)_2$.

(vii)Organotin(iv) sulphates, R_2SnSO_4 , (R=Me,Et, n-Pr).

(viii)Organotin(iv) carboxylates, $Ph_3SnOCOPh$ and n-$BuSn(OAc)_3$.

Full decomposition processes and mechanisms are presented for the majority of compounds studied, however, in some instances, (eg. the organotin carboxylates), since

successive decomposition stages closely overlapped, whenever it was possible, from decomposition temperatures, volatile product analysis, weight losses obtained from both the TG/DTA apparatus and the large scale pyrolysis equipment, the nature of the transient intermediates was proposed. The proposed machanisms are always in agreement with mechanisms determined.

The results obtained in the course of this study have shown that, even in relatively simple systems, complex decomposition pathways occur and require the use of a wide range of existing analytical techniques and the development of new ones. The equipment designed and constructed has proven to be of particular use in the elucidation of the decomposition mechanisms for these tin-containing compounds.

Typical of the mechanisms proposed as a result of this study are:

Formates

$$M_3Sn_4(CHOO)_{14}.8H_2O \rightarrow M_3Sn_4(CHOO)_{14} \rightarrow 3SnO + M_3Sn(CHOO)_8 + 5CO + CO_2 + O_2 + 3H_2$$

$$\rightarrow 4SnO + 3MO + \text{Gaseous Products.}$$

(M=Mn, Zn).

$$Ni_3Sn_4(CHOO)_{14}.8H_2O \rightarrow Ni_3Sn_4(CHOO)_{14} \rightarrow 3NiO + SnO + Sn_3(CHOO)_6 + MeOH + CO_2$$

$$\rightarrow 4SnO + 3NiO + \text{Gaseous Products.}$$

$$Co_3Sn_4(CHOO)_{14}.8H_2O \rightarrow Co_3Sn_4(CHOO)_{14} \rightarrow 4SnO + Co_3(CHOO)_6 + \text{Gaseous Products}$$

$$\rightarrow 4SnO + 3CoO + \text{Gaseous Products.}$$

Acetates,

$$ASn(CH_3COO)_3 \rightarrow SnO + CH_3COOA \rightarrow SnO + \tfrac{1}{2}A_2CO_3 + \tfrac{1}{2}C + CH_3COCH_3 + CO_2 \quad \delta\text{acetone}$$

(for A=Na,K).

$$(NH_4)Sn(CH_3COO)_3 \rightarrow Sn(CH_3COO)_2 + NH_3 \rightarrow SnO + CH_3COCH + CO_2 + CH_3COOH$$

$$CaSn_2(CH_3COO)_6 \rightarrow Ca(CH_3COO)_2 + SnO + Sn(CH_3COO)_2\uparrow \rightarrow \overset{CaC_2O_4}{+ SnO\ C_2H_6} + CO_2 + CH_3COCH_3$$

$$\rightarrow CaCO_3 + SnO + \tfrac{1}{2}CO_2$$

Oxalates.

$$Na_2Sn(C_2O_4)_2 \rightarrow 0.75Na_2O + 0.25|NaSn(C_2O_4)_2| + 0.75SnC_2O_4 + CO_2 + 0.250.$$

$$\rightarrow 0.75Na_2O + 0.25SnO + 0.25Na_2C_2O_4 + \delta CO_2 \rightarrow Na_2O + \tfrac{1}{2}C + 0.25SnO + 0.750$$

$$K_2Sn(C_2O_4)_2 \rightarrow SnO + K_2C_2O_4 \rightarrow SnO + K_2CO_3 + |CO| + 1\tfrac{1}{2}CO_2 + \tfrac{1}{2}C$$

$$CaSn(C_2O_4)_2 \rightarrow SnO + CaC_2O_4 \rightarrow SnO + CaCO_3 + |CO| + 1\tfrac{1}{2}CO_2 + \tfrac{1}{2}C$$

Malonates.

$$Na_2Sn_2(CH_2C_2O_4)_3 \rightarrow 2SnO + 2CH_3COONa \rightarrow Na_2CO_3 + COCH_3 + 4CO + CO_2$$

$$K_2Sn_2(CH_2C_2O_4)_3.H_2O \rightarrow 2SnO + 2CH_3COOK + \tfrac{1}{2}C \rightarrow K_2CO_3 + \cdot CH_3COCH_3 + CH_3OH + 2CO + 2CO_2 + \tfrac{1}{2}O_2$$

$$CaSn_2(CH_2C_2O_4)_3.2H_2O \rightarrow 2SnO + Ca(CH_3COO)_2 + \tfrac{1}{2}C \rightarrow CaC_2O_4 + C_2H_6 + CH_3OH + 3\tfrac{1}{2}CO_2$$

$$\rightarrow CaCO_3 + |CO|$$

$$(NH_4)_2Sn(CH_2C_2O_4)_3 \rightarrow (NH_4)_2C_2O_4 + SnO + Sn(CH_3COO)_2\uparrow + CO_2 + 2CO$$

$$\rightarrow 2NH_3 + 2CO_2 + H_2$$

Triphenyltin Hydroxide.

$$2nPh_3SnOH \rightarrow nPh_3SnOSnPh_3 \rightarrow (Ph_2SnO)_n + nPh_4Sn$$

$$+ nH_2O$$

$$n/2SnO_2 + n/2Ph_4Sn \qquad nSnO + n(Ph\text{-}Ph)$$

Alkyltin oxide polymers.

$$(R_2SnO)_n \rightarrow n(2R^{\cdot} + SnO) \rightarrow nR_2$$

$$\rightarrow n/2(R_4Sn + SnO_2)$$

Di-alkyltin Nitrates.

$$R_2Sn(NO_3)_2 \xrightarrow{H_2O} R_2Sn(OH)NO_3 + NO + O_2$$

$$\text{for Ph} \rightarrow |\tfrac{1}{2}(Ph_2)|Sn(OH)NO_3 + PhH \rightarrow NOPh + \tfrac{1}{2}O_2 + SnO_2$$

$$\text{for Et} \rightarrow SnO_2 + NO + |2Et^{\cdot}| + H^{\cdot} + O^{\cdot}$$

$$C_2H_6\downarrow + C_2H_4$$

Sulphates.

$R_2SnSO_4 \rightarrow 2R^{\cdot} + SnSO_4$ (R = Me,Et)

$n\text{-}Pr_2SnSO_4 \rightarrow 2C\uparrow + 8H\uparrow + C\downarrow + SnSO_4$

Carboxylates.

$$2Ph_3SnOCOPh \rightarrow \tfrac{1}{2}\left|\begin{matrix} & OCOPh & OCOPh & \\ Ph - & Sn - & Sn - & Ph \\ & OCOPh & OCOPh & \end{matrix}\right| + Ph_2 + |3Ph + Sn|^{*}$$

$\rightarrow\rightarrow PhSn(O)OCOPh + \tfrac{1}{2}Ph_2 + CO \rightarrow SnO_2 + Ph^{\cdot} + COPh^{\cdot}$

(* as $Ph_4Sn + (PH_3Sn)_2$)

$BuSn(OCOMe)_3 \rightarrow \tfrac{1}{2}|BuSn(OCOMe)_2|_2O \rightarrow BuSn(O)OCOMe +$
$+ \tfrac{1}{2}CH_3COCH_3 + \tfrac{1}{2}CO_2 \qquad \tfrac{1}{2}CH_3COCH_3 + \tfrac{1}{2}CO_2$

$\rightarrow SnO + Bu^{\cdot} + COBu^{\cdot}$

APPENDIX

Published Paper:

Thermal Decomposition Of Inorganic and Organometallic Compounds of Tin-I. Triphenyltin Hydroxide.

Polyhedron Vol. 4, No. 7, pp. 1293–1295, 1985
Printed in Great Britain

0277-5387/85 $3.00 + .00

THERMAL DECOMPOSITION OF INORGANIC AND ORGANOMETALLIC COMPOUNDS OF TIN—I. TRIPHENYLTIN HYDROXIDE

JOHN D. DONALDSON, SUSAN M. GRIMES,* ARTHUR F. LeC. HOLDING and MICHELLE HORNBY

Department of Chemistry, The City University, Northampton Square, London EC1V 0HB, U.K.

(*Received* 8 *August* 1984; *accepted after revision* 18 *December* 1984)

Abstract—The thermal decomposition of triphenyltin hydroxide in the temperature range 25–400°C has been studied. The decomposition products formed at each stage have been isolated and characterised. A decomposition scheme involving a reductive-elimination reaction is proposed. The proportions of this reaction and the accompanying reaction are dependent on the mode of heating.

The literature contains very few reports on the thermal decomposition of organotin(IV) compounds. The interpretation of pyrolysis reactions involved in the decomposition of a series of organotin(IV) adducts and carbohydrate derivatives has been shown to be difficult[1] because of the lack of information on the thermal decomposition of simple organotin(IV) compounds. This is particularly true of organotin–oxygen-containing derivatives and for this reason we have investigated the thermal behaviour of a number of relatively simple oxygen-containing compounds by simultaneous thermogravimetry and differential thermal analysis (TG/DTA).

Triphenyltin hydroxide was chosen as the first example for a detailed thermal analytical study including the identification of the product(s) formed at each stage of the decomposition by the use of appropriate techniques including IR, UV and ^{119}Sn Mössbauer spectroscopy, thin layer chromatography, X-ray powder diffraction data and elemental analyses.

EXPERIMENTAL

The thermal decompositions were carried out under a N_2 atmosphere in a vertical electrically heated furnace (temperature control ± 5°C). The sample was contained in a small pyrex dish and a glass probe, which could be cooled if necessary, was inserted into the furnace such that the bottom tip of the probe was about 5 mm above the sample. The slow stream of N_2 gas issuing from the furnace was passed through a trap cooled in liquid nitrogen to collect any volatile products. The sample was heated stepwise at 85, 310 and 400°C and maintained at each temperature for 2.5 h. After each heating stage the furnace was cooled to room temperature, the volatile product on the probe was collected and a sample of the non-volatile product removed for analysis.

The TG/DTA data were recorded using a Stanton Redcroft STA 780 simultaneous thermal analyser, IR data, as KBr discs, on a Perkin–Elmer 599 IR Spectrophotometer and UV spectra, in absolute ethanol, using a Perkin–Elmer 402 UV/visible Spectrophotometer. ^{119}Sn Mössbauer data were recorded at 78 K using a $BaSnO_3$ source as previously described.[2]

RESULTS AND DISCUSSION

The TG/DTA data show that Ph_3SnOH decomposes in three stages as detailed in Table 1, and the decomposition products identified are listed in Table 2.

From the percentage weight loss data, the first decomposition corresponds to the reaction

$$2Ph_3SnOH \xrightarrow{75°C} Ph_3SnOSnPh_3 + H_2O \quad (1)$$

and the second to

$$nPh_3SnOSnPh_3 \xrightarrow{290°C} (Ph_2SnO)_n + nPh_4Sn. \quad (2)$$

* Author to whom correspondence should be addressed.

Table 1.

Decomposition reaction	Temperature (°C)	Weight loss (%)	DTA feature
1	75	2.5	Endothermic
2	290	59.5	Endothermic
3	362	16.5	Endothermic

However, no simple decomposition reaction can be inferred from the percentage weight loss recorded in the third decomposition. In order to determine the products formed in the third decomposition, and to confirm the products postulated in the reactions (1) and (2), the pyrolysis of approximately 0.2 g Ph_3SnOH was carried out stepwise at temperatures slightly in excess of those recorded in Table 1 with product isolation and characterisation at each stage.

The IR and C, H analysis of (**I**) and the TG data are consistent with reaction (1) being the first decomposition step. The O–H bands at 3610 and 895 cm^{-1} in the IR spectrum of Ph_3SnOH are absent in (**I**); the percentage weight loss of 2.5 is close to that required (2.45). Characterisation of the non-volatile product (**II**) by IR and C, H analysis, and of the volatile product (**III**) by IR and UV spectroscopy identified them as $(Ph_2SnO)_n$ and Ph_4Sn respectively. For reaction (2) the percentage weight loss required is 59.3, and that found is 59.5.

The third decomposition reaction gives three final products, a non-volatile residue (**IV**), whose IR spectrum shows the absence of any organic species, and two volatile fractions (**V**) and (**VI**) of different volatility. Component (**VI**) was identified as Ph_4Sn from its IR spectrum. The IR spectrum of (**V**) was similar to that of (**VI**), but with one extra band at 749 cm^{-1}. The absorption band λ_{max} 250 nm in the UV spectrum of (**V**) suggested the presence of Ph–Ph. A TLC study using a 100:50:5 mixture of *n*-butanol:water:acetic acid[3,4] showed that (**V**) consisted of Ph–Ph with a small amount of Ph_4Sn, whereas (**VI**) consisted mostly of Ph_4Sn with a small amount of Ph–Ph (Ph–Ph, R_f 1.00; Ph_4Sn, R_f 0.00).

^{119}Sn Mössbauer spectroscopy on the non-volatile residue (**IV**) gave the following data, a Sn(II) doublet ($\delta = 2.76 \pm 0.02$ mm s^{-1}, $\Delta = 1.41 \pm 0.02$ mm s^{-1}), assignable to SnO, and a Sn(IV) singlet ($\delta = 0.12 \pm 0.01$ mm s^{-1}) assignable to SnO_2.

Table 2.

Temperature (°C)	Non-volatile product	Volatile product
85	$(Ph_3Sn)_2O$ (**I**)	H_2O
310	$(Ph_2SnO)_n$ (**II**)	Ph_4Sn (**III**)
400	Tin oxide (**IV**)	Ph–Ph*: Ph_4Sn (**V**)
		Ph–Ph: Ph_4Sn* (**VI**)

* Major component of (**V**) > (**VI**).

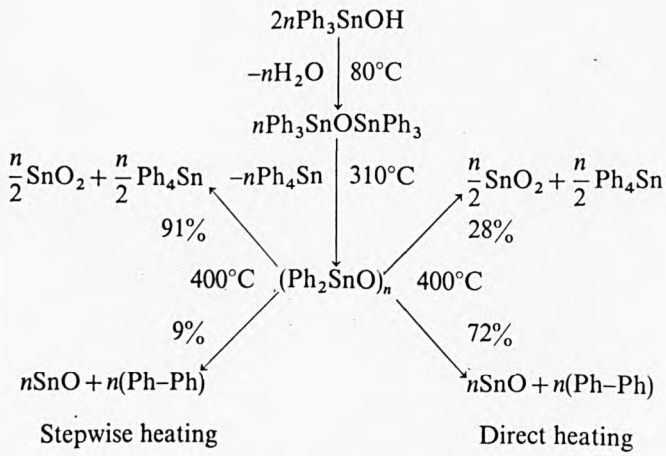

Fig. 1.

The volumetric determination of Sn(II) in the residue using ceric sulphate showed that the Sn(II) : Sn(IV) ratio was approximately 1 : 5.

When a sample of Ph_3SnOH was heated directly to 400°C more Ph–Ph and SnO were produced than when it was heated stepwise to the same temperature. By titrimetry the Sn(II) : Sn(IV) ratio in the residue in this case was approximately 5 : 1.

Thus for the third decomposition reaction, the contribution of the reductive elimination reaction

$$(Ph_2SnO)_n \xrightarrow{400°C} n(Ph\text{–}Ph) + SnO$$

to the overall decomposition of $(Ph_2SnO)_n$ when Ph_3SnOH is heated stepwise to 400°C is less than when it is heated directly to the same temperature.

The results show that the thermal decomposition of Ph_3SnOH by the two modes of heating are as shown in Fig. 1.

The results clearly show that the products of the thermal decomposition of even a simple compound such as Ph_3SnOH do depend on the exact conditions of pyrolysis.

Acknowledgement—The authors thank the International Tin Research Institute for the generous gift of organotin(IV) compounds.

REFERENCES

1. S. M. Grimes, PhD. Thesis, The City University, London (1982).
2. J. D. Donaldson and B. J. Senior, *J. Chem. Soc.* (*A*) 1966, 1769.
3. A. H. Chapman and J. W. Price, *Int. Pest Contr.* 1972, **14**, 11.
4. Y. Tanaka and T. Morikawa, *Japan Analyst* 1964, **13**, 753.